ENHANCED EFFICACY OF NANOTECHNOLOGY-DRIVEN APPROACHES AGAINST ANTIBIOTIC-RESISTANT BIOFILMS IN THE PRESENCE OF METABOLITES

By Naside Gozde Durmus

A Dissertation Submitted in Partial Fulfillment of the

Requirements for the Degree of Doctor of Philosophy in the Biomedical

Engineering Program at Brown University

Providence, Rhode Island

May 2013

This dissertation by Naside Gozde Durmus is accepted in its present form by the School of Engineering as satisfying the dissertation requirement for the degree of Doctor of Philosophy.

Date _____ _____

Anubhav Tripathi, Advisor

Date _____ _____

Thomas J. Webster, Advisor

Recommended to the Graduate Council

Date_____ _____

Shouheng Sun, Reader

Date_____ _____

Jeffrey Morgan, Reader

Date_____ _____

Robert Hurt, Reader

Approved by the Graduate Council

Date_____ _____

Peter M. Weber, Dean of the Graduate School

NASIDE GOZDE DURMUS

EDUCATION

Brown University — Providence, RI
Doctor of Philosophy in Biomedical Engineering — Fall 2009- Present

Boston University — Boston, MA
Master of Engineering in Biomedical Engineering — 2007-2009

Middle East Technical University (METU) — Ankara, Turkey
Bachelor of Science in Molecular Biology & Genetics, High Honors — 2003-2007

RESEARCH INTERESTS

Nanotechnology and its applications in medicine, biomimetic materials, tissue engineering, cell-material interactions at the nanoscale, targeted nanoparticle delivery for infection and disease control

HONORS AND AWARDS

- **Finalist for CIMIT Healthcare Prize**, awarded $10,000 research grant
- Society for Biomaterials STAR Award, Honorable Mention
- Graduate Student Recognition Award, Graduate School and Division of Biology and Medicine, Brown University
- International Affairs Travel Award, Brown University
- NSF Fellowship, 9th International Summer School on Biocomplexity from Gene to System2010
- NSF RI-EPSCoR and Slater Technology Fund Entrepreneurial Fellowship
- **Fulbright Scholarship**, ranked 1st in arts-sciences field in Turkey
- Outstanding Fulbright Scholars in Europe, selected by McKinsey& Company
- College of Engineering Fellowship, Boston University
- Scientific and Technological Research Council of Turkey (TUBITAK) Graduate Scholarship
- President's High Honor Circle, METU
- Turkish Government Scholarship for Undergraduate Education (Ranked in the top 1000 out of 2 million candidates in the National University Entrance Exam)
- 3rd Place in National Science Olympics in Turkey (in physics, chemistry and biology)

RESEARCH EXPERIENCE

Brown University
Nanomedicine Laboratory
PhD Candidate, **Advisor: Prof. Thomas J. Webster**

Metabolite Enabled Reduction of Bacterial Growth on Nanorough Surfaces

- Investigated the effects of surface topography to decrease bacterial (i.e., *Staphylococcus aureus)* attachment on biomedical devices
- Coated nanorough surfaces with sugar metabolites to decrease bacterial growth and biofilm formation on biomedical devices, especially endotracheal tubes

Metabolite Enhanced Efficacy of Magnetic Nanoparticles for Antibiotic-Resistant Biofilms

- Designed superparamagnetic iron oxide nanoparticles (SPION) to eradicate methicillin-resistant *Staphylococcus aureus (MRSA)* biofilms
- Investigated the use of metabolic stimulation to increase the efficacy of SPION treatment

Harvard-MIT Division of Health Sciences and Technology (HST)
Harvard Medical School
Summer Research Student, **Advisor: Prof. Ali Khademhosseini** Summer 2006

Three-Dimensional (3D) Porous Scaffolds for Tissue Engineering

- Created a novel, simple and inexpensive method to construct 3D cell-laden macroporous agarose scaffolds

Three-Dimensional (3D) Vascularized Tissue Engineering

- Developed model systems to optimize printed 3D constructs formed by cell laden hydrogels
- Analyzed the spatial distribution of cells within 3D agarose scaffolds in single and dual perfusion microfluidic channel constructs by MATLAB

Self-Assembly of Hydrogels for Tissue Engineering Applications

- Helped a graduate student to assemble patterned PEG microwells at the oil-water interface

METU-BIOMAT 2004- 2007
Undergraduate Student, **Advisor: Prof. Vasif Hasirci**

Controlled Drug Delivery Systems for Brain Cancer (Senior Project)

- Compared the *in vitro* effects of two anti-cancer agents; temozolomide and celecoxib, which are loaded in the porous PLGA foams
- Investigated *in vitro* optimal conditions by changing the foam pore size and drug concentration

PUBLICATIONS

Refereed Journal Publications:

1. **Durmus NG**, Taylor EN, Kummer KM, Webster TJ, "Enhanced efficacy of superparamagnetic iron oxide nanoparticles against antibiotic-resistant biofilms in the presence of metabolites", 2012. (resubmission to Advanced Materials)
2. **Durmus NG**, Webster TJ, "Eradicating antibiotic-resistant biofilms with silver-conjugated superparamagnetic iron oxide nanoparticles", Advanced Healthcare Materials (2012).
3. **Durmus NG**, Webster TJ, "Nanostructured Titanium: The Ideal Material for Improving Orthopedic Implant Efficacy?", Nanomedicine (2012).
4. **Durmus NG**, Taylor EN, Inci F, Kummer KM, Tarquinio KM, Webster TJ, "Fructose enhanced reduction of bacterial growth on nanorough surfaces", International Journal of Nanomedicine (2012).
5. Taylor EN, Kummer KM, **Durmus NG**, Leuba K, Tarquinio KM, Webster TJ, "Superparamagnetic iron oxide nanoparticles (SPION) for the treatment of antibiotic resistant biofilms", Small (2012).
6. Leuba K, **Durmus NG**, Webster TJ, "Short Communication: Carboxylate functionalized superparamagnetic iron oxide nanoparticles (SPION) for the reduction of S. aureus growth post biofilm formation", International Journal of Nanomedicine. (2012) (in press).
7. Kummer KM, Taylor EN, **Durmus NG**, and Webster TJ, "Effect of different sterilization treatments and varying anodized nanotubular Ti on bacteria growth", Journal of Biomedical Materials Research Part A (2012) (in press).
8. Xu F, Sridharan B, **Durmus NG**, Wang S, Yavuz AS, Gurkan UA, Demirci U, "Living sacrificial porogens to engineer decellularized porous scaffolds", PLoS ONE (2011).
9. Xu F, Wu J, Wang S, **Durmus NG**, Demirci U, "Microengineering Methods for Cell-Based High Throughput Drug Screening", Biofabrication (2011). (Featured article).
10. Park JH, Chung BG, Lee WG, Kim J, Brigham M, Shim J, Lee S, Hwang C, **Durmus NG**, Demirci U, Khademhosseini A, "Microporous cell-laden hydrogels for engineered tissue constructs", Biotechnology and Bioengineering (2010).
11. Lin RL, Montesano G, **Durmus NG**, Moon S, Lee G, Kayaalp E, Khademhosseini A, Hæggström E, Demirci U, "Creating and Perfusing 3D Tissue Constructs'', Analytical and Bioanalytical Chemistry (2009).

Publications in Preparation:

12. **Durmus NG**, Webster TJ, "Emerging nanotechnology approaches for the infection control and diagnosis in clinical settings" (to be submitted)
13. **Durmus NG**, Webster TJ, "Reduced bacterial growth and biofilm formation on nanorough SPION PVC composites" (to be submitted)
14. **Durmus NG**, Webster TJ, "Potentiating the antibacterial properties of magnetic nanoparticles through metabolic stimulation" (to be submitted)

Conference Proceedings:

15. **Durmus NG,** Taylor EN, Webster TJ, "Fructose enhanced efficacy of magnetic nanoparticles against antibiotic resistant biofilms", MRS Fall 2012 Proceedings.
16. **Durmus NG**, Taylor EN, Kummer KM, Webster TJ, "Fructose enhanced reduction of bacterial growth on nanorough surfaces", MRS Fall 2012 Proceedings.

17. **Durmus NG,** Taylor EN, Kummer KM, Webster TJ, "Fructose enhanced reduction of bacterial growth on nanorough surfaces without using antibiotics", North East Bioengineering Conference (NEBEC) 2012 Proceedings.

Book Chapters:

18. **Durmus NG**, Machado M, Yang L, Webster TJ, "Nanomedicine: Novel Approaches for the Treatment of Bone Disease", (in preparation).
19. Stout DA, **Durmus NG**, Webster TJ, "Synthesis of Carbon-based Nanomaterials for Tissue Engineering" in Nanomaterials in Tissue Engineering: Characterization, Fabrication and Applications edited by Gaharwar, Sant, Hancock, and Hacking (Cambridge, UK): Weeodhead (2012).
20. **Durmus NG**, Lin R, Moon S, Demirci D, Khademhosseini A, Demirci U, "Acoustics Based Biosensors'', in "Encyclopedia of Micro- and Nanofluidics'', Springer (2006).
21. **Durmus NG**, Lin R, Lee G, Montesano G, Demirci U, "3D Cell Printing Technologies for Tissue Engineering'', in "Micro- and Nanoengineering of the Cell Microenvironment: Technologies and Applications''; Artech House Publishing Inc. (2006).

Keynote Lecture/Invited Talks:

22. **Durmus NG**, Webster TJ, "Commercialization of Nanotechnology-based Medical Devices", Keynote Lecture given on behalf of Prof. Webster at 9th World Biomaterials Congress (WBC), China, 2012.
23. **Durmus NG**, Webster TJ, "Designing Small Materials for Big Challenges: The Past, Present, and Future of Nanomedicine", Invited Talk given on behalf of Prof. Webster at APMAS 2012, Turkey, 2012.

Oral Presentations:

24. **Durmus NG**, Taylor EN, Kummer KM, Webster TJ, "Metabolite enabled reduction of bacterial growth on nanorough surfaces", 9th World Biomaterials Congress (WBC), 2012.
25. **Durmus NG**, Taylor EN, Kummer KM, Webster TJ, "Metabolite enabled reduction of biofilm formation on nanorough surfaces", IMRC 2012, Cancun, Mexico, 2012.
26. **Durmus NG**, Taylor EN, Kummer KM, Webster TJ, "Metabolite-Enhanced Efficacy of Magnetic Nanoparticles for Antibiotic-Resistant Biofilms", SFB Fall Symposium, 2012.
27. **Durmus NG,** Taylor EN, Webster TJ, "Enhanced efficacy of magnetic nanoparticles against antibiotic resistant biofilms in the presence of metabolite", MRS Fall, Boston, MA, 2012.

Poster Presentations:

28. **Durmus NG**, Taylor EN, Kummer KM, Webster TJ, "Fructose-Enhanced Efficacy of Magnetic Nanoparticles for Antibiotic-Resistant Biofilms", BMES, Atlanta, 2012.
29. **Durmus NG**, Taylor EN, Kummer KM, Webster TJ, "Fructose enhanced reduction of bacterial growth on nanorough surfaces", MRS Fall, Boston, MA, 2012.
30. **Durmus NG**, Taylor EN, Kummer KM, Webster TJ, "Fructose enhanced reduction of bacterial growth on nanorough surfaces without using antibiotics", 38th North East Bioengineering Conference (NEBEC), Philadelphia, 2012.

31. Park JH, Chung BG, Lee WG, Kim J, Brigham M, Shim J, Lee S, Hwang C, **Durmus NG**, Demirci U, Khademhosseini A, "Cell-Encapsulated 3D Bio-Material Systems with Micro-pores and Micro-vasculatures", 13th International Conference on Miniaturized Systems for Chemistry and Life Sciences (MicroTAS), November 1-5, 2009, Korea.
32. **Durmus NG**, Bayam E, Yucel D, Hasirci V, "*In vitro* Antitumor Activity of Temozolomide and Celecoxib Loaded PLGA Discs Against Saos2 and Glioma C6 Cells'', TASSA Annual Conference in Harvard Medical School, 11-13 April, 2008, Boston, MA, USA.
33. **Durmus NG**, Bayam E, Yucel D, Hasirci V, "*In vitro* Antitumor Activity of Temozolomide and Celecoxib Loaded PLGA Discs Against Saos2 and Glioma C6 Cells'', FAST Annual Conference, 15 February, 2008, Boston, MA, USA.
34. **Durmus NG**, Bayam E, Yucel D, Hasirci V, "*In vitro* Antitumor Activity of Temozolomide and Celecoxib Loaded PLGA Discs Against Saos2 and Glioma C6 Cells", 13th Biomedical Science and Technology Symposium, August, 2007, Istanbul, Turkey.
35. **Durmus NG**, Bayam E, Yucel D, Hasirci V, "*In vitro* Antitumor Activity of Temozolomide and Celecoxib Loaded PLGA Discs Against Saos2 and Glioma C6 Cells'', 4th European Symposium on Biopolymers (ESP2007), October 2-4, 2007, Kusadasi, Turkey.

TEACHING AND MENTORING

Teaching Experience:

Teaching Assistant, Brown University Summer 2012
Exploring Engineering: Problem Solving in Biotech, Nanotech and Renewable Energy
Instructors: Prof. Thomas J. Webster and Prof. Karen Haberstroh

- This is an online pre-college course which emphasizes the three different fields of engineering. Students learn how to interpret data, use mathematics and science to solve complex engineering problems as well as working in teams.

Instructor at Summer@Brown, Brown University Summer 2011
CEEN 0903 Do You Want to Be an Engineer?

- This is a three-week pre-college course which introduces a variety of engineering topics and disciplines with a focus in mechanical, civil, electrical, computer, chemical, biomedical, and materials engineering.

Teaching Assistant, Brown University Spring 2011
BIOL 1120 Biomaterials, Instructor: Beth Anne Zielinski

- This course emphasizes the transition from tissue replacement to tissue repair strategies for advanced undergraduates and graduate students. Topics from science and technology, such as polymers, metals, ceramics, and materials obtained from biological sources or through recombinant biotechnology are covered.

Soil Bacteria Project Presenter May- June 2008

- Gave presentations in Boston area for the Fulbright Academy of Sciences (FAST) and National Science Foundation (NSF) project with the goal of educating the public on the important environmental roles of bacteria.

Mentoring:

- Kim Kummer, Master's student in Biomedical Engineering, Brown University
- Benjamin Geilich, Undergraduate student in Neuroscience Program, Brown University
- Kohana Leuba, Undergraduate student in Engineering, Brown University
- Naser Mahfouz, Undergraduate student in Engineering, Brown University
- Zai Ganesh, Undergraduate student in Biology Department, Brandeis University

SKILLS

Technical:

- **Molecular Biology, Tissue Engineering and Nanotechnology-Related Techniques:** Plasmid DNA isolation, RNA isolation, agarose gel electrophoresis, electroporation, bacterial transformation with plasmid DNA, human genomic DNA isolation, polymerase chain reaction (PCR), RT-PCR, SDS-PAGE, mammalian cell culture, cell viability and proliferation assays, agarose and collagen matrix preparation, protein and cell patterning, microfluidic channel fabrication, preparation of cell co-cultures, micro- and nanoparticle synthesis
- **Cell lines:** mouse embryonic stem cells (mES), AML12, NIH-3T3, Saos2, Glioma C6, HL cardiomyocytes, human mesothelial cells (LP9/TERT), bacteria cells
- **Microscopy:** Scanning electron microscope (SEM), atomic force microscopy (AFM), transmission electron microscopy (TEM), fluorescence microscopy and confocal microscopy with cells and nanoscale materials

Computer:

- **Programming:** MATLAB, Perl, UNIX
- **Databases:** Genbank, BLAST, MultALin, Protein Data Bank

Language: Turkish (native), German (beginner), French (beginner)

MEMBERSHIPS

- Sigma Xi Research Society, Brown University Chapter
- Fulbright Academy of Sciences and Technology (FAST)
- Turkish and American Scientists and Scholars Association (TASSA)
- State Alumni (for Fulbright Scholars)

ACKNOWLEDGMENTS

This thesis would have been impossible without the contribution of many colleagues, mentors and friends. First of all, I would like to acknowledge my advisor, Prof. Thomas Webster, for being such a supportive and generous advisor, thrusting in my scientific abilities and giving me the unique opportunity to do research under his guidance. His great energy, positivism and enthusiasm to do exciting research have always impacted me. He gave me the freedom to pursue my research ideas, encouraged me to become an independent researcher and under his guidance, my research has thrived. I had access to him whenever I needed to discuss my research data or I needed his advice. His insights have lead to the success of my PhD work and my career. Without his enthusiastic guidance and generous support, I could not have published so many papers, book chapters, proceedings and received any grants or awards in a very short amount of time.

I also want to acknowledge my co-advisor, Prof. Anubhav Tripathi, for his generous support and guidance. He was there helping, supporting and meeting me whenever I needed him, especially during the last period of my PhD. He gave me valuable advices and support for my career. I was always inspired by the endless support and advice that he has for his students. I also would like to thank Dean John Tyler at the Graduate School for his help, guidance and support during the rough times of my PhD. Without their guidance and support, I would not be finishing up my studies at Brown.

I also want to thank all of my friends in the Webster Nanomedicine group. In particular, I would like to thank Dr. Erik Taylor for teaching me the basic techniques in the bacteria

lab and for his collaboration on the antibacterial magnetic nanoparticles work. His talent and enthusiasm was crucial for the success of these studies. In addition, I would like to thank Kim Kummer for her help with the bacteria experiments and her company in the lab. Also, I thank Erik, Kim, George, Gavin, Linlin, David, Glareh, Vince and Mary for their friendship and support throughout my studies. Moreover, I would like to acknowledge, Center for Integration of Medicine and Innovative Technology (CIMIT) for partially funding my PhD studies through the Student Healthcare Prize.

I also thank all my teachers and mentors during my education who helped me to recognize my talents and ambition to do science. I want to express my gratitude to Prof. Vasif Hasirci at Middle East Technical University (Ankara, Turkey). He gave me the opportunity to join his group in my sophomore year at METU and I have started my first research project on drug delivery systems for cancer. In addition, I would like to thank Prof. Semahat Demir for her advice and mentorship (and for our fortune-telling sessions) throughout my PhD studies. She has been my greatest role model as a female engineer. I also would like to thank Prof. Metin Akay for his time, advice in his very busy schedule.

I am very lucky to have so many close and supportive friends and family. Cagdas Varel (Cagdis) has been one of my closest friend since college years. We always supported each other during the happiest and saddest moments in life and during PhD. He has been my second brother in life. Ozlem Arat has been my go-to person and my sister since my college years as well. Whenever I needed, she was always available to give me her endless support, calm me down whenever I was stressed out. She cheered me up during

the very rough times during my PhD years. I would also thank Yildiz Sinangil, for her support, for being my closest friend in Boston and for sharing the guilty pleasure of 'shopping'. I would also like to thank my friends and family in Turkey, who were always there supporting and missing me. I would like to thank Eda Ercan (Edos), Emine Tevattepe (Emik), Duygu Ertem (Conim), Ceren Sozver (Kankam), Ezgi Can Ozan, Gonca Karakus, Seher Bal Kocaman, Sedef Bal Kocaman, Gokce Sultan Tuzun for their endless love and friendship, even if we could not be together for a long time. In additon, I would like to thank Ozgur Arslan (Pozgurum), Hasan Onur Keles, Ragip Akbas, Melik Demirel, Ela Kucukpinar, Mahmut Akten, Yasemin Sanli. Without their company, my life would be miserable in the US.

I am also thankful to Utkan who has been with me throughout this journey. His endless support, encouragement and unconditional love constantly makes me a better person. His motivational speeches, his passion for what he does and his vision always influence me to push my limits, even in my weakest moments. He is my best friend, my 'cicim' and my greatest supporter in life.

Finally, I am deeply grateful to my mother, father and brother for their love, care and all the sacrifices that they have made for my education. My mother has been my best teacher, mentor and motivator in life. I also thank my grandfather and grandmother for their endless love and support. They looked after me and they were always proud of my every little success. My family's constant belief that I will be successful in whatever I do was the force which has motivated and pushed me to reach my goals.

DEDICATION

I dedicate this thesis to my family, especially to my mother (canim annem) Nefise.

TABLE OF CONTENTS

LIST OF FIGURES

CHAPTER 1

of infection to new locations. **B)** Confocal microscopy analysis of the each stage of biofilm formation. I-III represents *P. aeruginosa* stained with DAPI, IV represents *S. aureus* stained with chromosomal green fluorescent protein (GFP), and V represents *S. aureus* stained with Live/Dead assay.

Figure 1.4. Summary of the factors contributing to the biofilm formation on biomaterial surfaces. Rapid initial adhesion and attachment of bacteria is controlled by Van der Waals forces, hydrophobic and electrostatic interactions as well as protein adsorption on the biomaterial surface. Moreover, biomaterial surface roughness, texture, chemistry and hydrophobicity are among the contributing factors. Initial attachment and adhesion is followed by a more prolonged accumulation phase that involves cell proliferation and intercellular adhesion. Finally, micro-organisms may disaggregate from the macrocolonies and drift into the bloodstream resulting in metastatic and embolic complications.

Figure 1.5. Distinct metabolic states within a biofilm structure. Metabolic activity is a function of depth within the biofilm and is influenced by nutrient transport. Cells at the edges at the bulk liquid interface are the most metabolically active. On the other hand, cells deep within the biofilm can potentially remain dormant, limit nutrient uptake and slow their growth. Thus, they are able to survive an antibiotic treatment.

Figure 1.6. A model for biofilm drug resistance based on persister cell formation and survival. Initial treatment with antibiotic kills normal cells in both planktonic and biofilm populations. The host immune system kills planktonic persisters while persisters within the biofilm are protected by the EPS matrix. After the antibiotic therapy is discontinued, persisters resuscitate and repopulate the biofilm and the infection relapses.

Figure 1.7. Three main hypotheses for mechanisms of antibiotic resistance in biofilms. Biofilms restrict the antibiotic intake or penetration through the matrix. In addition, they develop resistant phenotypes with their antibacterial agent destroying enzymes. Horizontal gene transfer between the resistant bacteria also contributes. Moreover, they alter their growth rate, metabolism and cellular microenvironment, which also contribute to the inhibition of antibiotic penetration through the biofilm.

Figure 1.8. The use of nanomaterials is a growing new approach to the design of medical devices that have improved resistance to biofilm-mediated, drug-resistant, and device centered infections. For these anti-infection applications, various nanomaterials are being developed, such as nanoparticles and nanotubes, for direct use as biomedical devices; such nanomaterials can be used alone, incorporated onto surfaces, into composites, or as components in sensors such as zinc oxide (ZnO) nanoparticles, carbon nanotubes, titanium dioxide nanotube arrays, and silver nanoparticle-polymer composites, respectively in A-D. (Figures A, B, C, D. are from citations listed). These examples and others will be further reviewed here briefly to understand their antibacterial activity and potential applications.

Figure 1.9. Characterization of silver (Ag)/montmorillonite (MMT)/chitosan (Ct) bio-nanocomposites. TEM characterization indicated that in particle size and their size distribution decreased as UV irradiation time increased from three hours to 96 hours (**A-C, respectively**). Nanocomposites exhibited strong antibacterial properties against both gram-negative (*E. coli*) and gram-positive (*S. aureus* and MRSA) bacteria (**D**).

Figure 1.10. Biomedical applications of SPION. Representative TEM images of SPION with different sizes and chemical compositions: 8 nm/2.5 nm Fe/Fe3O4

nanoparticles (**a**) and 5 nm/5 nm Fe/Fe_3O_4 nanoparticles (**b**). SPION can be engineered for control of the magnetic core size, along with a polymer coating, targeting agents, peptide fragments, drugs, and fluorescent markers for various biomedical applications (**c**). For example, SPION are commonly used as image contrast agents in MRI due to their high biocompatibility (**d-f**).

Figure 1.11. Various toxicity mechanisms of nanoparticles against bacterial cells. Nanoparticles can disrupt and damage the bacterial cell membrane/wall, release heavy metal ions (i.e., Ag^{+} or Zn^{+2}), interrupt electron transport, cause production of ROS species which then damages the proteins, lipids and DNA.

Figure 1.12. Nanoroughness decreases bacterial attachment and biofilm formation on medical devices. In addition, biovolume of biofilms decreases on nanorough surfaces.

Figure 1.13. Metabolite-enabled eradication of bacterial persisters by antibiotics. **a)** Antibiotics do not eradicate *E. coli* persisters *in vitro*. On the other hand, percentage survival of persisters decreases when mannitol is used in combination with antibiotics. **b)** Metabolites also enhance the *in vivo* efficacy of antibiotics. *E. coli* biofilms on urinary-tract- inserted catheters are eradicated after treatment with mannitol (1.5 g/kg) plus gentamicin (1mg/kg). **c)** Metabolic network shows the efficiency of metabolite-enabled elimination of persister *E. coli*. Metabolites are color-coded according their ability to stimulate antibiotic action.

Figure 1.14. Using nanomaterial science to reduce infections. Metabolic microenvironment of the biofilms was manipulated to improve the antibacterial properties of magnetic nanoparticles (SPION) as well as nanorough device surfaces.

CHAPTER 2

ETT soaked into a 100 mM fructose solution.

Figure 2. 8. *S. aureus* optical density measurements after 24 hours. Planktonic bacteria growth decreased on NanoR surfaces soaked in a fructose (10 mM and 100 mM) solution. Data represents mean ± SEM, N=3. * $p < 0.05$ NanoR compared to NanoR soaked in 10 mM fructose, and NanoR soaked in 10 mM fructose compared to NanoR soaked in 100 mM.

Figure 2.8. *S. aureus* colony counts on PVC and NanoR surfaces soaked in a 10 mM fructose solution. Biofilm formation decreased on NanoR and PVC surfaces soaked in a 10 mM fructose solution. Data represents mean ± SEM, N = 4. *$p < 0.05$ NanoR soaked in 10 mM fructose compared to PVC control, # $p < 0.1$ NanoR compared to PVC control.

CHAPTER 3

Figure 3.1. Method used for the synthesis and isolation of superparamagnetic iron oxide nanoparticles (SPION). SPION were prepared by high temperature reflux of iron (III) acetylacetonate in triethylene glycol (**A**) in a round bottom boiling flask under magnetic stir while outfitted with a reflux condenser. SPION were isolated in a strong magnetic field produced by two DZX08-N52 neodymium magnets (4" diameter x 1/2" thick magnet) (**B-C**).

Figure 3.2. Schematic of *in vitro* screening assays used in the study. A single colony of *Mu50* strain of MRSA was grown in 3 mL of TSB for 18 hours at 37^0C, 200 rpm. Then, 200 µL of a 10^8 cells/mL solution was inoculated into each well of a 96-well microtiter plate. Thus, biofilms were established as some portion of inoculated bacteria attached to the surface of the plate during 24 hours incubation. After 24 hours, the culture medium

was replaced with unconjugated and metal conjugated SPION in TSB. In addition, different concentrations of a fructose solution (1 and 10 mM) were added to the SPION+TSB solution to investigate the effect of fructose on magnetic nanoparticle action. After 24 hours of treatment, three different assays were used to assess SPION activity on the MRSA biofilms. Optical density was measured at 562 nm ($OD_{562\ nm}$) to assess planktonic (free floating) bacteria growth within the solution (**Assay 1**). In addition, crystal violet (CV) staining was performed to quantify biofilm mass (**Assay 2**) and viable cell counts were performed to quantify colony forming units (CFU/mL) (**Assay 3**). To compare SPION action with conventional antibiotics, 1 mg/mL of vancomycin and gentamicin were tested using the same experimental design.

Figure 3.3. a) TEM image of unconjugated SPION (UC) prepared by refluxing Fe $(acac)_3$ in a TREG solution. TEM analysis demonstrated that dispersed nanoparticles were successfully synthesized and had an average size of 9.92 ± 3.14 nm (scale bar = 100 nm). **b)** Elemental composition of unconjugated and metal (Fe, Zn) conjugated SPION determined by ICP-AES. 10 mg/mL of a SPION solution (UC) was conjugated with 1 mM or 4 mM salts of $FeCl_3$ (Fe1, Fe4) and $ZnCl_2$ (Zn1, Zn4), respectively. The concentration of iron (Fe^{3+}) and zinc (Zn^{2+}) ions increased as the metal salt conjugations increased from 1 mmol (Fe1 and Zn1) to 4 mmol (Fe4 and Zn4). Data represents mean ± standard error of the mean (SEM), N = 3.

Figure 3.4. DLS analysis of unconjugated SPION. The average size was 19.93 ± 1.31 nm.

Figure 3.5. DLS analysis of iron-conjugated SPION. The average size was 23.3 ± 1.17 nm.

Figure 3.6. DLS analysis of zinc-conjugated SPION. The average size was 19.67 ± 0.72 nm.

Figure 3.7. The effect of fructose concentration on the planktonic growth of *Mu50* strain (MRSA). Bacterial growth was quantified by continuous optical density measurements for 24 hours. The presence of fructose in the culture medium did not significantly affect the planktonic growth of MRSA over 24 hours.

Figure 3.8. The effect of fructose concentration on the planktonic growth of *Mu50* strain (MRSA). Bacterial growth was quantified by colony forming units. Presence of fructose in the culture medium did not increase the biofilm formation over 24 hours.

Figure 3.9. SPION activity against planktonic MRSA growth after 24 hours. Unconjugated (UC) and metal-conjugated (Fe1, Fe4, Zn1 and Zn4) SPION significantly decreased the growth of planktonic bacteria (* $p < 0.001$). Metal-conjugated SPION had improved antibacterial activities compared to vancomycin ($^{\phi}$ $p < 0.01$). Data represents mean ± standard error of the mean (SEM), N = 3.

Figure 3.10. Enhanced anti-biofilm activity of SPION treatment in the presence of fructose metabolites. The anti-biofilm activity of 1mg/mL SPION against MRSA biofilms after 24 hours with and without 1 mM and 10 mM fructose solutions. The anti-biofilm efficacy of unconjugated SPION (UC) as well as 1 mM iron-conjugated SPION (Fe1) and 1 mM zinc-conjugated SPION (Zn1) against MRSA biofilms was significantly enhanced when fructose metabolites were added to the treatment. Data represents mean ± SEM. N = 3. *$p < 0.001$ compared to untreated biofilms; # $p < 0.05$ and ** $p < 0.01$ compared to the same treatment without fructose.

Figure 3.11. Representative colony forming units observed for the same dilution during the viable cell count experiments. a) Representative picture for an uncountable colony of

untreated MRSA biofilm at a 10^{-5} dilution. b) On the other hand, countable colonies were observed at the same dilution (10^{-5} dilution) when biofilms were treated with 1 mg/mL of unconjugated (UC) and 1 mmol and 4 mmol Fe^{+3} conjugated SPION (Fe1 and Fe4) treated MRSA biofilms in the presence and absence of a fructose solution. SPION significantly eradicated the MRSA biofilms. Moreover, 1 mM and 10 mM of a fructose solution clearly increased the eradication efficacy of UC and Fe1 on MRSA biofilms.

Figure 3.12. Fructose metabolites improved the eradication efficacy of unconjugated SPION (UC) against MRSA biofilms (b and c, respectively) after 48 hours, as compared to control biofilms (a). Live (green) and dead (red) cells were stained with BacLight Live/Dead utilizing Syto9 and propidium iodide stains. Scale bars represent 20 µm.

Figure 3.13. 1 mM of fructose metabolites improved the eradication efficacy of iron-conjugated SPION (Fe1) against MRSA biofilms (b and c, respectively) after 48 hours, as compared to control biofilms (a). Live (green) and dead (red) cells were stained with BacLight Live/Dead utilizing Syto9 and propidium iodide stains. Scale bars represent 20 µm.

Figure 3.14. 10 mM of fructose metabolites improved the eradication efficacy of zinc-conjugated SPION (Zn1) against MRSA biofilms (b anc c, respectively) after 48 hours, as compared to control biofilms (a). Live (green) and dead (red) cells were stained with BacLight Live/Dead utilizing Syto9 and propidium iodide stains. Scale bars represent 20 µm.

Figure 3.15. Comparison of the percentage survival of MRSA biofilms treated with 1 mg/mL of vancomycin and unconjugated and metal conjugated (Fe1, Fe4, Zn1 and Zn4) SPION in the presence of fructose metabolites. SPION treatments exhibited stronger

antibacterial properties than vancomycin, the antibiotic of last resort. The eradication by unconjugated SPION (UC) was about two orders of magnitude better than vancomycin ($p < 0.1$). Metal conjugations further increased the eradication efficacy of SPION (Fe1, Fe4, Zn1 and Zn4) ($p < 0.05$). Most importantly, fructose metabolites further enhanced the eradication efficacy of unconjugated (UC) and 1mmol iron (Fe1) and zinc (Zn1) conjugated SPION. Fructose metabolites also increased the efficacy of vancomycin on MRSA biofilms.

Figure 3.16. MRSA biofilm mass after 24 hours of SPION treatment. Fructose metabolites significantly improved the biofilm mass reduction efficiency of SPION conjugated with 1 mM (Fe1) and 4 mM iron (Fe4). In addition, vancomycin significantly reduced MRSA biofilm mass in the presence or absence of a fructose solution. On the other hand, gentamicin increased biofilm formation. Data represents mean ± standard error of the mean (SEM), N = 3. *$p < 0.05$ and # $p < 0.01$ compared to untreated control biofilms.

Figure 3.17. Activity of metal salts used in SPION synthesis ($ZnCl_2$ and $FeCl_3$) against the planktonic growth of MRSA after 24 hours of treatment. 1mg/mL $ZnCl_2$ showed significant activity against planktonic bacteria. However, the metal salts were not as effective as the nanophase unconjugated (UC) or metal conjugated SPION (Fe1, Fe4, Zn1, Zn4). Data represents mean ± SEM, N = 3. *$p < 0.05$ compared to untreated control biofilms.

Figure 3.18. The effect of metal salts used in SPION synthesis ($ZnCl_2$ and $FeCl_3$) on MRSA biofilm mass after 24 hours of treatment. 1mg/mL $ZnCl_2$ and $FeCl_3$ did not show

any significant effect in the presence or absence of a fructose solution. Data represents mean ± SEM, N = 3.

Figure 3.19. Qualitative analysis of the iron deposition by Prussian blue staining. Intensity of blue color increased in the presence of fructose metabolites, implying an increase in the iron deposition levels within the biofilm when fructose metabolites were present as carbon sources.

Figure 3.20. Intensity of blue color increased in the presence of fructose metabolites, implying an increase in the iron deposition levels within the biofilm when fructose metabolites were present as carbon sources.

Figure 3.21. Analysis of the uptake of SPION within the MRSA biofilms by quantifying the presence of iron (Fe^{3+}), sulphur (S^{2-}) and zinc (Zn^{2+}) ions by inductively coupled plasma atomic emission spectroscopy (ICP-AES) (**a, b and c, respectively**). The uptake of SPION by the biofilms included the nanoparticles within the cell, attached to the bacterial cell surface as well as in the biofilm matrix. The enhanced anti-biofilm efficacy of SPION treatments are mostly due to the significant increases in intracellular or membrane bound iron (Fe^{3+}) and sulphur (S^{2-}) within the MRSA biofilms.

Figure 3.22. TEM imaging of bacteria after SPION treatment. Growth inhibition and biofilm reduction by SPION is mediated by interactions with the MRSA membrane surface. **A)** Unconjugated (UC) SPION adsorb to the bacterial cell surface and damage the bacterial cell membrane. **B)** The uptake of SPION within the biofilm-forming cell increases in the presence of metabolites. SPION damage the cell membrane and better penetrate through the membrane surface (as indicated with the arrows) (scale bars = 100 nm).

Figure 3.23. The formation of reactive oxygen species (ROS) was increased when SPION was used in combination with fructose metabolites: **A)** untreated biofilms; **B)** biofilms treated with 1 mg/mL SPION; **C)** biofilms treated with 1 mg/mL SPION in combination with 1 mM fructose; **D)** biofilms treated with 1 mg/mL SPION in combination with 10 mM fructose. ROS formation increased when MRSA biofilms were treated with unconjugated SPION for 24 hours (**Figure 23B**), compared to untreated control biofilms (**Figure 23A**). Moreover, ROS generation further increased when 1 mM and 10 mM fructose metabolites were added to the SPION treatment (**Figure 23Cand 23D respectively**). Thus, enhanced anti-biofilm activity was due to the increased SPION penetration into the MRSA biofilms and generation of reactive oxygen species (ROS) in the presence of metabolites.

Figure 3.24. Quantification of color intensity after staining with CellRox Dep Red Sensor. Increased intensity implies an increase in the reactive oxygen species (ROS) formation when SPION were used in combination with fructose metabolites. Thus, enhanced anti-biofilm activity was due to the increased SPION penetration into the MRSA biofilms and the generation of ROS in the presence of metabolites.

Figure 3.25. Enhanced anti-biofilm activity of SPION treatment in the presence of fructose metabolites. The anti-biofilm activity of 1mg/mL SPION against *E. coli* biofilms after 24 hours with and without 1 mM and 10 mM fructose solutions. Anti-biofilm efficacy of unconjugated SPION (UC) as well as 1 mM iron-conjugated SPION (Fe1) and 1 mM zinc-conjugated SPION (Zn1) against MRSA biofilms was significantly enhanced when fructose metabolites were added to the treatment. Data represents mean ±

SEM. N = 3. * $p < 0.01$ compared to untreated biofilms; # $p < 0.001$ and φ $p < 0.1$ compared to the same treatment without fructose.

Figure 3.26. Representative images of anti-biofilm activity of unconjugated SPION treatment against *P. aeruginosa* in the presence of fructose metabolites. Biofilms were grown on glass slides for a week **(Figure 3.26a, c, and e).** Biofilm formation was decreased after 24 hours of SPION treatment (**Figure 3.26d**). The anti-biofilm activity of SPION was significantly enhanced when used in combination with fructose metabolites (**Figure 3.26f**).

Figure 3.27. The effect of increasing metabolite concentration while decreasing the SPION metal conjugation concentrations. MRSA biofilms were treated with 1 mg/mL of SPION conjugated with 0.5 mmol iron and zinc (denoted as Fe0.5 and Zn0.5, respectively), which also corresponded to a decrease in antibacterial Fe^{+3} and Zn^{+2} concentrations. The anti-biofilm activities of SPION were still significantly enhanced by increasing the fructose concentration to 100 mM ($p < 0.001$).

Figure 3.28. Fructose metabolites potentiate the antibacterial activities of SPION against *S. aureus* planktonic growth. Although 0.1 mg/mL SPION is not an antibacterial concentration, it significantly reduced the planktonic *S. aureus* growth in the presence of 10 mM or 100 mM fructose metabolites (* $p < 0.05$).

Figure 3.29. Potentiating the anti-biofilm properties of SPION through the use of metabolites. Presence of 1 mM, 10 mM and 100 mM fructose metabolites significantly increased the eradication efficacy of 0.1 mg/mL SPION, which is not an antibacterial dose ($p < 0.0001$). Most importantly, the efficacy of 0.1 mg/mL SPION was comparable to the activity of 1 mg/mL SPION, when used in combination with 100 mM fructose

metabolites. This might highlight the possibility of using metabolites as a novel method to decrease the toxicity of SPION treatments.

Figure 3.30. The effect of glucose metabolites on the anti-biofilm efficacy of 1mg/mL unconjugated SPION. 10 mM glucose metabolites significantly enhanced the SPION activity against *S. aureus* biofilms (* $p < 0.001$).

Figure 3.31. The effect of mannitol metabolites on the anti-biofilm efficacy of 1mg/mL unconjugated SPION. 1 mM and 10 mM mannitol metabolites significantly enhanced the SPION activity against *S. aureus* biofilms (* $p < 0.01$).

Figure 3.32. Possible mechanism for the observed enhanced anti-biofilm activity when fructose metabolites were added to the SPION treatment. Enhanced activity is due to the increased penetration of nanoparticles within the biofilm which leads to increases in ROS formation. The uptake of fructose metabolites might induce the catabolism of carbon sources and the generation of NADH. The bacterial electron transport chain oxidizes NADH and contributes to PMF. Then, bacterial cell death might occur due to the oxidative stress from ROS formation. First, superoxide (O_2^-) formation could be stimulated by the electron chain transport and O_2^- might damage Fe-S clusters, making more ferrous iron available for oxidation by the Fenton reaction. The Fenton reaction might lead to the formation of hydroxyl radicals (•OH), which can damage DNA, lipids and proteins. All of these events eventually cause bacterial cell death and the eradication of biofilms.

CHAPTER 4

Figure 4.1. Schematic of the novel strategy for infection treatment. Methicillin-resistant *Staphylococcus aureus* (MRSA) biofilms were established on microtiter plate surfaces. Biofilms then were treated with superparamagnetic iron oxide nanoparticles (SPION) conjugated with antibacterial silver salts. After 24 hours, antibiotic-resistant biofilms were significantly eradicated. Anti-biofilm efficacy of the silver-conjugated SPION treatment was also improved by an external magnetic field. Thus, this novel treatment can be targeted to the infection site, disrupt and eradicate the biofilm, in the presence of a magnetic field.

Figure 4.2. TEM analysis of the magnetic nanoparticles used in the study**. a)** Unconjugated SPION (UC) prepared by refluxing iron (III) acetylacetone in triethylene glycol (TREG) (scale bar = 50 nm). **b)** Silver-conjugated SPION (scale bar = 100 nm).

Figure 4.3. Characterization of unconjugated (UC) and silver-conjugated SPION. **a)** Size distribution histogram of unconjugated SPION. Average particle size is 18.17 ± 1.34 nm. **b)** Size distribution histogram of silver-conjugated SPION. Average particle size is 176.5 ± 27 nm.

Figure 4.4. Characterization of unconjugated (UC) and silver-conjugated SPION. Elemental composition of unconjugated (UC) and silver-conjugated SPION determined by ICP-AES. 10 mg/mL of a SPION solution was conjugated with 1 mM or 4 mM salt of $AgNO_3$. ICP-AES indicated that silver was successfully conjugated to SPION. The concentration of silver (Ag^+) ions increased as the silver metal salt conjugations increased from 1 mmol to 4 mmol. Data represents mean ± standard error of the mean (SEM), N=3.

Figure 4.5. Optimization of the antibacterial dose of silver-conjugated SPION. Antibacterial activity of silver-conjugated SPION was assessed at three different concentrations (0.01 mg/mL, 0.1 mg/mL and 1 mg/mL). When the concentration of silver-conjugated SPION increased from 0.1 to 1 mg/mL, planktonic MRSA growth rate significantly decreased from 88.14 ± 2.28% to 57.91 ± 1.57% (* $p < 0.001$). On the other hand, 0.01 mg/mL silver-conjugated SPION did not have any significant antibacterial effect. In addition, the concentration of SPION had a significant effect on planktonic MRSA growth rate. 1 mg/mL was significantly more effective than 0.01 mg/mL and 0.1 mg/mL silver-conjugated SPION (*$p < 0.001$). Data represents mean ± standard error of the mean (SEM), N= 3.

Figure 4.6. Antibacterial properties of silver-conjugated SPION against MRSA biofilms. Biofilm mass significantly decreased when MRSA biofilms were treated with 1 mg/mL silver-conjugated SPION. Biofilm mass further decreased when an external field was present (*$p < 0.01$).

Figure 4.7. Representative colony forming units. An uncountable colony was observed for the untreated MRSA biofilm at a 10^{-5} dilution whereas countable colonies were observed at the same dilution when biofilms were treated with 1 mg/mL silver-conjugated SPION. Thus, silver-conjugated SPION treatment significantly eradicated the MRSA biofilms.

Figure 4.8. The eradication efficacy of silver-conjugated SPION against MRSA biofilms as compared to control biofilms. Live (green) and dead (red) cells were stained with Baclight Live/Dead utilizing Syto®9 and propidium iodide stains. Scale bars represent 20 μm.

Figure 4.9. Planktonic MRSA growth further decreased when an external magnetic field was present (*p < 0.001). All of these results show that the anti-biofilm efficacy of silver-conjugated SPION treatment is improved in the presence of an external magnetic field.

Figure 4.10. Analysis of the uptake of silver-conjugated SPION within the MRSA biofilms by quantifying the presence of iron (Fe^{3+}), sulfur (S^{2-}) and silver (Ag^{+}) ions by inductively coupled plasma atomic emission spectroscopy (ICP-AES). The enhanced anti-biofilm efficacy of SPION treatments are due to the significant increases in intracellular or membrane bound iron (Fe^{3+}) (**$p < 0.001$), sulfur (S^{2-}) (*$p < 0.05$) and silver (Ag^{+}) (**$p < 0.001$), which indicates an increased uptake of silver-conjugated SPION within the MRSA biofilms. An external magnetic field further increased the intracellular or membrane-bound Fe^{3+} ($^{\#}p < 0.1$), S^{2-} ($^{\#\#}p < 0.01$) and Ag^{+} within the biofilm and improved the antimicrobial activity of silver-conjugated SPION. Data represents mean ± standard error of the mean (SEM), N= 3.

CHAPTER 5

Figure 5.1. *S. aureus* optical density measurements after 24 hours. Planktonic bacteria growth significantly decreased on PVC+ 2% SPION nanocomposites, compared to conventional PVC surfaces (* $p < 0.001$). Data represents mean ± SEM, N=3.

Figure 5.2. *S. aureus* biofilm formation on nanocomposite surfaces after 24 hours Biofilm formation decreases on PVC+ 2% nanocomposites by ~73%, compared to conventional PVC surfaces. Data represents mean ± SEM, N=3.

Figure 5.3. Representative colony forming unit observed for the dilutions over the 4-log range during the viable cell count experiments. Uncountable colony units were observed

at 10^{-1} and 10^{-2} dilutions on conventional PVC surfaces. On the other hand, countable colonies were observed at the same dilution (10^{-2} dilution) when S. aureus was cultured on PVC+2% SPION nanocomposites.

Figure 5.4. Schematic overview of the proposed infection prevention technology: PVC+SPION nanocomposites. This broadly applicable multifunctional platform technology will: **a)** decrease the initial bacterial attachment on the medical device surface (i.e. catheter surface); **b)** further reduce bacterial biofilm formation on the surface by using magnetic nanoparticles that can be targeted to the infected site on demand. Moreover, the nanoroughness of the nanocomposites surfaces can be increased to further improve the anti-biofilm properties (as shown in Chapter 2).

Figure 5.5. Schematic diagram of peritoneal dialysis (PD). PD is a simple home-based solution to big growing problem of end stage renal disease. However, infections can occur on the catheter surface or at the catheter-exit sites while patients perform PD at their home setting.

LIST OF TABLES

Chapter 1. Introduction

1.1. Burden and Impact of Healthcare-associated Infections (HAIs)

When antibiotics were first introduced, they were believed to be the end of bacterial infections.[1] However, due to their extensive use (which has been estimated to be over 1 million tons since the 1940's), the emergence of multi-drug resistant bacteria has become one of the greatest global problems in public health today.[2] The number and frequency of multi-drug resistant microorganisms have been mounting worldwide rendering antibiotic therapies costly and, most of the time, unsuccessful.[3] On the other hand, there has been a descending trend in the development of new antibiotics, creating a critical void on global health.

Invasive medical devices (such as central venous catheters, urinary tract catheters, renal dialysis shunts, peritoneal dialysis catheters as well as prosthetic heart valves, cardiac pacemakers, total artificial hearts, joint replacements or other orthopedic devices) have become an integral part of modern healthcare.[4] While these devices are used in many areas of medicine for diagnostic and therapeutic purposes, device-associated infections as well as device-associated hospital infections have been a critical concern for many years (**Figure 1.1**).[5-8] Contamination of a medical device usually occurs by inoculation with only a few microorganisms from the skin or mucous membranes of the patient during implantation. In addition, the presence of pathogens could be due to in-hospital contamination since they are usually acquired from the hands of the surgical or clinical staff. The World Healthcare Organization (WHO) defines HAI as: "An infection

occurring in a patient during the process of care in a health-care facility which was not present or incubating at the time of admission. This includes infections acquired in the hospital but appearing after discharge, and also occupational infections among clinical staff."[9-11] Between 5 and 10% of patients admitted to acute-care hospitals usually acquire one or more infections.[7]

HAIs are worldwide acknowledged as the most frequent adverse event in health care. The impact of HAIs includes prolonged hospital stays and associated health care costs, massive financial burden on the health care systems, long-term disability and increased resistance to antimicrobial agents.[9,12] For instance, HAIs affect approximately 2 million patients each year in the United States (US), result in up to 100,000 excess deaths, and lead to an estimated cost to the U.S. health care system of more than $35 billion per year.[7,8] Thus, infection control is critical for patient safety and there exists an urgent need for innovative studies to develop infection prevention strategies in the clinical setting.

1.1.1. Infections Associated with Medical Devices: Clinical Impact and Implications for Patient Safety

At the global level, clinical reports estimate that at least 50% of HAIs are device-related.[6] There are four types of infections which account for more than 80% of the HAIs: urinary catheter infections (mostly catheter-associated), surgical site infections, bloodstream infections (mostly associated with the use of an intravascular device), and

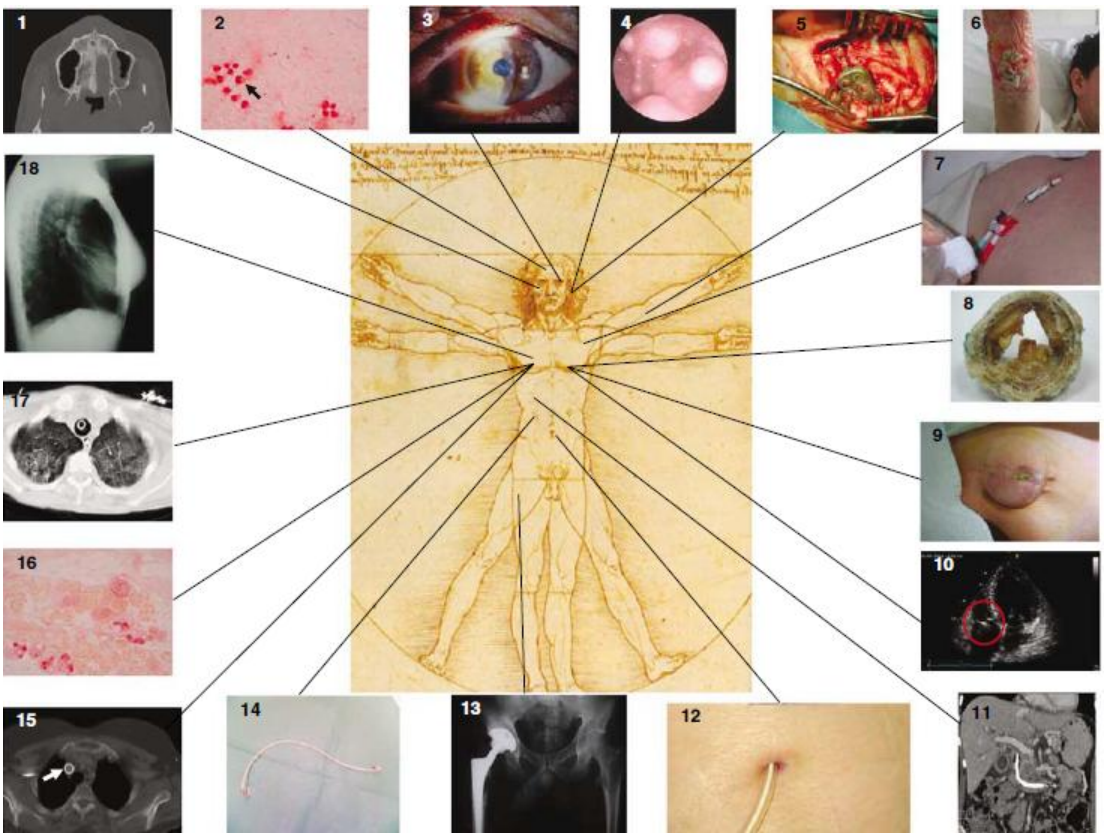

Figure 1.1. Diversity of biofilm-associated infections. (1) Computed tomography scan showing chronic sinusitis. (2) Central nervous system shunt infection. (black arrow indicates a gram-positive cocci in the cerebrospinal fluid). (3) Contact lens-associated keratitis. (4) Chronic otitis media. (5) Cochlear implant infection. (6) Burn-related infection. (7) Intravascular catheter infection (a Hickman type catheter is shown). (8) Prosthetic valve endocarditis. (9) Pacemaker infection. (10) Electrophysiological wire endocarditis (vegetation shown in circle). (11) Biliary stent infection. (12) Peritoneal dialysis catheter infection. (13) Prosthetic joint infection. (14) Urinary stent infection. (15) Intravascular stent infection (superior vena cava stent marked with white arrow). (16) Pulmonary infection in cystic fibrosis patient. Gram stain showing Gram-negative bacilli encased in an alginate matrix. (17) Ventilator associated pneumonia. (18) Breast implant infection.[13,14]

80%, 37% and 21% for urinary tract infections, bloodstream infections and pneumonia, respectively.[15] In addition, 25% of all medical device-related infections involve patients with pneumonia (mostly ventilator-associated pneumonia). Also, 70% of device-related infections in intensive care units (ICUs) are due to microorganisms that are resistant to one or more antibiotics.[4]

Catheters are widely used in hospitals for a number of applications, such as liquid drainage-injection and instrument access. [15] Patients have one or more vascular catheters in place during their hospital stay. In addition, 15 million central venous catheter (CVC) days occur in ICUs each year.[4,16] Despite their frequent use, bacterial infection is a major problem for catheters. Bacteria infect approximately 54% of all catheters which could lead to serious complications for the patient. Mortality rate of catheter-associated infections varies from 12% to 25%.[15] In addition, catheter-associated urinary-tract infections (CAUTI) are the most common type of HAI, which affect 1 million patients in acute- and extended-care settings. Moreover, 3 million CVCs are used annually in the U.S. and 3% to 7% of the time, an infection occurs. This also might result in bloodstream infections (BSI). For instance, CVCs resulting in bloodstream infections occur in about 4-5 out of every 1000 CVCs inserted[17,18] with an attributed cost per infection estimated at $34,508–$56,000.[19,20] In addition, CVC-associated BSIs are associated with a mortality rate of up to 11.5% and additional hospital stay length of 9-12 days.[21] Thus, the total annual cost of caring for patients with CVC-associated BSIs ranges from $296 million to $2.3 billion.[16]

Ventilator-associated pneumonia (VAP), an infection in the lung of the patients who undergo mechanical ventilation, is associated with much higher mortality and costs.[7] The mortality rates are reported to be in the range of 24-50% and reach as high as 73% when lung infection is caused by high-risk pathogens such as *Pseudomonas* and *Acinetobacter* species.[22] Moreover, it has been indicated that a positive diagnosis of VAP can increase hospital costs by $40,000 in mean charges per patient ($104,983 ± $91,080 costs when VAP occurs vs. $63,689 ± $75,030 costs when VAP does not occur during mechanical ventilation).[23,24] Prolonged endotracheal intubation is one of the greatest risk factors for VAP. During the ventilation process, patients incapable of breathing are intubated with polyvinyl chloride (PVC) endotracheal tubes (ETTs). PVC ETTs provide surfaces where bacteria can attach and proliferate from the contaminated oropharyngeal space to the sterile bronchoalveolar area.[22,23,25,26] Many studies have shown that the pathogenesis of VAP is associated with the colonization of the aerodigestive tract with pathogenic bacteria and aspiration of contaminated secretions.[24,27] These complications result in significant patient morbidity and mortality. For example, colonization of ETTs and the upper respiratory tract by *P. aeruginosa* precedes over 90% of VAP cases, 40% of which are fatal, despite antibiotic therapy. Moreover, the risk of VAP increases by 3% per day during the first five days of mechanical ventilation and by 2% between days five and ten.[25,28-31] Hence, there exists an unmet clinical need to create antibacterial surfaces that resist biofilm formation to reduce the risk of infection.[26]

1.1.2. Current Strategies to Limit Medical Device Infections

There are three main strategies to limit biomedical device-related infections in the clinical settings. These can be listed as: to prevent the infection (or the formation of the biofilms), to treat the infection through surgery, and/or to use drugs to limit the spread of the infection. A summary of these strategies are listed in **Table 1.1.**

Table 1.1. Conventional Strategies to Limit Medical Device Infections in Healthcare Settings

Strategy	Method	Disadvantages
Prevention	Sterilization of medical device surfaces	Inefficient to remove all sources of contamination from health personnel's hands, the patient's skin, and other surfaces
Prevention	Antibacterial coatings	Limited lifetime, might decrease device performance, toxic
Surgery	Removal of the medical device and washing of the infected area	Extra healthcare cost, impaired mobility, device might fail
Surgery	Retention	Only useful for early stages of bloodstream infections
Drugs	I.V. or oral antibiotics	Poor targeting to the infection site, antibacterial resistance

The first step for prevention of infection is the sterilization of the medical device surfaces. Common sterilization methods include ethylene gas (EtO) sterilization, autoclaving, hydrogen peroxide gas plasma as well as using chemical disinfectants.[32] However, hospital environment is a constant source of bacteria: microorganisms can

originate from patient's own skin microflora, exogenous microflora from the healthcare personnel, or from the contaminated infusates. [5] There is no conventional technology to detect and remove all sources of contamination from areas such as hospital beds, health workers hands, the patient's skin, and other surfaces before and during a clinical operation (or intubation).

Medical device surfaces can be coated to release antibacterial agents to further prevent infections. For example, nitric oxide releasing coatings have been developed to reduce the surface adhesion of gram-negative and gram-positive pathogens.[33] Moreover, metallic silver has been coated on catheters and orthopedic fixation pins. Although the adhesion and biofilm formation on catheters were significantly reduced *in vitro*, there was no significant decrease in bacterial adhesion in *in vivo* studies.[33,34] The major problems with medical device coatings include the decreased mechanical stability and delamination of coatings. In addition, coatings have a limited lifetime due to their delamination *in vivo*. The performance of implanted medical devices is also decreased due to reduced mammalian cell adhesion and tissue integration near the device.[35] Thus, medical device coatings are only temporary solutions to limit infections, especially for devices that are exposed to bacteria continuously (such as with catheters or endotracheal tubes, where the coating may only delay the onset of infection).

Once the device is infected, the standard treatment is the removal of the infected device when possible and its replacement with combined antibiotic therapy.[4] If the patient shows signs of severe sepsis and septic shock, removal of the device is

recommended.[4] The standard clinical procedure usually involves the washout of the infected area which contains the sticky biofilm and then removal of the device which is followed by immediate antibiotic treatment.[36] However, these procedures are expensive and create an extra cost to the patient and might result in decreased life quality. [37]

Retention of devices (or the removal of infected tissue) and antibacterial therapy is more recently considered as a favorable procedure in terms of ease of surgery, time, and cost-effectiveness.[36] However, adverse events have been observed with the use of local antibiotics. For example, events of acute renal failure and ototoxicity after combined local and systemic antibiotic treatments have been reported.[37] Moreover, another serious consideration is to consequently select and favor the emergence of antibiotic-resistant strains during the antibiotic therapy. For instance, gentamicin-loaded bone cements caused the emergence and recovery of a gentamicin-resistant staphylococcal strain after 5 years *in situ*.[37,38] Other problems with antibiotic treatments, especially through oral or intravenous routes, include the formation of an immune-incompetent zone (fibrous capsule formation), poor availability of drugs at the site of infection, and the increased biofilm formation. [39,40]

1.2. Clinical Problem: Biofilm Formation

In 1933, Arthur T. Henrici first described a biofilm with these words: ‘‘… it is quite evident that for the most part water bacteria are not free floating organisms, but grow upon submerged surfaces’’.[13,41,42] Today, biofilms can simply be defined as communities of microorganisms that are adherent to a biotic or abiotic surface.[41,43] These are complex heterogeneous communities embedded in an extracellular polymeric substance (EPS) matrix, which is composed of polysaccharides, nucleic acids, proteins and lipids.[44,45] Biofilm formation appears early in fossil records (~3.25 billion years ago), particularly in hydrothermal environments.[43] For instance, biofilm microcolonies have been identified in the ~3.4-billion-year-old South African Kornberg formation[43,46] as well as in the 3.2-billion-year-old deep-sea hydrothermal rocks of Pilbara Craton, Australia.[43,47] In modern hydrothermal environments, similar biofilm structures can be found in hot springs and deep-sea vents. Thus, biofilm formation is an ancient and a key component of bacterial survival mechanisms from diverse environmental conditions.

Device-related infections were the first clinical infections to be identified as having a biofilm etiology.[43] The surfaces of invasive medical devices serve as substrates for bacterial attachment, growth, colonization and biofilm formation (Figure 1.2).[48] Host inflammatory responses also can facilitate the formation of biofilms as the inflammatory proteins (i.e. fibronectin, fibrinogen) facilitate bacteria adhesion to the device surface.[43] In today’s healthcare environment, clinical data estimates that more than 65% of all bacterial infections are due to biofilm-forming bacteria (**Figure 1.1**). For instance, infection rates are approximately 2% for joint prostheses, 2% for breast implants, 4% for

mechanical heart valves, 4% for pacemakers and defibrillators, 10% for ventricular shunts, and 40% for ventricular-assisted devices.[13] **Table 1.2** lists some of the common biofilm-associated infections and mostly isolated microorganisms from these infection sites. Bacterial species that are commensal with the human body such as *Staphylococcus epidermidis* as well as bacteria commonly found in aquatic environments such as *Pseudomonas aeruginosa* comprises more than 50% of the biofilm-associated infections. Bacteria commonly isolated from these devices include gram-positive *Enterococcus faecalis, Staphylococcus aureus,* and *Streptococcus viridians* as well as gram-negative *Escherichia coli, Klebsiella pneumonia* and *Proteus mirabilis*.[5] Moreover, biofilm infections may be caused by a mixture of species of bacteria or fungi (i.e., *Candida albicans*).

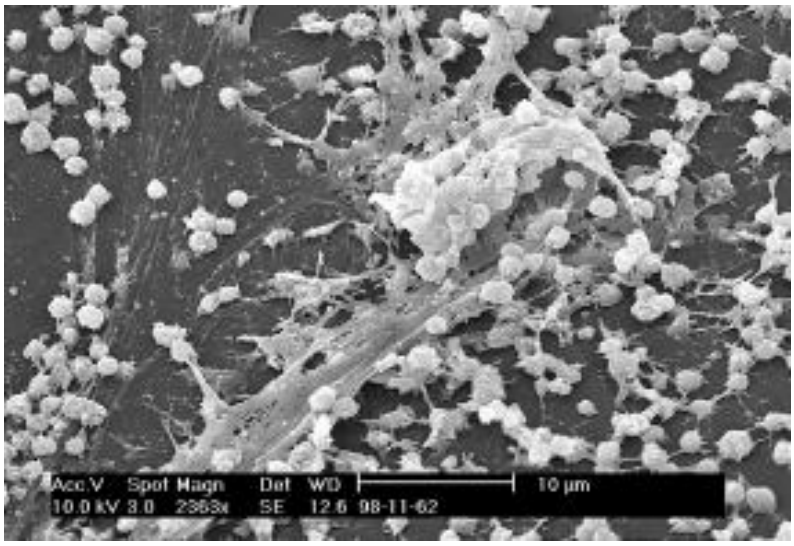

Figure 1.2. Scanning electron microscopy analysis of a *Staphylococcus* biofilm on the inner surface of a needleless connector. Exopolysaccharide (EPS) matrix of the biofilm appears either as thin strands connecting the cells to the surface and one another or as sheets of amorphous material on a surface. [5]

Table 1.2. Some common biofilm-associated infections and commonly isolated microorganisms [49]

Infection/Disease	Commonly Isolated Microorganisms
HAI-related (nosocomial) infections	
Sutures	*S. epidermidis* and *S. aureus*
Catheter-exit sites	*S. epidermidis* and *S. aureus*
Urinary catheter cystitis	*S. epidermidis, E. coli, Enterococcus faecalis, Proteus mirabilis, P. aeruginosa* and *K. pneumoniae*
Central venous catheters	*S. epidermidis, S. aureus, Candida albicans, P. aeruginosa, K. pneumoniae* and *Enterococcus faecalis*
Peritoneal-dialysis (CAPD) peritonitis	Various bacteria and fungi
Endotracheal tubes	*P. aeruginosa, S. epidermidis, S. aureus, H. influenzae, S. pneumoniae, Acinetobacter* species and *Klebsiella* spp
Mechanical heart valves	*S. epidermidis, S. aureus* and *C. albicans*
Orthopedic devices	*S. epidermidis* and *S. aureus*
Vascular grafts	Gram-positive cocci
Hickman catheters	*S. epidermidis* and *C. albicans*
Cystic fibrosis pneumonia	*P. aeruginosa* and *Burkolderia cepacia*
Musculoskeletal infections	Gram-positive cocci
Periodontitis	Gram-negative anaerobic oral bacteria
Dental caries	Acidogenic gram-positive cocci

1.2.1. Pathogenesis of Biofilm Formation

The steps of biofilm formation on a medical device are summarized in **Figure 1.3**. Biofilms are a stable point in a biological cycle that includes initiation, maturation, maintenance, and dissolution. Biofilm formation is thought to begin when bacteria sense environmental conditions, such as nutrient availability and pH, which trigger the transition to life on a surface.[49] Bacteria undergo a transition from planktonic (free-floating cells to sessile (surface-attached) cells in response to environmental conditions. [49]

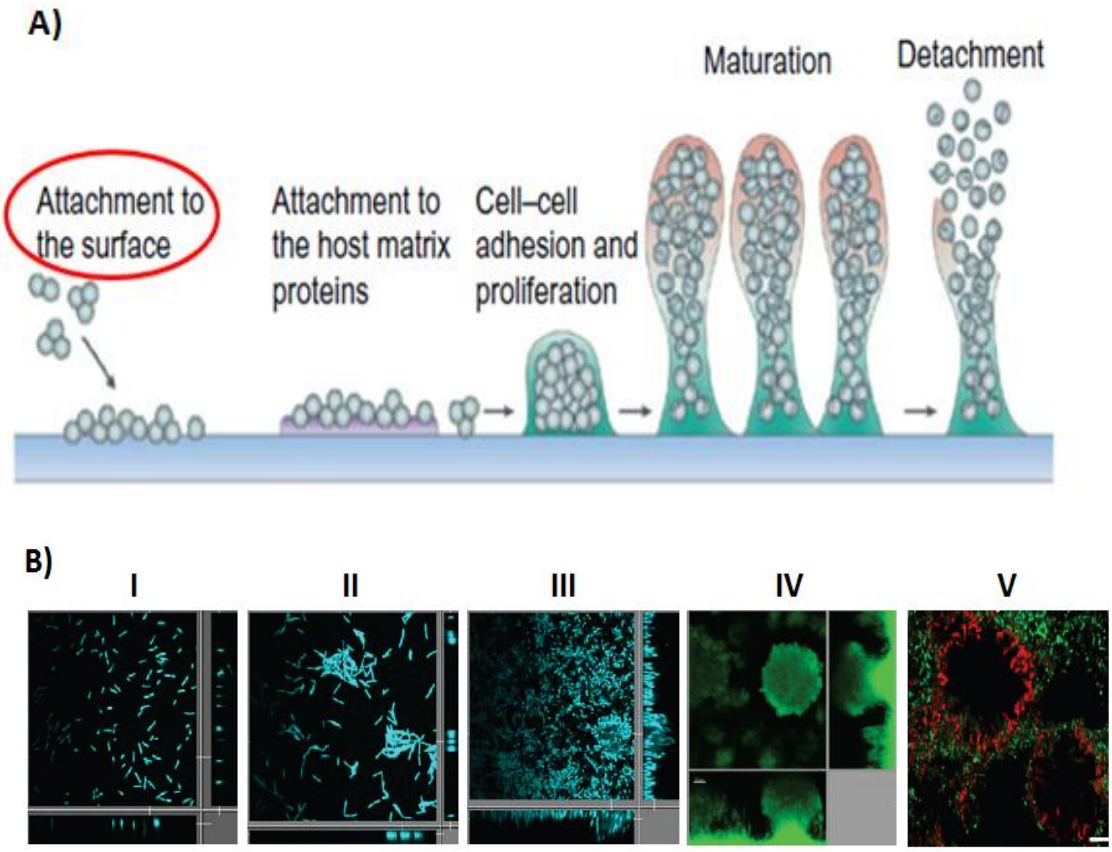

Figure 1.3. Pathogenesis of biofilm-associated infections. **A)** Initial step in biofilm formation is bacterial adhesion and attachment to the device surface. After adhesion, production of a biofilm begins with bacterial secretion of polysaccharides and proteins. Biofilm development in the colony is then controlled through the release of detergent-like peptides and proteolytic activity in exposed layers which can also mediate the spreading of infection to new locations.[50] **B)** Confocal microscopy analysis of the each stage of biofilm formation. I-III represents *P. aeruginosa* stained with DAPI, IV represents *S. aureus* stained with chromosomal green fluorescent protein (GFP), and V represents *S. aureus* stained with Live/Dead assay. [11,12]

Recent proteomic studies have indicated that biofilm formation (i.e., the formation of *P. aeruginosa* biofilms) proceeds as a regulated sequence of five developmental stages.[43,51,52] Stages one and two are generally identified by a loose or transient association with the surface, followed by robust adhesion. Stages three and four include the aggregation of bacterial cells into microcolonies and subsequent growth and maturation. Stage five is characterized by a return to transient motility where *P. aeruginosa* biofilm cells are sloughed or shed. These developmental stages have been also identified in *E. coli* biofilms.[53] Moreover, same dynamic processes, such as moving over surfaces, growth cycles and detachment and reattachment, have been observed in non-motile species, such as *S. epidermidis*[14] and *S. aureus* [43].

The crucial step for biofim formation relies on the ability of the microorganism to attach to the material surface. Attachment depends on bacterial cell surface characteristics as well as the material characteristics. The mechanism of bacterial adhesion is a complex process which includes the initial instantaneous and reversible physical phase which is followed by a time-dependent and irreversible molecular and cellular phase, all driven by physiochemical forces as well as cellular and molecular interactions. Bacterial adhesion takes place due to the initial attraction of cells to the polymer surface followed by adsorption and attachment. Bacteria move to the material surface due to physical forces and chemical factors, such as polarity, surface electrostatic forces, gravitational forces, surface tension, London-van der Waal's forces, Brownian motion and hydrophobic forces.[4,54-56] Physical interactions can be further defined as long-range (>50 nm) and short-range (< 5 nm) interactions. Long-range interactions are non-specific forces that are

dominant when the bacteria are first interact with the material surface. They act as a function of the distance (between the cell and the material) and surface energy. Then, the short-range interactions become more dominant at closer proximity due to hydrogen bonds, ionic and dipole-dipole interactions.[55,56] Molecular and cellular factors also play a crucial role in the bacterial attachment and proliferation of the biofilm. Different species use different cell-cell signaling molecules to proliferate and colonize on the device surface. For example, *S. epidermidis* has specific polysaccharide adhesion molecules, including the surface-associated autolysin, atlE, and the capsular polysaccharide intercellular adhesin (PSA).[57] Biofilm-associated protein Bap is involved in the adhesion and cell proliferation of *S. aureus* biofilms.[4] Moreover, polysaccharide/adhesin (PS/A) is involved in initial adhesion and slime production.[58] In later stages of adhesion, implanted medical devices becomes rapidly coated with host plasma and connective tissue proteins, including fibronectin, fibrinogen, vitronectin, laminin, and collagen.[4,59] Adhesion of *S. aureus* is dependent on the presence of host-tissue ligands, i.e., fibronectin, fibrinogen, and collagen. *S. aureus* adheres to these ligands via microbial surface proteins, commonly referred to as "microbial surface components recognizing adhesive matrix molecules" (MSCRAMM). The most common and well-characterized MSCRAMM include fibronectin-binding proteins FnbpA and FnbpB.[4,60]

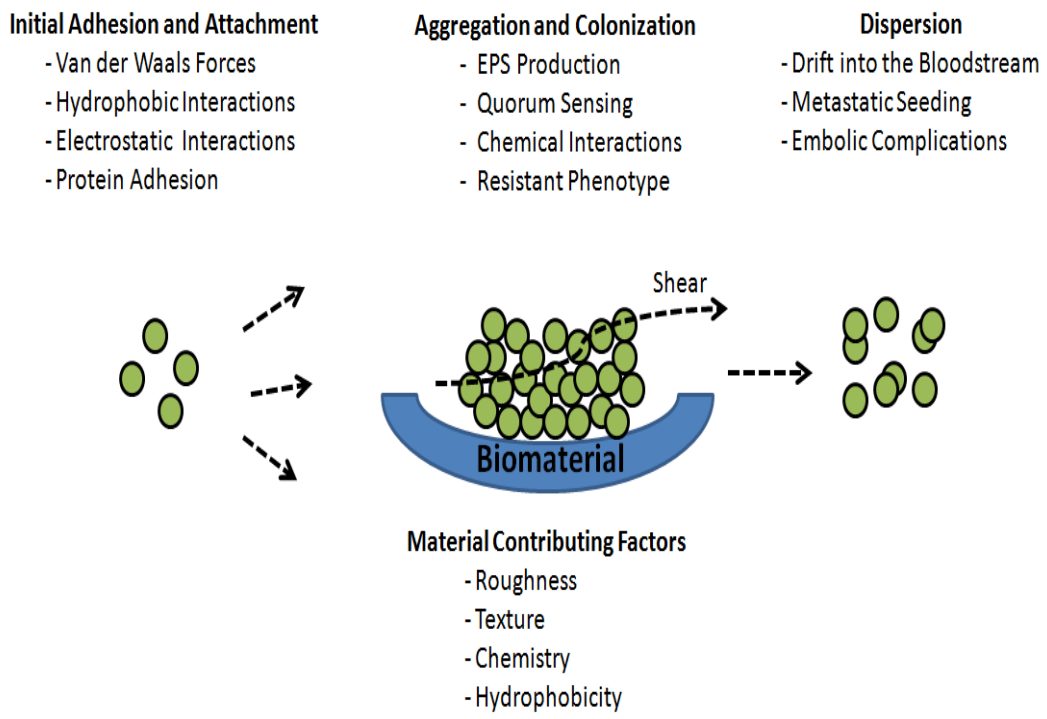

Figure 1.4. Summary of the factors contributing to the biofilm formation on biomaterial surfaces.[4] Rapid initial adhesion and attachment of bacteria is controlled by Van der Waals forces, hydrophobic and electrostatic interactions as well as protein adsorption on the biomaterial surface. Moreover, biomaterial surface roughness, texture, chemistry and hydrophobicity are among the contributing factors. Initial attachment and adhesion is followed by a more prolonged accumulation phase that involves cell proliferation and intercellular adhesion. Finally, micro-organisms may disaggregate from the macrocolonies and drift into the bloodstream resulting in metastatic and embolic complications.

1.2.2. Why Is It So Difficult to Eradicate Biofilms?

Biofilms growing in natural and industrial environments are resistant to bacteriophages and chemically diverse anti-biofouling agents used in the industrial processes.[45,49] Structure and gene expression significantly contributes to the survival of biofilm forming cells. Biofilms are both heterogeneous in both time and space. The basic structural unit of the biofilm is called a "microcolony". Bacteria themselves account for a variable fraction of the total biofilm volume (typically, 5-35%). Confocal microscopy analysis revealed that the rest of the biofilm consists of highly hydrated structures of 73-98% extracellular matrix material, open channels and void spaces.[56] For instance, the solid component of the *S. aureus* glycocalyx or slime layer is composed of teichoic acids (80%), bacterial and host proteins.[61] The nutrients can circulate through the open channels to the all layers within the biofilm.[49,62] This preserves the viability of the bacteria and their proliferation capacity. In addition, there are gradients of oxygen, nutrients and electron acceptors throughout the biofilm due to its heterogeneous structure. This also leads to different gene expression in different regions of a biofilm. Varying expression patterns were demonstrated on a cell-cell basis for multiple cell wall-associated proteins throughout the cell clusters within the biofilm.[61,63] Hence, sessile biofilm-forming bacteria can withstand host immune responses and become much less susceptible to antibiotics than their individual planktonic counterparts.[43,49,63] It is hypothesized that biofilms evade antimicrobial challenges by multiple mechanisms as discussed below.

1) Restricted or Slow Penetration

One of the main hypotheses for biofilm resistance is the restricted penetration or failure of an antimicrobial agent to penetrate within the full depth of the biofilm. Polymeric materials within the EPS matrix are known to retard the diffusion of antibiotics. In addition, it has been shown that solutes diffuse at slower rates within biofilms than they do in water.[64] Mathematical models also predicted that a formidable penetration barrier would be established if the antimicrobial agent is deactivated in the outer layers of the biofilm faster than it diffuses.[49] On the other hand, there are several studies which showed that antibiotics can penetrate through the biofilms.[45,49] For example, fluoroquinolones (i.e., ciprofloxacin) rapidly diffuse deep into biofilms of *P. aeruginosa*[65] and *K. pneumoniae*.[13,66] In addition, Stone *et al.* developed a method to visualize biofilm cells in contact with tetracycline, which relied on the fact that tetracycline fluoresces when activated by a UV light source. It has been demonstrated that uropathogenic *E. coli* and K-12 strains of *E. coli* were permeable to tetracycline.[67] Vancomycin can also reach the inner layers of *S. epidermidis* biofilms.[68] The biofilm matrix is mostly water, therefore, antibiotics can diffuse through the matrix. However, restricted antibiotic penetration can occur if the antibiotic gets deactivated within the biofilm. For example, ampicillin can penetrate through the biofilm of a β-lactamase-negative strain but not the biofilm formed by the β-lactamase-positive wild type strain of *K. pneumonia*. In the wild type biofilm, ampicillin is deactivated in the surface layers more rapidly than it diffuses.[66,69] Moreover, restricted penetration occurs if antibiotics are adsorbed into the biofilm EPS matrix. Aminoglycosides (i.e., tobramycin) are positively charged antimicrobial agents. They bind to negatively charged exopolysaccharides within

the matrix. This functions as ion-exchange resins capable of binding to antibiotics and restricts aminoglycoside penetration.[13,69,70] All of these studies suggests that penetration is not directly correlated with susceptibility to the antibiotic[65] but it depends on the bacteria strain and the antibiotic used.[71]

2) Resistant Phenotype: Antimicrobial Destroying Enzymes and Gene Transfer

Biofilm research has established unique differences in the gene expression between planktonic and sessile bacteria which imply physiological alterations occur during biofilm formation. For example, Brözel *et al*. identified 11 proteins that had different expression levels during various stages of *P. aeruginosa* biofilm formation.[71,72] In another study, Whitely *et al.* identified 20 differentially expressed genes in *P. aeruginosa* biofilms compared with planktonic cells when cultures were exposed to high levels (5 μg/mL) of tobramycin.[73] In addition, biofilm-forming bacteria cells can upregulate their stress-response genes and switch to resistant phenotypes upon exposure to antibiotics.[13] Expression of chromosomally encoded β-lactamase in *P. aeruginosa* biofilms is upregulated after prolonged exposure to β-lactam antibiotics.[74] Ampicillin is also rapidly chelated and inactivated by β-lactamase enzymes within the *K. pneumoniae* biofilms.[66] Moreover, Mah *et. al.* identified a gene, *ndvB*, that is only expressed in *P. aeruginosa* biofilms for the synthesis of periplasmic glucans.[75] Glucans are hypothesized to physically interact with antibiotics (i.e., tobramycin) and slow or stop their diffusion from the periplasmic space to their site of action in the cytoplasm. An alternative hypothesis suggested that glucans may not entirely account for all of the antibiotic resistance of biofilm cells but may contribute to the resistance by slowing the diffusion of

antibiotics into the biofilm. This may allow bacteria additional time to adapt and become resistant to the antibiotic.[73,75]

Moreover, antibiotic resistance might be facilitated through the horizontal gene transfer (HGT) between neighboring cells within the biofilm.[13] The resistance is acquired by mutational change or by the acquisition of resistance-encoding genes that are transferred from another bacterial species. For example, antibiotic resistance of *Bacteroides* species, a predominant species in the human colon, has increased from about 30% to more than 80% of strains through the conjugal transfer of the tetracycline resistance gene, *tetQ*.[76] Quorum-sensing signaling systems synchronize target gene expression and coordinate biological activity within biofilms.[3] For example; N-acylhomoserine lactones are secreted by *P. aeruginosa* in deep regions of the biofilm. These quorum sensors interact with transcriptional activators to direct expression of several factors that facilitate bacterial persistence enabling *P. aeruginosa* to evade the effects of antimicrobial agents.[14]

3) Altered Cellular Microenvironment and Metabolism

According to the third main hypothesis, at least some of the cells in a biofilm experience nutrient limitation and therefore exist in a slow-growing or starved state.[49] **Figure 1.5** summarizes the four distinct metabolic states determined in an *in vitro* biofilm model: 1) aerobically growing cells (high metabolic activity), 2) fermentative cells (intermediate activity), 3) low metabolic activity and 4) dormant cells (including very slow growing or dead cells).[61,71] Metabolic activity in a biofilm cell cluster is a function

of depth within the biofilm and is influenced by nutrient transport. The cells exposed to the upper air oxygen-rich interface and lower liquid-nutrient rich interface are metabolically active.

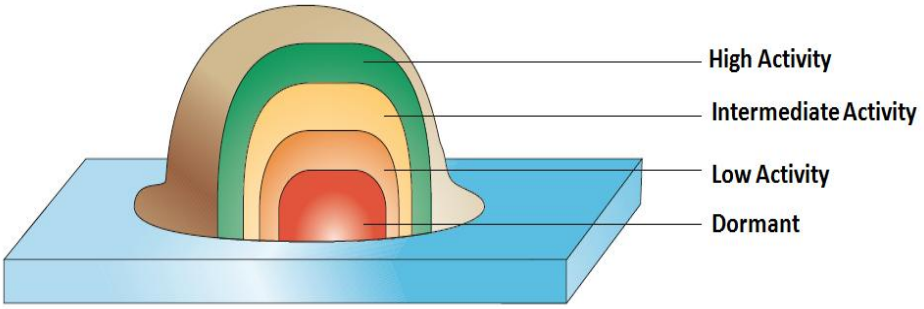

Figure 1.5. Distinct metabolic states within a biofilm structure. Metabolic activity is a function of depth within the biofilm and is influenced by nutrient transport. Cells at the edges at the bulk liquid interface are the most metabolically active. On the other hand, cells deep within the biofilm can potentially remain dormant, limit nutrient uptake and slow their growth. Thus, they are able to survive an antibiotic treatment.[71]

However, the majority of cells in a biofilm are dormant and located in an anoxic environment.[77] These slow growing or non-growing cells have a protected phenotype and they are not very susceptible to antimicrobial agents. These cells have been referred to as "persisters" and may be present in relatively high numbers in the deep biofilm.[61,77] **Figure 1.6** summarizes the model for biofilm drug resistance based on persister cell formation and survival.

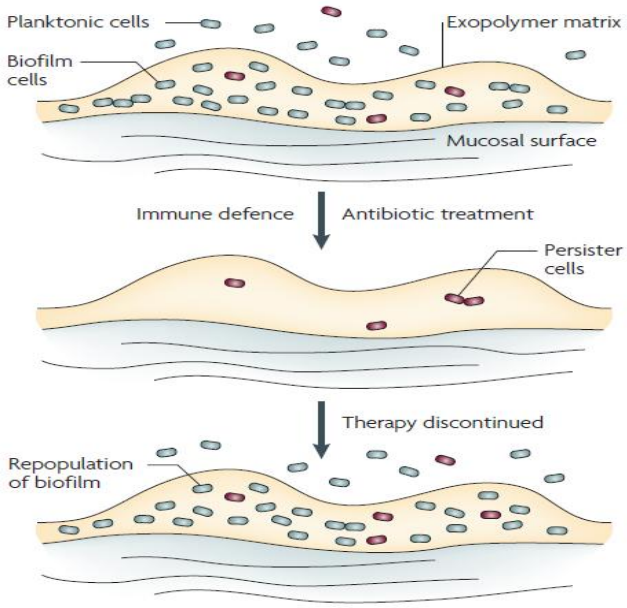

Figure 1.6. A model for biofilm drug resistance based on persister cell formation and survival. Initial treatment with antibiotic kills normal cells in both planktonic and biofilm populations. The host immune system kills planktonic persisters while persisters within the biofilm are protected by the EPS matrix. After the antibiotic therapy is discontinued, persisters resuscitate and repopulate the biofilm and the infection relapses.[78]

In 1944, for the first time, Lee *et. al.* showed the important role of growth rate on antibiotic activity.[79] They found that penicillin activity was impaired when bacteria grew slowly. The same phenomenon was observed for other antibiotics as well. For example, resting cells were fully resistant to ampicillin and tetracycline. In addition, although streptomycin and ciprofloxacin were still active against the cells in the stationary phase, their antibacterial activity was lower than that observed for exponentially growing bacteria. [80,81]

Altered biochemical microenvironments within the biofilm also contribute to increased resistance. Nutrient gradients and increased bacterial density through biofilm microcolonies result in waste accumulation and an altered microenvironment: low pH, low O_2 levels, high CO_2 levels, low divalent cation and pyrimidine concentration, and low hydration levels.[13] For example, low oxygen levels reduce the antimicrobial activity of aminoglycosides.[13,82] Also, although ciprofloxacin penetrated through the *P. aeruginosa* biofilm, it was only active against the cells in the regions with high O_2 levels and high metabolic activity.[66] These results indicated that oxygen limitation and low metabolic activity in the interior of the biofilm, not poor antibiotic penetration, are correlated with *P. aeruginosa* biofilm antibiotic resistance. Further, nutrient limitation within the biofilm layers plays a critical role. Anderl *et. al*. suggested that the antibiotic resistance could be explained by nutrient limitation within the biofilm leading at least some of the cells to a stationary phase. This mechanism was supported by experimental characterization of nutrient availability and growth status in *K. pneumoniae* biofilms. For example, the average growth rate of bacteria in biofilms was only 0.032/hour compared to the growth rate of planktonic bacteria of 0.59/hour measured in the same medium. Glucose did not reach to the deeper layers and oxygen penetrated only into the upper 100 μm. In addition, the catalase activity was elevated in biofilm bacteria to a level similar to that of stationary-phase planktonic cells. Transmission electron microscopy revealed that bacteria were affected by ampicillin near the periphery of the biofilm but were not affected in the interior. Taken together, all of these results indicated that nutrient limitation occurs locally within the biofilm, leading to zones in which the bacteria enter

the stationary phase and are growing slowly or not at all. In these inactive regions, bacteria are less susceptible to killing by antibiotics. [83]

In conclusion, formation of sessile biofilm communities provides a resistance mechanism against host immune responses and antibacterial agents.[49] **Figure 1.7** summarizes the three main hypotheses for antibiotic resistance of biofilms. The inherent resistance of biofilms on material surfaces and the lack of new antibacterial agents cause a real-world problem as many persistent and chronic bacterial infections occur in the medical and industrial settings. Therefore, there is an urgent clinical need for novel alternative treatment strategies to eradicate these persister infections.

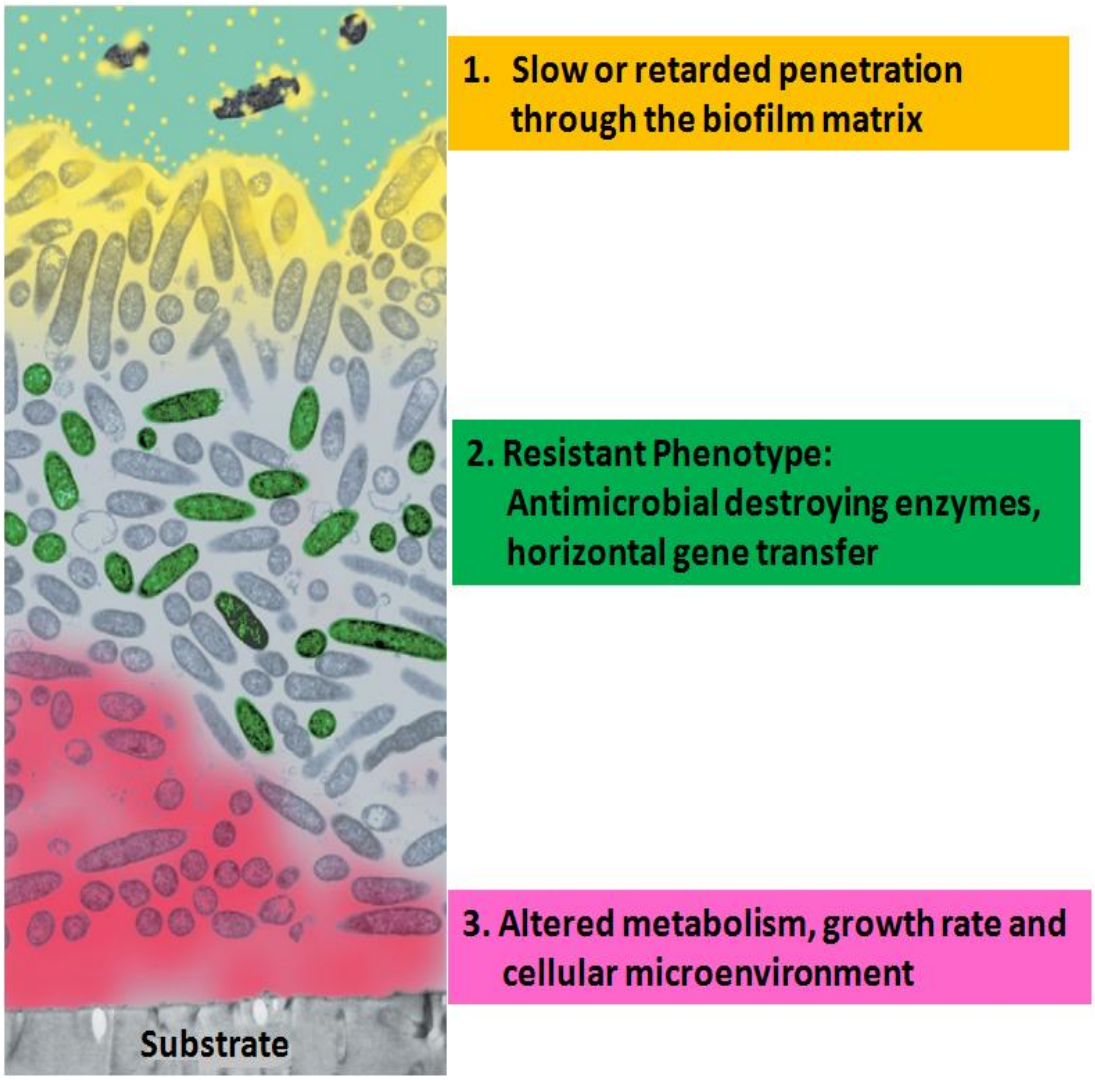

Figure 1.7. Three main hypotheses for mechanisms of antibiotic resistance in biofilms.[69] Biofilms restrict the antibiotic intake or penetration through the matrix. In addition, they develop resistant phenotypes with their antibacterial agent destroying enzymes. Horizontal gene transfer between the resistant bacteria also contributes. Moreover, they alter their growth rate, metabolism and cellular microenvironment, which also contribute to the inhibition of antibiotic penetration through the biofilm.

1.3. The Emerging Nanomedicine Landscape

1.3.1. The Promise of Nanotechnology and Nanoscale Materials

Nanotechnology is defined as the “the design, characterization, production and application of structures, devices and systems by controlling the shape and size at the nanoscale (<100 nm)”. The seminal concepts of nanotechnology were first mentioned in "There's Plenty of Room at the Bottom," a talk given by Nobel laureate Richard Feynman at an American Physical Society meeting at Caltech on December 29, 1959. Although he did not mention the term “nano”, Feynman described a process that builds molecular machines with “atomic precision”, using one set of precise tools to build and operate another proportionally smaller set, so on down to the needed scale. In 1974, the term ‘‘nanotechnology’’ was first used in Norio Taniguchi’s paper. Ever since, the role of nanotechnology and the various applications of controlling material properties at the nanoscale (1 nm = 10^{-9} m) were investigated.

There has been a growing interest in using nanomaterials, materials with basic structural units, grains, particles, fibers or other constituent components smaller than 100 nm in at least one dimension, for various applications in medicine, such as tissue regeneration, disease and infection prevention, diagnosis, and treatment.[84] Due to their dramatically increased surface area, surface roughness and surface area to volume ratio, nanomaterials possess unique properties such as enhanced magnetic, catalytic, optical, electrical, and mechanical properties which do not exist at other length scales.[15,84-86] Moreover, most of the cellular events within biological systems occur at the nanometer scale. The size of proteins and inorganic materials within the extracellular matrix of a

eukaryotic cell are in a range from several nanometers to a few hundred nanometers. For example, the osteoblast (bone-forming) extracellular matrix consists of inorganic hydroxyapatite crystals which are 50 nm in length and 2-5 nm in width. In addition, type I collagen fibers, which have fibrils of 300 nm in length, 0.5 nm in width and a periodicity of 67 nm, are the main organic component.[15] Since the nanostructured materials are the same length scale as native tissues, they can be used to develop biomimetic materials. Thus, nanomaterials have been extensively investigated for various biomedical applications such as tissue engineering scaffolds, novel tissue substitutes, *in vitro* diagnostics sensors, controlled drug delivery systems and contrast agents for *in vivo* imaging with a significantly improved performance (**Figure 1.8**).[87]

For instance, carbon nanotubes (CNTs) exhibit exceptional mechanical strength (i.e., Young's modulus strength of more than 1 TPa tensile strengths of up to 63 GPa) resulting from covalent sp2 bonds and tunable electrical properties.[15] Thus, the use of CNTs as conductive neural biomaterials, in situ sensors, drug delivery vehicles, or tissue engineering scaffolds has been investigated.[86,87] In addition, quantum dots (QDs) exhibit unique optical properties due to the quantum confinement effect which makes their energy levels quantized with values directly related to their size.[88] Compared with traditional organic fluorophores used for diagnostic and imaging applications, QDs exhibit superior properties, such as higher levels of fluorescence brightness (~10 to 20 times brighter)[89], large absorption coefficients across a wide spectral range of excitation[88,90] as well as high resistance to photo bleaching.[15,91] Indeed, QDs are several thousand times more photostable than the conventional organic dyes such as Texas Red.[91]

Hence, QDs are highly desirable for long-term 3D imaging or cell tracking studies. In addition, titanium (Ti) and its alloys have been widely used as implant materials for orthopedic applications due to their excellent wear, corrosion resistance, light weight but strong mechanical and acceptable biocompatibility properties.[35] Various methods have been applied to create nanostructured titanium surfaces. For example, nanotubular morphologies (with diameters less than 100 nm) can be synthesized on conventional Ti surfaces through anodization and the diameter of TiO_2 nanotubes can be controlled by adjusting reaction parameters such as electrolyte type and concentration, voltage, duration, and temperature.[35,92,93] Nanostructured Ti has been mostly explored for implant orthopedic applications[35], offering increased bone-forming cell attachment, growth and proliferation[94,95], control over stem cell differentiation[96], better osseointegration and decreased inflammation[97-99] as well as decreased bacterial attachment[100-103]. Moreover, magnetic particles, i.e. superparamagnetic iron oxide particles (SPION), have been used in magnetic resonance imaging (MRI) as contrast agents[104], drug delivery[105], stem cell tracking[106], assembly of 3D tissue constructs[107,108], magnetic separation (e.g., protein separation) and ultrasensitive diagnostic assays[109].

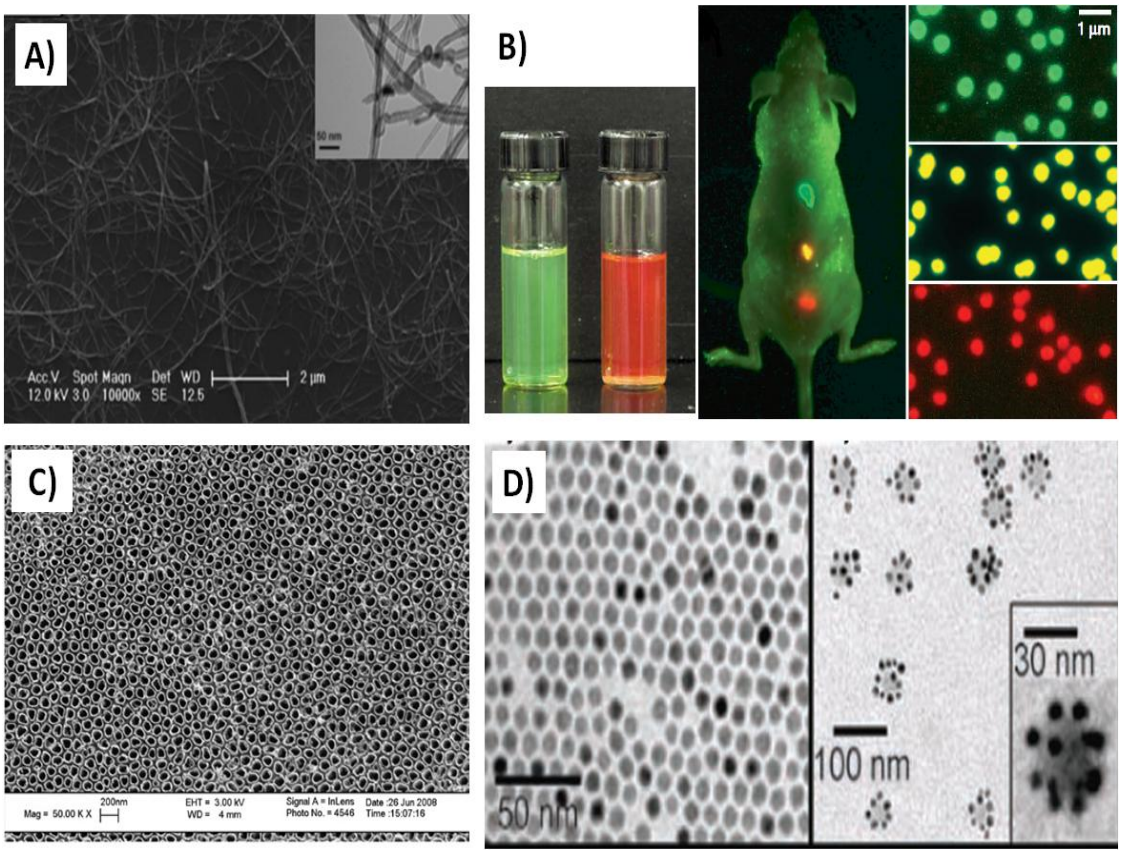

Figure 1.8. The use of nanomaterials is a growing new approach to the design of medical devices that have improved resistance to biofilm-mediated, drug-resistant, and device centered infections. For these anti-infection applications, various nanomaterials are being developed, such as nanoparticles and nanotubes, for direct use as biomedical devices; such nanomaterials can be used alone, incorporated onto surfaces, into composites, or as components in sensors such as zinc oxide (ZnO) nanoparticles, carbon nanotubes, titanium dioxide nanotube arrays, and silver nanoparticle-polymer composites, respectively in A-D. (Figures A[110], B.[89,91],C.[103] D. [111] are from citations listed). These examples and others will be further reviewed here briefly to understand their antibacterial activity and potential applications.

1.3.2. Nanomaterials for Infection Control

As discussed earlier, antibiotic resistance and the emergence of multi-drug resistant strains has prompted the development of alternative strategies to treat bacterial diseases. Among them, nanomaterials have emerged as novel antimicrobial agents. Especially, antibacterial nanoparticles (NPs) which consist of metals and metal oxides (i.e., silver nanoparticles, zinc oxide nanoparticles, titanium nanoparticles), naturally occurring antibacterial substances (i.e., antibacterial peptides, chitosan), carbon-based nanomaterials and nitric-oxide (NO) releasing nanoparticles have been explored in detail and their potential use for *in vitro* and *in vivo* infection control has been demonstrated.[112] Moreover, many recent studies have shown that changes in the surface features at the nanometer scale can interfere with bacterial functions.[23,26,113-119] Here, we will first review the antibacterial toxicity mechanisms and applications of nanoparticles. Then, some recent antibacterial material designs utilizing nanotechnology to inhibit medical device-related infections will be reviewed.

1.3.2.1. Antibacterial Nanoparticles

Antibacterial nanoparticles consist of nanophase materials with intrinsic bactericidal properties such as metal and metallic oxide nanoparticles, carbon nanotubes and fullerenes, naturally occurring antimicrobial peptides and chitosan.[15,112,120-122] There are also nanomaterials that act as drug carrier for antibacterial agents such as nitric oxide (NO) and antibiotics. High surface area to volume ratios and unique chemico-physical properties of these NPs are believed to contribute to their antimicrobial activities. Among various types of NPs, superparamagnetic iron oxide NPs (SPION) with different surface

coatings (i.e., gold and silver) show highest antibacterial activity against biofilms. These magnetic NPs also have the capability to better penetrate into biofilm in the presence of an external magnetic field.[120,123-125] In addition, nanoparticle chemistry, size, shape as well as zeta potential are among the most relevant properties affecting antibacterial activity. These distinctive nanoparticles can directly interact with the bacteria cells, disrupt and penetrate through the cell wall/membrane, interrupt transmembrane electron transfer. Moreover, they can produce secondary products, i.e. reactive oxygen species (ROS), or release ions that cause damage to the cellular components such as proteins and DNA.

1.3.2.1.1. Antimicrobial Peptides and Chitosan

Naturally occurring chitin and certain peptides have been long recognized for their wide-spectrum antimicrobial properties. Chitosan is a partially deacetylated chitin and is a high-molecular-weight linear polycationic heteropolysaccharide; comprising of β-1,4-linked D-glucosamine and *N*-acetyl-D-glucosamine.[15,112,126,127] It is commercially extracted from shrimp and crab shells.[127] Due to its unique polycationic nature, chitosan has a wide-range antibacterial activity against fungi, bacteria and viruses. In addition, chitosan exhibits higher antibacterial activity against Gram-positive bacteria than Gram-negative bacteria.[15] Interactions between the polycationic particle surface and the negatively-charged bacterial cell wall and cytoplasmic membranes might cause osmotic instability, membrane disruption, and leakage of intracellular elements.[127-129] Antibacterial activity depends on the type of chitosan, degree of polymerization, molecular weight and solvent.[126] For example, low molecular weight chitosan is more

effective against gram-negative bacteria; i.e. *E. coli*, *K. pneumoniae* and *P. aeruginosa*, while the high molecular weight chitosan is more effective against the gram-positive bacteria; i.e. *S. aureus* and *S. epidermidis*. This could be due to the intrinsic differences in the cell wall structure of gram-negative and gram-positive bacteria.[130] Chitosan has been recently synthesized in the nanoparticle form. Qi *et. al*. synthesized chitosan nanoparticles based on the ionic gelation of chitosan with tripolyphosphate anions.

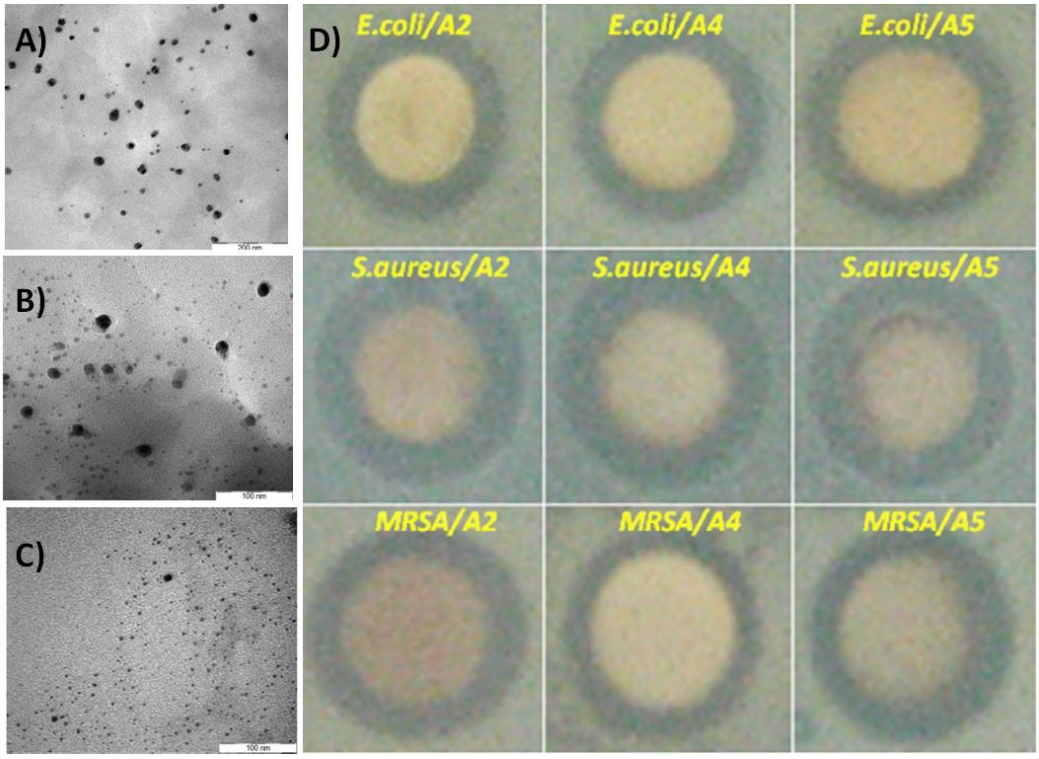

Figure 1.9. Characterization of silver (Ag)/montmorillonite (MMT)/chitosan (Ct) bio-nanocomposites. TEM characterization indicated that in particle size and their size distribution decreased as UV irradiation time increased from three hours to 96 hours (**A-C, respectively**). Nanocomposites exhibited strong antibacterial properties against both gram-negative (*E. coli*) and gram-positive (*S. aureus* and MRSA) bacteria (**D**).[131]

In addition, they synthesized copper-loaded chitosan nanoparticles by adsorbing copper ions onto the chitosan nanoparticles via ion-exchange resins and surface chelation to form copper-loaded nanoparticles.[132] Their antibacterial activities were tested against *E. coli*, *S. choleraesuis*, *S. typhimurium*, and *S. aureus*. Compared to conventional chitosan, both chitosan nanoparticles and copper-loaded chitosan nanoparticles exhibited stronger antibacterial properties. Their minimum inhibitory concentration (MIC) against *E. coli* and S. aureus was less than 0.25 μg/ml; whereas conventional chitosan had a MIC of 20 μg/ml against both bacteria.[133] Antibacterial properties of chitosan derivatives have been also characterized. For example, Shameli *et.al.* synthesized silver (Ag)/montmorillonite (MMT)/ chitosan (Ct) bionanocomposite films through UV-radiation.[131] Chitosan, montmorillonite (MMT), and $AgNO_3$ were used as the natural polymeric stabilizer, solid support, and silver precursor, respectively. Nanocomposites were synthesized under different UV irradiation times: one hour, three hours, 18 hours, 48 hours, and 96 hours, respectively. The increase in UV irradiation time caused a decrease in particle size and size distribution. According to the inhibition zone experiments, Ag/MMT/Ct nanocomposites showed strong antibacterial properties against both gram-negative (*E. coli*) and gram-positive (*S. aureus* and MRSA) bacteria (**Figure 1.9**).[131]

1.3.2.1.2. Silver (Ag) Nanoparticles

The antibacterial properties of silver have been known since the ancient times. It has been used in wound dressings, catheters, water disinfecting filters for bacterial infection control in the forms of metallic silver, silver nitrate, silver sulfadiazine and silver zeolite.[112,134,135] By manipulating their size at the nanoscale, antibacterial activities of

silver can be significantly increased. This is due to their high-surface area-to-volume ratio which results in increased reactivity. Ag nanoparticles exhibit wide-spectrum antibacterial activities against *S. aureus*, *S. epidermidis*, *E.coli*, *K. pneumoniae*, *B. subtilis*, *P. aeruginosa*, *Salmonella typhi* as well as MRSA, multidrug-resistant *P. aeruginosa*, ampicillin-resistant *E. coli* and erythromycin-resistant *S. pyogenes*.[136-142] It is also known that gram-positive bacteria are less susceptible to Ag nanoparticles than gram-negative bacteria, which is due to the differences in cell wall composition.[143] The gram-negative bacteria have a thin (~7–8 nm) layer of peptidoglycan, which is not rigid.

Negatively charged Ag nanoparticles might attack the gram-negative bacteria cell wall by metal depletion, as shown in the literature.[144] On the other hand, gram-positive bacteria have a thick (~20–80 nm) peptidoglycan layer, which forms a 3D rigid structure by cross linking of linear polysaccharide chains cross-linked by short peptides. Thus, the penetration of Ag nanoparticles through the rigid cell wall is low. Moreover, nanoparticle size and shape are among the other factors that influence their activity. Morones *et. al.* characterized the antibacterial effects of Ag nanoparticles of size 1-100 nm against *E. coli*. Nanoparticles smaller than 10 nm had the highest percentage of interactions with bacteria and showed the best antibacterial activity.[145] In another study, Panacek *et al.* synthesized size-controlled Ag nanoparticles ranging from 25-100 nm. The 25 nm particles showed the highest activity.[146] Thus, the antimicrobial activity of Ag NPs is inversely dependent on size. [112,134] In addition, Pal *et. al.* reported the effect of spherical, rod and triangular Ag nanoparticles against *E. coli*. Truncated triangular particles with a [134] lattice plane as the basal plane displayed the strongest bactericidal action, compared with spherical and rod-shaped nanoparticles or Ag^{+} ions. [147]

Ag particles can be coated on many different medical device surfaces or different materials to prevent biofilm formation. Roe *et. al.* formed a thin layer (~100 nm) of silver nanoparticles on catheter surfaces.[148] Sustained release of silver from the catheter surfaces significantly inhibited the *in vitro* and *in vivo* biofilm formation of *E. coli*, *Enterococcus*, *S. aureus*, coagulase-negative staphylococci, *P. aeruginosa* and *C. albicans* over a period of 10 days.[148] In addition, silicon nanowires (SiNWs) decorated with Ag nanoparticles (SiNW@Ag) showed strong antibacterial properties against *B. subtilis* and *E. coli*. The minimum inhibitory concentration (MIC) of SiNW@Ag was 1.1 µg/mL, while the MIC of Ag nanoparticles was 2.7 µg/mL.[149]

1.3.2.1.3 Zinc Oxide (ZnO) Nanoparticles

ZnO nanoparticles are highly attractive antibacterial agents due to their low cytotoxicity toward mammalian cells, low production cost, white appearance, and UV-blocking properties.[15,112] Similar to Ag nanoparticles, antibacterial properties also depend on the concentration and the size of particles. For example, Jones *et. al.* showed that smaller ZnO nanoparticles (8 nm) reduced 99% of *S. aureus* planktonic growth, whereas ultrafine ZnO powder (41 mm) and ZnO nanopowder (50-70 nm) reduced 50% of planktonic growth.[150] Antibacterial properties of ZnO nanoparticles can be improved by photoactivation. When nanoparticles were exposed to UV light at 254 nm for 30 minutes, a 40% increase in bacterial growth inhibition was observed, compared with the non-photoacvitated particles.[150] In addition, ultrasound stimulation can increase the activity of ZnO nanoparticle treatments against *S. aureus*. Seil *et. al.* showed that the addition of

ultrasound stimulation further reduced a 76% increase in antibacterial activity, compared to nanoparticles alone.[151]

1.3.2.1.4 Titanium Dioxide (TiO_2) Nanoparticles

TiO_2 nanoparticles unique particles and mostly studied for their photo-catalytic antimicrobial properties. TiO_2 nanoparticles exhibit very strong and wide-spectrum antimicrobial properties upon receiving irradiation with near-UV light and UVA against *E. coli*, *P. aeruginosa*, *S. aureus*, *Enterococcus faecium* and *C. albicans*.[112,152] In addition, photo activated TiO_2 nanoparticles can inactivate bacterial endospores (Bacillus cereus).[153] The MIC concentrations are in the range of 0.1–1 mg/mL.[154]

The bactericidal mechanism of TiO_2 is mainly related to the production of reactive oxygen species (ROS) in the presence of near-UV and UV-A irradiation. When in the presence of both oxygen and light, the primary ROS with antimicrobial activity generated by TiO_2 nanoparticles are hydroxyl radicals, superoxide, and hydrogen peroxide. Upon irradiation, an electron is transferred from the valence band to the conduction band, forming an electron (e_{cb}^-) – hole (h_{vb}^+) pair (Equation 1). The reactions of electrons (e_{cb}^-) and hole (h_{vb}^+) with water molecules on TiO_2 surfaces form hydroxyl radicals ($^{\cdot}OH$) and superoxide (O_2^-) (Equation 2 and 3). [15,155]

$$TiO_2 + h\nu \rightarrow (h_{vb}^+ + e_{cb}^-) \qquad \textbf{(Equation 1)}$$

$$h_{vb}^+ + H_20 \rightarrow {}^{\cdot}OH + H^+ \qquad \textbf{(Equation 2)}$$

$$e_{cb}^- + O_2 \rightarrow O_2^- \qquad \textbf{(Equation 3)}$$

These free radicals can then further react to product hydrogen peroxide (H_2O_2) (Equation 5 and 6) or through combination of the hydroxyl radicals produced from Equation 2 (as shown in Equation 7).

$O2^- + H^+ \rightarrow HO2^\cdot$ **(Equation 5)**

$HO2^\cdot + e^-H^+ \rightarrow H_2O_2$ **(Equation 6)**

$OH^\cdot + OH^\cdot \rightarrow H_2O_2$ **(Equation 7)**

Generation of ROS initially damages the bacterial cell membrane via oxidation and then impairs many crucial biological functions, such as respiration and oxidative phosphorylation reactions.[112] Antibacterial properties of TiO_2 nanoparticles can be improved by visible light or metal doping. Metal doping improves the visible light absorbance and increases its photocatalytic activity under UV irradiation.[156] Ag-doped TiO_2 nanoparticles reduced the reaction time required for complete removal time of *E. coli* (10^7 CFU/mL) from 65 minutes to 16 minutes in UVA light, by the silver surface plasmons which facilitate the electron–hole separation and provides more surface area for light adsorption.[157-159]

1.3.2.1.5. Nitric oxide (NO)-Releasing Nanoparticles

Nitric oxide has important functions in immune system reactions to microbes and has shown promising antibacterial properties in many studies. For example, macrophages and other inflammatory cells produce NO to battle foreign microbes.[160] In addition, gaseous NO has broad-spectrum antimicrobial properties against gram-positive and

gram-negative bacteria, nitrosating DNA, proteins as well as membrane-bound lipids due to the formation of peroxynitrite ($ONOO^-$) and dinitrogen trioxide (N_2O_3). MIC of gaseous nitrogen is 200 µg/mL. [161,162] On the other hand, it is extremely hard to deliver and target gaseous NO as an antibacterial agent. Recent studies have shown promising developments that nanoparticle-based scaffolds can store and deliver gaseous NO. For example, Hetrick *et. al.* synthesized NO-releasing silica nanoparticles via co-condensation of tetraalkoxysilane with aminoalkoxysilane modified with diazeniumdiolate NO donors. 400 µg/mL of NO-releasing silica nanoparticles killed 90% of viable *P. aeruginosa* after 2 hours of treatment, while 800 µg/mL nanoparticle treatment resulted in 100% bacterial cell death.[163] Antibacterial concentrations of NO-releasing silica nanoparticles were not toxic to the mammalian cells. NO-releasing particles were also found to be effective against Gram-negative (*E. coli*) and Gram-positive (*S. aureus*, *S. epidermidis* and MRSA) bacteria as well as fungi (*C. albicans*).[112]

1.3.2.1.6. Superparamagnetic Iron Oxide Nanoparticles (SPION)

The applications of small iron oxide particles in *in vitro* diagnostics have been practiced for nearly 50 years.[164] Especially, SPIONs are used in various biomedical applications such as magnetic resonance imaging (MRI) for contrast enhancement, drug delivery, stem cell tracking, heat source in magnetic fluid hyperthermia or magnetic separation technologies (e.g., rapid DNA sequencing) and ultrasensitive diagnostic assays.[165] Several types of iron oxide nanoparticles have been characterized. Magnetite (Fe_3O_4) or maghemite (γ-Fe_2O_3) are 5-20 nm in diameter and they are promising candidates for biomedical applications due to their high biocompatibility and ease of synthesis. For

example, some SPION, such as Ferumoxytol and Feridex, are FDA-approved and used in clinical studies as MRI contrast agents.[107] In addition, surfaces of SPION can be further functionalized with different bioactive molecules and tailor-made surface coatings, which give them further ability to deliver specific molecules.[164] Moreover, SPION are in a superparamagnetic state at room temperature. Their magnetization can be saturated under an external magnetic field, but in the absence of this field their net magnetic moments are often randomized to zero by thermal agitation. SPION are desirable for targeted and controlled delivery of drugs and therapeutic agents.[111] Thus, due to their unique properties, SPION hold great promise for many biomedical applications (**Figure 1.10**).

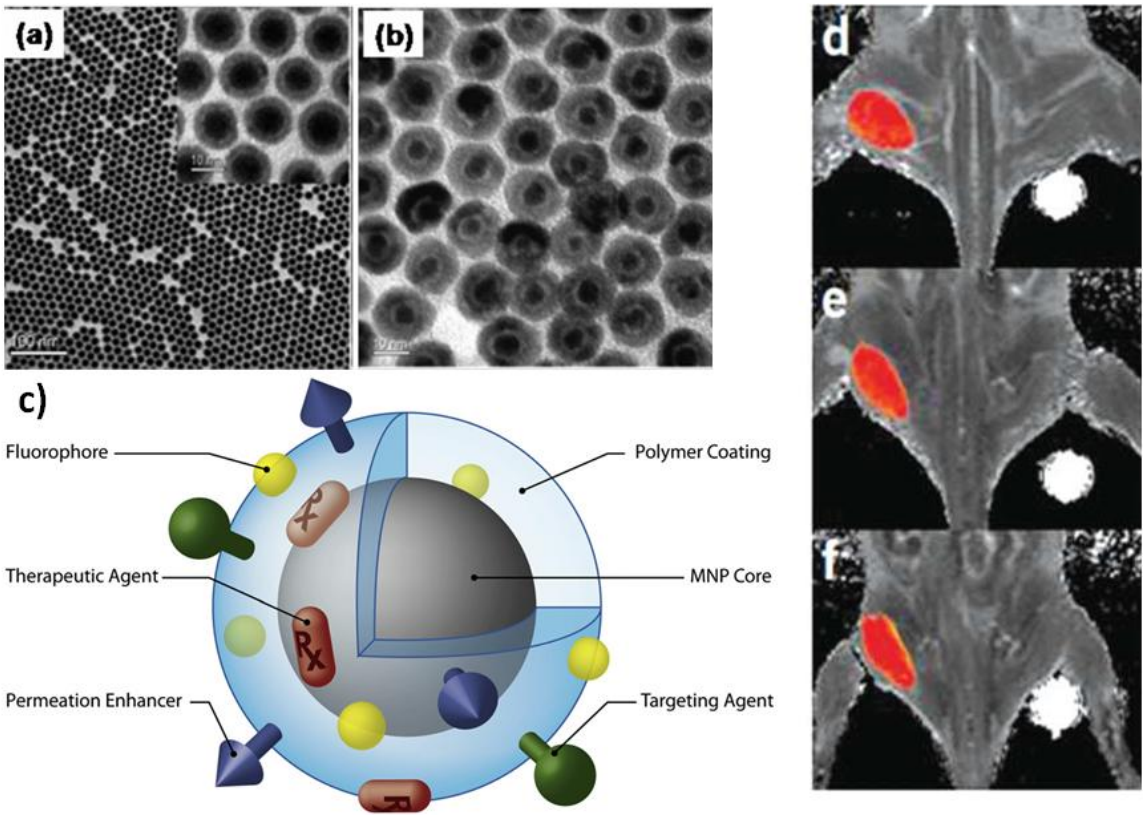

Figure 1.10. Biomedical applications of SPION. Representative TEM images of SPION with different sizes and chemical compositions: 8 nm/2.5 nm Fe/Fe3O4 nanoparticles (**a**) and 5 nm/5 nm Fe/Fe_3O_4 nanoparticles (**b**).[166] SPION can be engineered for control of the magnetic core size, along with a polymer coating, targeting agents, peptide fragments, drugs, and fluorescent markers for various biomedical applications (**c**).[167] For example, SPION are commonly used as image contrast agents in MRI due to their high biocompatibility (**d-f**).[168]

Although metal oxides have been extensively characterized for their antibacterial properties, little is known about the antibacterial activity of SPION. Tran *et. al*. synthesized SPION with an average size of 9 ± 4 nm.[169] These particles found to be antibacterial against *S. aureus*, shown by a decrease in the ratio of live to dead cells. 3 mg/mL SPION significantly inhibited *S. aureus* planktonic growth after 4, 12 and 24 hours. In another study, Taylor *et. al.* showed that 2 mg/mL SPION (average size = 8 nm) reduced *S. epidermidis* growth by 65% compared to untreated bacterial cells.[170] Azam *et. al.* investigated the activity of Fe_2O_3 nanoparticles against gram-negative (*E. coli* and *P. aeruginosa*) and gram-positive (*S. aureus* and *B. subtilis*) bacteria.[171] Minimum bactericidal concentrations were 65 ± 1.5 µg/mL, 120 ± 2.3 µg/mL, 80 ± 1.5 µg/mL, and 78 ± 1.4 µg/mL for *E. coli*, *P. aeruginosa, S. aureus* and *B. subtilis, respectively.* Fe_2O_3 nanoparticles were less antibacterial than ZnO nanoparticles. In addition, nanocomposites of iron and silver particles have been synthesized and characterized for their antibacterial and antifungal activities. For example, Prucek *et. al.* synthesized two types of magnetic composites: $Ag@Fe_3O_4$ and γ-$Fe_2O_3@Ag$.[172] Ag nanoparticles (~5 nm) were caught at the surfaces of Fe_3O_4 magnetic cores (~70 nm) to form $Ag@Fe_3O_4$. On the other hand, γ-$Fe_2O_3@Ag$ nanocomposites were composed of larger silver nanocores (~20-40 nm), which are surrounded by ultra small γ-Fe_2O_3 nanoparticles (~5 nm). Both nanocomposites exhibited very strong antibacterial and antifungal activities against clinical bacterial strains, such as *P. aeruginosa,* S. *epidermidis,* methicillin-resistant *S. epidermidis*, methicillin-resistant *S. aureus* (MRSA), vancomycin-resistant *Enterococcus faecium* (VRE) and ESBL-positive *K. pneumoniae* as well as clinical fungal strains such as *C. albicans, C. tropicalis* and *C. parapsilosis*. MIC values for bacterial strains ranged

from 15.6 mg/L to 125 mg/L, while MIC for fungal strains ranged from 1.9 mg/L to 31.3 mg/L. In addition, Mahmoudi *et. al.* developed new classes of engineered multimodal nanoparticles comprising a magnetic core and either a silver or a gold ring with a ligand gap.[124] Both silver- and gold-coated SPION significantly increased the number of dead *S. aureus* and *S. epidermidis* cells after 24 hours of treatment, compared to bare SPION. Moreover, antibacterial properties were enhanced in the presence of an external field.

1.3.2.1.7. Toxicity Mechanisms of Nanoparticles against Bacteria

The exact mechanisms of antibacterial activities of nanoparticles against various bacteria are not fully understood. The mechanisms of nanoparticle toxicity depend on composition, surface modification, intrinsic properties, and the bacterial species. Nanoparticles can attach to the membrane of bacteria by electrostatic interaction and disrupt the integrity of the bacterial membrane. Nano- toxicity is generally triggered by the induction of oxidative stress by free radical formation, that is, the ROS, following the administration of nanoparticles. Formation of ROS damages the cellular and viral components, interrupts energy transduction, and inhibits enzyme activity and DNA synthesis.

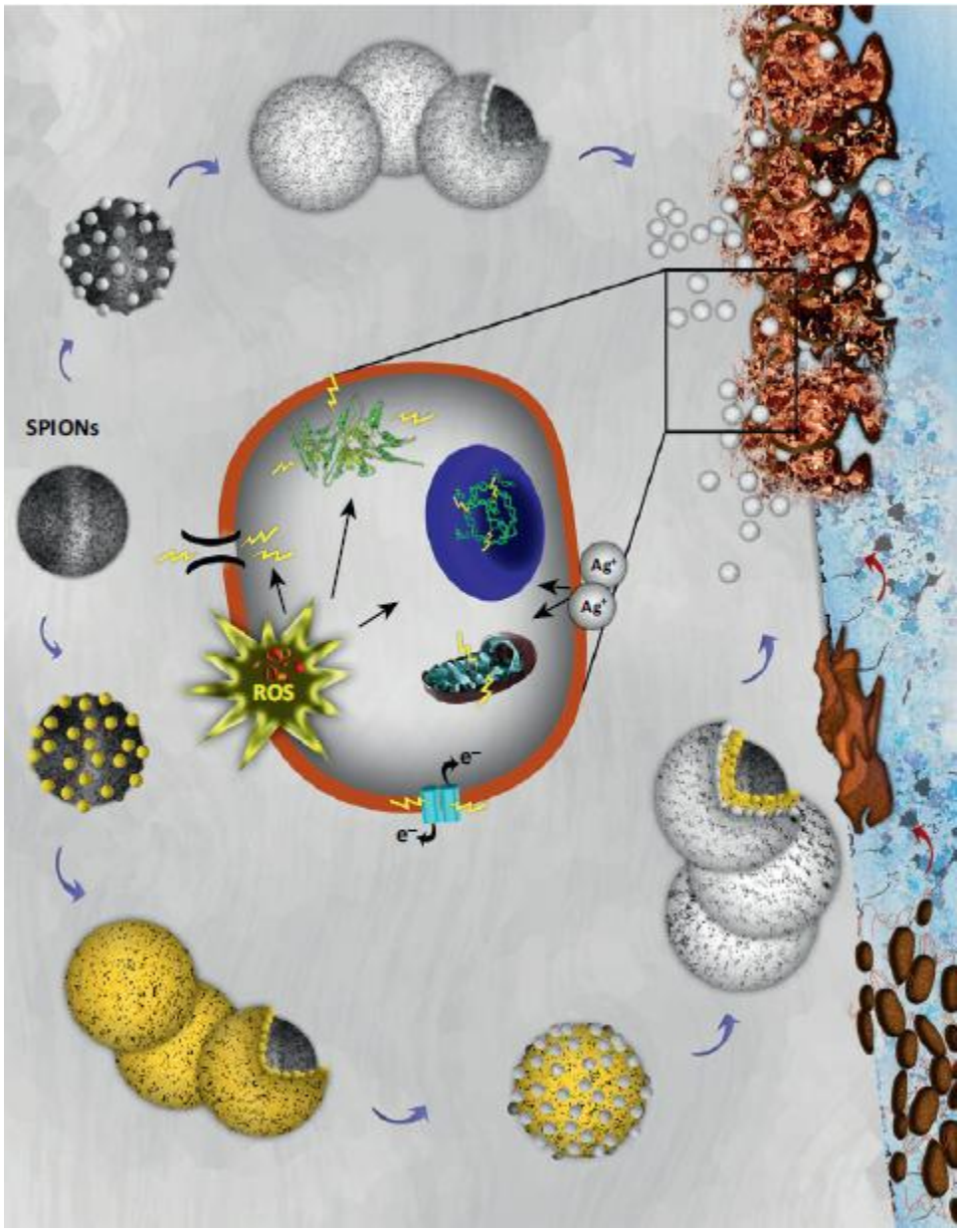

Figure 1.11. Various toxicity mechanisms of nanoparticles against bacterial cells.[124] Nanoparticles can disrupt and damage the bacterial cell membrane/wall, release heavy metal ions (i.e., Ag^{+} or Zn^{+2}), interrupt electron transport, cause production of ROS species which then damages the proteins, lipids and DNA.

1.3.2.2. Nanostructured Antibacterial Surfaces

Conventional biomaterials do not have nanoscale roughness. Nanoscale materials provide roughness and feature dimensions at the nano level which can influence bacteria behavior.[23,119] An *in vitro* study recently reported decreased *S. epidermidis* attachment on nanostructured ZnO and titania (TiO_2) compared to microstructured surface features.[118] *Puckett et al.* compared the adhesion of *S. aureus, S. epidermis*, and *P. aeruginosa* on conventional Ti, anodized Ti and nanorough Ti. It was shown that nanorough Ti fabricated by e-beam evaporation decreased the bacterial adherence the most, compared to conventional Ti.[103] *Ercan et al.* coupled nanotubular Ti with a 15-30V electrical stimulation and observed a significant decrease in *S. aureus* biofilm formation after 2 days of culture.[100] Moreover, nanostructured Ti can be loaded with antibiotics or nanoparticles as coatings for implant materials to reduce the infection risk. For example, *Popat et al.* fabricated 80 nm and 400 nm nanotubes on Ti through anodization and filled them with different concentrations of gentamicin.[102] It was shown that drug-eluting nanotubes significantly decreased initial *S. epidermis* adhesion on the surface. Increased osteoblast cell differentiation was also observed on gentamicin-filled nanotubular Ti.[102] Moreover, *Zhao et al.* incorporated Ag nanoparticles into nanotubes.[173] The nanotubes loaded with Ag nanoparticles killed all the planktonic bacteria in the culture medium during the first four days. Most importantly, nanostructured Ag incorporated Ti prevented bacterial adhesion for 30 days, which could be long enough to prevent an infection after surgery in the early and intermediate stages of implantation.[173] Many studies have shown that the anti-bacterial effects of nanotopographies are due to the changes in surface energy leading to changes in the initial adsorbed protein layer which modulates

intercellular interactions.[174] Nanorough features may increase the surface area and surface energy of medical devices which leads to altered select protein adsorption.[117] For example, increased protein adsorption (specifically vitronectin) and interactions on nanostructured titanium surfaces has resulted in improved functions of osteoblasts (bone forming cells).[117,175-177] Moreover, a ~40% reduction in bacteria colony forming units was observed on nanorough polyvinyl chloride (PVC) endotracheal tube (ETT) surfaces compared to conventional ETTs.[23,26] These studies indicated that there is a great potential to create antibacterial surfaces via engineering medical device surface roughness at the nanoscale.

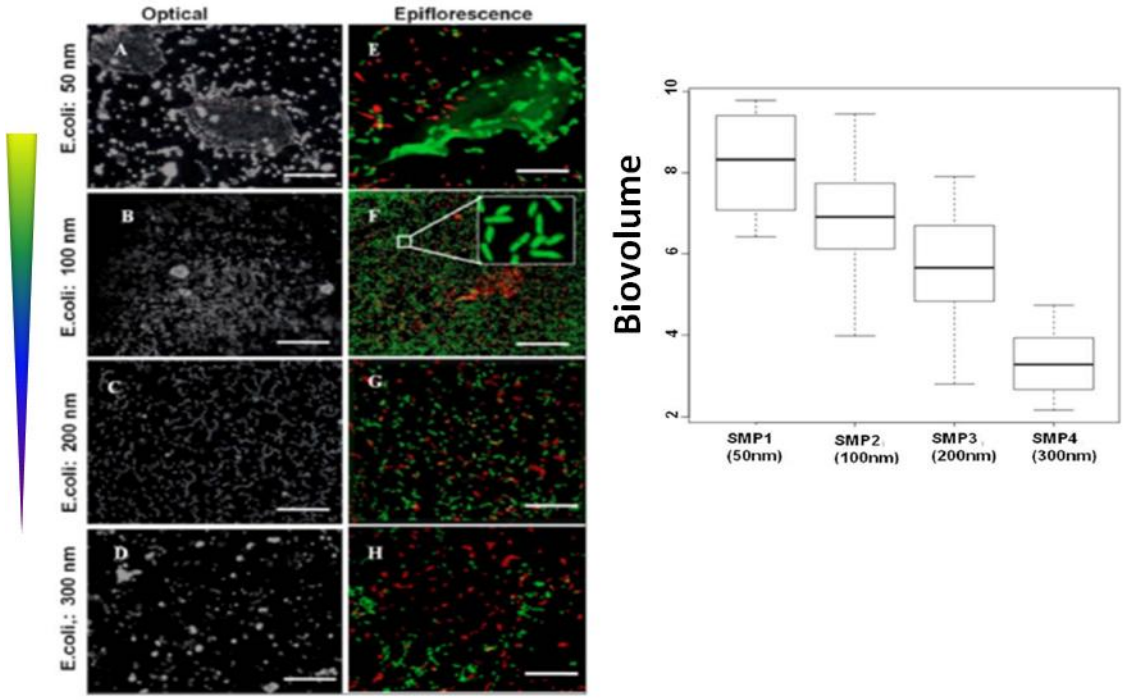

Figure 1.12. Nanoroughness decreases bacterial attachment and biofilm formation on medical devices. In addition, biovolume of biofilms decreases on nanorough surfaces.[178]

1.4. Metabolic Regulation of Antibiotic Resistance

The eradication of biofilms can be controlled by changing the surrounding microenvironment and biological conditions.[81] As mentioned earlier, persister bacteria are a subpopulation of dormant cells that form biofilms in chronic infections.[45,179] They enter a metabolic hibernation state and shut down their metabolism completely. This enables them to survive antibiotic treatment and become resistant. Recent studies by Allison *et. al.* provided evidence that the addition of certain metabolites, such as fructose, could increase the efficiency of antibiotics used to treat of both gram-negative and gram-positive persisters (**Figure 1.13**).[179] Bacteria are stimulated into an active state using sugars combined with an antibiotic, which renders them vulnerable to antibiotic treatments and eradication from the medical device surfaces. [179] The potentiation of antibacterial properties does not rely on growth resumption and it is effective in both aerobic and anaerobic conditions. It proceeded by the generation of a proton-motive force which facilitates the uptake of antibiotics. They demonstrated that persisters, although dormant, are primed for metabolite uptake, central metabolism and respiration. Furthermore, it has been shown that this approach can improve the *in vivo* treatment of chronic infections in a mouse urinary tract infection model. Thus, metabolic stimulation establishes a new strategy for eradicating bacterial persisters that is based on metabolism, and highlights the importance of the metabolic environment to antibiotic treatment.

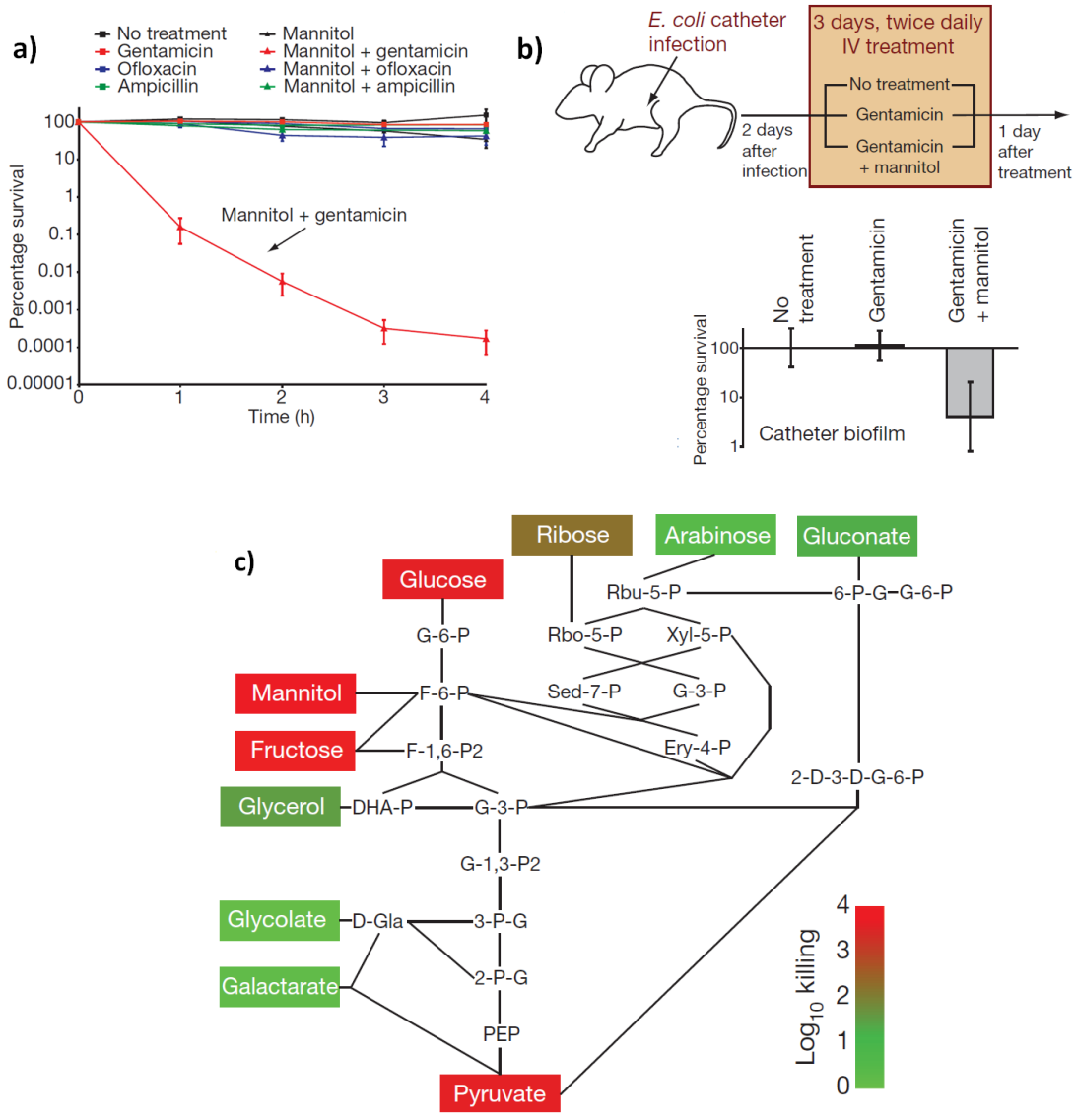

Figure 1.13. Metabolite-enabled eradication of bacterial persisters by antibiotics. **a)** Antibiotics do not eradicate *E. coli* persisters *in vitro*. On the other hand, percentage survival of persisters decreases when mannitol is used in combination with antibiotics. **b)** Metabolites also enhance the *in vivo* efficacy of antibiotics. *E. coli* biofilms on urinary-tract- inserted catheters are eradicated after treatment with mannitol (1.5 g/kg) plus gentamicin (1mg/kg). **c)** Metabolic network shows the efficiency of metabolite-enabled elimination of persister *E. coli*. Metabolites are color-coded according their ability to stimulate antibiotic action. [179]

The goal of this thesis is, for the first time, to integrate two novel approaches, i.e. nanotechnology and metabolic stimulation, to eradicate antibiotic-resistant biofilms (**Figure 1.14**). We hypothesized that combining the antibacterial properties of ***i) nanostructured surfaces*** *or* ***ii) magnetic nanoparticles (SPION)*** with metabolic stimulation (i.e. fructose) can further decrease bacterial growth and biofilm formation without the use of antibiotics. We manipulated the metabolic microenvironment of the biofilms to improve the antibacterial properties of magnetic nanoparticles (SPION) as well as nanorough device surfaces. In chapter 2, we demonstrate that engineered nanoscale topographies provide surfaces that are more resistant to bacterial growth than conventional polyvinyl chloride (PVC). We also show, for the first time, that the presence of fructose on the nanorough PVC decreases the number of planktonic *S. aureus* in the solution and biofilm formation, without use of any antibiotics. In chapter 3, for the first time, we showed that metabolic stimuli (i.e. fructose) can further enhance the uptake and eradication efficacy of SPION treatment to eradicate MRSA, *E. coli* and *P. aeruginosa* biofilms. In addition, biofilm eradication by the engineered SPION was significantly better than vancomycin, the antibiotic of last resort. This chapter establishes a simple and low-cost strategy for the eradication of persistent biofilms which could lead to alternative clinical treatments to vancomycin, which MRSA has already developed a resistance towards. In chapter 4, the effect of an external field to eradicate antibiotic-resistant biofilms with SPION has been investigated. We demonstrate that SPION conjugated with antibacterial silver salts exhibit strong eradication properties against the antibiotic-resistant (MRSA) biofilms. In addition, antibacterial properties of silver-conjugated SPION were improved when an external magnetic field was applied due as their

magnetic core enabled them to penetrate into the biofilms. Chapter 5 shows the antibacterial properties of a platform technology, where SPION are embedded within the PVC surfaces. Potential applications of the platform technology in various healthcare settings also have been reviewed.

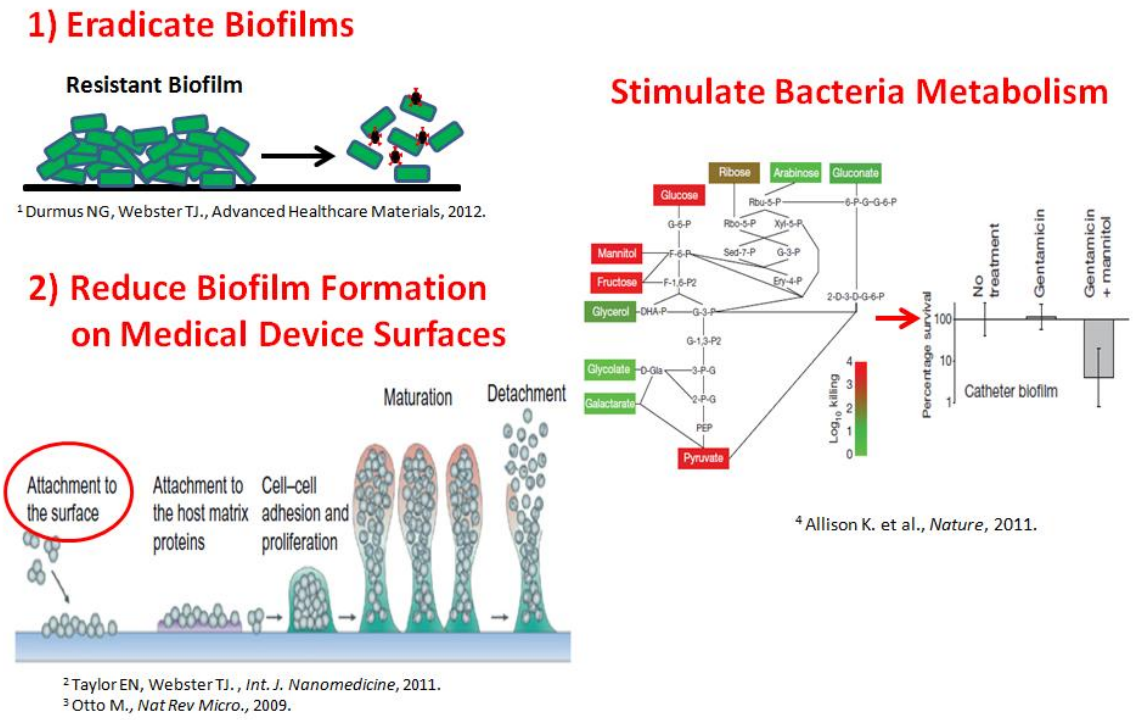

Figure 1.14. Using nanomaterial science to reduce infections. Metabolic microenvironment of the biofilms was manipulated to improve the antibacterial properties of magnetic nanoparticles (SPION) as well as nanorough device surfaces.[50,123,179]

1.5. Contributions to the Field

Although many studies have investigated different implant chemistries, new drugs and antibacterial agents, nanotechnology, or the science that deals with technologies on the scale of one billionth of a meter (10^{-9} m = 1 nm), is only recently being investigated as a means for infection control on medical devices. Many of these studies are usually targeted towards planktonic (free-floating) bacterial growth. On the other hand, persistent infections are often attributed to the formation of biofilms [180,181],which is the focus of this thesis. Moreover, the uptake of antibacterial treatments by the biofilm is also low as many agents cannot penetrate to the full depth of the biofilm.[182] The metabolic microenvironment of the biofilm is crucial and metabolites that can trigger and enable eradication have great potential to improve the treatment of antibiotic-resistant infections in the clinical settings.[125,170] In this thesis, we described a simple and low-cost dual-sided approach which uses superparamagnetic iron oxide particles (SPION) in combination with fructose metabolites as a new therapeutic option to existing antimicrobial strategies. This strategy offers further improved efficacy of magnetic nanoparticles against persistent MRSA infections by manipulating the biofilm extracellular metabolic microenvironment, creating a new nanotechnology-driven approach. . In addition, SPION treatments better eradicated the resistant biofilms than vancomycin, the antibiotic of last resort. Thus, this work establishes a simple, broad-spectrum and low-cost strategy for the better eradication of persistent biofilms, as a new therapeutic option to existing antibacterial strategies. Moreover, metabolic stimulation further decreased the growth and biofilm formation on nanostructured biomaterials (especially PVC-based device

surfaces). Thus, this thesis, for the first time, highlighted the importance of biofilm metabolic microenvironment for the nanotechnology-driven approaches.

It is envisioned that simple and inexpensive approaches developed in this thesis could lead to novel alternative treatments to the only current clinical option, vancomycin, which MRSA has started to develop a resistance towards. Once their *in vitro* and *in vivo* toxicity are well-characterized, these novel SPION treatments could lead to successful clinical outcomes for infection control. Moreover, combining metabolic stimulation with nano-material science has the potential to impact the future surface engineering of medical devices and invasive biomaterials and biomedical devices. These approaches can lead to successful clinical outcomes in terms of minimizing infections, longer medical device lifetimes, and decreasing antibiotic usage. All of these events might support decreased antibiotic resistance in the clinical settings.

Chapter 2. Fructose Enhanced Reduction of Bacterial Growth on Nanorough Surfaces

2.1. Introduction

Ventilator-associated pneumonia (VAP) is the most common hospital-acquired infection among patients requiring mechanical ventilation.[183-185] Patients are intubated with endotracheal tubes (ETTs) which interact with the surrounding airway epithelium during the ventilation process. However, ETTs provide surfaces where bacteria can attach, colonize and proliferate from the contaminated oropharyngeal space to the sterile bronchoalveolar area.[23,25] The pathogenesis of VAP is shown in **Figure 2.1.** Prolonged intubation leads to the colonization of upper respiratory tract by pathogens such as *Pseudomonas aeruginosa* (*P. aeruginosa*) and *Staphylococcus aureus* (*S. aureus*) and increases the risk of lung infection by six to twenty folds.[28-30,184,185] In addition, the risk of VAP increases by 3% per day during the first five days of mechanical ventilation and by 2% between days five and ten.[25,28-31]

Previous attempts to reduce the incidence of infection due to PVC ETTs have explored a variety of methods to change tube surface properties, including the use of antimicrobial and anti-bacteria adherent coatings, and the incorporation of antimicrobial agents directly onto the device.[25,186,187] However, these strategies have had limited success, principally due to issues relating to poor mechanical performance of either the coating or the impregnated device, or inappropriate drug elution profiles.[23] Therefore,

there exists an unmet clinical need to create surfaces that resist bacterial attachment and growth to reduce the risk of infection.

There is a great variation in the species responsible for VAP infection, in addition to the possibility of multiple organisms being involved in a single infection.[183] This great variation in organisms makes it difficult to specify which organism, or combination of organisms, are involved in every specific case. The etiology of VAP depends on the time of onset, duration of hospitalization and hospital settings.[24,183] *Staphylococcus aureus*, *Streptococcus pneumoniae*, and *Haemophilus influenzae* usually predominate in the early onset of VAP.[22,183] In addition, aerobic gram-negative bacteria, including members of the family *Enterobacteriaceae*, have been isolated in both the early and late onset of pneumonia.[22] *Pseudomonas aeruginosa*, *Acinetobacter* and *Enterobacter* species are often isolated from late-onset pneumonia.[22] Trauma intensive care unit (TICU) patients are at high risk of infection with *S. aureus*. *P. aeruginosa* is isolated most frequently in patients with VAP occurring greater than 4 days after the start of mechanical ventilation (19.7%) while *S. aureus* is isolated most frequently in patients whose VAP is diagnosed during the first 4 days (23.7%).[183] Not surprisingly, intubation increases the risk of lung infections by six to twenty fold.[28-30,184,185]

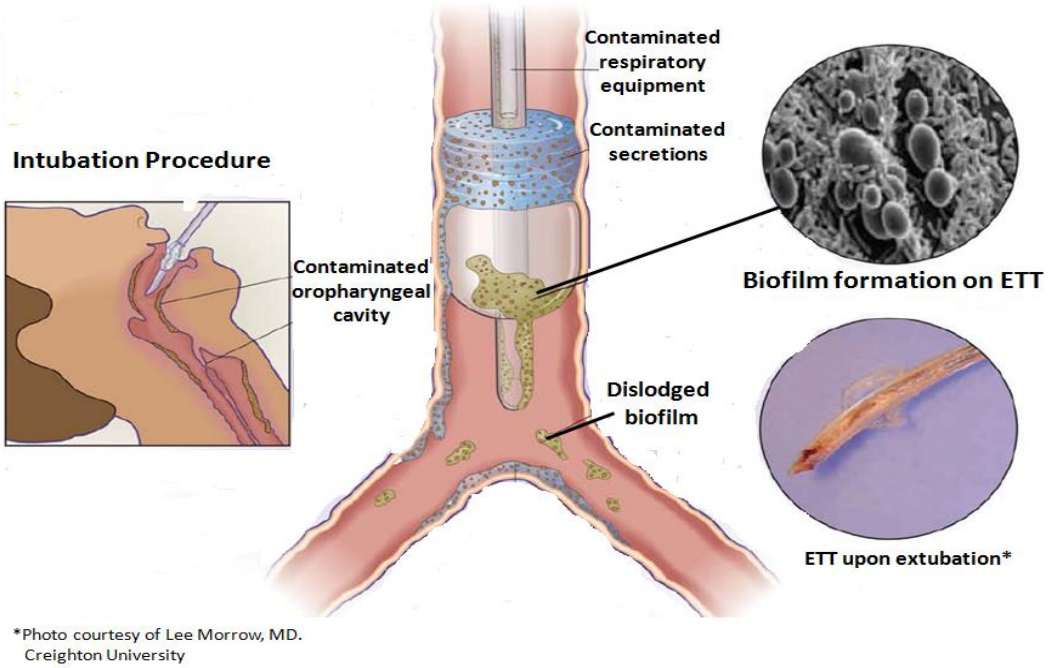

Figure 2.1. Pathogenesis of Ventilator-Associated Pneumonia (VAP). [188]

Surfaces of invasive medical devices (such as ETTs) serve as substrates for bacterial attachment, growth, colonization and biofilm formation.[48] Bacterial biofilms are complex heterogeneous communities embedded in an extracellular polymeric substance (EPS) matrix which is composed of polysaccharides, nucleic acids, proteins and lipids.[44,45] Formation of these sessile (adherent, immobile bacteria) communities provides a resistance mechanism against host immune responses and antibacterial agents. [49] Inherent resistance of biofilms on material surfaces causes a real-world problem as many persistent and chronic bacterial infections occur in medical and industrial settings.

Recently, many studies have shown that changes in the surface topography at the nanometer level can interfere with bacterial functions.[23,26,113-119] Conventional biomaterials (such as PVC ETTs) do not have nanoscale roughness. Nanoscale materials

provide roughness and dimensions at the nano level which might influence bacteria behavior.[23,119] For example, an *in vitro* study recently reported decreased *Staphylococcus epidermidis* (*S. epidermidis*) attachment on nanostructured ZnO and titania (TiO_2) compared to microstructured surface features.[118] It was also demonstrated that the attachment of different pathogenic strains (*S. aureus*, *S. epidermidis* and *P. aeruginosa*) could be controlled by changing titanium surface roughness and ultrafine crystallinity at the nano level.[117] Many studies have shown that these effects of surface nanotopographies are due to changes in surface energy leading to changes in the adsorbed protein layer which modulates intercellular interactions.[174] For example, increased protein adsorption and bioactivity on nanostructured Ti surfaces has resulted in improved functions of osteoblasts (bone forming cells).[117,175-177] Moreover, a ~40% reduction in colony forming units was observed on nanorough PVC ETT surfaces compared to conventional ETTs.[23,26] These studies indicated that there is a great potential to create antibacterial surfaces via engineering surface roughness at the nanoscale.

In addition to the antibacterial effects of surface nanoroughness, eradication of biofilms can be also controlled by changing the surrounding micro- and nano-environment and biological conditions. Persister bacteria represent a population of dormant cells which can form biofilms in chronic infections.[45,179] Persisters enter a metabolic hibernation state and shut down their metabolism. This enables them to survive during the antibiotic treatment and become resistant. A recent study provided evidence that the addition of certain metabolites, such as fructose, could increase the efficiency of antibiotics which are used to treat of both gram-negative and gram-positive persisters.[179]

In this approach, persister bacteria are stimulated into an active state using fructose metabolites. Fructose molecules enter the bacterial metabolism through glycolysis and stimulate the shut-down metabolism of persister cells. As a result, changes in the bacterial metabolism stimulate the uptake of antibiotics. Therefore, fructose metabolites combined with an aminoglycoside antibiotic (i.e., gentamicin) render biofilm forming bacteria vulnerable to antibiotic treatments and eradicate them from the medical device surfaces.[179] Metabolites which can trigger and enable the dispersal of biofilms have a great potential to treat infections in the clinical settings.

In this chapter, the antibacterial effect of nanorough topographies with sugar metabolites were combined in an effort to further decrease bacterial growth and biofilm formation on ETTs without using antibiotics. *S. aureus* was chosen as the target bacteria as it is one of the major causes of fatal nosocomial infections as well as community-associated infections. In addition, it is the most frequently isolated bacteria in patients whose episode of VAP was diagnosed during the first days of mechanical ventilation.[183,189] First, commercially available polyvinyl chloride (PVC) ETTs were enzymatically degraded to create nanoscale surface roughness. Then, nanorough (NanoR) ETTs were soaked into different concentrations of a fructose solution. Planktonic bacterial growth in the surrounding culture medium and biofilm formation of *S. aureus* on ETT surfaces were observed and quantified after 24 hours. For the first time, results are presented that show the presence of a specific metabolite, i.e. fructose, on the nanorough surfaces decreases the number of planktonic bacteria in the solution and biofilm formation after 24 hours.

2.2. Materials and Methods

2.2.1. PVC ETT Material Preparation and Nanoroughening

Commercially available Sheridan® 6.0 mm ID, uncuffed ETTs (Hudson RIC, Temecula, CA) were cut vertically into 0.6 cm x 0.3 cm segments using a rectangular hole punch. Nanorough (NanoR) topographies on the PVC ETT surface were created using a lipase from Rhizopus arrhizus (Sigma-Aldrich, St. Louis, MO) at a 0.1% concentration in 1M potassium phosphate buffer (PBS) at a pH of 7.2 (Fisher Scientific). PVC samples were soaked in the lipase solution at 37°C at 200 revolutions per minute (rpm) for 24 hours. After 24 hours, the lipase solution was replaced with a fresh solution and the samples were soaked for additional 24 hours. Then, the NanoR samples were removed and rinsed three times with double distilled water. The NanoR and untreated PVC samples were air dried overnight (~12 hours) at room temperature, and then they were sterilized at Rhode Island Hospital using ethylene oxide gas.

2.2.2. PVC Surface Modification with Metabolites

D-Fructose (Fisher Scientific, Pittsburg, PA) was dissolved in double distilled water. 10 mM and 100 mM fructose solutions were sterilized via a polytetrafluoroethylene (PTFE) syringe filter with a 0.2 µm pore size (Fisher Scientific, Pittsburg, PA). To coat surfaces with the fructose, sterilized PVC samples prepared above were soaked in either 10 mM or 100mM fructose solutions and incubated overnight (~12 hours) in a sterile hood. Then, the samples were air dried in the sterile hood.

2.2.3. Surface Characterization

2.2.3.1. Scanning Electron Microscopy (SEM)

Surface topography of the materials was visualized using a SEM (LEO 1530VP FE-4800 Field-Emission SEM, Carl Zeiss SMT, Peabody, MA) according to standard operating procedure. Samples were imaged with an accelerating voltage of 20 kV using variable pressure.

2.2.3.2. Atomic Force Microscopy (AFM)

Samples were characterized by using atomic force microscopy (AFM) at scan areas of 5μm x 5 μm. Specifically, the topography of the PVC substrates were evaluated with AFM (Asylum-1 MFP-3D AFM System, Santa Barbara, CA) under tapping mode using a 9 ± 2 nm AFM tip at a scan rate of 0.5 Hz. The root-mean-squared (RMS) roughness, which is the standard deviation of the height value in the selected line, was determined in five random fields per sample. In Equation 2.1, RMS is calculated as the standard deviation of the Z values (in vertical direction) within the given area and stands for height direction roughness where Zn is the current Z value; Zave is the average Z value within the given area. N is the number of points within the given area.

$$\mathrm{RMS} = \sqrt{\sum_{i=1}^{N} \frac{(Zn - Zave)^2}{N}} \qquad \textbf{(Equation 2.1)}$$

2.2.3.3 Contact Angle Measurements

Water contact angles were investigated using a drop shape analysis system (EasyDrop, Kruss, Hamburg, Germany). The contact angle from 1 µL of double distilled water sessile droplets (60 seconds after being dropped on the surface) was measured for each sample.

2.2.4 Bacteria Assays

2.2.4.1. Bacteria Culture

The experimental strategy employed in our work is shown in **Figure 2.2**. *Staphylococcus aureus* (ATCC #25923, American Type Culture Collection, Mannassas, VA) was hydrated and streaked for isolation on a tryptic soy agar plate. Following growth, a single isolated colony was selected and inoculated in 3 mL tryptic soy broth (TSB) media (MP Biomedicals, Solon, OH). The bacteria culture was grown on an incubator shaker for 18 hours at 37^0C at 200 rpm until it reached the stationary phase.

2.2.4.2. Bacterial Growth and Biofilm Formation Analyses

First, the optical density of the overnight culture at 562 nm (OD_{562}) was adjusted to 0.52, which corresponds to cell number of 10^9. Then, the cultures were serially diluted to obtain 10^3 cells/mL bacteria in solution. 100 µL of a 10^3 bacteria solution was seeded onto a single well of a flat bottom 96-well plate (BD, Franklin Janes, New Jersey) containing either NanoR or an untreated PVC sample soaked in a 10 mM and 100 mM fructose solution (Fisher Scientific, Pittsburg, PA). Unsoaked NanoR and PVC samples

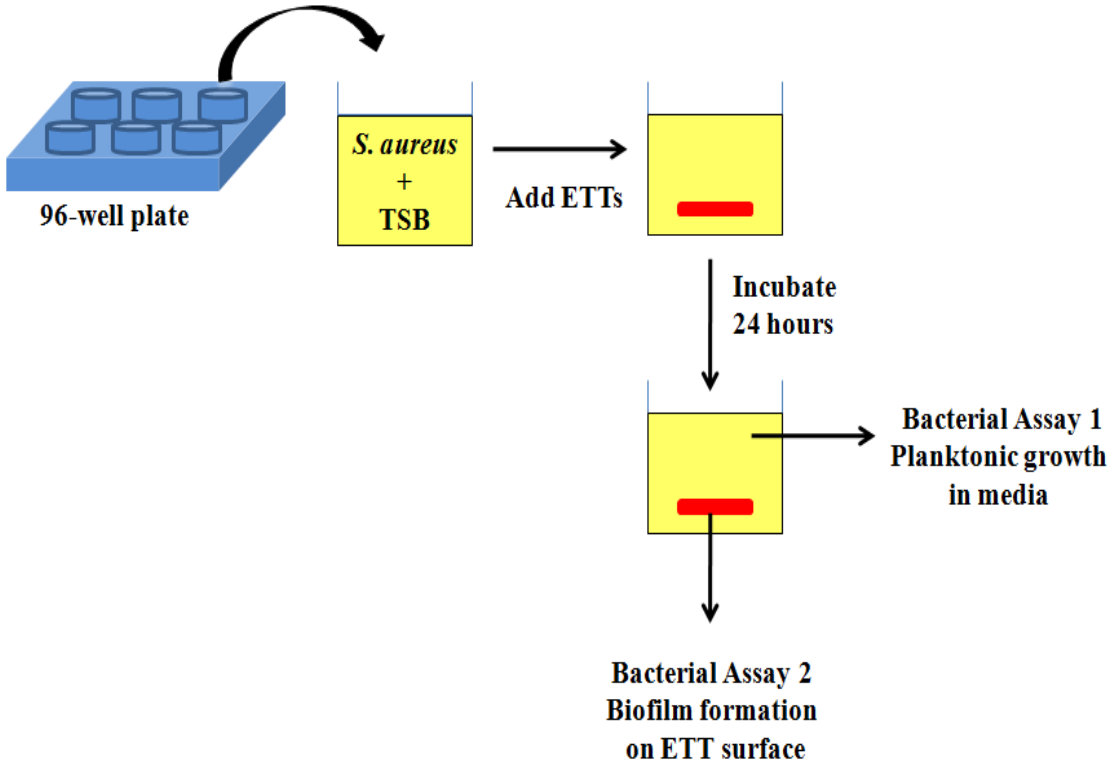

Figure 2.2. Schematic of bacteria assays. Commercially available polyvinyl chloride (PVC) endotracheal tubes (ETTs) were enzymatically degraded to create nanoscale surface roughness. Then, control PVC and nanorough (NanoR) ETTs were soaked into different concentrations of a fructose solution. Bacterial survival in the medium (Assay 1) and biofilm formation on the ETT surfaces (Assay 2) were quantified.

were used as controls. The plate was then placed in a stationary incubator at 37^0C with 5% CO_2. After 24 hours, samples were removed with a pair of sterile forceps. The optical density of the plate was then measured at 562 nm using a SpectraMax M5 plate reader (Molecular Devices, Sunnyvale, CA) to analyze planktonic bacteria growth. To remove sessile bacteria from the PVC surface, a vortexing method was used and a cell viability assay was performed to measure colony forming units/mL (CFU/mL). Specifically, each PVC sample was placed in 1 mL of PBS (Fisher Scientific, Pittsburg, PA) and vortexed at 3000 rpm for 10 minutes. The cells were then serially diluted in PBS (Fisher Scientific, Pittsburg, PA) over a 3-log range. 10 µL of each dilution were plated on tryptic soy agar plates and incubated at 37°C overnight. After overnight incubation, colony forming units were counted for each sample to quantify biofilm formation on the ETT surfaces. CFU/mL values were calculated using the following formula:

$$CFU/mL = ([(Number\ of\ Colonies) \times (Dilution\ Factor)] / 0.01\ mL) \quad \textbf{(Equation 2.2)}$$

2.2.5. Statistical Analysis

All experiments were performed in triplicates and repeated at least three times to validate repeatability and reproducibility. Data were represented as the mean ± standard error of the mean (SEM). Results were analyzed for statistical significance using Student's *t*-test. Three different significance levels ($p < 0.01$, $p < 0.05$, and $p < 0.1$) were noted.

2.3. Results and Discussion

2.3.1. Material Characterization

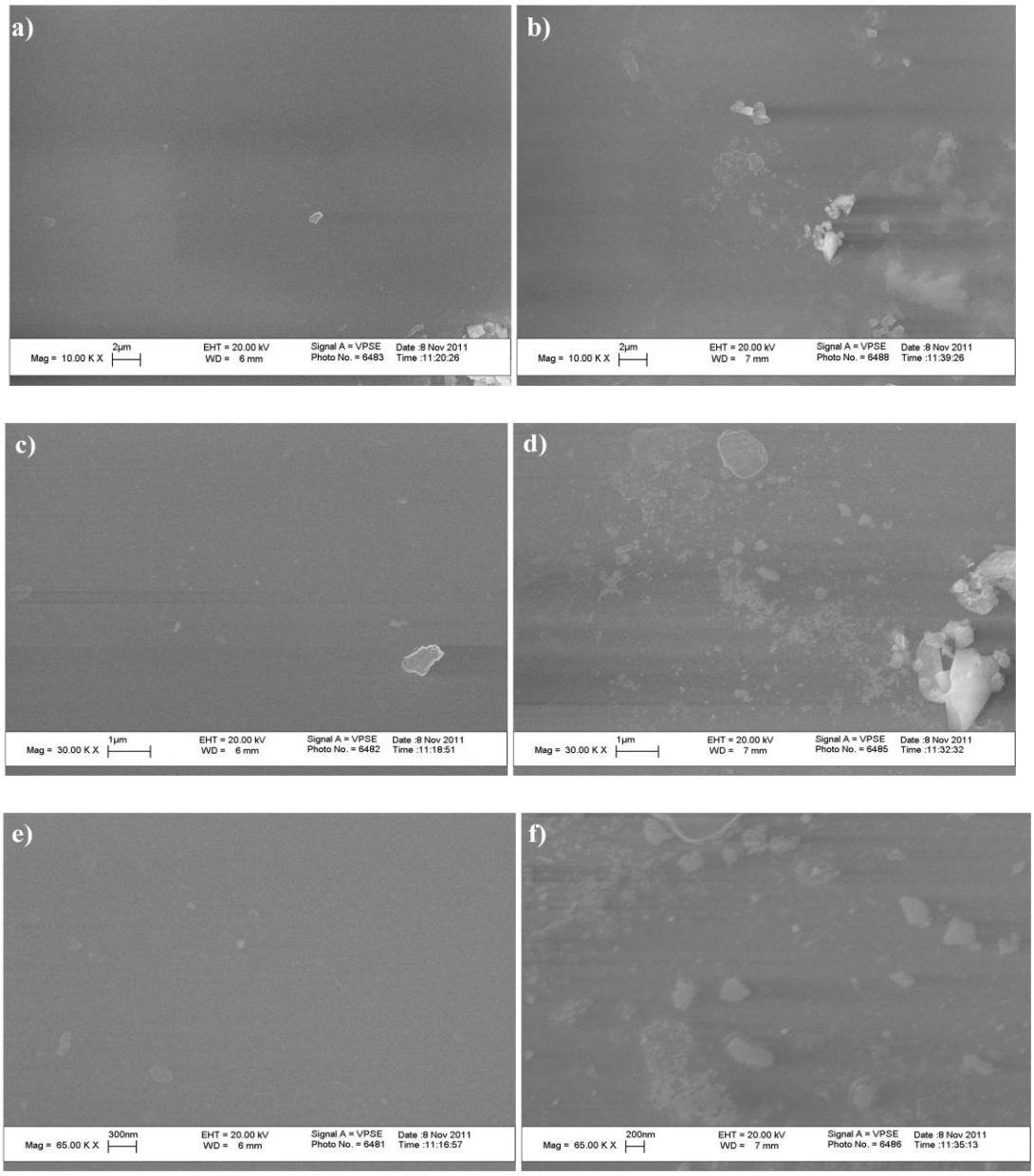

Figure 2.3. SEM images of untreated PVC and NanoR PVC. Untreated PVC samples revealed a smooth surface (**a, c, and e**) (10, 30 and 65 KX, respectively). On the other hand, NanoR PVC samples revealed a rough surface at the micron, submicron and nanometer level (**b, d, and f**) (10, 30 and 65 KX, respectively).

SEM analysis indicated that the lipase treatment degraded conventional PVC surfaces and created nanoscale features (**Figure 2.3**). In addition, AFM micrographs revealed distinct topographies in control surfaces compared to NanoR PVC surfaces (**Figure 2.4 a-b**). As expected, control PVC surfaces were smooth compared to NanoR PVC. Roughness of untreated PVC was 0.704 ± 0.192 nm while it was 8.440 ± 1.282 nm for NanoR PVC as measured by AFM at 5 µm X 5µm scans **(Table 1)**. SEM images also confirmed that PVC was smooth compared to NanoR PVC surfaces. In addition, coating the surface with fructose decreased the nanoscale topography and nanoroughness for both the control PVC and NanoR PVC surfaces soaked in different fructose concentrations (**Figure 2.4 c- f**). The decrease in the surface roughness was more apparent in the NanoR samples. Coating the NanoR surface with 10 mM fructose decreased the roughness from 8.440 ± 1.282 nm to 1.214 ± 0.144 nm. Surface roughness was significantly higher for NanoR ETT soaked in 10 mM fructose solution than control PVC ETTs ($p < 0.01$). As the fructose concentration increased to 100 mM, RMS values decreased from 8.440 ± 1.282 nm to 1.034 ± 0.175 nm. Surface roughness of NanoR ETT soaked in the 100 mM fructose solution was also significantly higher than control PVC ETTs ($p < 0.1$).

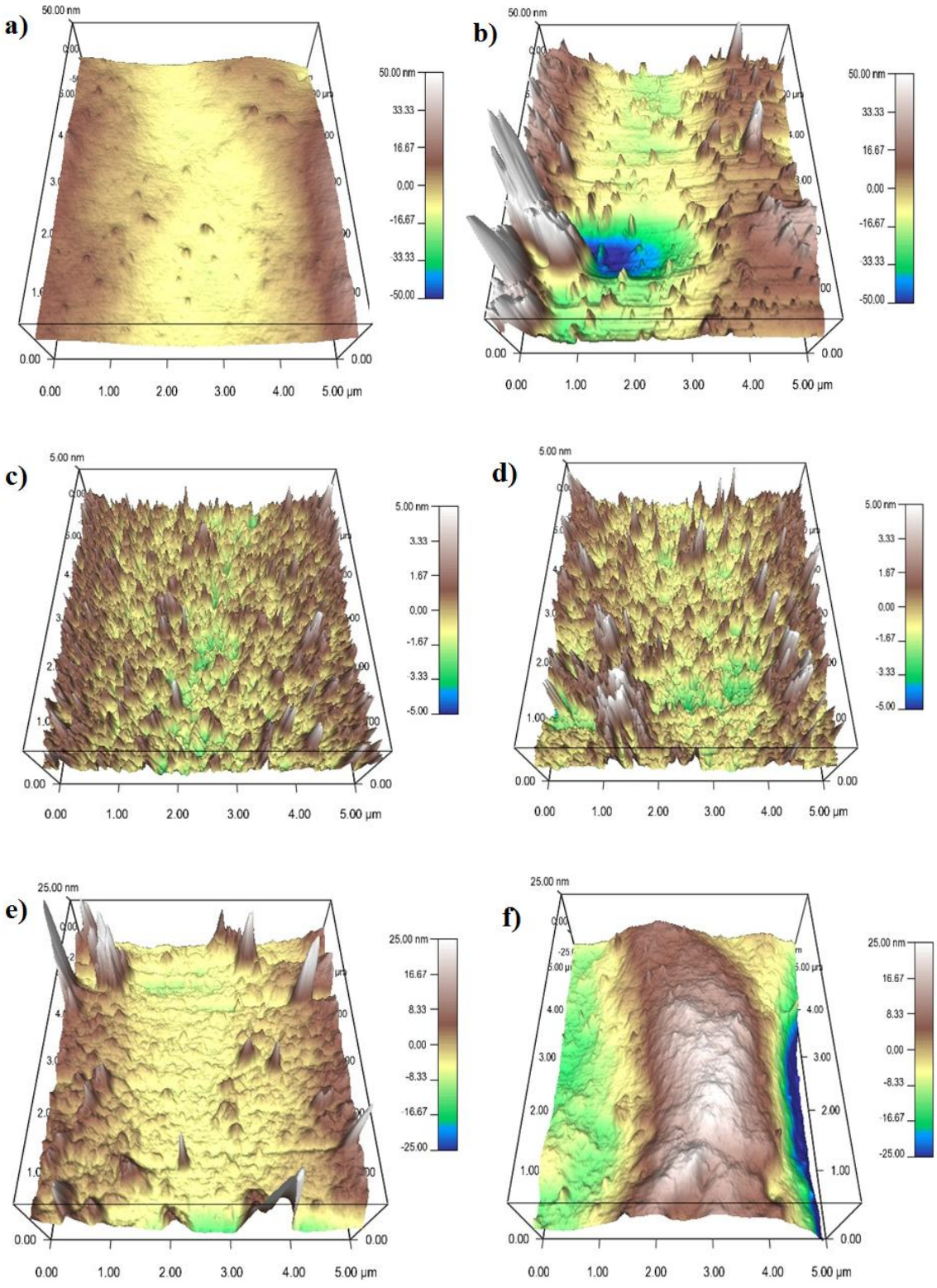

Figure 2.4. AFM micrographs showing the topography of **(a, b)** control PVC and NanoR PVC, **(c, e)** Control PVC soaked in 10 and 100 mM fructose, and **(d, f)** NanoR

PVC soaked in 10 and 100 mM fructose, respectively. Micrographs revealed distinct differences in nanotopographies between the control PVC and NanoR PVC surface soaked in different metabolite concentrations.

Table 2.1. RMS values of PVC and NanoR PVC surfaces before and after soaking in two different concentrations (10 and 100 mM) of a fructose solution. RMS values were calculated from the AFM scan areas of 5 µm x 5 µm. Data represents mean ± SEM, n = 5. * $p < 0.05$ compared to control PVC ETT surface. # $p < 0.01$ NanoR PVC soaked in a 10 mM fructose solution compared to control PVC ETT.

	Root Mean Square Roughness (RMS)
PVC	0.704 ± 0.192 nm
PVC soaked in 10 mM fructose	0.592 ± 0.037 nm*
PVC soaked in 100 mM fructose	0.702 ± 0.029 nm
NanoR	8.440 ± 1.282 nm#
NanoR soaked in 10 mM fructose	1.214 ± 0.144 nm#
NanoR soaked in 100 mM fructose	1.034 ± 0.175 nm^

The rougher surfaces have more surface energy and fructose coated the rougher regions on the NanoR surfaces, which decreased the roughness and made surfaces smoother. Deposition of fructose crystals was also clearly visibly apparent on the surfaces, and more deposition was observed when NanoR surfaces coated with 100 mM fructose (**Figure 2.5**). The effect of fructose coating on surface roughness was also observed for untreated PVC surfaces. The RMS decreased on PVC soaked in 10 mM fructose from 0.704 ± 0.192 nm to 0.592 ± 0.037 nm. On the other hand, RMS value of PVC soaked in 100 mM fructose was 0.702 ± 0.037 nm. This increase in roughness compared to PVC soaked in 100 mM could be due to the excess deposition of fructose crystals on the surface (**Figure 2.5**).

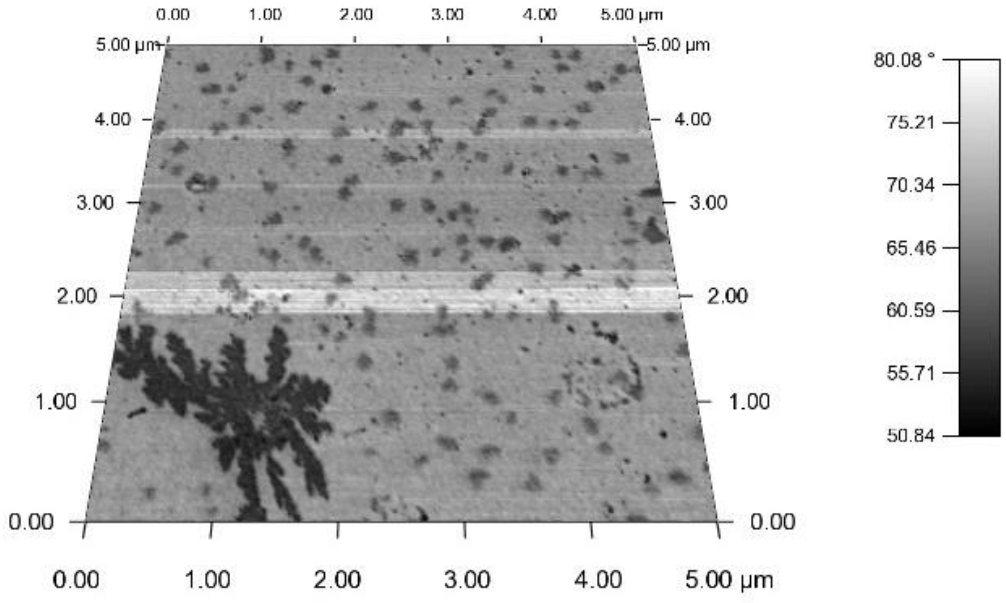

Figure 2.5. Fructose deposition on NanoR PVC surfaces soaked in a 100 mM fructose solution.

Since surface nanoroughness can provide more surface area and make the surface more hydrophobic due to greater water surface tension interactions,[176,190-193] the hydrophobicity of the PVC and NanoR surfaces were characterized **(Table 2.2)**. The NanoR surface had a contact angle of $70.36^0 \pm 1.18$ and it was significantly more hydrophilic than the control PVC surface, which had a contact angle of $88.62^0 \pm 1.12$ ($p < 0.01$). In this case, surface nanoroughness provided more wetting for the PVC ETTs. Moreover, coating surfaces with fructose decreased the hydrophobicity of both the NanoR and control PVC samples.

The decrease in the contact angle was more apparent for the control PVC. Specifically, conventional PVC surface soaked in a 10 mM fructose solution had a contact angle of $72.98^0 \pm 0.45$, while the PVC soaked in a 100 mM fructose solution had contact angle of $69.02^0 \pm 1.43$. In addition, contact angles of the NanoR PVC soaked in 10 mM and 100 mM solution were significantly different than the contact angles of control PVC with water ($p < 0.01$). The NanoR PVC surfaces soaked in 10 mM fructose solution had a contact angle of $68.10^0 \pm 3.19$ while the contact angle of the NanoR soaked in 100 mM fructose solution was $64.18^0 \pm 3.46$. Representative contact angle measurement pictures of conventional and NanoR PVC are shown in **Figure 2.6** and **2.7**.

Table 2.2. Water contact angles on PVC and NanoR PVC surfaces before and after soaking into two different concentrations (10 mM and 100 mM) of a fructose solution. Values are mean ± SEM, n = 5. * $p < 0.01$ compared to control PVC ETT surface.

	Contact Angle with H_20
PVC	$88.62^0 \pm 1.12$
PVC soaked in 10 mM fructose	$72.98^0 \pm 0.45^*$
PVC soaked in 100 mM fructose	$69.02^0 \pm 1.43^*$
NanoR	$70.36^0 \pm 1.18^*$
NanoR soaked in 10 mM fructose	$68.10^0 \pm 3.19^*$
NanoR soaked in 100 mM fructose	$64.18^0 \pm 3.46^*$

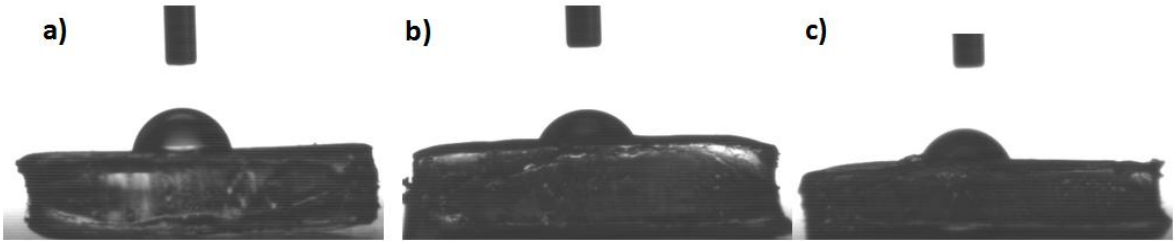

Figure 2.6. Representative contact angle pictures of control PVC ETTs. **a)** PVC ETT, **b)** PVC ETT soaked in a 10 mM fructose solution, **c)** PVC ETT soaked into a 100 mM fructose solution.

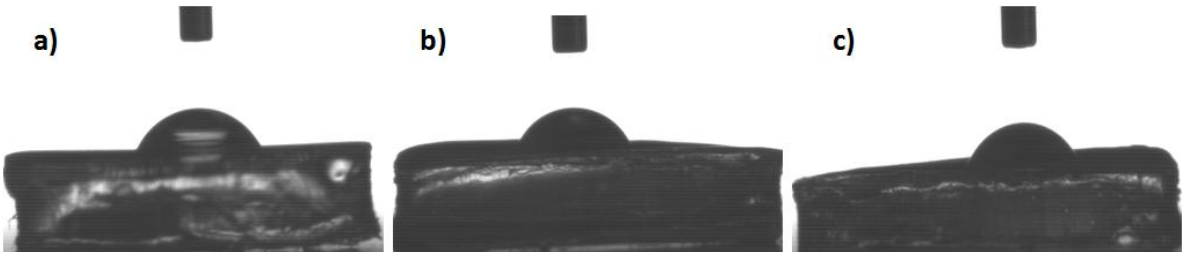

Figure 2. 7. Representative contact angle pictures of NanoR PVC ETTs. **a)** NanoR PVC ETT, **b)** NanoR PVC ETT soaked in a 10 mM fructose solution, **c)** NanoR PVC ETT soaked into a 100 mM fructose solution.

2.3.2. Bacteria Studies:

Figure 2.8 shows the effect of the fructose treatment on planktonic *S. aureus* bacteria that were suspended in the surrounding culture medium. The growth of planktonic bacteria decreased on NanoR surfaces soaked into a 100 mM fructose solution compared to conventional PVC surfaces as well as PVC soaked in respective amounts of fructose. In addition, less planktonic bacteria was observed on NanoR PVC surfaces soaked in a 100 mM fructose solution compared to NanoR PVC surfaces soaked in a 10 mM fructose solution. Therefore, it was clear that fructose reduced planktonic *S. aureus* bacteria growth and bacterial reduction was dependent on the fructose concentration on the nanorough surfaces.

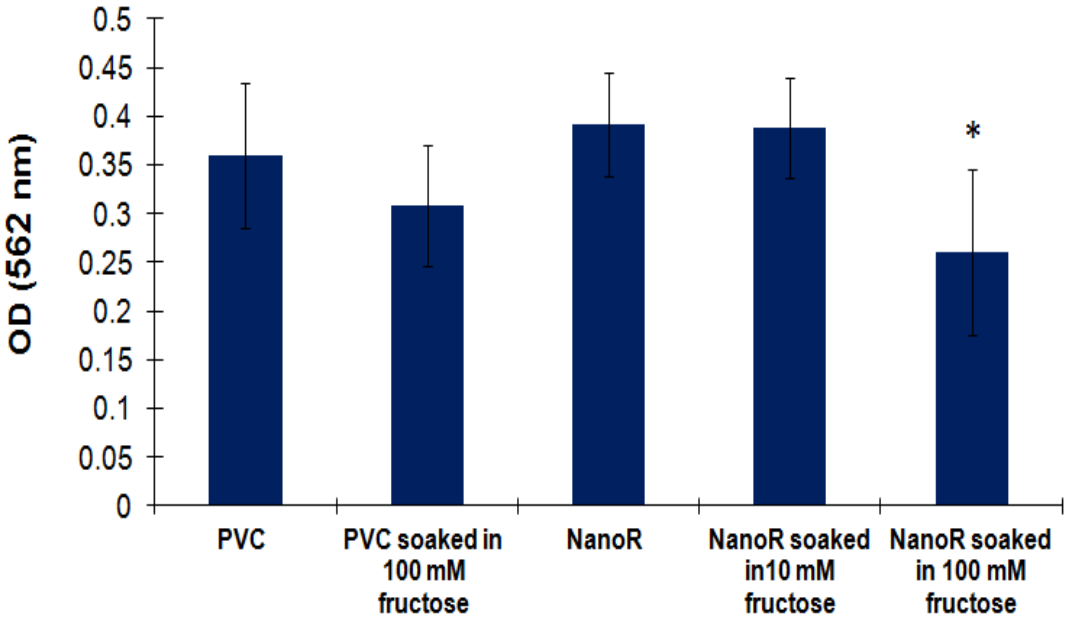

Figure 2. 8. *S. aureus* optical density measurements after 24 hours. Planktonic bacteria growth decreased on NanoR surfaces soaked in a fructose (10 mM and 100 mM) solution. Data represents mean ± SEM, N=3. * $p < 0.05$ NanoR compared to NanoR soaked in 10 mM fructose, and NanoR soaked in 10 mM fructose compared to NanoR soaked in 100 mM.

Figure 2.9 shows the *S. aureus* colony counts on PVC and NanoR surfaces soaked in a 10 mM fructose solution. According to these results, fructose treatment decreased the biofilm formation on both PVC and NanoR surfaces after 24 hours. A 38% decrease was observed in the growth of *S. aureus* on PVC surfaces soaked in 10 mM fructose solution compared to unsoaked PVC surfaces. In addition, biofilm formation significantly decreased (45%) on NanoR surfaces compared to the control PVC surfaces ($p < 0.1$). In addition, a 60% decrease (~ 0.4 log reduction) in biofilm formation was observed on

NanoR surfaces soaked in a 10 mM fructose solution compared to conventional PVC surfaces ($p < 0.05$). More importantly, all of these results were accomplished without using any antibiotics.

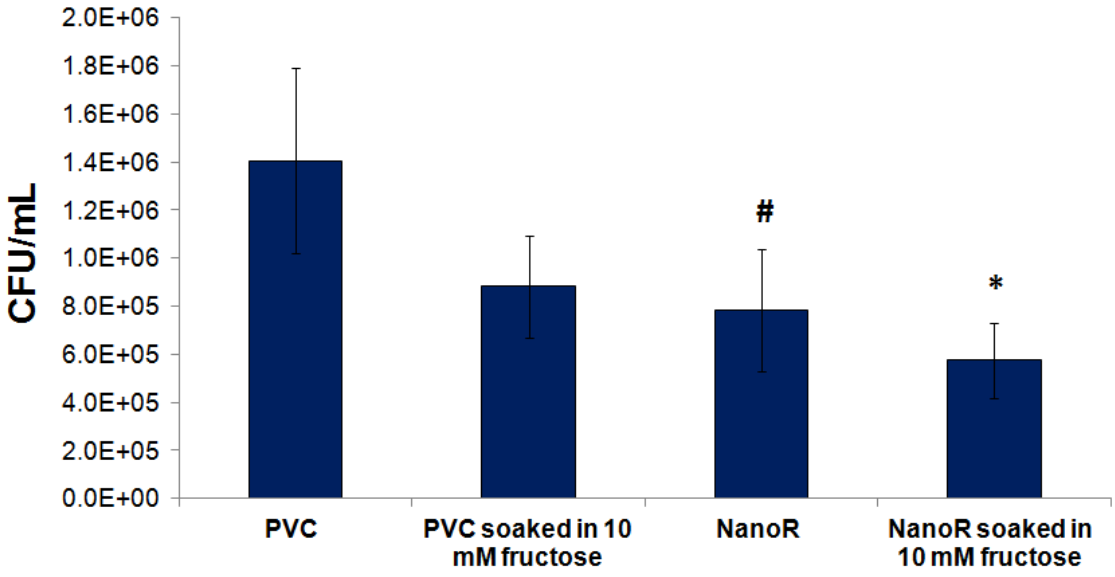

Figure 2.8. *S. aureus* colony counts on PVC and NanoR surfaces soaked in a 10 mM fructose solution. Biofilm formation decreased on NanoR and PVC surfaces soaked in a 10 mM fructose solution. Data represents mean ± SEM, N = 4. *$p < 0.05$ NanoR soaked in 10 mM fructose compared to PVC control, # $p < 0.1$ NanoR compared to PVC control.

2.4. Discussion

Biofilms develop a protected growth which allows survival in a hostile environment. As a result, bacterial persisters are a dormant population and they are tolerant to antibiotic treatment.[45,49,179] These persister structures within the biofilms form channels in which nutrient circulation occurs. However, the uptake of some antibiotics, such as aminoglysocides, requires a promotion motive force (PMF). As the biofilm forming bacteria are in a dormant state, they do not uptake and metabolize antibiotics. Thus, bacterial resistance to antibiotics develops. If the metabolites which enter to the upper glycolysis metabolism (i.e., glucose, fructose and mannitol) are added into the microenvironment as carbon sources, the efficiency of gentamicin increases. As the metabolism and PMF of the persisters are induced, metabolite stimulation increases the uptake of antibiotics and their killing efficiency.[179] In addition, these sessile biofilm communities can give rise to non-sessile bacterium and these planktonic bacteria can rapidly multiply and disperse within the solution. Planktonic bacteria must expose themselves to deleterious agents in their environment while the biofilm forming persisters protect themselves from harsh environmental conditions, such as antibiotics.[49]

As the planktonic bacteria are dispersed within the surrounding medium due to the presence of fructose on the ETT surface, surface roughness at the nanoscale could minimize the contact between the bacteria cell wall and the NanoR ETT surface. This might inhibit the electrostatic interactions responsible for initial bacterial attachment on the surface.[23] Accumulation of proteins on nanorough surfaces might also affect initial bacterial adhesion though a thick anti-bacterial protein layer. This layer could decrease

interactions at the bacteria-nanorough surface interface. Thus, this passivation effect could reduce the bacterial attachment and biofilm formation.[32] Moreover, metabolites on both PVC and NanoR ETT surfaces might induce metabolism of biofilm forming S. aureus. All of these events might lead to the reduction of both planktonic bacteria growth and biofilm formation on NanoR surfaces that are soaked in fructose solutions, without the use of any antibiotics. The effect of combining nanostructured surfaces with other metabolites which enter bacterial metabolism through glycolysis (such as glucose, mannitol, and pyruvate) should be studied in the future studies.

2.5. Conclusions

In summary, as presented here for the first time, the presence of fructose on nanorough (NanoR) PVC surfaces decreases the number of planktonic *S. aureus* in solution and biofilm formation, without the use of any antibiotics. In addition, it was shown that engineered nanoscale topographies provide surfaces that are more resistant to bacterial growth than conventional PVC without the use of any antibiotics. Such results have important implications. First, the design of nanorough engineered surfaces decreases bacterial adhesion on surfaces. In addition, the reduction of biofilm forming bacteria can be improved through the use of specific metabolites on nanorough surfaces. It is envisioned that this method has the potential to impact the future surface engineering of ETTs as well as catheters, invasive biomaterials and biomedical devices leading to more successful clinical outcomes in terms of longer lifetimes, minimized infections and decreased antibiotic usage; all of these events can support decreased antibiotic resistance, necessary for the future of world-wide healthcare.

Chapter 3. Enhanced Efficacy of Superparamagnetic Iron Oxide Nanoparticles Against Antibiotic-Resistant Biofilms in the Presence of Metabolites

3.1. Introduction

When the antibiotics were first introduced, they were believed to be the end of bacterial infections.[1] However, due to their extensive use (which has been estimated to be over 1 million tons since 1940's), the emergence of multi-drug resistant bacteria is one of the greatest global problems in public health today.[2] The number and frequency of antibiotic resistant microorganisms are mounting worldwide which renders antibiotic therapies costly and most of the time, unsuccessful.[3] On the other hand, there is a descending trend in the development of new antibiotics creating important implications on global health and economy. Especially, antibiotic resistance and the lack of new antibacterial agents create significant complications and treatment challenges in the clinical setting leading to healthcare-associated infections (HAI). HAI are among the top leading causes of death in the United States and affect approximately 1.7 million patients each year, resulting in up to 100,000 excess deaths, and leading to an estimated cost of more than $35 billion per year.[194,195]

The emergence of methicillin-resistant *Staphylococcus aureus* (MRSA) has been the steadily growing cause of healthcare- and community-associated infections.[1,196,197] *S. aureus* is a gram-positive bacteria which commonly colonize on the human skin and has

developed many epidemic waves of antibiotic resistance since the mid 1940's.[197] *S. aureus* can cause a wide range of diseases, such as skin and soft-tissue infections, bloodstream infections, pneumonia, infective endocarditis and osteomyelitis.[1] Moreover, MRSA is responsible for half of the 14 million skin and soft-tissue infections as well as 100,000 serious blood infections and more than 15,000 deaths a year in the United States.[198,199] This often necessitates the use of vancomycin to treat these infections since it has the most reliable antimicrobial activity against MRSA[200,201] and is the last remaining antibiotic which MRSA strains are susceptible to.[197] On the other hand, a small portion of MRSA has started to develop resistance to vancomycin leading to treatment failures in the clinic. For example, a clinical strain of MRSA with reduced susceptibility to vancomycin, *Mu50*, first emerged in Japan in 1996.[200,202] In addition, a similar strain was isolated in United States in 1997.[201,203] The effectiveness of vancomycin as a treatment option is therefore diminishing due to the emergence of these vancomycin-intermediate *S. aureus* (VISA) and vancomycin-resistant *S. aureus* (VRSA) strains. [197]

These antibiotic resistance and persister infections are attributed to formation of sessile bacterial communities, called biofilms. Bacterial biofilms are complex heterogeneous communities embedded in an extracellular polymeric substance (EPS) matrix which is composed of polysaccharides, nucleic acids, proteins and lipids.[180,181] Bacteria undergo a transition from free-living, planktonic cells to sessile, surface-attached biofilms in response to environmental conditions.[181] Sessile bacteria can withstand host immune responses, and they are much less susceptible to antibiotics than their non-attached individual planktonic counterparts. One mechanism of biofilm antibiotic resistance is the

failure of an antibiotic to penetrate the full depth of the biofilm. The biofilm matrix is known to retard the diffusion of antibiotics, and solutes in general diffuse at slower rates within biofilms than they do in water. Another mechanism posits that at least some of the cells in a biofilm experience nutrient limitation and therefore exist in a slow-growing or starved state. Slow growing or non-growing cells are not very susceptible to many antimicrobial agents.[180,181] Formation of these sessile communities provides a resistance mechanism against host immune responses and antibiotics. Therefore, there is an urgent clinical need to develop novel treatments targeting bacterial biofilms to reduce the risk of infection, without resorting to antibiotics for which bacteria are developing a resistance towards.

There is a growing interest in the use of nanotechnology and the use of novel materials with at least one dimension below 100 nm for the treatment of bacterial infections, without resorting to the antibiotics. For instance, many carbon-based nanomaterials such as fullerenes (C60) [203], carbon nanotubes (CNTs) [204,205] and graphene [206] as well as metal-based nanoparticles including silver (Ag) [205,207], gold (Au) [208], magnesium oxide (MgO) [209] and zinc oxide (ZnO) [210] have shown antibacterial properties. Nanoparticles which possess magnetic properties, superparamagnetic iron oxide particles (SPION), have also shown promising bactericidal effects. [169,211] On the other hand, these studies usually targeted planktonic bacterial growth and there are a limited number of studies which actually targeted the bacterial biofilms. [125,170] In addition, as the yield of antibacterial nanoparticle uptake by the biofilm is low, nanoparticles cannot penetrate to the full depth of the biofilm, which creates another problem. [182]

The metabolic microenvironment of the biofilm is crucial and metabolites that can trigger and enable eradication have great potential to improve the treatment of antibiotic-resistant infections in the clinical settings. Changes in the metabolism might alter bacterial susceptibility to antibiotics.[204] As persister bacteria cells enter a metabolic hibernation state and shut down their metabolism, they are able to survive and become resistant to the antibiotic treatment. Recently, it has been shown that specific carbon sources (such as fructose) could be useful to increase the efficiency of antibiotics (i.e., gentamicin) and eradicate the persisters.[179] Persister bacteria are stimulated into an active metabolic state which is enough to uptake the metabolites by recovering the proton-motive force (PMF). As a result, antibiotic uptake by the biofilms increase and then antibiotics enter the bacterial metabolism and cause the death of persister cells. Moreover, it has been recently shown that fructose metabolites enhance the reduction of bacterial growth and biofilm formation on nanorough polyvinyl chloride (PVC) surfaces.[212] Thus, metabolites that can trigger and enable the eradication of biofilms have great potential to treat antibiotic resistant infections in the clinical settings.

In this chapter, without using antibiotics, two novel approaches, i.e. nanotechnology and metabolic stimulation nanomaterial science are integrated to design novel treatments to remove the antibiotic resistant biofilms while improving their efficacy by increasing their uptake by the biofilms, without using antibiotics. A simple, broad-spectrum and low-cost dual-sided approach which uses superparamagnetic iron oxide particles (SPION) in combination with fructose metabolites was developed. First, it was demonstrated that superparamagnetic iron oxide nanoparticles (SPION) can be conjugated with different

metal ions (such as iron, zinc) to eradicate both gram-positive MRSA and gram-negative (i.e., *E. coli* and *P. aeruginosa*) biofilms. These novel nanoparticles also exhibited significantly stronger antibacterial characteristics compared to conventional antibiotics, such as gentamicin, and especially vancomycin, the antibiotic of last resort. Most importantly, for the first time, it is shown that SPION biofilm eradication efficacy was significantly improved in the presence of fructose metabolites due to the increased nanoparticle uptake by the MRSA biofilms, creating a new nanotechnology-driven approach. Thus, this work establishes a simple, broad-spectrum and low-cost strategy for the better eradication of persistent biofilms, as a new therapeutic option to existing antibacterial strategies.

Materials and Methods

3.2.1. Synthesis of Superparamagnetic Iron-Oxide Nanoparticles (SPION)

SPION were synthesized using a variation of the high temperature synthesis method in triethylene glycol (TREG). 2 mmol of iron (III) acetylacetone (**$Fe(acac)_3$**) was dissolved in 25 mL of TREG in a round bottom boiling flask with magnetic stirring. This solution was heated gradually to 278°C and incubated at this temperature for 30 minutes. After this gentle reflux, the solution was cooled slowly to room temperature (**Figure 3.1**).

3.2.2. Conjugating SPION with Metals

After synthesis, SPION were conjugated with 4 mmol dimercaptosuccinic acid (DMSA). DMSA was used as a capping agent, and the solution was incubated overnight for reaction. Then, the synthesized SPIONs were precipitated in 200 mL of 100% ethanol saturated with ammonium sulfate ((NH4)2SO4) and isolated with a strong magnetic field (4" x 1" x 1" thick magnet, 4871 Gauss, and Neodymium; K&J magnetics, Jamison, PA). Particles were then purified several times in ethanol and dried at room temperature. Afterwards, the DMSA capping agent was further conjugated with metals such as silver (Ag), zinc (Zn), and iron (Fe). 10 mg/mL SPION solution was placed in a centrifuge tube and diluted to 1:10 in ethanol with 1 mM or 4 mM salts of AgNO3, ZnCl2, and FeCl3, respectively. Solutions were then incubated on a shaker overnight at 90 rpm. After overnight incubation, nanoparticles were purified by placing the mixture in a magnetic field by a thick magnet parallel to the beaker. The purification step was repeated three

times, and the magnetic field allowed purification of magnetic components, while non-magnetic components were washed away.

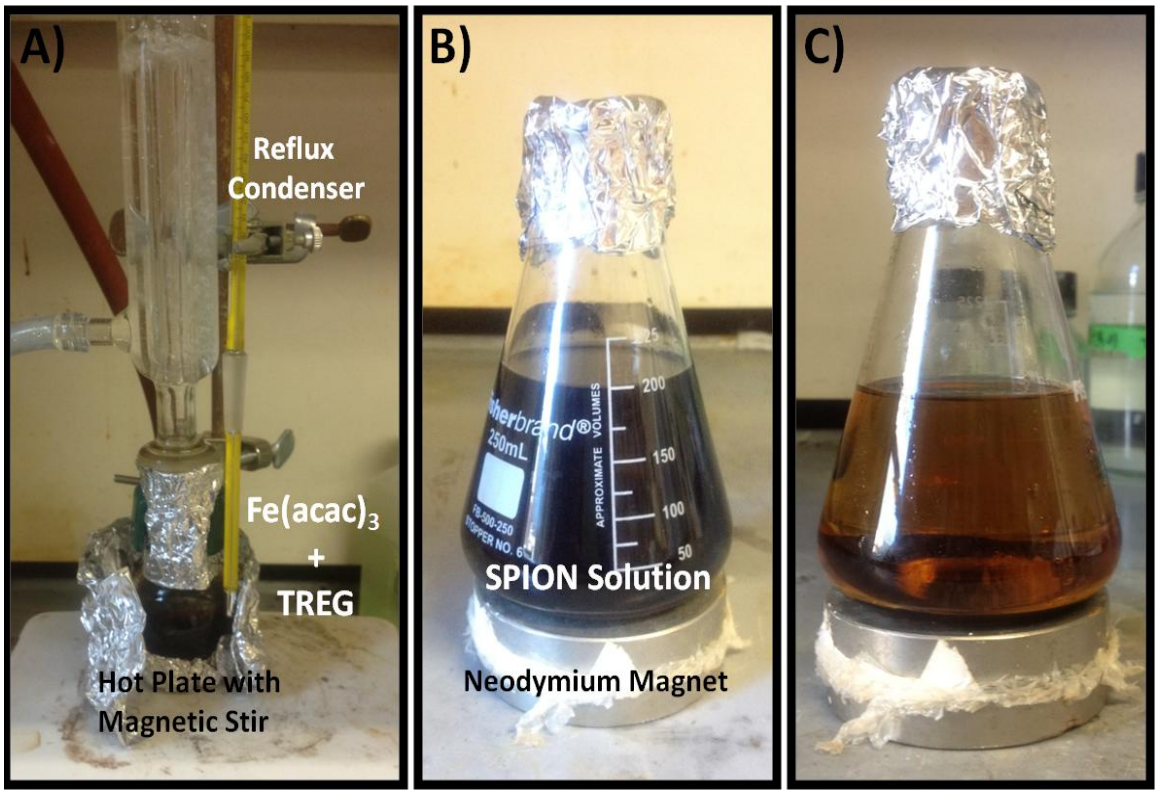

Figure 3.1. Method used for the synthesis and isolation of superparamagnetic iron oxide nanoparticles (SPION). SPION were prepared by high temperature reflux of iron (III) acetylacetonate in triethylene glycol (**A**) in a round bottom boiling flask under magnetic stir while outfitted with a reflux condenser. SPION were isolated in a strong magnetic field produced by two DZX08-N52 neodymium magnets (4" diameter x 1/2" thick magnet) (**B-C**).

3.2.3. Characterization of SPION

SPION morphology was visualized using a transmission electron microscope (TEM). For this, dispersions of SPION were dried on carbon coated copper grids. Samples were imaged by a Philips JOEL 140 kV TEM (Philips, New York, NY). Particle size was calculated by the Image J program, Version 1.41 (National Institutes of Health, Bethesda, MD). In addition, inductively coupled plasma atomic emission spectroscopy (ICP-AES) was used to quantitatively confirm the presence of metals in the purified metal conjugated SPION and concentrations of each metal was compared with the unconjugated SPION. First, standard solutions of iron (Fe^{3+}), zinc (Zn^{2+}), and sulfur ions (S^{2-}) were prepared in a 2% solution of HNO_3 at 100 parts per million (ppm) to obtain a standard curve. 50 µL of unconjugated and metal conjugated SPION solutions were then dissolved by aqua regia (nitric acid and hydrochloric acid at a volumetric ratio of 1:3). The SPION + aqua regia solution was evaporated to dissolve nanoparticles and all metal salts. Then, 5 ml of 2% nitric acid (HNO_3) were added to each SPION+ aqua regia solution and the samples were analyzed. For dynamic light scattering analysis (DLS), unconjugated (UC), iron and zinc conjugated SPION were diluted 1:1000 in double deionized water after they were sterile filtered by a 0.2 µm filter (Corning; low protein binding #431219). A Zetasizer Nano ZS (Malvern Instruments) was used and five readings were taken for each sample. In addition, magnetization measurements were performed using vibrating sample magnetometry (VSM, LakeShore 7400; Chicago, IL, USA) at T= 300 K. To prepare samples for VSM, SPION were centrifuged and the supernatant was discarded. Then, nanoparticles were dispersed in ethanol, centrifuged again and the supernatant was discarded. Isolated nanoparticles were dried at room

temperature for several days. Nanoparticle powders were weighed and then placed in a capsule for hysteresis experiments at T= 300 K.

3.3.4. Bacteria Culture

A *Mu50* strain of MRSA (ATCC #**700699**, American Type Culture Collection, Mannassas, VA) was hydrated and streaked for isolation on a tryptic soy agar plate. Following growth, a single isolated colony was selected and inoculated in 3 mL of tryptic soy broth (TSB) media (MP Biomedicals, Solon, OH). The bacteria culture was grown on an incubator shaker for 18 hours at 37^0C at 200 revolutions per minute (rpm) until it reached the stationary phase.

3.3.5. Biofilm Growth and Treatment

Overnight cultures which had an optical density of 0.52 at 562 nm were diluted at a ratio of 1:90 in fresh TSB, corresponding to a 10^8 cells/mL solution. 200 µL of this solution was inoculated onto each well of a 96-well microtiter plate (Fisher Scientific, Pittsburgh, PA) and incubated for 24 hours at 37^0C to allow for biofilm formation. After 24 hours, the culture medium was replaced with 1 mg/mL of unconjugated (UC) and metal conjugated SPION in fresh TSB solution. In addition, different concentrations of a fructose solution (1 and 10 mM) were added to the SPION+TSB solution to investigate the effect of fructose on magnetic nanoparticle action. To compare the inhibitory properties of the synthesis components or a panel of antibiotics including vancomycin, gentamicin and to SPION, such components were tested under the same experimental design. 1 mg/mL vancomycin and gentamicin were sterilized with a sterile, 0.2 µm PTFE filter (Fisher Scientific, Pittsburgh, PA). After 24 hours of treatment, planktonic bacteria

growth was assessed by measuring optical density at 562 nm. In addition, the amount of biofilm remaining was assayed by crystal violet (CV) staining or viable cell counting, as described below (**Figure 3.2**).

3.2.6. Crystal Violet (CV) Staining Assay

CV staining was used to quantify biofilm density after 24 hours of treatment. First, the TSB culture medium was removed and each well was rinsed with 1X PBS. Then, 200 µL of a 0.1% CV solution in water was added to each well and incubated for 15 minutes. Then, wells were rinsed three times with 175 µL of PBS. The plate was air dried at room temperature for two days. Then, CV was dissolved in 200 µL of 100% ethanol, and optical density was measured at 562 nm. Optical readings of control solutions with SPION or antibiotics, but without bacteria, were subtracted from the corresponding readings.

3.2.7. Viable Cell Count Assay

Viable bacteria cell counts were obtained by disrupting biofilms formed at the bottom of the microtiter plate in a sonicating water bath. First, a 96-well microtiter plate was rinsed three times with 200 µL of 1X PBS. 150 µL of 1X PBS was added into each well and the microtiter plate was covered with a sterile tape. The plate was placed in an Ultrasonics 5510 sonic water bath (Branson, Danbury, CT) and sonicated for 30 min at 40 kHz to dislodge biofilms into the PBS solution. Then, serial dilutions were performed and 10 µL of each dilution was spot-plated on tryptic soy agar (TSA) plates. Colony forming units (CFU) were counted after overnight incubation at 37°C.

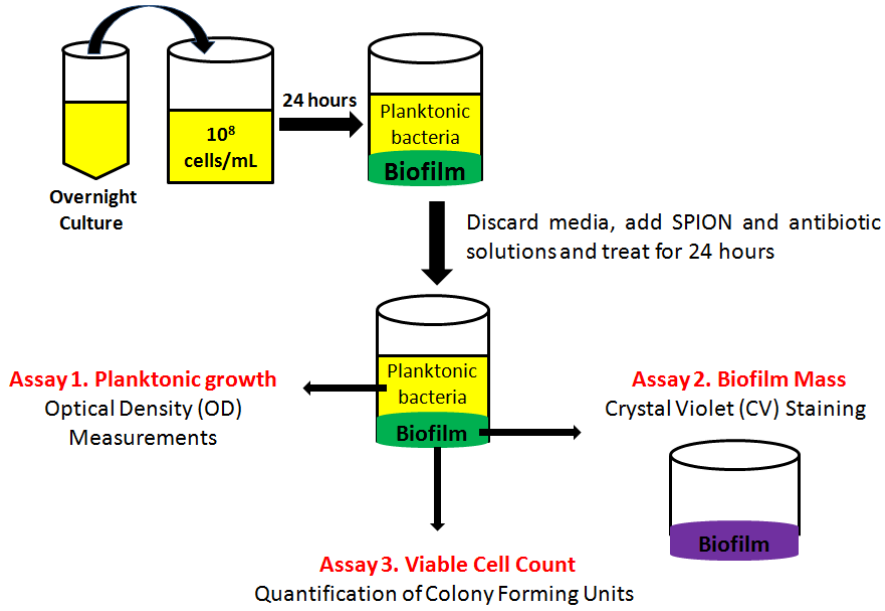

Figure 3.2. Schematic of *in vitro* screening assays used in the study. A single colony of *Mu50* strain of MRSA was grown in 3 mL of TSB for 18 hours at 37^0C, 200 rpm. Then, 200 µL of a 10^8 cells/mL solution was inoculated into each well of a 96-well microtiter plate. Thus, biofilms were established as some portion of inoculated bacteria attached to the surface of the plate during 24 hours incubation. After 24 hours, the culture medium was replaced with unconjugated and metal conjugated SPION in TSB. In addition, different concentrations of a fructose solution (1 and 10 mM) were added to the SPION+TSB solution to investigate the effect of fructose on magnetic nanoparticle action. After 24 hours of treatment, three different assays were used to assess SPION activity on the MRSA biofilms. Optical density was measured at 562 nm ($OD_{562\ nm}$) to assess planktonic (free floating) bacteria growth within the solution (**Assay 1**). In addition, crystal violet (CV) staining was performed to quantify biofilm mass (**Assay 2**) and viable cell counts were performed to quantify colony forming units (CFU/mL) (**Assay 3**). To compare SPION action with conventional antibiotics, 1 mg/mL of vancomycin and gentamicin were tested using the same experimental design.

3.2.8. Iron Uptake and Deposition into the Biofilm

The amount of iron deposited into the biofilms was qualitatively determined by a Prussian blue assay, a histology stain creating a blue by-product in the presence of iron. MRSA biofilms were grown for 48 hours using overnight by inoculating 0.5 mL of a 10^8 cells/mL solution in a 12 well plate on glass slides. Then, the biofilms were treated with 1 mg/mL of unconjugated SPION (UC) and 1 mM metal conjugated SPION (Fe1 and Zn1) in fresh TSB solution for 24 hours. In addition, different concentrations of a fructose solution (1 and 10 mM) were added to the SPION+TSB solution to investigate the effect of fructose on SPION deposition in the biofilm. Untreated biofilms were used as controls. Prussian blue staining was carried out using a 10% solution of potassium ferrocyanide mixed just prior to staining with an equal proportion of 10% hydrochloric acid (HCl) (this combination reacts and produces a blue colored precipitate in the presence of iron). 1 mL of this mixture was added to the biofilm and allowed to react with the MRSA biofilms for 15 minutes. After 15 minutes of incubation, samples were washed three times with PBS to get rid of the excess potassium ferrocyanide (C6N6FeK4) and HCl solution. Iron deposition within the MRSA biofilms was qualitatively analyzed based on the amount of blue staining. In addition, the intensity of blue color was quantified by Image J, Version 1.45s.

3.2.9. Analysis of SPION uptake by the Biofilm

The amount of SPION taken up by the biofilm was measured by inductively coupled plasma atomic emission spectroscopy (ICP-AES) via quantifying the presence of iron (Fe^{3+}), sulfur (S^{2-}) and zinc (Zn^{2+}) ions. As previously described, MRSA biofilms were grown in 96-well plates and they were treated with unconjugated (UC), iron (Fe1) and

zinc (Zn1) conjugated SPION for additional 24 hours. After 24 hours, each well was washed three times with PBS to remove SPION that were not taken up by the biofilms or SPION which were membrane-unbound. Then, the biofilms were digested in a 50% nitric acid (HNO_3) solution[182] and the microtiter plate was shaken for 30 minutes at 150 rpm. Then, 200 µL of acid digested bacteria solution were then diluted in 2% nitric acid solution and samples were analyzed by ICP-AES. The amount of iron (Fe^{3+}), sulfur (S^{2-}) and zinc (Zn^{2+}) ions in SPION treated biofilms were compared with untreated control samples.

3.2.10. TEM imaging of Bacteria after SPION Treatment

Bacterial cells were grown in vitro for 24 hours using overnight inoculums. Then, bacteria were treated with 1 mg/ml of unconjugated SPION for two hours, and the supernatant was collected. The cells were then rinsed with 1 ml of phosphate buffered saline, and the supernatant was collected. Then, the supernatant was centrifuged at 5000 rpm for 5 minutes, and fixed with 2.5% glutaraldehyde in 0.1M sodium cacoadylate buffer at pH 7.4 with 0.1M sucrose, then gently agitated, and resuspended for 1 hour. After 1 hour, the pellet was rinsed three times with the buffer solution (Electron Microscopy Sciences, Hatfield, PA), followed by resuspension in 1% osmium tetraoxide (Electron Microscopy Sciences, Hatfield, PA) as a contrast agent in buffer. A firm pellet was formed after centrifugation at 10,000 rpm for 5 minutes. The pellet was then rinsed in deionized water three times, suspended in 2% agar. The water within the samples was removed by successive ethanol rinses of 25%, 50%, 75%, 95%, 100%, 100%, and 100%, allowing between 20-40 minutes for each stage. Finally, the pellet was fixed with resin

(Electron Microscopy Sciences, Hatfield, PA) using successive curing stages in ethanol of 1:2, 1:1, 3:1, and finally 100% resin which was cured for 18 hours at 60°C.

3.2.11. Statistical Analysis

All experiments were performed in triplicate and repeated at least three times to validate repeatability and reproducibility. Data are represented as the mean ± standard error of the mean (SEM). Results were analyzed for statistical significance using analysis of variance (ANOVA) followed by a Student's t-test. Three different significance levels ($p < 0.01$, $p < 0.05$, and $p < 0.1$) were noted.

3.3. Results and Discussion

3.3.1 Characterization of Magnetic Nanoparticles

3.3.1.1. Characterization of SPION Morphology

Figure 3.3a shows the unconjugated SPION (UC) morphology as characterized by transmission electron microscopy (TEM). Unconjugated SPION were synthesized using a variation of the high temperature synthesis method in triethylene glycol (TREG). To increase the solubility and dispersion of the nanoparticles, SPION were chelated with dimercaptosuccinic acid (DMSA) as it has been previously shown that SPION coated with DMSA possess increased solubility and dispersion in water, cell medium and physiological fluids.[213]

SPION as produced could not be separated from solution with a magnet because of their small size and because they did not form agglomerates, so 175 mL of 100% ethanol saturated with ammonium sulfate was added, producing larger agglomerates which could then be isolated. DMSA is also known to form disulfide bonds, so SPION were refrigerated and stored in 100% ethanol to prevent oxidation. These SPION prior to coating were well dispersed in bacterial cell media. TEM analysis demonstrated that the dispersed nanoparticles were successfully synthesized with an average size of 9.92 ± 3.14 nm without large scale aggregation (**Figure 3.3a**). This analysis showed that SPION could be synthesized with DMSA as a capping and coating agent.

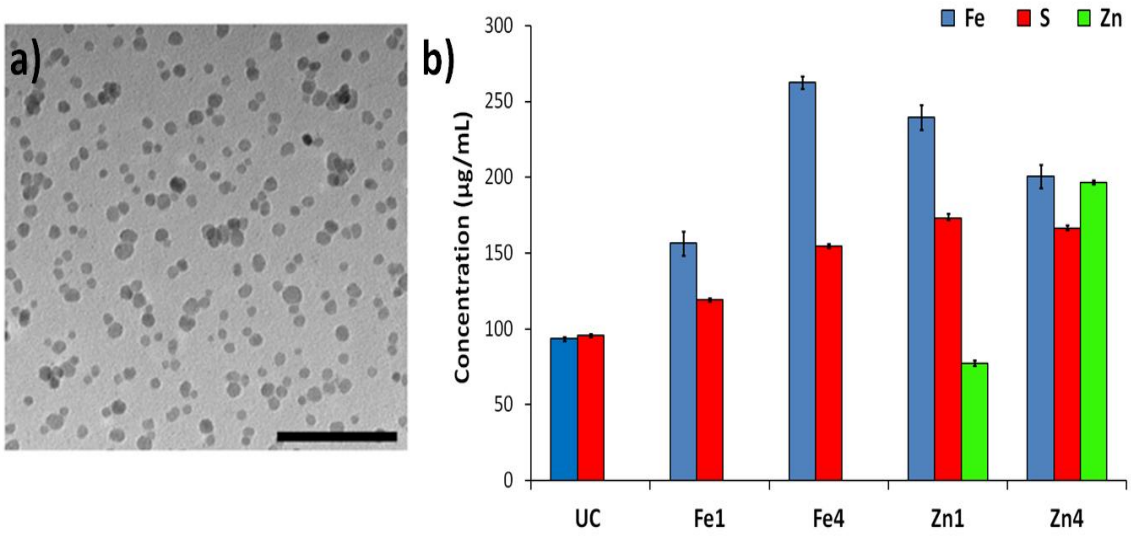

Figure 3.3. **a)** TEM image of unconjugated SPION (UC) prepared by refluxing Fe $(acac)_3$ in a TREG solution. TEM analysis demonstrated that dispersed nanoparticles were successfully synthesized and had an average size of 9.92 ± 3.14 nm (scale bar = 100 nm). **b)** Elemental composition of unconjugated and metal (Fe, Zn) conjugated SPION determined by ICP-AES. 10 mg/mL of a SPION solution (UC) was conjugated with 1 mM or 4 mM salts of $FeCl_3$ (Fe1, Fe4) and $ZnCl_2$ (Zn1, Zn4), respectively. The concentration of iron (Fe^{3+}) and zinc (Zn^{2+}) ions increased as the metal salt conjugations increased from 1 mmol (Fe1 and Zn1) to 4 mmol (Fe4 and Zn4). Data represents mean ± standard error of the mean (SEM), N = 3.

3.3.1.2. Chemical Composition of SPION

The analysis of SPION chemical composition by inductively coupled plasma atomic emission spectroscopy (ICP-AES) showed that the metal salt conjugations were successful (**Figure 3.3b**). Increased sulfur concentration (S^{2-}) indicated that DMSA attached to the unconjugated SPION (UC) surface, and increases in iron (Fe^{3+}) and zinc (Zn^{2+}) concentrations indicated that these metals were successfully conjugated. Moreover, the concentration of iron (Fe^{3+}) and zinc (Zn^{2+}) ions increased as the metal salt conjugations increased from 1 mmol (denoted as Fe1 and Zn1) to 4 mmol (denoted as Fe4 and Zn4, respectively).

3.3.1.3. Zeta Potential for Surface Charge of SPION

The zeta potential of the zinc conjugated SPION decreased to -43.2 mV compared to -35.5 mV for unconjugated SPION, while the zeta potential of iron conjugated SPION increased to -34.0 mV (**Table 1**). Changes in the zeta potential might indicate that zinc metals were incorporated into the polydisulfide layer within DMSA while iron metals were associated with DMSA the surface, resulting in an increase in the zeta potential compared to unconjugated SPION (UC).

3.3.1.4. Dynamic Light Scattering (DLS) Analysis of SPION Size

Dynamic light scattering analysis indicated zinc conjugated SPION had a similar size (19.67 ± 0.72 nm) while iron conjugated SPION were larger (23.3 ± 1.17 nm) compared to unconjugated SPION (UC) (19.93 ± 1.31 nm) (**Table 1**).

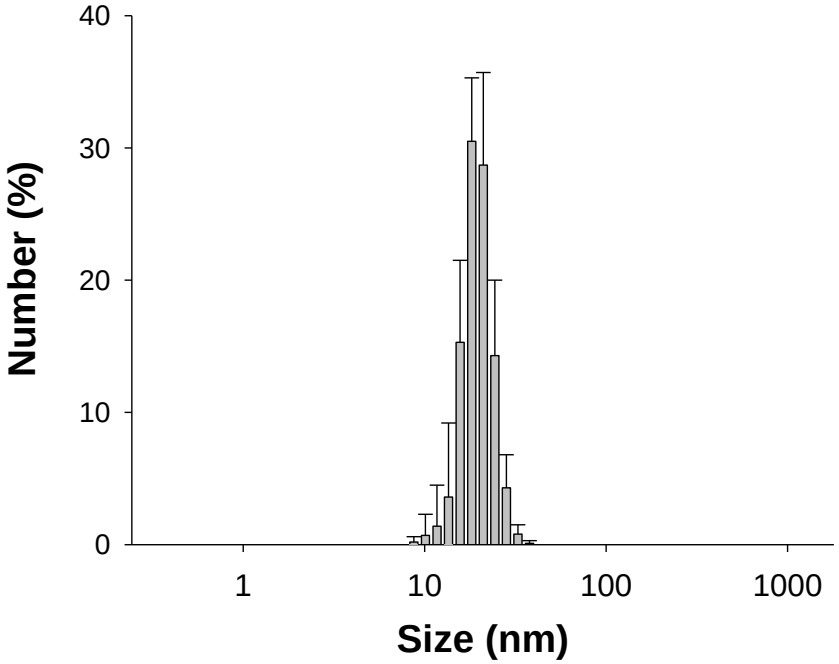

Figure 3.4. DLS analysis of unconjugated SPION. The average size was 19.93 ± 1.31 nm.

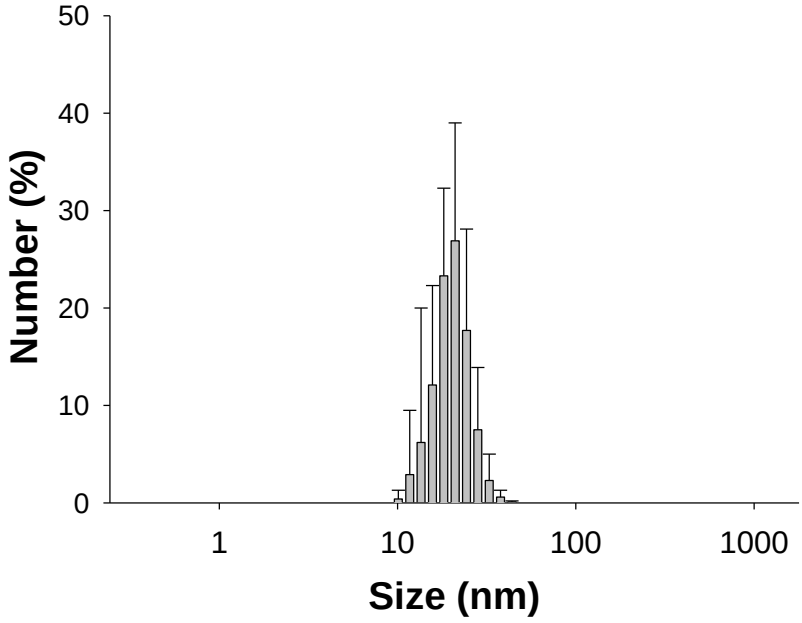

Figure 3.5. DLS analysis of iron-conjugated SPION. The average size was 23.3 ± 1.17 nm.

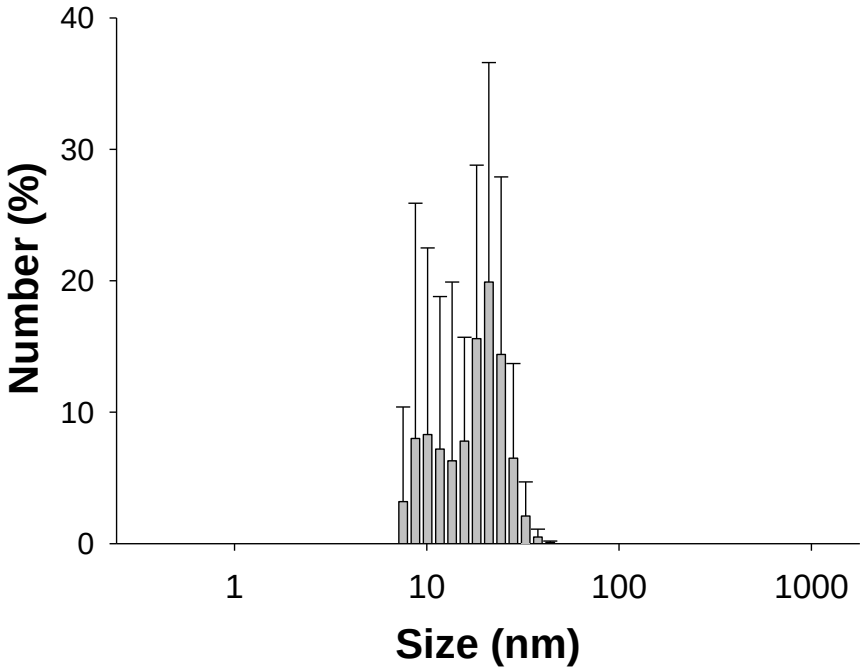

Figure 3.6. DLS analysis of zinc-conjugated SPION. The average size was 19.67 ± 0.72 nm.

3.3.1.5. Magnetic Properties of SPION

In addition, the magnetic properties of the dried unconjugated and conjugated SPION were assessed using vibrating sample magnetometry. The superparamagnetic properties of the nanoparticles were preserved after the metal conjugations, which is a desired property to specifically target the nanoparticles to the infection sites (**Table 1**). Unconjugated SPION (UC) showed saturation magnetization of 58.625 emu/g, which corresponds to 63.7% of the magnetic moment of bulk magnetite (Fe_3O_4) (92 emu/g).[214] On the other hand, the saturation magnetization of zinc and iron conjugated SPION were lower than that in the unconjugated SPION (UC) to ~25% of Fe_3O_4, 23.875 emu/g and

22.635 emu/g, respectively. This could be due to a number of reasons. First, it could be due to the incorporation of non-magnetic ions during synthesis. Another reason could be the changes in the crystal structure of some iron from magnetic maghemite (γ-Fe_2O_3) or non-magnetic hematite (FeO). For example it is known that DMSA will oxidize the surface of Fe3O4 during the coating process. DMSA is also a chelator, so addition of other metals could modify this oxidation process and might change the crystal structure. In addition, other studies in the literature observed a decrease in magnetic properties when SPION were coated with different metals.[124] For example, gold- and silver-coated SPION had a lower magnetic moment compared to bare SPIONs due to their higher shell thickness.[124] Moreover, it has been shown that the magnetic properties of SPION depend on particle size.[215,216] Smaller nanoparticles tend to have a larger magnetic moment.[216] As the iron- and zinc-conjugated SPION are larger compared to unconjugated SPION, their magnetic properties might decrease. Decreases in magnetic saturation could be due to the incorporation of non-magnetic metal ions or to the increased size of the zinc or iron conjugated SPION. Thus, the present analysis indicated that the magnetic properties of the multifunctional SPION used in this study were in the range for various biomedical applications, 20-30 emu/g[217] and are adequate for particle penetration within the bacterial biofilms.

Table 3.1. Characterization of size, zeta potential and magnetic moment of the different magnetic nanoparticles used in this study. (emu/g = electromagnetic units per gram).

	Mean Size	Zeta Potential	Magnetic Moment
Unconjugated SPION	18.17 ± 1.34 nm	-35.5 ± 3.55 mV	58.625 emu/g
Iron-conjugated SPION	27.69 ± 1.20 nm	-34.0 ± 3.40 mV	23.875 emu/g
Zinc-conjugated SPION	19.67 ± 0.72 nm	-40.1 ± 0.40 mV	22.625 emu/g

3.3.2. Antibacterial Studies

The antibacterial and anti-biofilm activity of SPION were then evaluated against the Mu50 strain of *S. aureus* (MRSA) biofilms. The effect of conjugated metal concentrations on SPION by conjugating with different concentrations (1 mM and 4 mM) of iron and zinc were investigated. Moreover, the inhibitory effects of SPION were compared to different conventional antibiotics including gentamicin, and vancomycin. A novel and high throughput *in vitro* screening assay was developed to assess the activities of different nanoparticles and antibiotics against both planktonic (free-floating) MRSA and MRSA biofilms (Figure 2). First, biofilms were established as the inoculated bacteria attached to the surface of a microtiter plate during 24 hours of incubation. The initial bacteria concentration used to establish biofilms was 10^8 CFU/mL, which is similar to the lethal dose (LD_{50}) of MRSA infections (3-5 * 10^7 CFU/mL).[218] After 24 hours, the biofilms were treated with 1 mg/mL of unconjugated (UC), 1mM and 4 mM iron conjugated SPION (Fe1 and Fe4) as well as 1mM and 4 mM zinc conjugated SPION (Zn1 and Zn4). In addition, different concentrations of the fructose solution (1 mM and 10 mM) are added to the SPION treatments to investigate the effect of carbon sources on the antibacterial activity of magnetic nanoparticles. After 24 hours of treatment, SPION antibacterial and anti-biofilm activity was accessed by analyzing the planktonic MRSA growth, MRSA biofilm mass and viable bacteria within the biofilms.

3.3.2.1. The Effect of Fructose on MRSA Growth

The effect of fructose concentration (1 mM, 10 mM, 50 mM and 100 mM) on the planktonic MRSA growth was investigated after 24 hours. Optical density was measured every four minutes to get the bacterial growth curves. Presence of fructose in the culture medium did not increase the planktonic growth over 24 hours (**Fig. 3.7**). Moreover, bacterial growth was quantified by colony forming units. According to this analysis, biofilm formation did not increase in the presence of fructose metabolites after 24 hours (**Fig. 3.8**). Thus, the presence of metabolites in the culture medium has no significant effect on MRSA growth or biofilm formation.

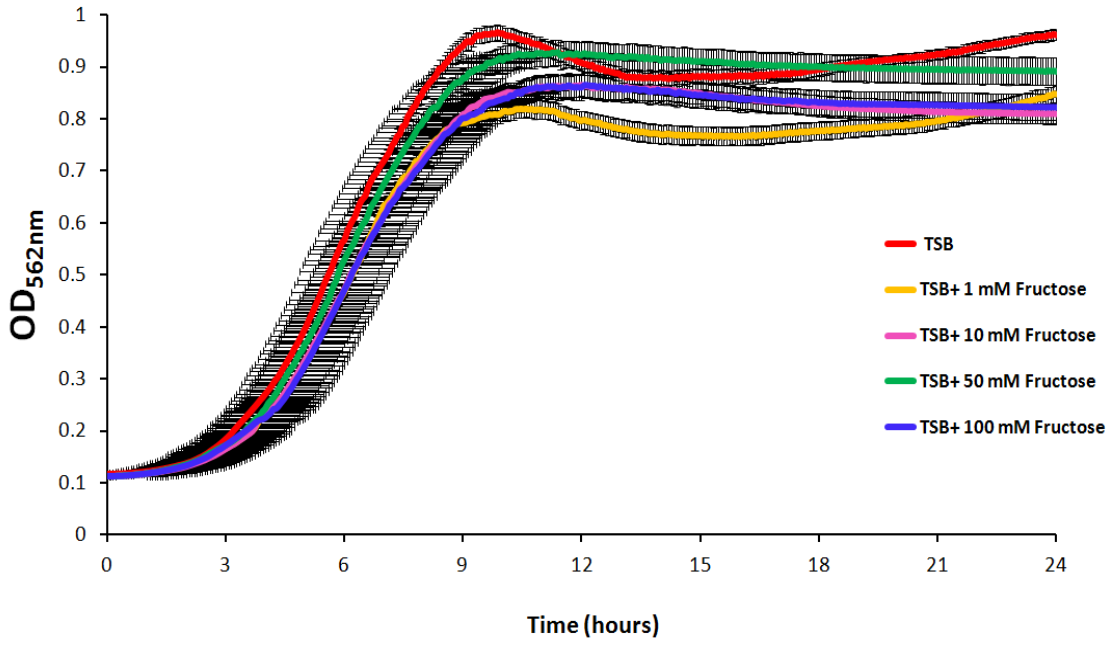

Figure 3.7. The effect of fructose concentration on the planktonic growth of *Mu50* strain (MRSA). Bacterial growth was quantified by continuous optical density measurements for 24 hours. The presence of fructose in the culture medium did not significantly affect the planktonic growth of MRSA over 24 hours.

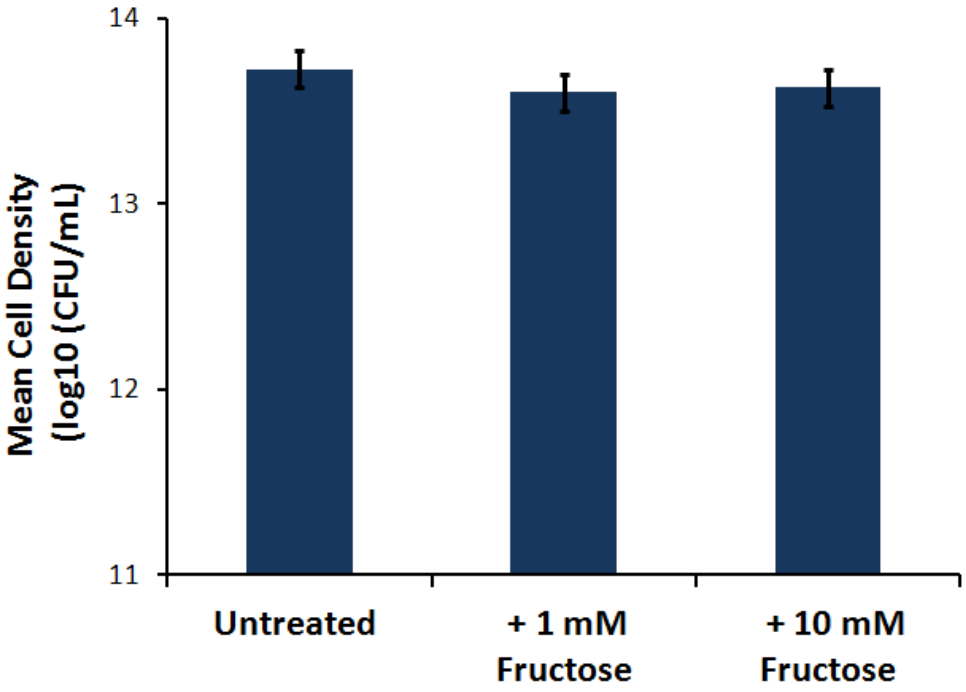

Figure 3.8. The effect of fructose concentration on the planktonic growth of *Mu50* strain (MRSA). Bacterial growth was quantified by colony forming units. Presence of fructose in the culture medium did not increase the biofilm formation over 24 hours.

3.3.2.2. SPION Activity Against Planktonic MRSA Growth

Activity of 1 mg/mL unconjugated (UC) and metal conjugated (Fe1, Fe4, Zn1, Zn4) SPION was compared with the same concentration of antibiotics, gentamicin and vancomycin in the absence or presence of a fructose solution (**Figure 3.9**). 1 mg/mL of dry weight unconjugated SPION (UC) corresponded to an iron concentration of 233.55 ± 51.18 µg/mL whereas 1 mg/mL dry weight of iron-conjugated SPION (Fe1) had an iron concentration of 270.72 ± 42.14 µg/mL. In addition, 1 mg/mL of dry weight zinc-conjugated SPION (Zn1) had a zinc concentration of 61.03 ± 6.13 µg/mL. Vancomycin

and unconjugated SPION (UC) significantly decreased the planktonic bacteria growth with and without a fructose solution ($p < 0.001$). Metal conjugated (Fe1, Fe4, Zn1, Zn4) SPION better eradicated the planktonic bacteria ($p < 0.001$), compared to unconjugated SPION. Moreover, metal-conjugated SPION better inhibited planktonic bacteria growth compared to vancomycin ($\phi\ p < 0.01$).

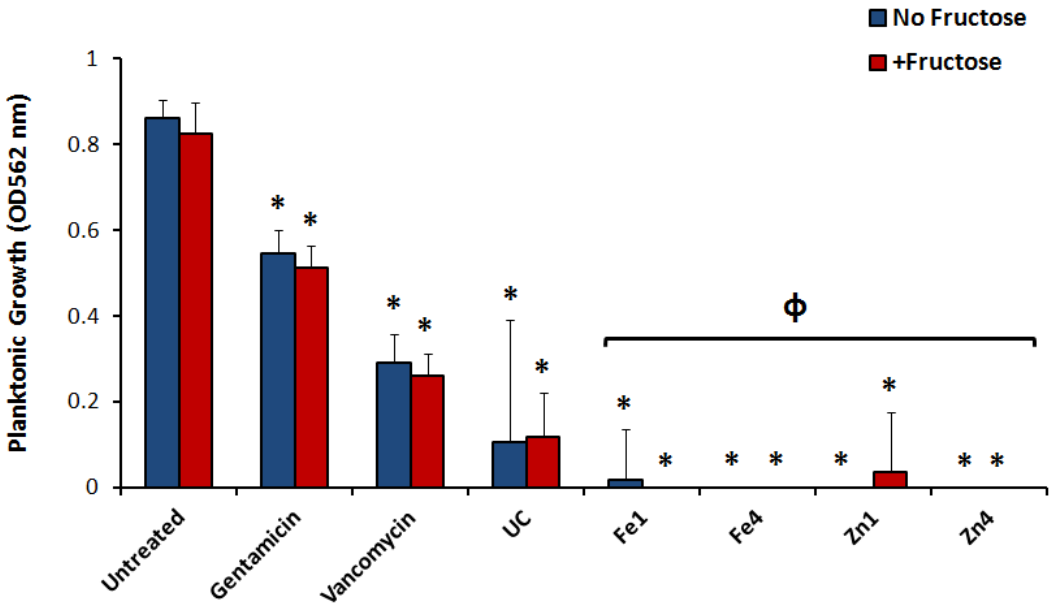

Figure 3.9. SPION activity against planktonic MRSA growth after 24 hours. Unconjugated (UC) and metal-conjugated (Fe1, Fe4, Zn1 and Zn4) SPION significantly decreased the growth of planktonic bacteria (* $p < 0.001$). Metal-conjugated SPION had improved antibacterial activities compared to vancomycin ($^{\phi}\ p < 0.01$). Data represents mean ± standard error of the mean (SEM), N = 3.

3.3.2.3 Anti-Biofilm Properties of SPION in the Presence of Fructose Metabolites

The anti-biofilm activity of 1mg/mL SPION against the MRSA biofilms after 24 hours with and without 1 mM and 10 mM fructose solution were then evaluated (**Figure 3.10**). A 6.34 ± 0.77 order of magnitude decrease in viable bacteria counts was observed when MRSA biofilms were treated with unconjugated SPION (UC) ($p < 0.001$). In addition, conjugating with 1 mM and 4 mM Fe^{3+} (Fe1 and Fe4) as well as Zn^{+2} (Zn1 and Zn4) further decreased viable MRSA within the biofilm ($p < 0.001$). In addition, conjugating SPION with 1 mM and 4 mM Fe^{3+} (Fe1 and Fe4) as well as Zn^{+2} (Zn1 and Zn4) further decreased viable MRSA within the biofilm ($p < 0.001$). For example, a 6.62 ± 0.76 log reduction was observed when MRSA biofilms were treated with Fe1, while treatment with Fe4 increased the anti-biofilm activity to a 6.57 ± 0.63 log reduction. In addition, the anti-biofilm activity of zinc-conjugated SPION was significantly improved when the metal conjugation concentrations increased from 1 mM to 4 mM ($p < 0.05$). A 6.87 ± 0.99 log reduction was observed when MRSA biofilms were treated with Zn1, while Zn4 treatment increased the anti-biofilm activity to a 7.15 ± 0. 91 log reduction (which corresponds to a ~ 0.3 log or 46.8±7.8% increase in activity).

Next, the effect of fructose metabolites on SPION anti-biofilm activity was investigated against MRSA biofilms (**Figure 3.10**). It has been recently shown that the addition of specific metabolites (i.e., fructose) to the biofilm extracellular microenvironment could sensitize the persister cells and potentiate the activity of antibiotics.[179] The persister

bacteria are primed to uptake the metabolites which enables bacteria killing by the antibiotics. Moreover, fructose metabolites enhanced the reduction of bacterial growth and biofilm formation on nanostructured polyvinyl chloride (PVC) surfaces.[219] Most significantly, for the first time, it was observed that the anti-biofilm efficacy of unconjugated SPION (UC) ($p < 0.05$) as well as 1 mM Fe^{3+} conjugated SPION (Fe1) ($p < 0.05$) and 1 mM Zn^{+2} conjugated SPION (Zn1) conjugated SPION ($p < 0.01$) against MRSA biofilms was significantly increased when fructose metabolites were present as carbon sources (The representative colony forming units observed for the same dilution for the untreated biofilm vs. SPION treated biofilms during the viable cell count experiments are shown in **Figure 3.11**). For example, there was a 81% increase in anti-biofilm efficacy when 1 mM fructose was added to the 1 mg/mL unconjugated SPION (UC) treatment. The efficacy was further improved when 1 mM fructose was added to the 1 mM iron-conjugated SPION (Fe1) treatment, which resulted in a 65.5% increase in antibacterial activity, compared to Fe1 treatment alone. Moreover, 10 mM fructose improved the efficacy of 1 mM zinc conjugated SPION (Zn1) by 22.7 %. On the other hand, the presence of fructose metabolites did not potentiate the efficacy of 4 mM iron (Fe4) or zinc (Zn4) conjugated SPION, which might indicate that there is a maximum iron/metabolite and zinc/metabolite concentration threshold in the bacterial metabolism to cause cell death.

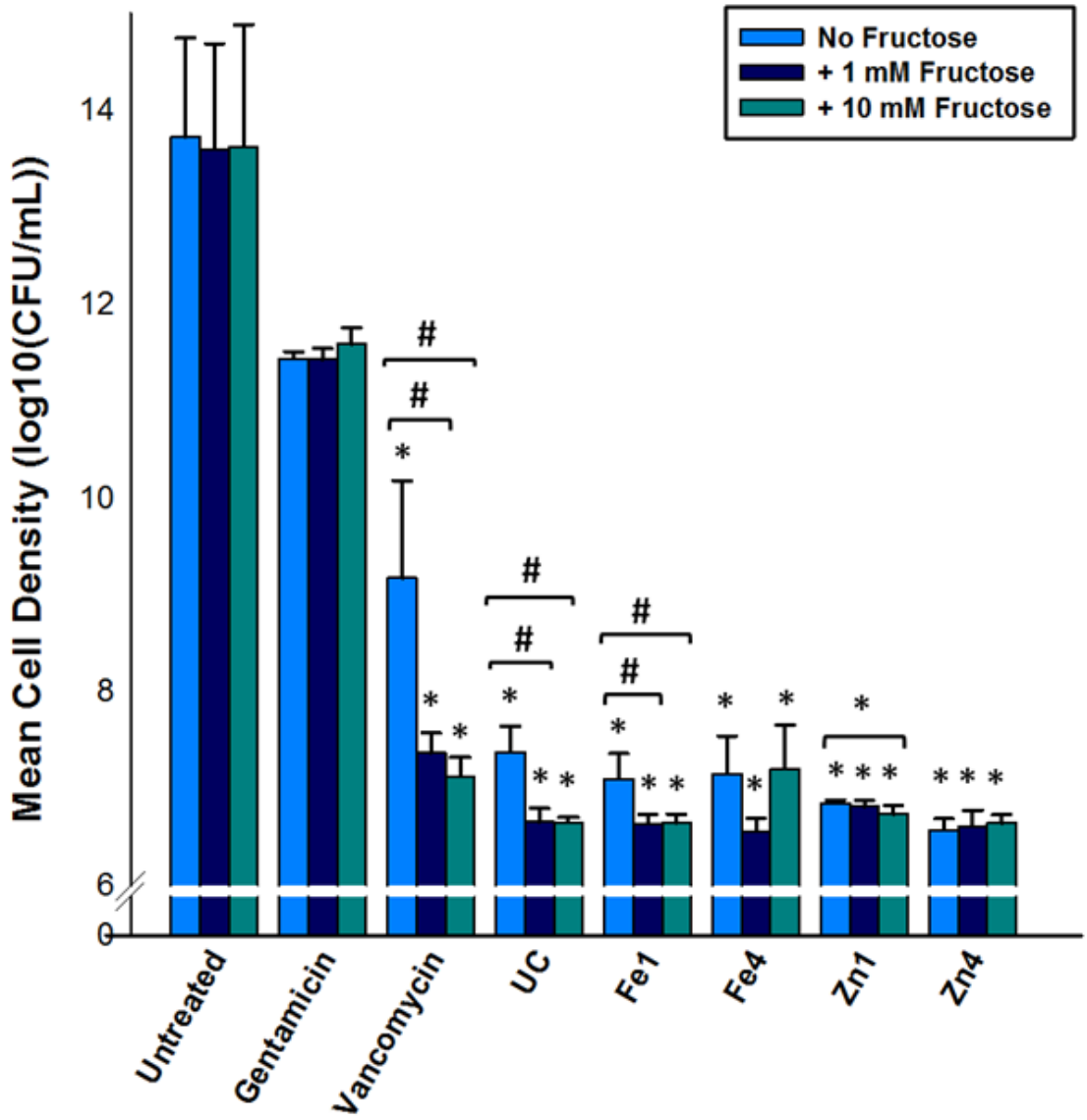

Figure 3.10. Enhanced anti-biofilm activity of SPION treatment in the presence of fructose metabolites. The anti-biofilm activity of 1mg/mL SPION against MRSA biofilms after 24 hours with and without 1 mM and 10 mM fructose solutions. The anti-biofilm efficacy of unconjugated SPION (UC) as well as 1 mM iron-conjugated SPION (Fe1) and 1 mM zinc-conjugated SPION (Zn1) against MRSA biofilms was significantly enhanced when fructose metabolites were added to the treatment. Data represents mean ± SEM. N = 3. *$p < 0.001$ compared to untreated biofilms; # $p < 0.05$ and ** $p < 0.01$ compared to the same treatment without fructose.

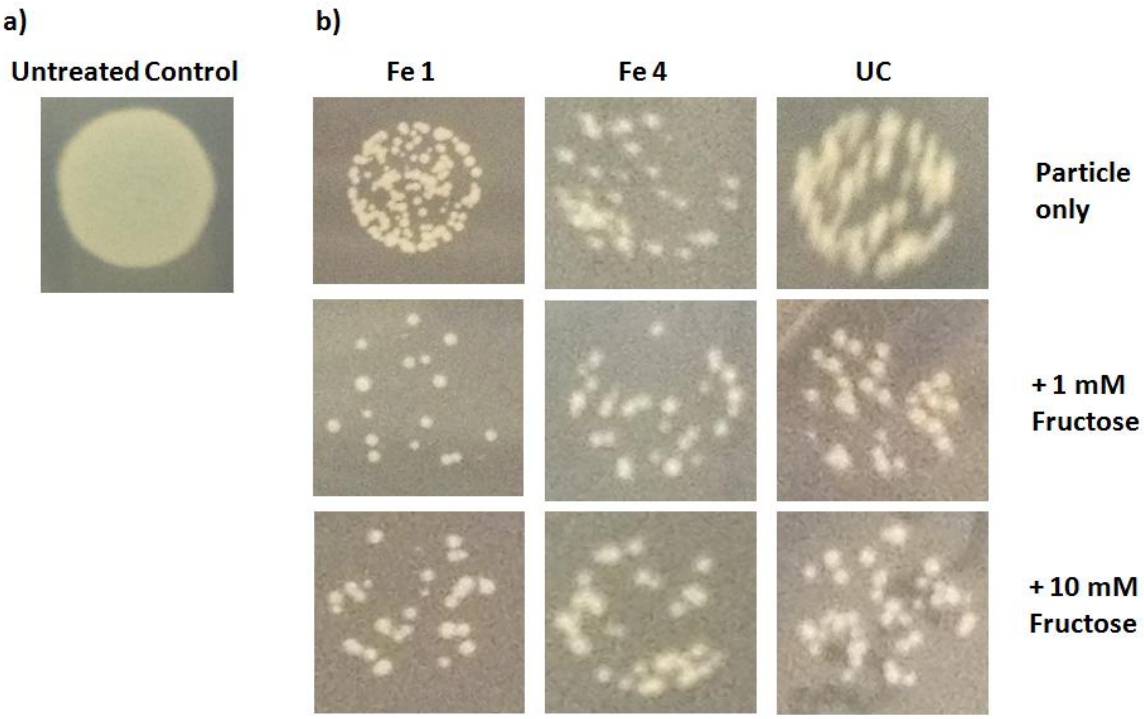

Figure 3.11. Representative colony forming units observed for the same dilution during the viable cell count experiments. a) Representative picture for an uncountable colony of untreated MRSA biofilm at a 10^{-5} dilution. b) On the other hand, countable colonies were observed at the same dilution (10^{-5} dilution) when biofilms were treated with 1 mg/mL of unconjugated (UC) and 1 mmol and 4 mmol Fe^{+3} conjugated SPION (Fe1 and Fe4) treated MRSA biofilms in the presence and absence of a fructose solution. SPION significantly eradicated the MRSA biofilms. Moreover, 1 mM and 10 mM of a fructose solution clearly increased the eradication efficacy of UC and Fe1 on MRSA biofilms.

3.3.2.4. Fluorescent Microscope Analysis of Biofilms

The MRSA biofilms were grown on glass slides for 24 hours. Then, biofilms were treated with unconjugated (UC) as well as iron and zinc-conjugated SPION for an additional 24 hours. Representative fluorescence microscope images clearly demonstrated that unconjugated SPIONM disrupted the biofilms and the eradication efficacy was improved in the presence of fructose (**Figure 3.12**). Moreover, iron and zinc-conjugated SPION disrupted the biofilms better than the unconjugated SPION and eradication was further improved when fructose metabolites were added to the SPION treatment after 24 hours (**Figure 3.13 and 3.14, respectively**).

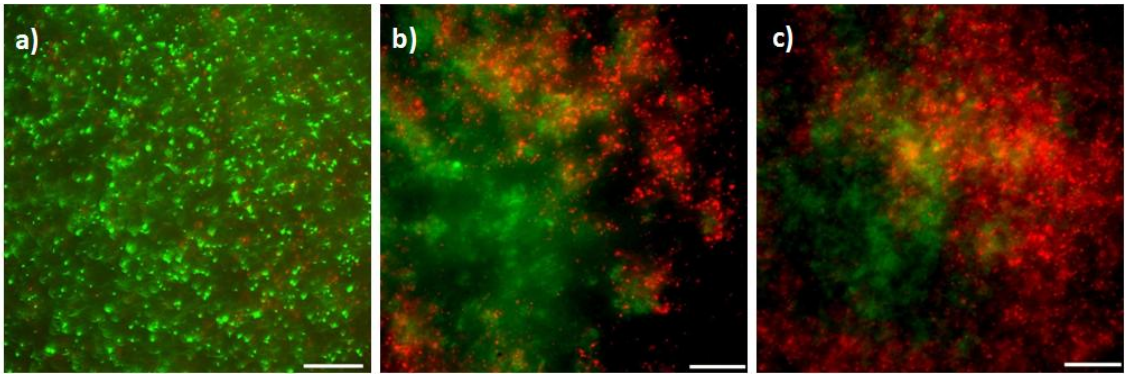

Figure 3.12. Fructose metabolites improved the eradication efficacy of unconjugated SPION (UC) against MRSA biofilms (b and c, respectively) after 48 hours, as compared to control biofilms (a). Live (green) and dead (red) cells were stained with BacLight Live/Dead utilizing Syto9 and propidium iodide stains. Scale bars represent 20 µm.

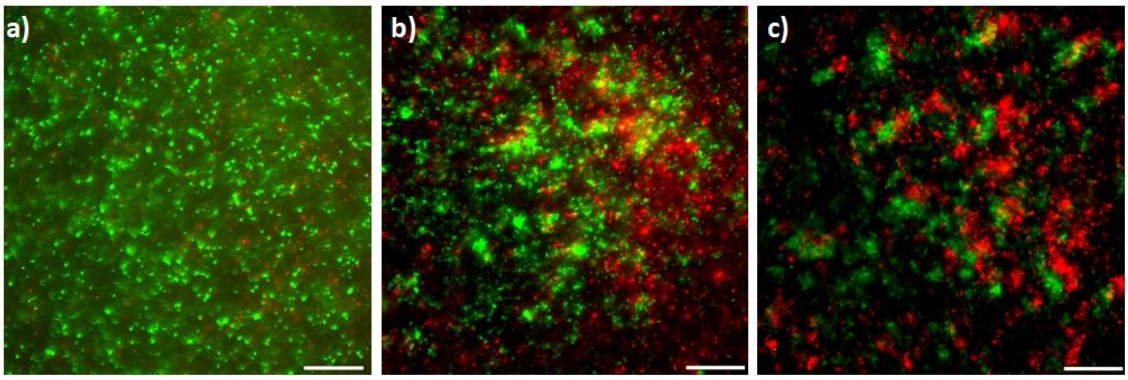

Figure 3.13. 1 mM of fructose metabolites improved the eradication efficacy of iron-conjugated SPION (Fe1) against MRSA biofilms (b and c, respectively) after 48 hours, as compared to control biofilms (a). Live (green) and dead (red) cells were stained with BacLight Live/Dead utilizing Syto9 and propidium iodide stains. Scale bars represent 20 µm.

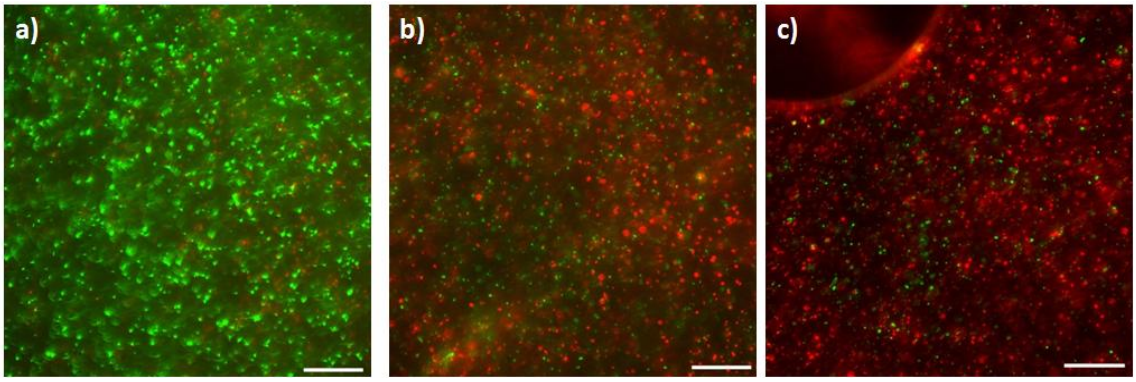

Figure 3.14. 10 mM of fructose metabolites improved the eradication efficacy of zinc-conjugated SPION (Zn1) against MRSA biofilms (b anc c, respectively) after 48 hours, as compared to control biofilms (a). Live (green) and dead (red) cells were stained with BacLight Live/Dead utilizing Syto9 and propidium iodide stains. Scale bars represent 20 µm.

3.3.2.5. Comparison of SPION Activity with Conventional Antibiotics

Next, the anti-biofilm activity was compared with conventional antibiotics. Gentamicin was not as effective as different SPION treatments used in the study. 1 mg/mL gentamicin treatment resulted in a 2.29 ± 0.95 log reduction (**Figure 3.10**). Although this *in vitro* anti-biofilm activity might seem significant, there is strong clinical evidence that gentamicin cannot eradicate MRSA biofilms and therefore cannot be a treatment option for MRSA. [196,220-223] Vancomycin remains as the last clinical option which MRSA strains are susceptible to.[197] In the present *in vitro* analysis, 1 mg/mL of vancomycin treatment resulted in a 4.55 ± 0.2 log reduction in colony forming units, compared to untreated biofilm controls ($p < 0.001$). Moreover, it has been shown for the first time that the anti-biofilm efficacy of vancomycin could be significantly improved in the presence of both 1 mM and 10 mM fructose metabolites ($p < 0.05$) (**Figure 3.10**). Moreover, all of the conjugated SPION were significantly more effective than vancomycin against MRSA biofilms ($p < 0.05$). Moreover, we compared the anti-biofilm activity of all of unconjugated and metal conjugated (Fe1, Fe4, Zn1, Zn4) SPION to vancomycin, by quantifying the percentage survival of MRSA biofilms (**Figure 3.15**). Unconjugated SPION (UC) eradicated MRSA biofilms by ~two-orders of magnitude better than vancomycin ($p < 0.1$). In addition, metal conjugation further increased the bacteria eradication ability of SPION (Fe1, Fe4, Zn1 and Zn4) and they were significantly more effective than the only clinically available option to treat MRSA infections ($p < 0.05$), vancomycin. Most significantly, fructose metabolites further enhanced the eradication efficacy of unconjugated (UC) and 1mmol iron (Fe1) and zinc (Zn1) conjugated SPION ($p < 0.05$).

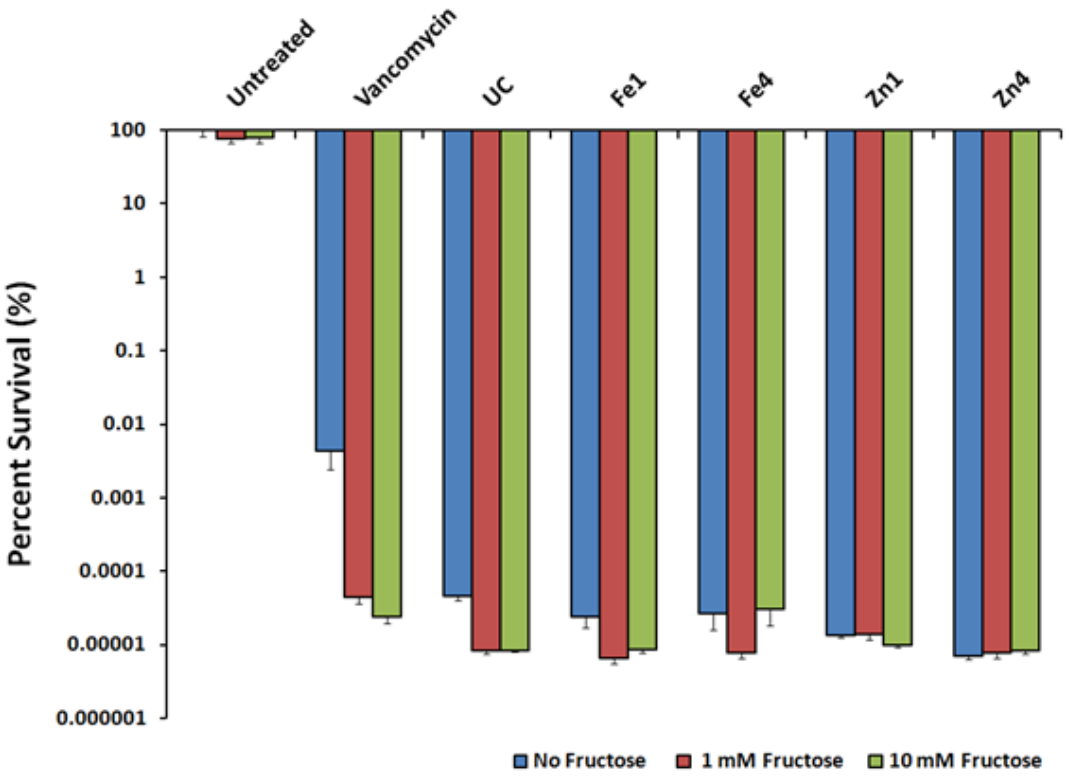

Figure 3.15. Comparison of the percentage survival of MRSA biofilms treated with 1 mg/mL of vancomycin and unconjugated and metal conjugated (Fe1, Fe4, Zn1 and Zn4) SPION in the presence of fructose metabolites. SPION treatments exhibited stronger antibacterial properties than vancomycin, the antibiotic of last resort. The eradication by unconjugated SPION (UC) was about two orders of magnitude better than vancomycin ($p < 0.1$). Metal conjugations further increased the eradication efficacy of SPION (Fe1, Fe4, Zn1 and Zn4) ($p < 0.05$). Most importantly, fructose metabolites further enhanced the eradication efficacy of unconjugated (UC) and 1mmol iron (Fe1) and zinc (Zn1) conjugated SPION. Fructose metabolites also increased the efficacy of vancomycin on MRSA biofilms.

3.3.2.6. Analysis of Biofilm Mass after SPION Treatment

The MRSA biofilm mass after the SPION treatment in the presence of fructose metabolites was also compared to biofilm mass after conventional antibiotic treatments. **Figure 3.16** shows the biofilm mass after 24 hours with and without 1 mM fructose solution. For the first time, it was observed that 1 mM and 4 mM Fe^{3+} (Fe1 and Fe4, respectively) conjugated SPION better decreased the biofilm mass in the presence of fructose compared to the Fe1 and Fe4 treatment alone ($p < 0.05$). In addition, vancomycin significantly decreased the biofilm mass, both with and without fructose. Thus, iron-conjugated SPION treatments showed similar biofilm mass eradicating activity to vancomycin when they were used in combination with fructose metabolites. Crystal violet stains the bacterial cells as well as any material adhering (i.e., biofilm matrix components) to the surface of the microtiter plate.[224,225] Unexpected higher crystal violet optical density readings for some SPION species (especially unconjugated SPION) might indicate that more matrix proteins were released after treatment compared with vancomycin. On the other hand, gentamicin significantly increased biofilm mass and biofilm formation compared to control group, which did not receive any treatment. In earlier studies, gentamicin and other aminoglycoside antibiotics has also been found to induce biofilm formation.[40] Biofilm mass analysis showed that SPION were more effective than gentamicin to eradicate biofilm mass.

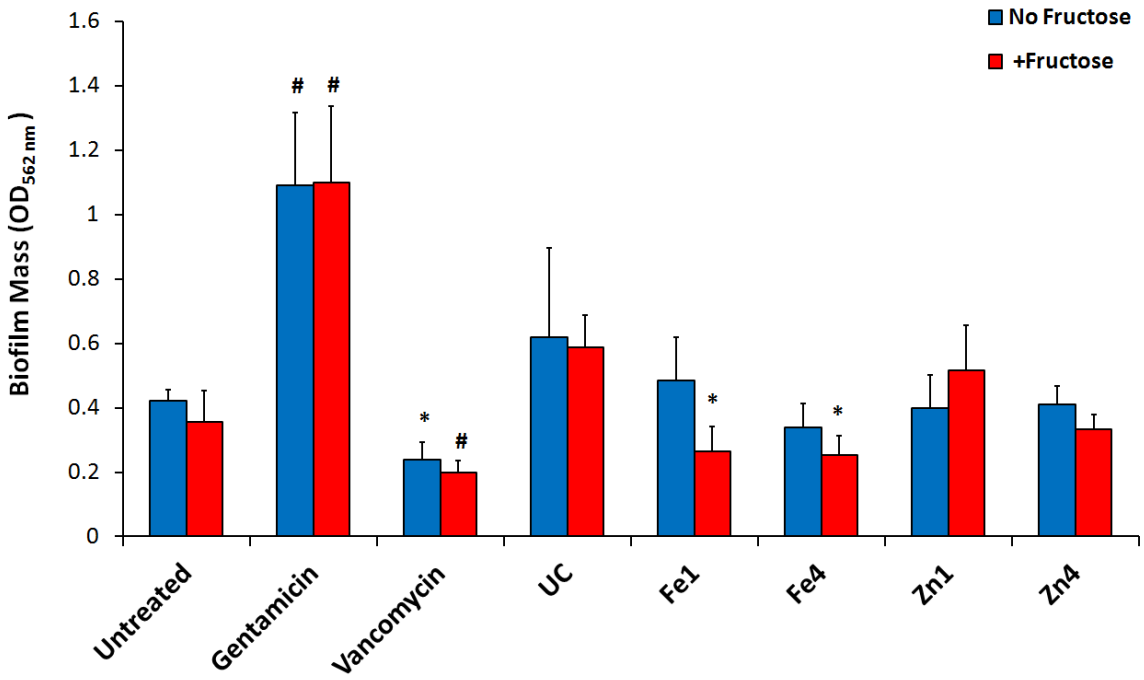

Figure 3.16. MRSA biofilm mass after 24 hours of SPION treatment. Fructose metabolites significantly improved the biofilm mass reduction efficiency of SPION conjugated with 1 mM (Fe1) and 4 mM iron (Fe4). In addition, vancomycin significantly reduced MRSA biofilm mass in the presence or absence of a fructose solution. On the other hand, gentamicin increased biofilm formation. Data represents mean ± standard error of the mean (SEM), N = 3. *$p < 0.05$ and # $p < 0.01$ compared to untreated control biofilms.

3.3.3.7. Antibacterial Activities of Metals Salts used in SPION Synthesis

Metal salts $FeCl_3$ and $ZnCl_2$ used for SPION conjugation did not have any significant activity to eradicate the biofilm mass, which indicated that iron and zinc are more effective towards bacteria at the nanoscale (**Fig. 3.17 and 18**).

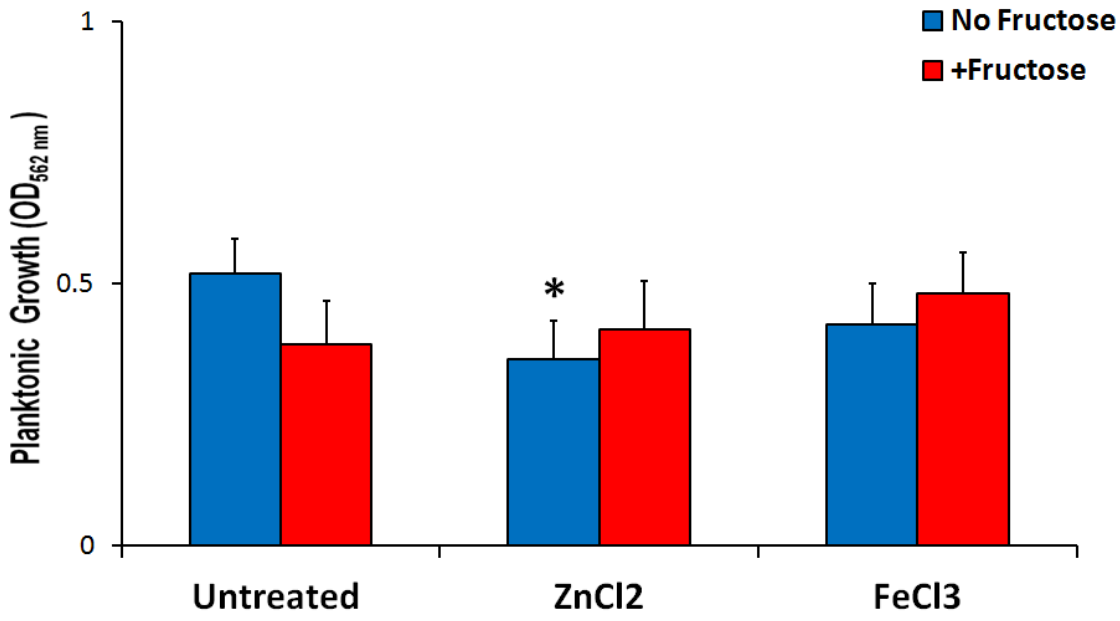

Figure 3.17. Activity of metal salts used in SPION synthesis ($ZnCl_2$ and $FeCl_3$) against the planktonic growth of MRSA after 24 hours of treatment. 1mg/mL $ZnCl_2$ showed significant activity against planktonic bacteria. However, the metal salts were not as effective as the nanophase unconjugated (UC) or metal conjugated SPION (Fe1, Fe4, Zn1, Zn4). Data represents mean ± SEM, N = 3. *$p < 0.05$ compared to untreated control biofilms.

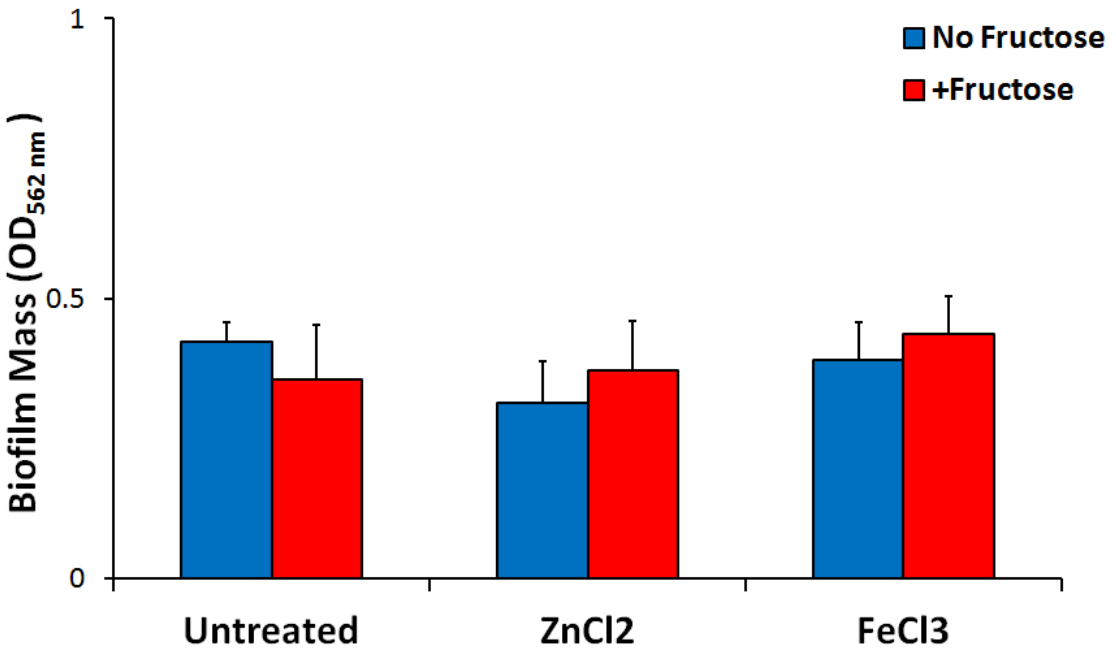

Figure 3.18. The effect of metal salts used in SPION synthesis ($ZnCl_2$ and $FeCl_3$) on MRSA biofilm mass after 24 hours of treatment. 1mg/mL $ZnCl_2$ and $FeCl_3$ did not show any significant effect in the presence or absence of a fructose solution. Data represents mean ± SEM, N = 3.

Taken together, all of these bacterial studies clearly indicate that metal conjugated and unconjugated SPION outperform the only clinically available antibiotic (vancomycin) to treat resistant biofilm infections and hold a great promise to be the next generation of antibacterial treatments.

3.3.2.8. Mechanism for Enhanced SPION Anti-Biofilm Activity in the Presence of Metabolites

From these results, it was hypothesized that the increase in the SPION anti-biofilm efficacy in the presence of a metabolic stimuli is due to the increased uptake of SPION by the biofilms.

3.3.2.8.1. Increased Uptake of Nanoparticles within the Biofilms

First, this hypothesis was tested by qualitatively analyzing the iron deposition within the biofilm by Prussian blue staining, a histology stain creating a blue by-product in the presence of ferric iron (Fe^{+3}) ions. Specifically, iron deposition was analyzed for the combinations which showed an increase in anti-biofilm efficacy: unconjugated SPION (UC) in the presence of 1 and 10 mM, 1 mM iron conjugated SPION (Fe1) in the presence of 1 mM fructose and 1 mM zinc conjugated SPION (Zn1) in the presence of 10 mM fructose. No blue color formation was observed in the untreated control biofilms (**Figure 3.19**). The blue color intensity increased in the presence of fructose metabolites, implying an increase in the iron deposition levels within the biofilm when fructose metabolites were present as carbon sources (**Figure 3.19 and 3.20**).

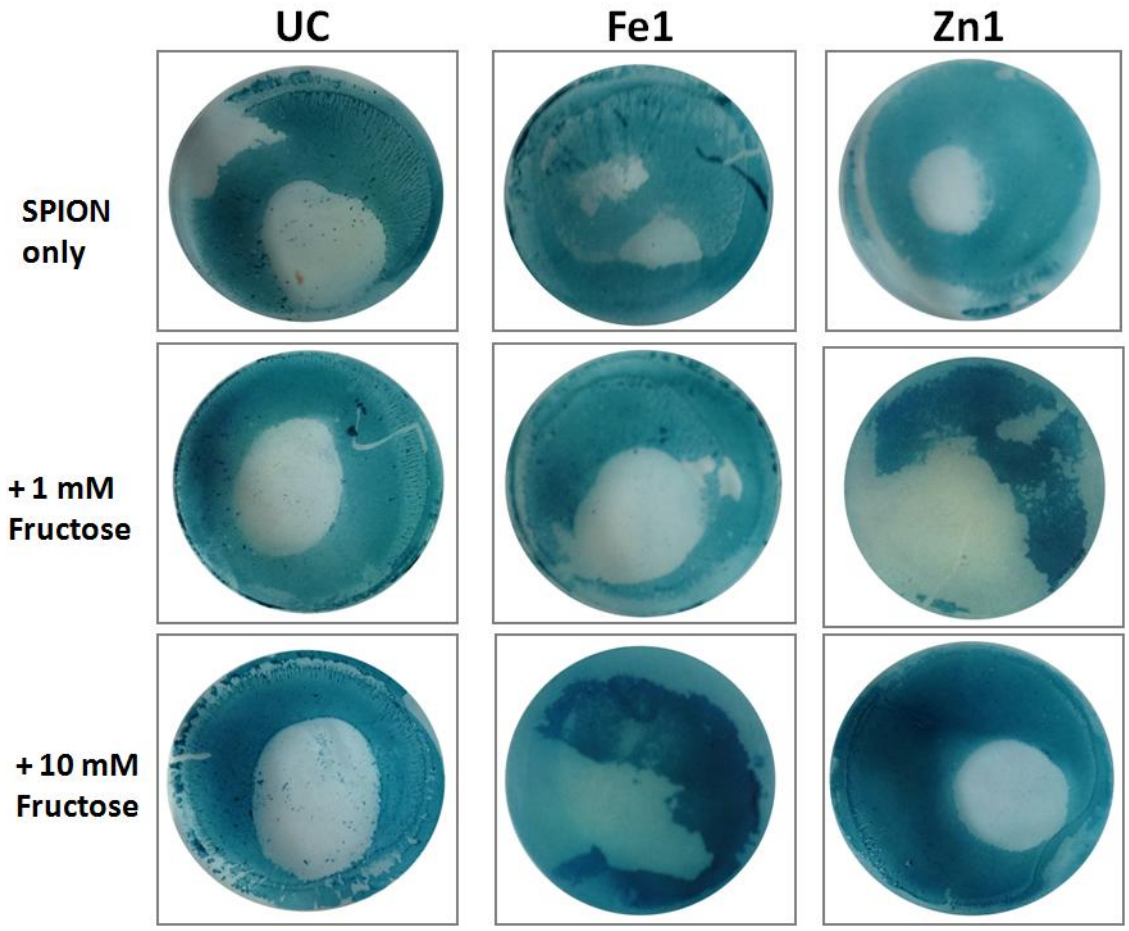

Figure 3.19. Qualitative analysis of the iron deposition by Prussian blue staining. Intensity of blue color increased in the presence of fructose metabolites, implying an increase in the iron deposition levels within the biofilm when fructose metabolites were present as carbon sources.

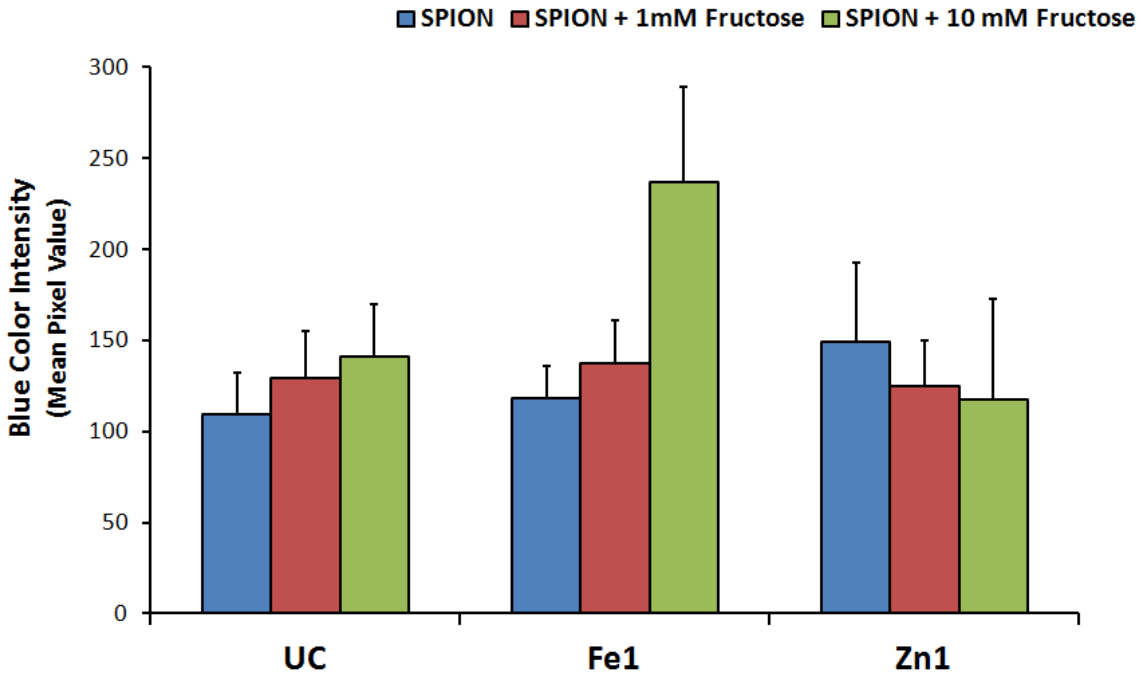

Figure 3.20. Intensity of blue color increased in the presence of fructose metabolites, implying an increase in the iron deposition levels within the biofilm when fructose metabolites were present as carbon sources.

Then, the uptake of SPION within the MRSA biofilms was analyzed by quantifying the presence of iron (Fe^{3+}), sulfur (S^{2-}) and zinc (Zn^{2+}) ions by inductively coupled plasma atomic emission spectroscopy (ICP-AES) (**Figure 3.19a-c**). The uptake of SPION by the biofilms includes the nanoparticles within the cell, attached to the bacterial cell surface as well as in the EPS matrix of the biofilm. First, significant increases in intracellular or membrane-bound iron (Fe^{3+}) concentrations for all the SPION treatments (UC, Fe1 and Zn1) in the presence or absence of 1 mM or 10 mM fructose, compared to untreated biofilms ($p < 0.01$) was observed. In addition, the intracellular or membrane-bound iron

(Fe^{3+}) concentration increased from 2.972 ± 0.548 µg/mL to 7.989 ± 1.901 µg/mL when biofilms were treated with Fe1 in the presence of 10 mM fructose ($p < 0.05$). The fructose concentration also had a significant effect on Fe^{3+} uptake. The Fe^{3+} concentration increased from 3.550 ± 0.745 µg/mL to 7.989 ± 1.901 µg/mL when the fructose concentration in Fe1 treatment increased from 1 mM to 10 mM ($p < 0.05$). The Fe^{3+} concentration also increased from 2.775 ± 0.770 µg/mL to 3.533 ± 0.571092 µg/mL when biofilms were treated with Zn1 in the presence of 10 mM fructose. Moreover, significant increases in intracellular or membrane-bound sulfur (S^{2-}) concentrations in the presence of fructose metabolites were observed. For example, the S^{2-} concentration increased from 2.714 ± 0.375 µg/mL to 4.420 ± 0.908 µg/mL when biofilms were treated with unconjugated SPION (UC) in the presence of 10 mM fructose ($p < 0.1$). The fructose concentration also had a significant effect on the S^{2-} concentration. The S^{2-} concentration increased from 2.744 ± 0.428 µg/mL to 4.910 ± 0.980 µg/mL when the fructose concentration in Fe1 treatment increased from 1 mM to 10 mM ($p < 0.05$). Although we observed significant increase in intracellular or membrane-bound zinc (Zn^{2+}) levels Zn1 treatment in the presence or absence of 1 mM or 10 mM fructose ($p < 0.001$) in the biofilm viability analysis, the effect of fructose on Zn^{2+} uptake was not significant. Therefore, the enhanced anti-biofilm efficacy of Zn1 treatment is mostly due to the significant increases in intracellular or membrane bound iron (Fe^{3+}) within the MRSA biofilms.

a)

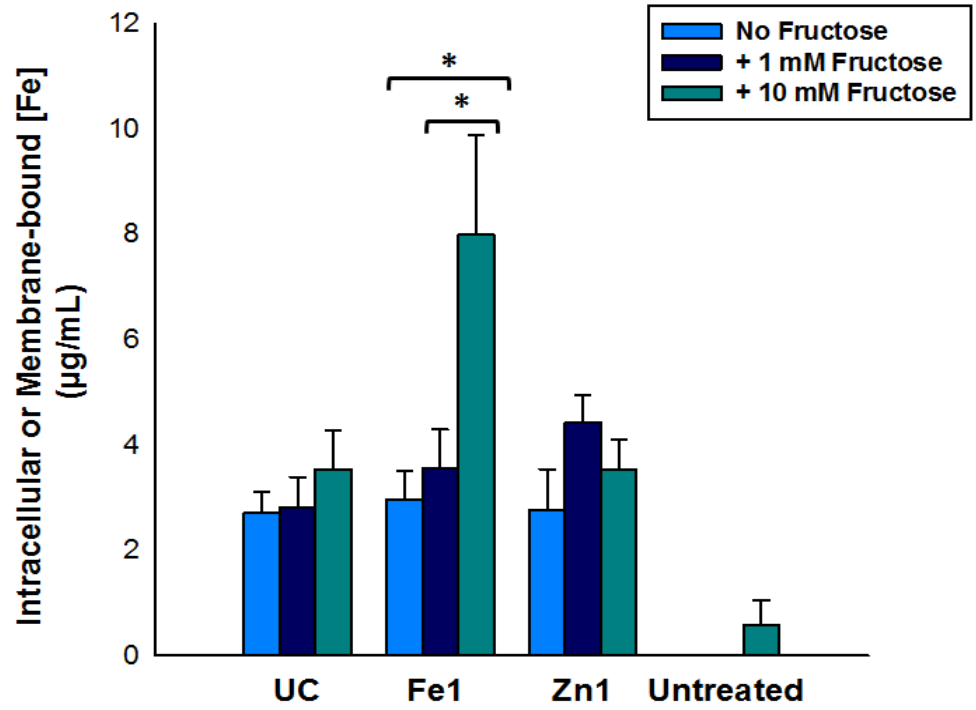
Intracellular or Membrane-bound [Fe] (µg/mL)
12
10
8
6
4
2
0
*
*
No Fructose
+ 1 mM Fructose
+ 10 mM Fructose
UC
Fe1
Zn1
Untreated

b)

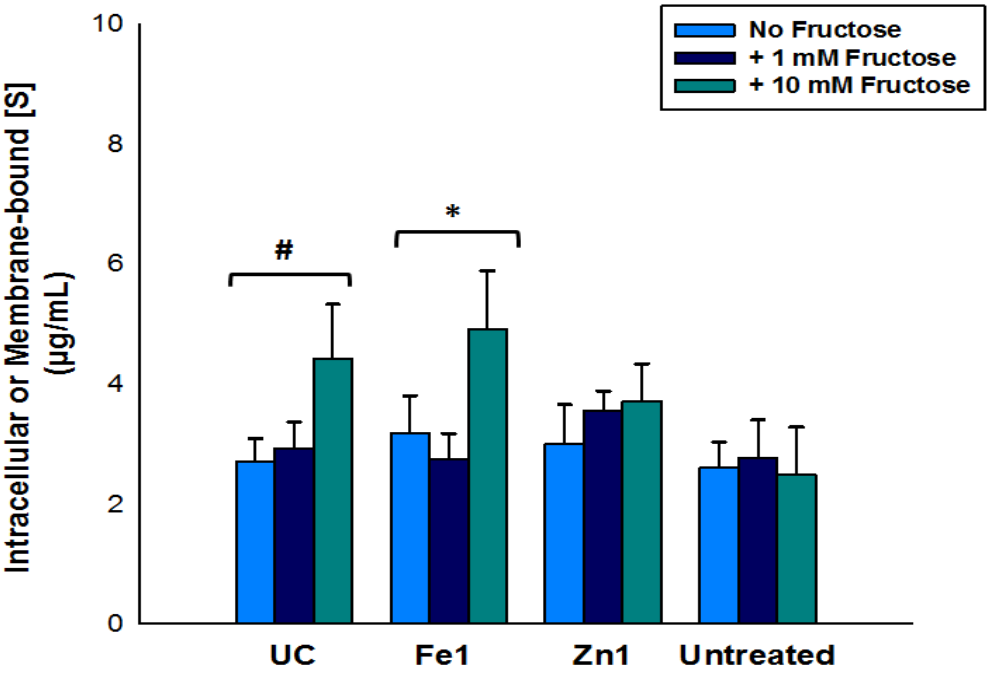
Intracellular or Membrane-bound [S] (µg/mL)
10
8
6
4
2
0
#
*
No Fructose
+ 1 mM Fructose
+ 10 mM Fructose
UC
Fe1
Zn1
Untreated

c)

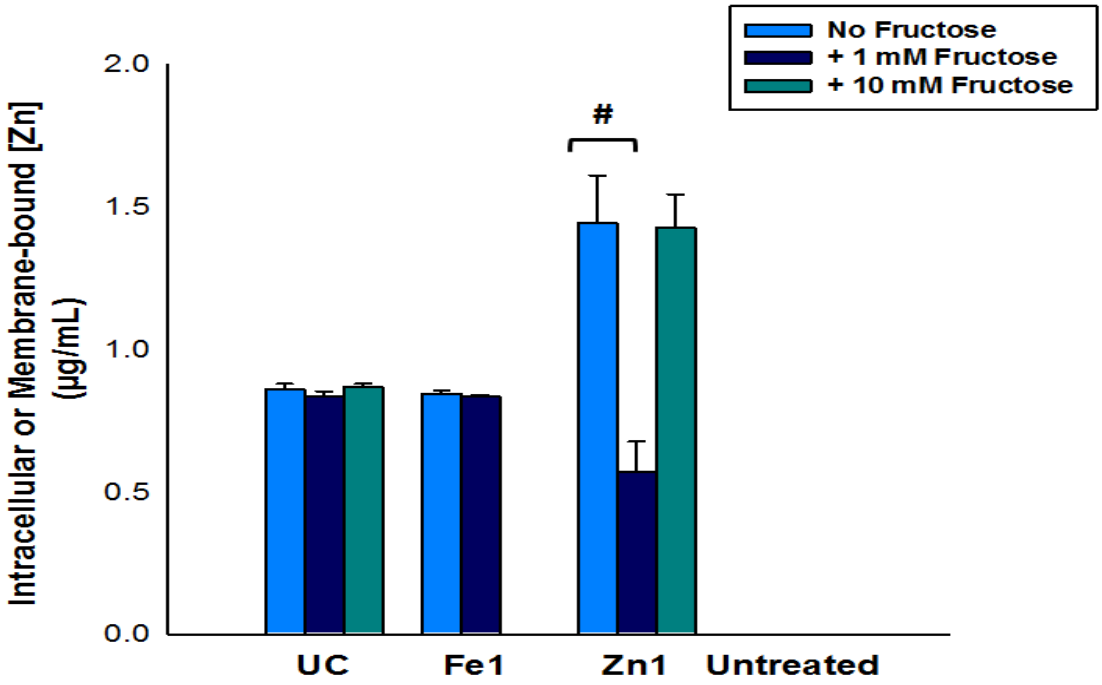

Figure 3.21. Analysis of the uptake of SPION within the MRSA biofilms by quantifying the presence of iron (Fe^{3+}), sulphur (S^{2-}) and zinc (Zn^{2+}) ions by inductively coupled plasma atomic emission spectroscopy (ICP-AES) (**a, b and c, respectively**). The uptake of SPION by the biofilms included the nanoparticles within the cell, attached to the bacterial cell surface as well as in the biofilm matrix. The enhanced anti-biofilm efficacy of SPION treatments are mostly due to the significant increases in intracellular or membrane bound iron (Fe^{3+}) and sulphur (S^{2-}) within the MRSA biofilms.

3.3.2.8.2. TEM Analysis of SPION Uptake within the MRSA Biofilms

To strengthen the hypothesis, TEM analysis was also performed to image the bacterial cells after SPION as well SPION+ fructose treatment. **Figure 22** shows the representative TEM images of bacterial cells after 24 hours of SPION and SPION + fructose treatment, respectively.

TEM analysis showed that the growth inhibition and biofilm reduction by SPION is mediated by interactions with the MRSA membrane surface. Unconjugated SPION mostly adsorb to the bacterial surface and damage the bacterial cell membrane (**Figure 3.22a**). In the presence of fructose metabolites, the number of intracellular and membrane-bound SPION particles is increased (**Figure 3.22b**). White arrows indicate particles taken up and particle clusters inside the bacteria. The bacterial cell membrane is more damaged as the SPION better penetrates the membrane surface in the presence of fructose metabolites. This data is consistent and further supported with the ICP analysis, which quantifies the particle uptake (**Figure 3.21**).

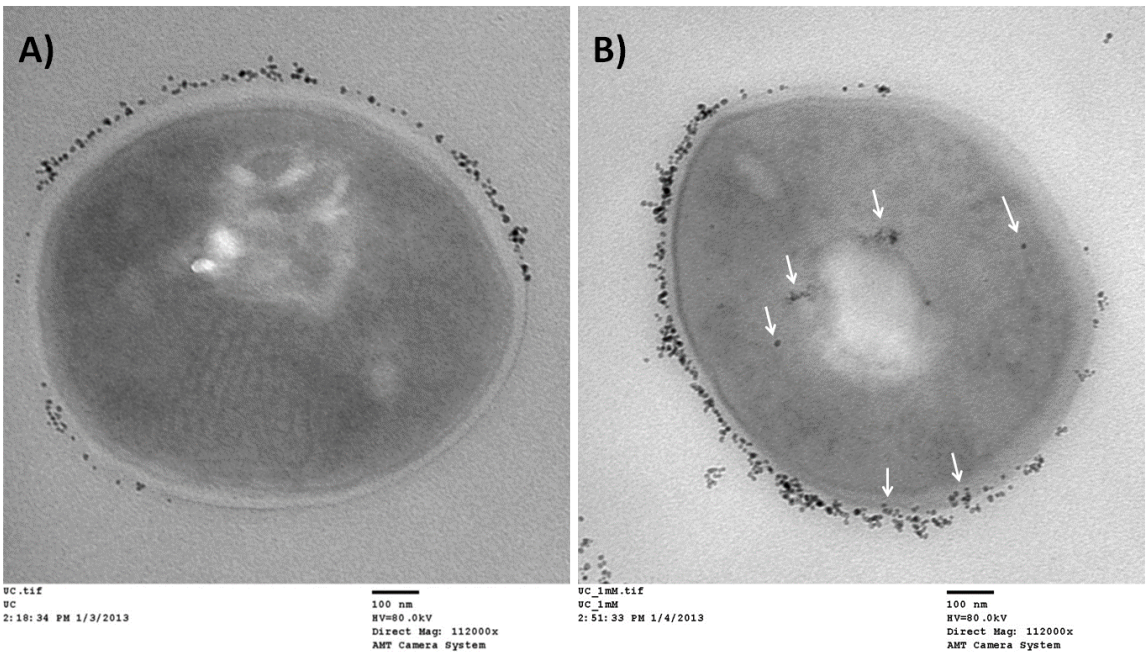

Figure 3.22. TEM imaging of bacteria after SPION treatment. Growth inhibition and biofilm reduction by SPION is mediated by interactions with the MRSA membrane surface. **A)** Unconjugated (UC) SPION adsorb to the bacterial cell surface and damage the bacterial cell membrane. **B)** The uptake of SPION within the biofilm-forming cell increases in the presence of metabolites. SPION damage the cell membrane and better penetrate through the membrane surface (as indicated with the arrows) (scale bars = 100 nm).

3.3.3.8.3. Increased Reactive Oxygen Species Formation

Furthermore, the effect of enhanced nanoparticle uptake on reactive oxygen species (ROS) formation was investigated. It has been shown that SPION could induce bacterial cell death through the formation of ROS.[226-229] After 24 hours of SPION treatment, biofilms were stained with DAPI and a CellRox Deep ROS sensor which measures the oxidative stress levels in cells **(Fig. 3.23).** ROS formation increased when MRSA biofilms were treated with unconjugated SPION for 24 hours (**Fig. 3.23b**), compared to untreated control biofilms (**Fig. 3.23a**). Moreover, ROS generation increased when 1 mM and 10 mM fructose metabolites were added to the SPION treatment (**Fig. 3.23 c and d, respectively**). In addition, the red color intensity was quantified after staining with a CellRox Deep ROS sensor (**Figure 3.24**). Increased intensity also proved that there was an increase in ROS formation when SPION are used in combination with fructose metabolites. Thus, the enhanced anti-biofilm activity due to the increased SPION penetration into the MRSA biofilms and generation of reactive oxygen species (ROS) in the presence of metabolites was validated here.

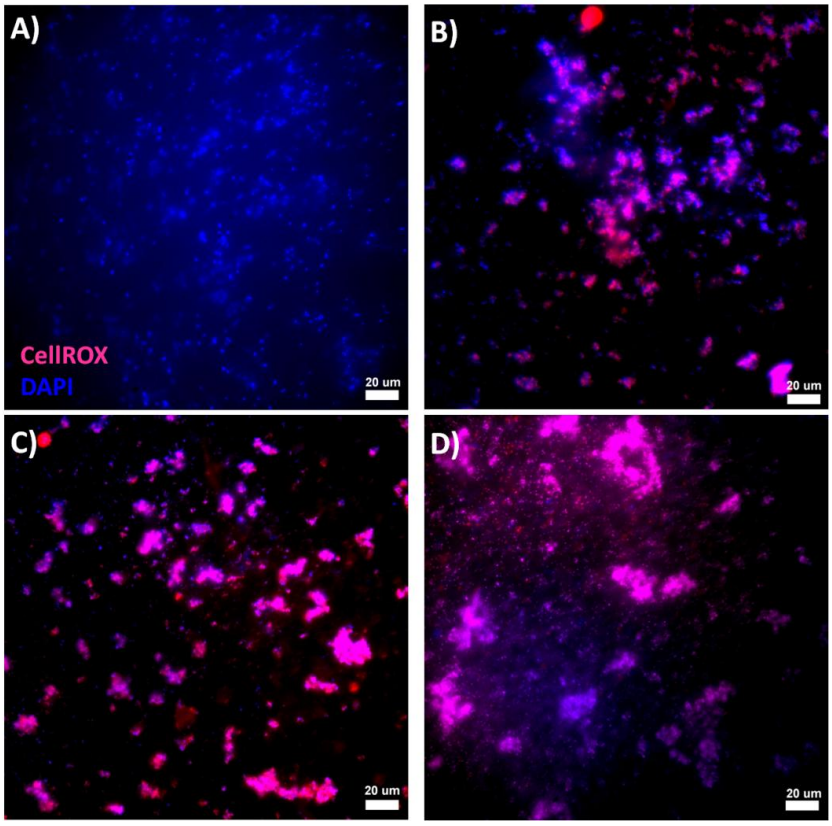

Figure 3.23. The formation of reactive oxygen species (ROS) was increased when SPION was used in combination with fructose metabolites: **A)** untreated biofilms; **B)** biofilms treated with 1 mg/mL SPION; **C)** biofilms treated with 1 mg/mL SPION in combination with 1 mM fructose; **D)** biofilms treated with 1 mg/mL SPION in combination with 10 mM fructose. ROS formation increased when MRSA biofilms were treated with unconjugated SPION for 24 hours (**Figure 23B**), compared to untreated control biofilms (**Figure 23A**). Moreover, ROS generation further increased when 1 mM and 10 mM fructose metabolites were added to the SPION treatment (**Figure 23Cand 23D respectively**). Thus, enhanced anti-biofilm activity was due to the increased SPION penetration into the MRSA biofilms and generation of reactive oxygen species (ROS) in the presence of metabolites.

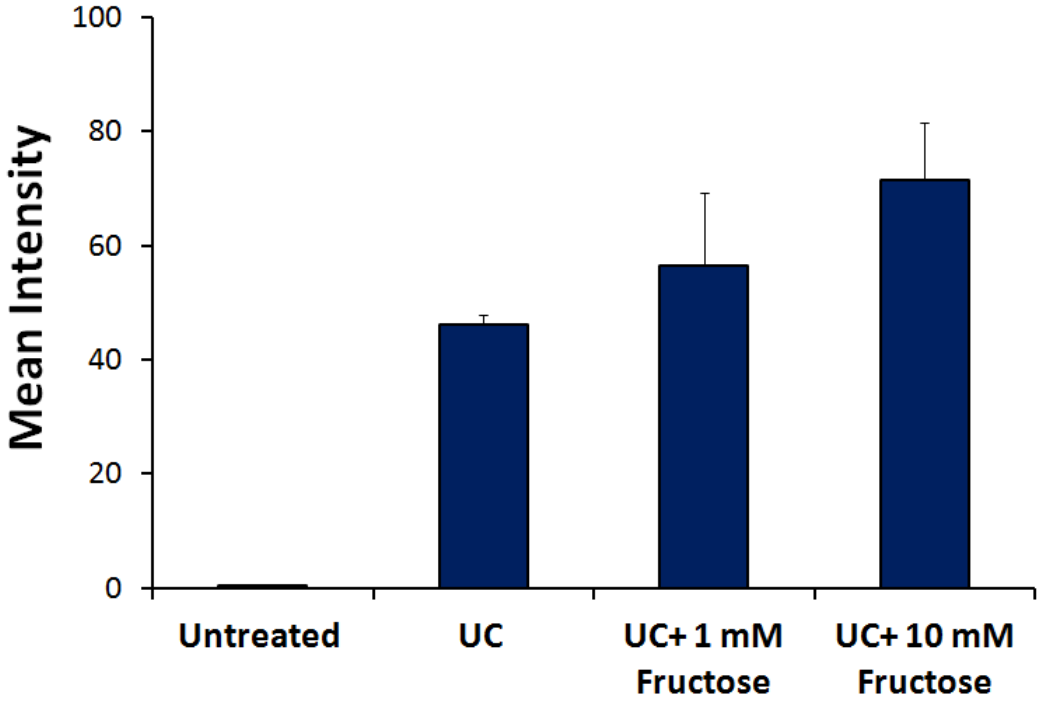

Figure 3.24. Quantification of color intensity after staining with CellRox Dep Red Sensor. Increased intensity implies an increase in the reactive oxygen species (ROS) formation when SPION were used in combination with fructose metabolites. Thus, enhanced anti-biofilm activity was due to the increased SPION penetration into the MRSA biofilms and the generation of ROS in the presence of metabolites.

3.3.4. Antibacterial and Anti-biofilm Assessment of SPION against *E.coli* Biofilms and the Effect of Fructose Metabolites

The anti-biofilm activity of SPION against the gram-negative *E. coli* biofilms and the effect of fructose on the antibacterial efficacy were also validated (**Figure 3.25**). For example, a 4.15 ± 0.40 order of magnitude decrease in viable bacteria counts was observed when E. coli biofilms were treated with unconjugated SPION (UC) ($p < 0.01$). In addition, conjugating SPION with 1 mM and 4 mM Fe^{3+} (Fe1 and Fe4) as well as Zn^{+2} (Zn1 and Zn4) further decreased viable E. coli within the biofilm ($p < 0.01$). The anti-biofilm activity of both iron and zinc conjugated SPION was y improved when the metal conjugation concentrations increased from 1 mM to 4 mM. For example, a 4.42 ± 0.29 log reduction was observed when MRSA biofilms were treated with Fe1, while treatment with Fe4 increased the anti-biofilm activity to a 4.61 ± 0.23 log reduction. In addition, a 4.58 ± 0.21 log reduction was observed when biofilms were treated with Zn1, while Zn4 treatment increased the anti-biofilm activity to a 5.31 ± 0. 41 log reduction (which corresponds to a ~ 0.7 log increase in activity) ($p < 0.05$).

Next, the effect of fructose metabolites on SPION anti-biofilm activity against E. coli biofilms was investigated. It was observed that the anti-biofilm efficacy of unconjugated SPION (UC) as well as 1 mM iron-conjugated SPION (Fe1) and 1 mM zinc-conjugated SPION (Zn1) against MRSA biofilms was significantly enhanced when fructose metabolites were added to the treatment. For example, there was a 1.02 ± 0.02 log increase (~ 90.6%) in anti-biofilm efficacy when 10 mM fructose was added to the

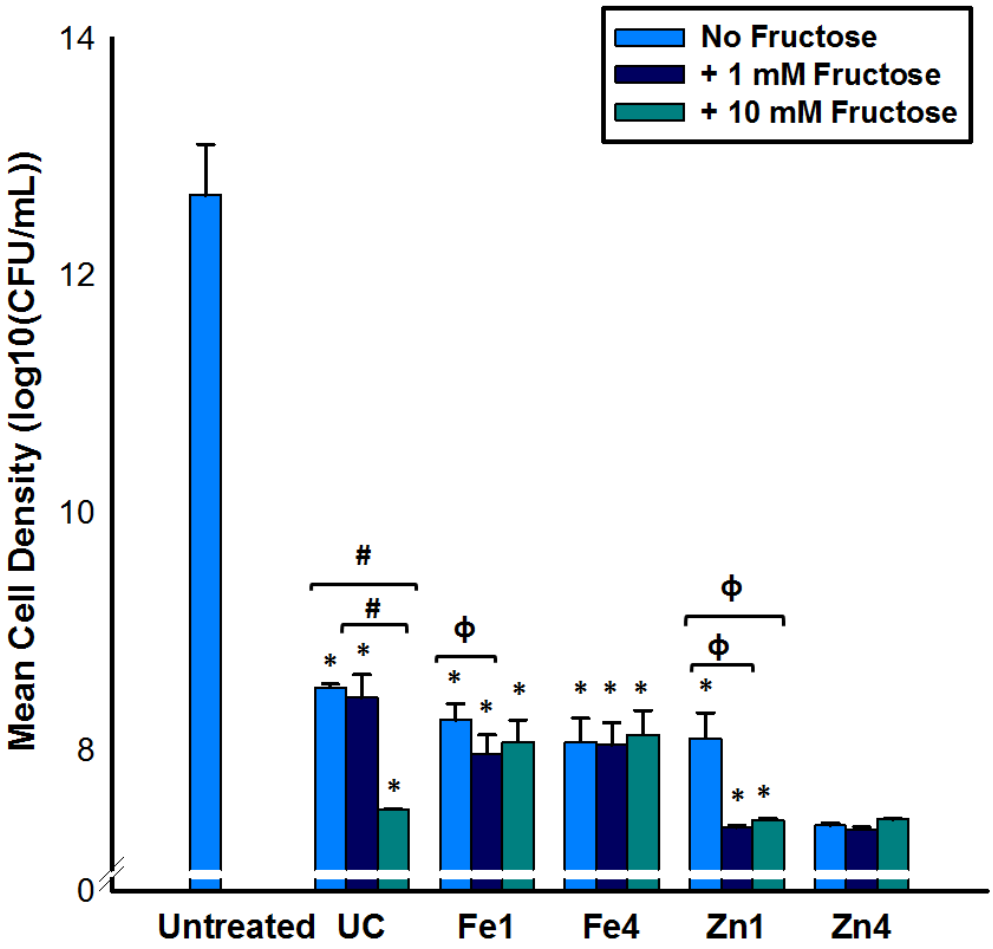

Figure 3.25. Enhanced anti-biofilm activity of SPION treatment in the presence of fructose metabolites. The anti-biofilm activity of 1mg/mL SPION against *E. coli* biofilms after 24 hours with and without 1 mM and 10 mM fructose solutions. Anti-biofilm efficacy of unconjugated SPION (UC) as well as 1 mM iron-conjugated SPION (Fe1) and 1 mM zinc-conjugated SPION (Zn1) against MRSA biofilms was significantly enhanced when fructose metabolites were added to the treatment. Data represents mean ± SEM. N = 3. * $p < 0.01$ compared to untreated biofilms; # $p < 0.001$ and φ $p < 0.1$ compared to the same treatment without fructose.

1 mg/mL unconjugated SPION (UC) treatment ($p < 0.001$). The efficacy was further improved when 1 mM fructose was added to the 1 mM iron-conjugated SPION (Fe1) treatment, which resulted in a 52.7 % increase in antibacterial activity, compared to Fe1 treatment. Moreover, there was a 0.75 ± 0.20 log increase (~ 82.2%) in efficacy when 1 mM fructose were used in combination with 1 mM zinc conjugated SPION (Zn1) ($p < 0.1$). In addition, 10 mM fructose enhanced the efficacy of 1 mM zinc conjugated SPION (Zn1) by 0.69 ± 0.20 log, which corresponds to a ~79.4 % increase in activity ($p < 0.1$). On the other hand, the presence of fructose metabolites did not potentiate the efficacy of 4 mM iron (Fe4) or zinc (Zn4) conjugated SPION, which is consistent with the previous analysis with MRSA biofilms. This might indicate that there is a maximum iron/metabolite and zinc/metabolite concentration threshold in the bacterial metabolism to cause cell death.

3.3.5. Antibacterial and Anti-biofilm Assessment of SPION against *P. aeruginosa* Biofilms and the Effect of Fructose Metabolites

The developed method was also validated on *P. aeruginosa* (**Figure 3.26**), another gram-negative bacterium which plays a critical role in hospital-acquired infections. Figure 26a, 24c and 24e shows the biofilms grown on glass slides for a week. Then, biofilms were treated with 1 mg/mL unconjugated (UC) SPION as well as UC SPION in combination with 10 mM fructose metabolites. After 24 hours of treatment, the samples were washed with phosphate buffered saline (PBS) and imaged. Images clearly showed that biofilm formation was decreased after 24 hours of SPION treatment (**Figure 3.26d**). Moreover, the anti-biofilm activity of SPION was significantly enhanced when used in combination

with fructose metabolites (**Figure 3.26f**). Better eradication of the biofilm was observed compared with the samples just treated SPION.

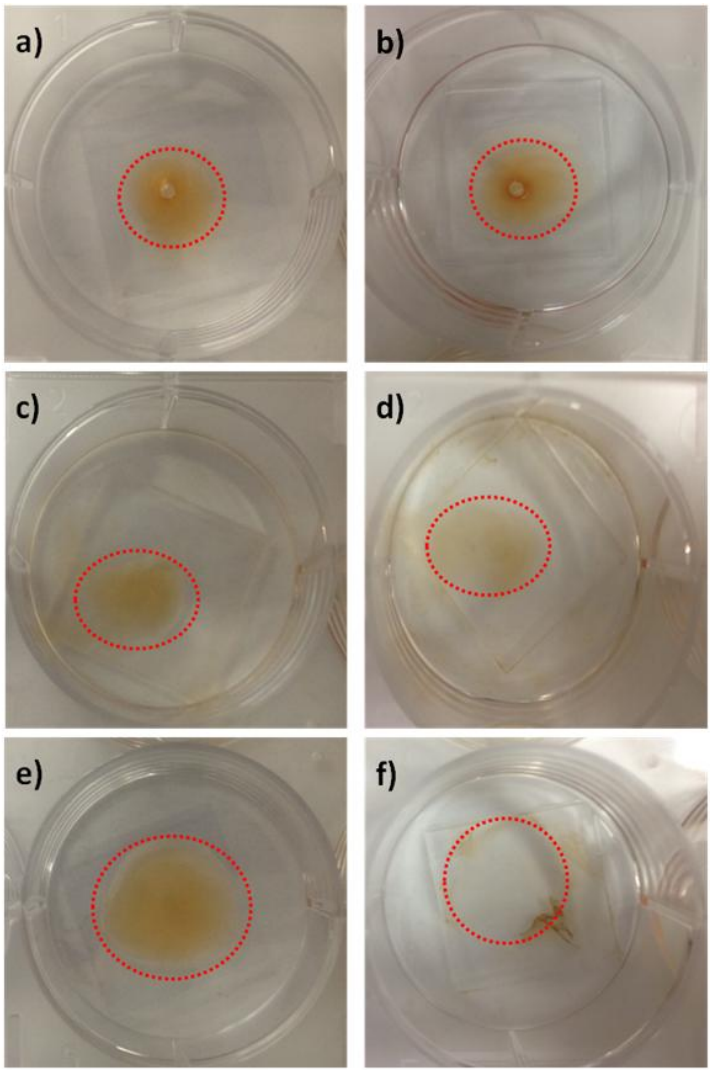

Figure 3.26. Representative images of anti-biofilm activity of unconjugated SPION treatment against *P. aeruginosa* in the presence of fructose metabolites. Biofilms were grown on glass slides for a week **(Figure 3.26a, c, and e).** Biofilm formation was decreased after 24 hours of SPION treatment (**Figure 3.26d**). The anti-biofilm activity of SPION was significantly enhanced when used in combination with fructose metabolites (**Figure 3.26f**).

3.3.6. The Effect of Increasing Metabolite Concentration while Decreasing SPION Metal Conjugation Concentrations

The effect of increasing metabolite concentration while decreasing SPION metal conjugation concentrations was also investigated. MRSA biofilms were treated with 1 mg/mL of SPION conjugated with 0.5 mM iron and zinc (denoted as Fe0.5 and Zn0.5, respectively). This also corresponded to a decrease in antibacterial Fe^{+3} (116 ± 11.56 µg/mL) and Zn^{+2} (23.57 ± 1.67 µg/mL) concentration. On the other hand, the anti-biofilm activities of SPION were enhanced by increasing the fructose concentration to 100 mM ($p < 0.001$) **(Figure 3.27)**. As SPION with lower conjugation concentrations could still target and eradicate the biofilm, this could also result in less toxic effects to healthy mammalian cells surrounding the infection site.

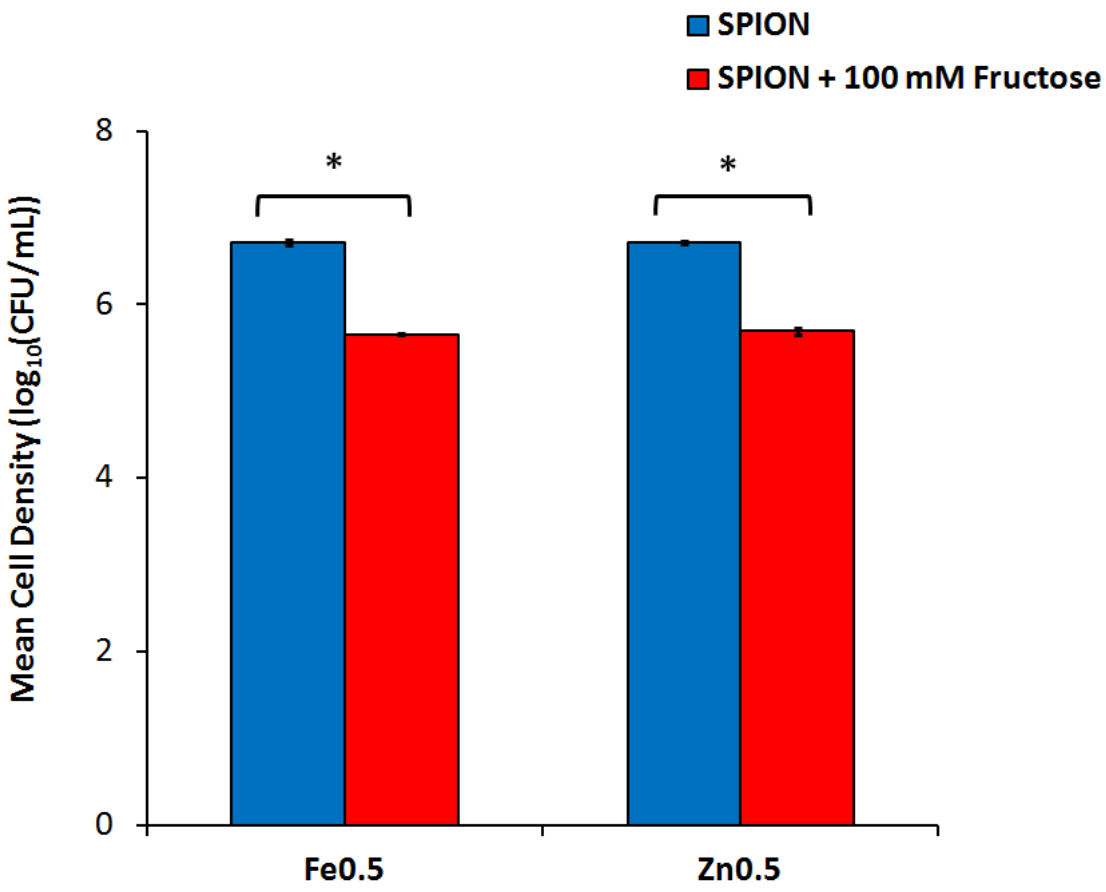

Figure 3.27. The effect of increasing metabolite concentration while decreasing the SPION metal conjugation concentrations. MRSA biofilms were treated with 1 mg/mL of SPION conjugated with 0.5 mmol iron and zinc (denoted as Fe0.5 and Zn0.5, respectively), which also corresponded to a decrease in antibacterial Fe^{+3} and Zn^{+2} concentrations. The anti-biofilm activities of SPION were still significantly enhanced by increasing the fructose concentration to 100 mM ($p < 0.001$).

3.3.7. Potentiating SPION Through the Use of Metabolites

The potential of using metabolites to potentiate the antibacterial and anti-biofilm efficacy of SPION was investigated. As shown earlier, the antibacterial dose of SPION to eradicate MRSA biofilms was 1 mg/mL. On the other hand, 0.1 mg/mL SPION did not have any significant antibacterial activity on planktonic *S. aureus* (**Figure 3.28**). On the other hand, 0.1 mg/mL SPION significantly reduced the planktonic *S. aureus* growth in the presence of 10 mM or 100 mM fructose metabolites ($p < 0.05$).

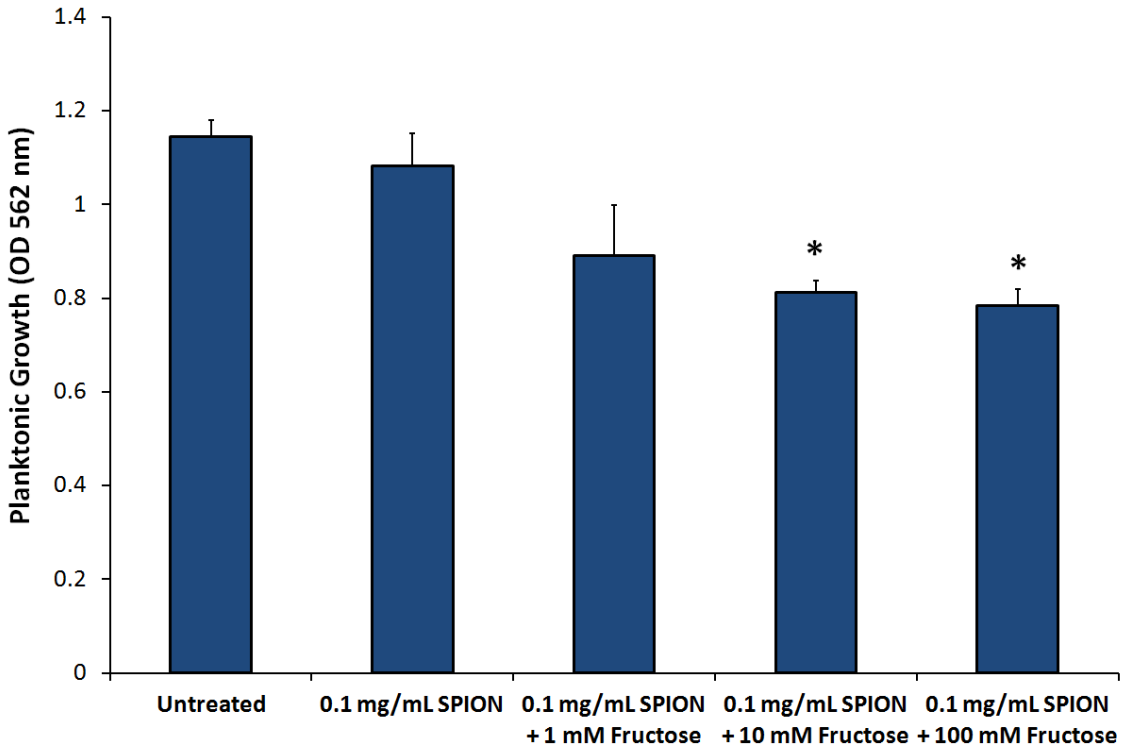

Figure 3.28. Fructose metabolites potentiate the antibacterial activities of SPION against *S. aureus* planktonic growth. Although 0.1 mg/mL SPION is not an antibacterial concentration, it significantly reduced the planktonic *S. aureus* growth in the presence of 10 mM or 100 mM fructose metabolites (* $p < 0.05$).

Moreover, we have investigated the potential of using metabolites to potentiate the SPION anti-biofilm efficacy. We have compared the anti-biofilm activities of 1 mg/mL SPION and 1 mg/mL SPION (**Figure 3.29**). The mean cell density after 0.1 mg/mL SPION treatment was 10.01 ± 0.43 CFU/mL, whereas it was 7.38 ± 0.26 CFU/mL after 1 mg/mL SPION treatment. Presence of 1 mM, 10 mM and 100 mM fructose metabolites significantly increased the eradication efficacy of 0.1 mg/mL SPION, which is not an antibacterial dose ($p < 0.0001$). For example, the mean cell density significantly decreased to 8.49 ± 0.45 CFU/mL in the presence of 1 mM fructose ($p < 0.0001$). Most importantly, the mean cell density further decreased to 7.70 ± 0.08 CFU/mL when used in combination with 100 mM fructose metabolites ($p < 0.0001$). This shows that the efficacy of 0.1 mg/mL SPION becomes comparable to the activity of SPION which is 10 times concentrated. These data has important implications. First, it shows that the metabolic stimulation can potentiate SPION. As lower SPION concentrations (i.e., a concentration 10 times lower than the actual antibacterial dose) could still target and eradicate the persistent biofilm, this could also result in less toxic effects to healthy mammalian cells surrounding the infection site. This highlights the possibility of using metabolites as a novel method to decrease the toxicity of SPION treatments.

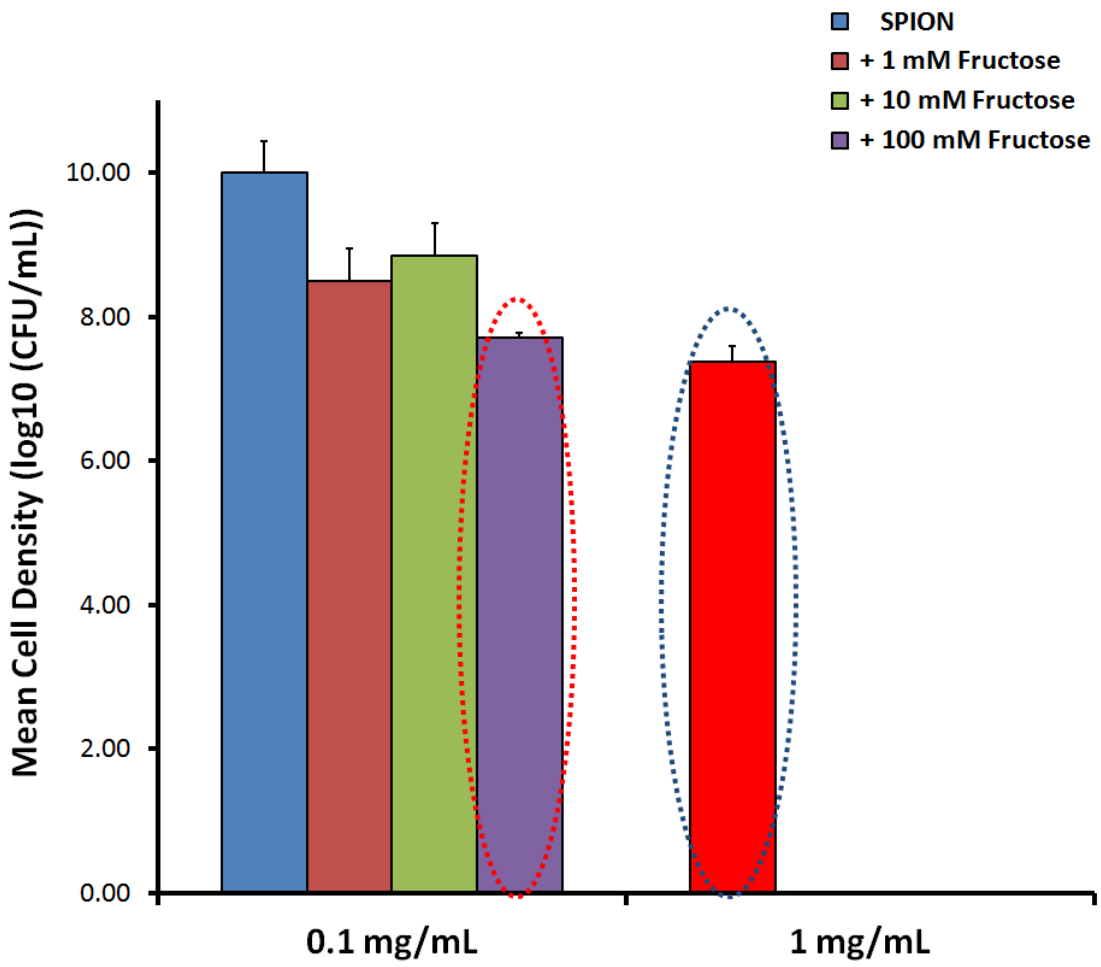

Figure 3.29. Potentiating the anti-biofilm properties of SPION through the use of metabolites. Presence of 1 mM, 10 mM and 100 mM fructose metabolites significantly increased the eradication efficacy of 0.1 mg/mL SPION, which is not an antibacterial dose ($p < 0.0001$). Most importantly, the efficacy of 0.1 mg/mL SPION was comparable to the activity of 1 mg/mL SPION, when used in combination with 100 mM fructose metabolites. This might highlight the possibility of using metabolites as a novel method to decrease the toxicity of SPION treatments.

3.3.8. Screening of Other Metabolites

Other metabolites, such as glucose and mannitol were also screened. Both metabolites enhanced the efficacy of 1 mg/mL unconjugated SPION (UC) against *S. aureus* biofilms. For example, the mean cell density decreased from 8.56 ± 0.9 CFU/mL to 6.62 ± 0.09 CFU/mL, when unconjugated SPION (UC) was used in combination with 10 mM glucose (*p < 0.001)* (**Figure 3.30**). In addition, both 1 mM and 10 mM mannitol metabolites significantly enhanced the SPION activity against *S. aureus* biofilms (* *p < 0.01*) (**Figure 3.31**). For example, the mean cell density decreased from 8.56 ± 0.9 CFU/mL to 7.24 ± 0.43 CFU/mL and 7.43 ± 0.46, when unconjugated SPION (UC) was used in combination with 1 mM and 10 mM mannitol, respectively.

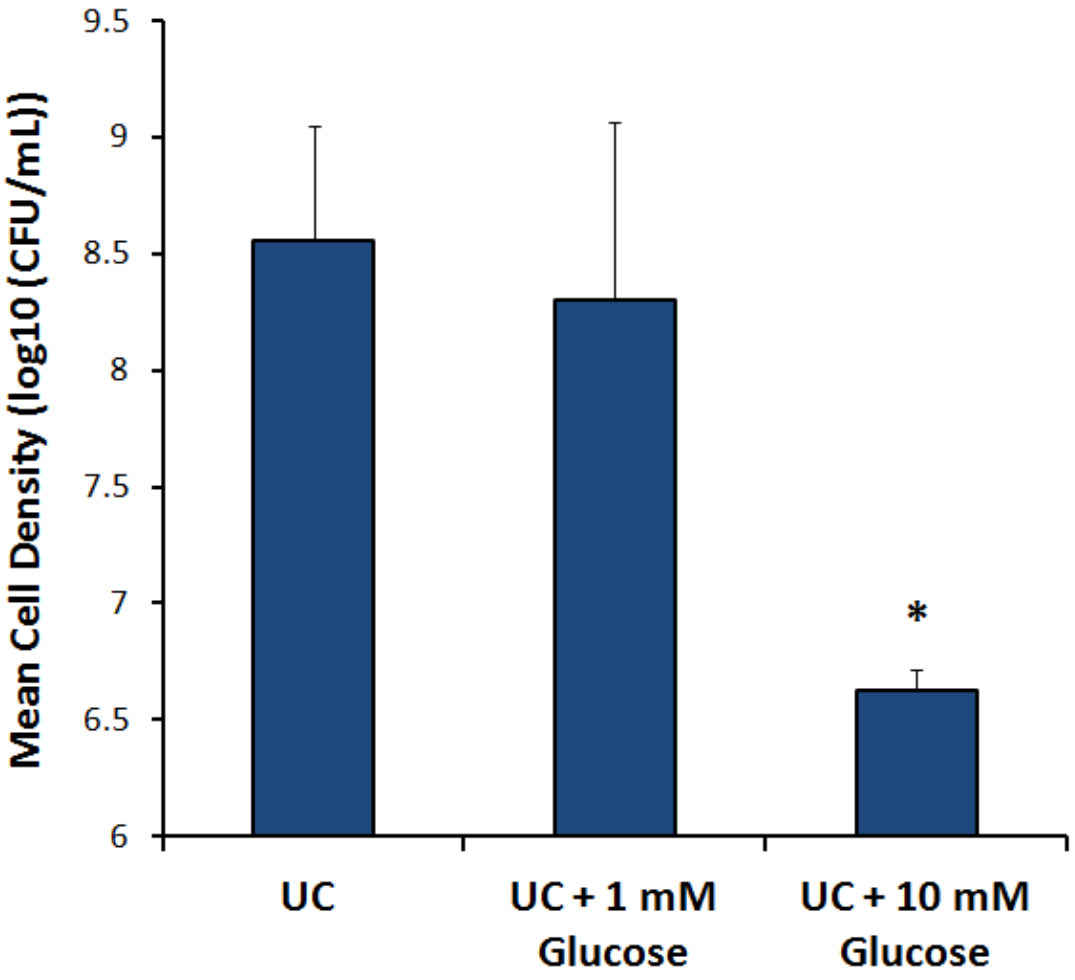

Figure 3.30. The effect of glucose metabolites on the anti-biofilm efficacy of 1mg/mL unconjugated SPION. 10 mM glucose metabolites significantly enhanced the SPION activity against *S. aureus* biofilms (* $p < 0.001$).

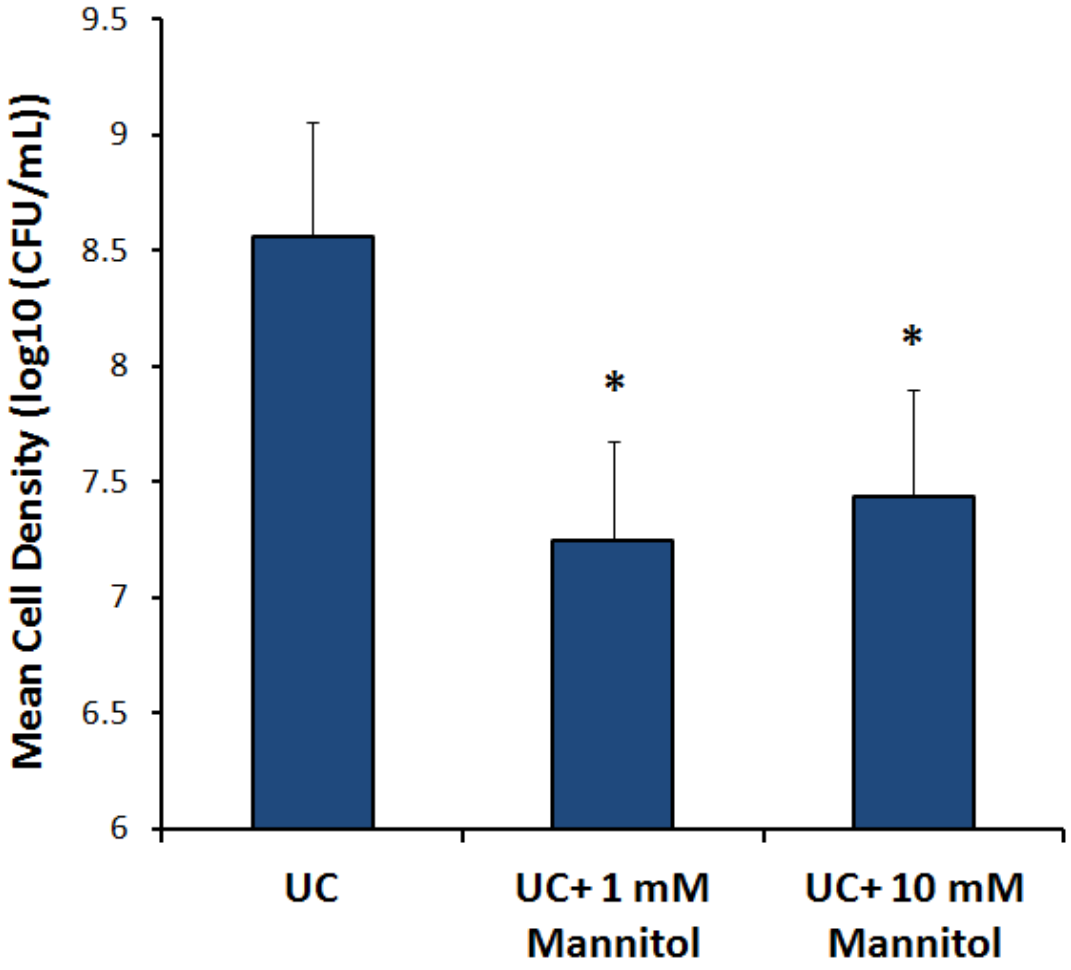

Figure 3.31. The effect of mannitol metabolites on the anti-biofilm efficacy of 1mg/mL unconjugated SPION. 1 mM and 10 mM mannitol metabolites significantly enhanced the SPION activity against *S. aureus* biofilms (* $p < 0.01$).

Here, a low-cost, simple and broad-spectrum approach to eradicate antibiotic resistant biofilms through the use of SPION as well as enhancing SPION efficacy through metabolic stimuli (i.e., fructose) was established. This approach is effective against both gram-negative and gram-positive bacteria. A possible mechanism for the enhanced anti-biofilm activity of SPION in the presence of fructose is summarized in **Fig. 3.32.** It is reasoned that the enhanced SPION activity is due to the increased uptake of nanoparticles by the biofilm which increases the concentrations of iron and sulfur and the generation of ROS. Recently, it has been shown that metabolite enabled eradication of biofilms occurs through the catabolism of metabolites and generation of NADH. Bacterial electron transport chain oxidizes NADH and contributes to the proton motive force (PMF). As a result, antibiotic uptake and the killing of persisters are facilitated.[179] The same mechanism could take place during the fructose-enhanced eradication of biofilms, as the SPION uptake also increased in the presence of fructose. Bacterial death might occur due to oxidative stress since ROS formation was increased. Superoxide (O^{2-}) formation could be stimulated by the electron chain transport and O^{2-} might then damage iron-sulfur (Fe-S) clusters, making more ferrous iron available for oxidation by the Fenton reaction. The Fenton reaction leads to the formation of hydroxyl radicals (•OH), which damages DNA, lipids and proteins.[230,231] All of these events eventually cause bacterial cell death and the eradication of biofilms.

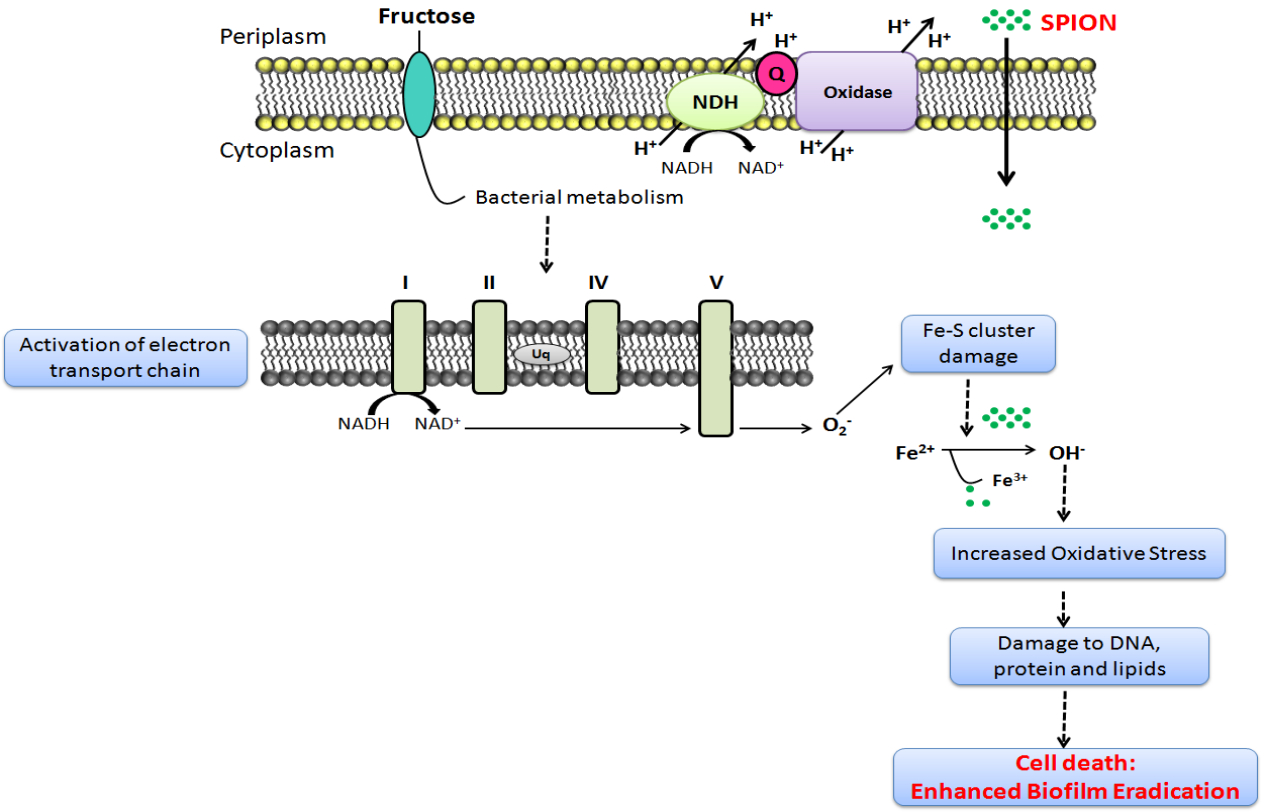

Figure 3.32. Possible mechanism for the observed enhanced anti-biofilm activity when fructose metabolites were added to the SPION treatment. Enhanced activity is due to the increased penetration of nanoparticles within the biofilm which leads to increases in ROS formation. The uptake of fructose metabolites might induce the catabolism of carbon sources and the generation of NADH. The bacterial electron transport chain oxidizes NADH and contributes to PMF. Then, bacterial cell death might occur due to the oxidative stress from ROS formation. First, superoxide (O_2^-) formation could be stimulated by the electron chain transport and O_2^- might damage Fe-S clusters, making more ferrous iron available for oxidation by the Fenton reaction. The Fenton reaction might lead to the formation of hydroxyl radicals (•OH), which can damage DNA, lipids and proteins. All of these events eventually cause bacterial cell death and the eradication of biofilms.

3.4. Conclusions

Overall, this chapter highlighted the promising possibility of using superparamagnetic iron oxide particles as a new therapeutic option to the current antimicrobial strategies against MRSA infections. In addition, the efficacy of superparamagnetic iron oxide particles against persistent infections was further improved by manipulating the biofilm metabolic microenvironment, creating a new the nanotechnology-driven approach. The promising capability of using superparamagnetic iron oxide particles in combination with fructose metabolites as a new therapeutic option to existing antimicrobial strategies was highlighted. These results have important implications. First, we have shown that SPION are more effective than the currently used antibiotics for treating MRSA biofilms (especially, vancomycin). In addition, SPION can be conjugated with different antibacterial metals to increase their anti-biofilm properties. Moreover, for the first time, the presence of fructose metabolites was shown to enhance the efficacy of the SPION against MRSA, *E. coli* and *P. aeruginosa* biofilms. Thus, this approach has a broad spectrum against both gram-positive and gram-negative bacteria. Biofilms develop a protected mode of growth and shut down their metabolism. Fructose metabolites might induce the metabolism and increase the uptake of SPION by the biofilms. It is envisioned that this simple and inexpensive approach could lead to novel alternative treatments to the only clinical option, vancomycin, which MRSA has started to develop a resistance towards. Once their *in vitro* and *in vivo* toxicity are well-characterized, these novel SPION treatments could lead to successful clinical outcomes in terms of minimized infections, longer medical device lifetimes, and decreased antibiotic usage. All of these events can support decreased antibiotic resistance in the clinical settings.

Chapter 4. Eradicating Antibiotic-Resistant Biofilms with Silver-conjugated Superparamagnetic Iron Oxide Nanoparticles

4.1. Introduction

Invasive medical devices (such catheters, implants, artificial joints and endotracheal tubes) have become an integral part of healthcare [4]. While these devices are used in many areas of medicine for diagnostic and therapeutic purposes, device-associated infections as well as device-associated nosocomial infections have been a critical concern for many years[5,6,194,195]. At the global level, at least 50% of nosocomial infections are device-related[6]. In addition, between 5 and 10% of patients admitted to acute care hospitals, acquire one or more infections [195]. These events affect approximately two million patients each year in the United States, result in up to 100,000 excess deaths, and lead to an estimated cost to the U.S. health care system of more than 35 billion U.S. dollars per year [194,195].

Staphylococcus aureus (*S. aureus*) has been one of the growing causes of healthcare and community-associated infections.[1,196,197] *S. aureus* can cause skin and soft-tissue infections, bloodstream infections, pneumonia, infective endocarditis and osteomyelitis [1]. Moreover, the emergence of methicillin-resistant *S. aureus* (MRSA) is a serious clinical problem since MRSA is responsible for 50% of the 14 million skin and soft-tissue infections, 100,000 blood infections which all together leads to more than 15,000 deaths

per year in the United States [198,199]. Currently, the only clinically available antibiotic to treat MRSA infection is vancomycin. On the other hand, vancomycin-intermediate *S. aureus* (VISA) and vancomycin-resistant *S. aureus* (VRSA) strains have emerged due the prevalent use of vancomycin.[201-203,232] The formation of sessile and heterogeneous bacterial communities, called biofilms, is the main contributing factor to the bacterial antibiotic resistance. *S. aureus* becomes resistant by producing an extracellular polymeric substance (EPS) matrix which is composed of polysaccharides, nucleic acids, proteins and lipids.[180,181] Sessile bacteria embedded in this EPS matrix can withstand host immune responses and become less susceptible to antibiotics as they fail to penetrate through the biofilm. Therefore, there is an urgent clinical need to develop novel antibacterial therapies to eradicate biofilms and thus reduce infections in the healthcare and community settings.

Recent advances in nanotechnology hold a great potential to develop novel strategies to eradicate biofilms, instead of antibiotics. Fullerenes (C60)[203], carbon nanotubes (CNTs) [204 205] and graphene [206] as well as silver (Ag) [205,207], gold (Au) [208], magnesium oxide (MgO) [209] and zinc oxide (ZnO) [210] nanoparticles have shown promising antibacterial properties. However, these nanoparticles cannot penetrate to the full depth of the biofilm and uptake within the biofilm is usually low[182]. Nanoparticles which possess magnetic properties, superparamagnetic iron oxide particles (SPION), have been extensively used in various biomedical applications for magnetic imaging, bioseperation, biodetection as well as targeted drug and gene delivery [111]. Although there are limited number of studies which actually target the biofilms, SPION have shown promising bactericidal effects

[125,169,170,211]. A novel infection treatment could be developed through the design of multifunctional SPION, which can be targeted to the infection site, disrupt and eradicate the biofilm, in the presence of a magnetic field.

In this study, it was demonstrated that SPION conjugated with antibacterial silver salts exhibit strong eradication properties against the antibiotic-resistant (MRSA) biofilms (**Figure 4.1**). Silver-conjugated SPION significantly decreased the number of planktonic MRSA in the surrounding medium as well as the MRSA biofilm mass. In addition, antibacterial properties of silver-conjugated SPION were improved when an external magnetic field was applied as their magnetic core enabled them to penetrate into the biofilms. Moreover, the enhanced anti-biofilm efficacy of SPION treatments were due to the significant increases in intracellular or membrane bound iron, sulfur and silver, and thus increases in SPION uptake within the MRSA biofilms.

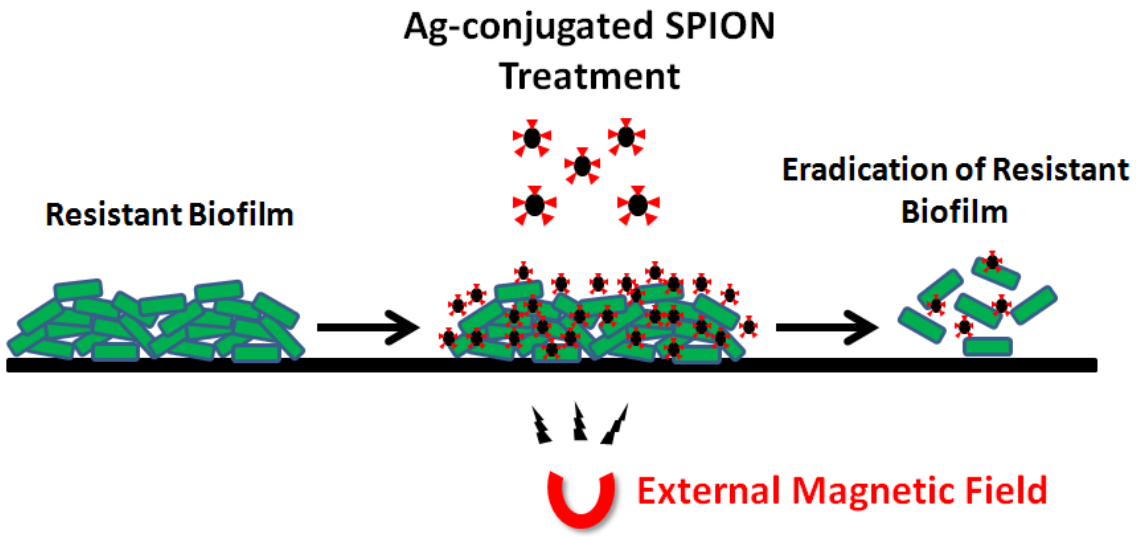

Figure 4.1. Schematic of the novel strategy for infection treatment. Methicillin-resistant *Staphylococcus aureus* (MRSA) biofilms were established on microtiter plate surfaces. Biofilms then were treated with superparamagnetic iron oxide nanoparticles (SPION) conjugated with antibacterial silver salts. After 24 hours, antibiotic-resistant biofilms were significantly eradicated. Anti-biofilm efficacy of the silver-conjugated SPION treatment was also improved by an external magnetic field. Thus, this novel treatment can be targeted to the infection site, disrupt and eradicate the biofilm, in the presence of a magnetic field.

4.2. Materials and Methods

4.2.1. Synthesis of Superparamagnetic Iron-Oxide Nanoparticles

SPION were synthesized using a variation of the high temperature reflux method in triethylene glycol (TREG).[233] 2 mmol of iron (III) acetylacetone (**Fe $(acac)_3$**) was dissolved in 25 mL of TREG in a round bottom boiling flask. Then, the solution was heated gradually to 278°C with constant magnetic stirring and incubated for 30 minutes. After this gentle reflux, the solution was cooled slowly to room temperature. SPION were then conjugated with 4 mmol dimercaptosuccinic acid (DMSA), which was used as a capping agent. The SPION + DMSA solution was incubated overnight to react. Then, the synthesized SPION were precipitated in 200 mL of 100% ethanol saturated with ammonium sulfate $(NH_4)_2SO_4$). SPION were isolated in a strong magnetic field (4" x 1" x 1" thick magnet, 4871 Gauss, and Neodymium; K&J magnetics, Jamison, PA). Particles were then purified several times in ethanol and air dried at room temperature.

4.2.2. Conjugating SPION with Silver Salts

The DMSA capping agent was further conjugated with antibacterial silver (Ag) metals. 10 mg/mL SPION solution was diluted in ethanol (1:10) with 1 mM salts of $AgNO_3$. Then, the solution was incubated overnight and shaken at 90 rpm. After overnight incubation, silver conjugated SPION were isolated in a strong magnetic field (4" x 1" x 1" thick magnet, 4871 Gauss, and Neodymium; K&J magnetics, Jamison, PA) where non-magnetic components are washed away. The purification step was repeated three times.

4.2.3. Characterization of Unconjugated and Silver-conjugated SPION

Unconjugated SPION morphology was evaluated by transmission electron microscopy (TEM). A drop of SPION sample dispersed in ethanol was placed on a copper grid and dried. Samples were imaged by a Philips C20 TEM (Philips, New York, NY). In addition, the particle size was analyzed by dynamic light scattering (DLS). Unconjugated SPION and silver-conjugated SPION were prepared in sterile TSB. TSB alone maintained as a control, and treated the same as the other SPION solutions. Samples were prepared by diluting 100 µl of each solution into 0.9 ml double deionized water. Then, diluted samples were filtered using a 0.2 µm filter (Fisher Scientific, Pittsburg, PA). For DLS readings, a Zetasizer Nano ZS (Malvern Instruments) was used and the particle size was analyzed by the Dispersion Technology software. Samples were repeated in 5 replicates for each reading. Moreover, inductively coupled plasma atomic emission spectroscopy (ICP-AES) was used to confirm the presence of silver in the metal conjugated SPION. First, standard solutions of iron (Fe^{3+}), sulfur ions (S^{2-}) and silver (Ag^{1+}) were prepared in a 2% solution of HNO_3 at 100 parts per million (ppm) to obtain a standard curve. 50 µL of unconjugated (UC) and silver conjugated (Ag) SPION solutions were then dissolved in aqua regia solution (nitric acid and hydrochloric acid at a volumetric ratio of 1:3). The SPION + aqua regia solution was evaporated to dissolve nanoparticles and all silver salts. Then, 5 ml of 2% nitric acid was added to each SPION + aqua regia solution and the samples were analyzed with ICP-AES. Iron, sulfur and silver concentrations of the silver conjugated SPION were compared with the unconjugated SPION (UC).

4.2.4. Bacteria Culture

The Mu50 strain of MRSA (ATCC #700699, American Type Culture Collection, Mannassas, VA) was hydrated and streaked for isolation on a tryptic soy agar plate. Following growth and isolation, a single isolated colony was selected and inoculated in 3 mL of a tryptic soy broth (TSB) media (MP Biomedicals, Solon, OH). The bacteria culture was grown on an incubator shaker for 18 hours at 37^0C, 200 revolutions per minute (rpm) until it reached the stationary phase.

4.2.5. Biofilm Growth and Treatment

Overnight cultures which had an optical density of 0.52 at 562 nm were diluted at a ratio of 1:90 in fresh TSB, corresponding to a 10^8 cells/mL solution. 200 µL of this solution was inoculated onto each well of a 96-well microtiter plate (Fisher Scientific, Pittsburgh, PA) and incubated for 24 hours at 37^0C to allow for biofilm formation. After 24 hours, the culture medium was replaced with 1 mg/mL of silver conjugated (Ag) SPION in fresh TSB solution. After 24 hours of treatment, planktonic bacteria growth was assessed by the optical density at 562 nm. In addition, the amount of biofilm remaining was assayed by crystal violet (CV) staining, as described below.

4.2.6. Crystal Violet (CV) Staining Assay

CV staining was used to quantify biofilm density after 24 hours of treatment. First, the TSB culture medium was removed and each well was rinsed with 1X PBS. Then, 200 µL of a 0.1% CV solution in water was added to each well and incubated for 15 minutes.

Then, wells were rinsed three times with 175 µL of PBS. The plate was air dried at room temperature for two days. Then, CV was dissolved in 200 µL of 100% ethanol, and the optical density was measured at 562 nm. Optical readings of control solutions with silver-conjugated SPION without bacteria were subtracted from the corresponding readings.

4.2.7. Viable Cell Count Assay

Viable bacteria cell counts were obtained by disrupting biofilms formed at the bottom of the microtiter plate in a sonicating water bath. First, a 96-well microtiter plate was rinsed three times with 200 µL of 1X PBS. 150 µL of 1X PBS was added into each well and the microtiter plate was covered with a sterile tape. The plate was placed in a water bath (Branson Ultrasonics 5510, Danbury, CT) and sonicated for 30 min at 40 kHz to dislodge biofilms into the PBS solution. Then, serial dilutions were performed and 10 µL of each dilution was spot-plated on tryptic soy agar (TSA) plates. Colony forming units (CFU) were counted after an overnight incubation at 37°C.

4.2.8. Analysis of SPION Uptake within the Biofilm

The amount of silver-conjugated SPION taken up by the biofilm was measured by inductively coupled plasma atomic emission spectroscopy (ICP-AES) via quantifying the presence of iron (Fe^{3+}), sulfur (S^{2-}) and silver (Ag^{+}) ions. As previously described, MRSA biofilms were grown in 96-well plates and they were treated with silver-conjugated SPION. After 24 hours of treatment, wells were washed three times with PBS to remove SPION that were not taken up by the biofilms or SPION which were

membrane-unbound. Then, the biofilms were digested in a 50% nitric acid (HNO_3) solution and the microtiter plate was shaken for 30 minutes at 150 rpm. Then, 200 µL of the acid digested bacteria solution was then diluted in 2% nitric acid solution and samples were analyzed by ICP-AES. The amount of iron (Fe^{3+}), sulfur (S^{2-}) and silver (Ag^{+}) ions in SPION treated biofilms were compared to untreated control samples.

4.3. Results and Discussion

4.3.1. Characterization of Silver-conjugated SPION

Figure 4.2 shows the unconjugated SPION (UC) and silver-conjugated morphology characterized by transmission electron microscopy (TEM). Unconjugated SPION were synthesized using a variation of the high temperature reflux method in triethylene glycol (TREG).[233] SPION were chelated with dimercaptosuccinic acid (DMSA) to increase the solubility and dispersion of particles in water, cell medium and physiological fluids.[213] TEM analysis demonstrated that SPION were successfully synthesized with an average size of 10.07 ± 1.54 nm.

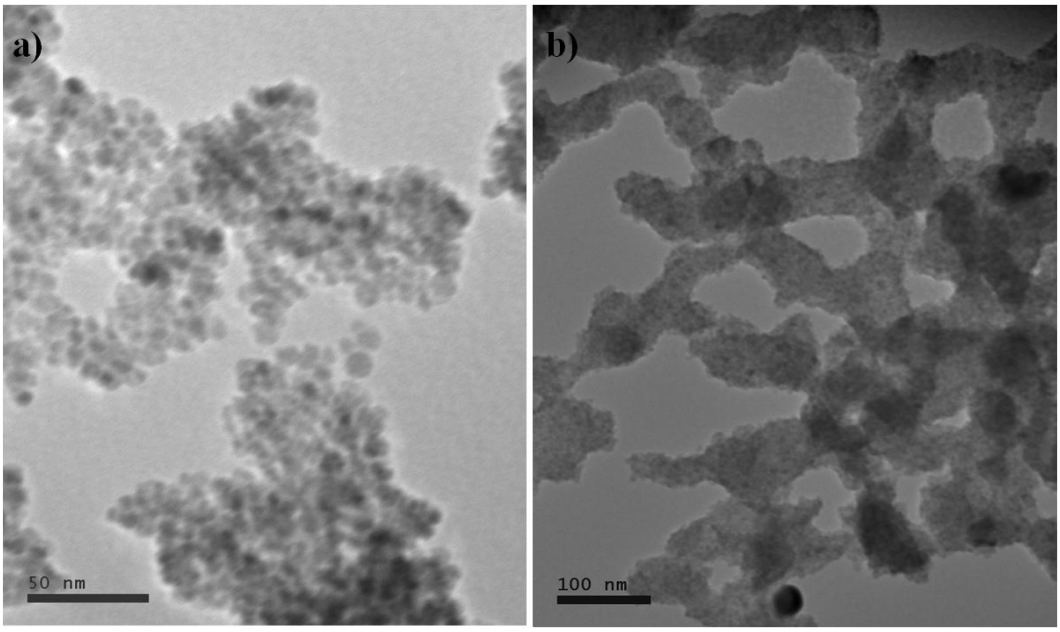

Figure 4.2. TEM analysis of the magnetic nanoparticles used in the study**. a)** Unconjugated SPION (UC) prepared by refluxing iron (III) acetylacetone in triethylene glycol (TREG) (scale bar = 50 nm). **b)** Silver-conjugated SPION (scale bar = 100 nm).

On the other hand, dynamic light scattering (DLS) analysis showed larger particle sizes. Unconjugated SPION had a mean hydrodynamic diameter of 18.17 ± 1.34 nm (**Figure 4.3a).** DLS measures the hydrodynamic diameter and the measurements could be influenced by nanoparticle aggregation or coating agents.[234,235] The acquired particle size measurements were fundamentally different from the particle sizes measured by TEM, where the discrete particle size is measured.[235] Therefore, larger particle size analysis from DLS measurements were expected since dimercaptosuccinic acid (DMSA) was used as a capping agent during unconjugated SPION (UC) synthesis. In addition, silver-conjugated SPION had a mean hydrodynamic diameter of 176.5 ± 27 nm, which was approximately ten times larger than the unconjugated SPION (**Figure 4.3b**). Silver can interact and bind to proteins in the bacteria culture medium, particularly to their thiol (S-H) groups.[236,237] This could lead to silver-conjugated SPION aggregation and increases in the DLS particle size measurements. In addition, chemical composition of SPION was analyzed by composition by inductively coupled plasma atomic emission spectroscopy (ICP-AES). ICP-AES analysis showed that that silver salt conjugations were successful (**Figure 4.4**). Increased sulfur concentration (S^{2-}) indicated that DMSA capped to the unconjugated SPION (UC) surface, and increases in silver (Ag^{+}) concentration showed that silver metals were also successfully conjugated. Moreover, concentration of silver (Ag^{+}) increased as the metal salt conjugations increased from 1 mmol to 4 mmol.

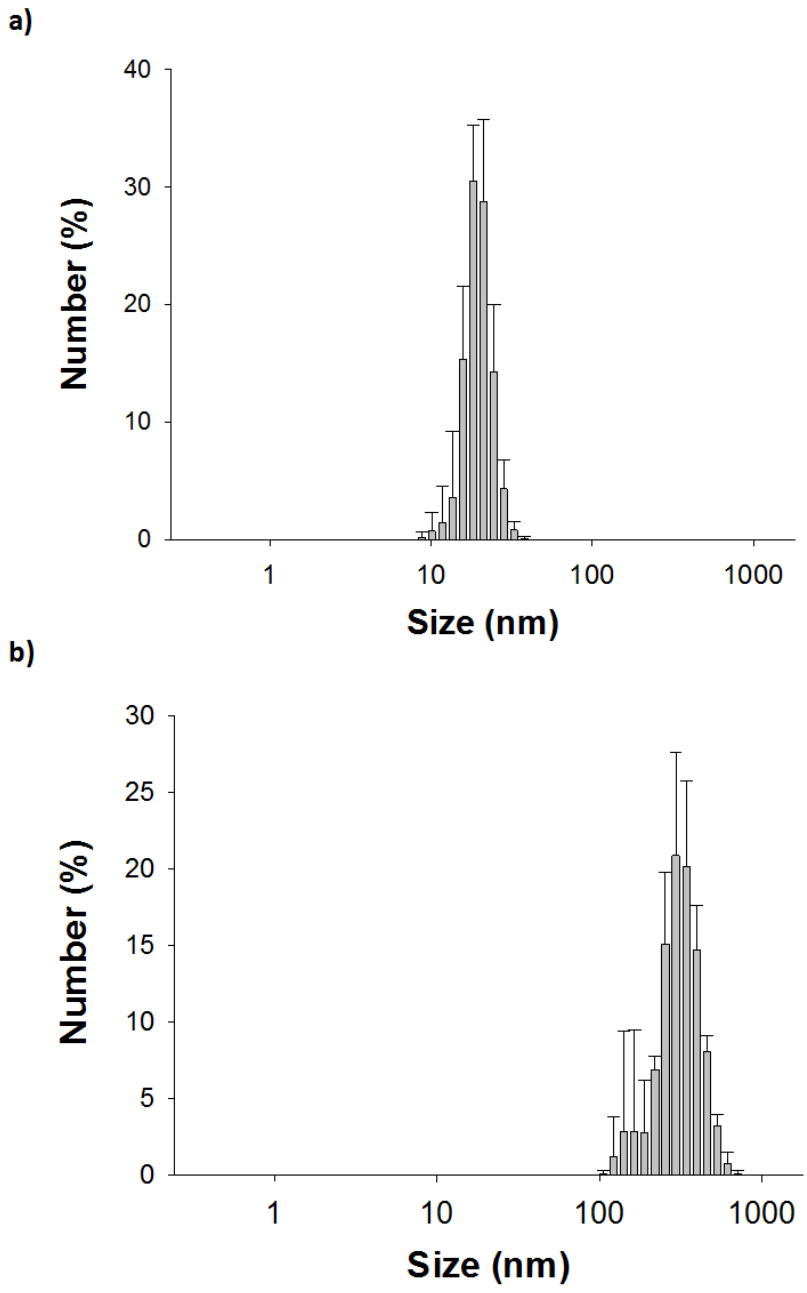

Figure 4.3. Characterization of unconjugated (UC) and silver-conjugated SPION. **a)** Size distribution histogram of unconjugated SPION. Average particle size is 18.17 ± 1.34 nm. **b)** Size distribution histogram of silver-conjugated SPION. Average particle size is 176.5 ± 27 nm.

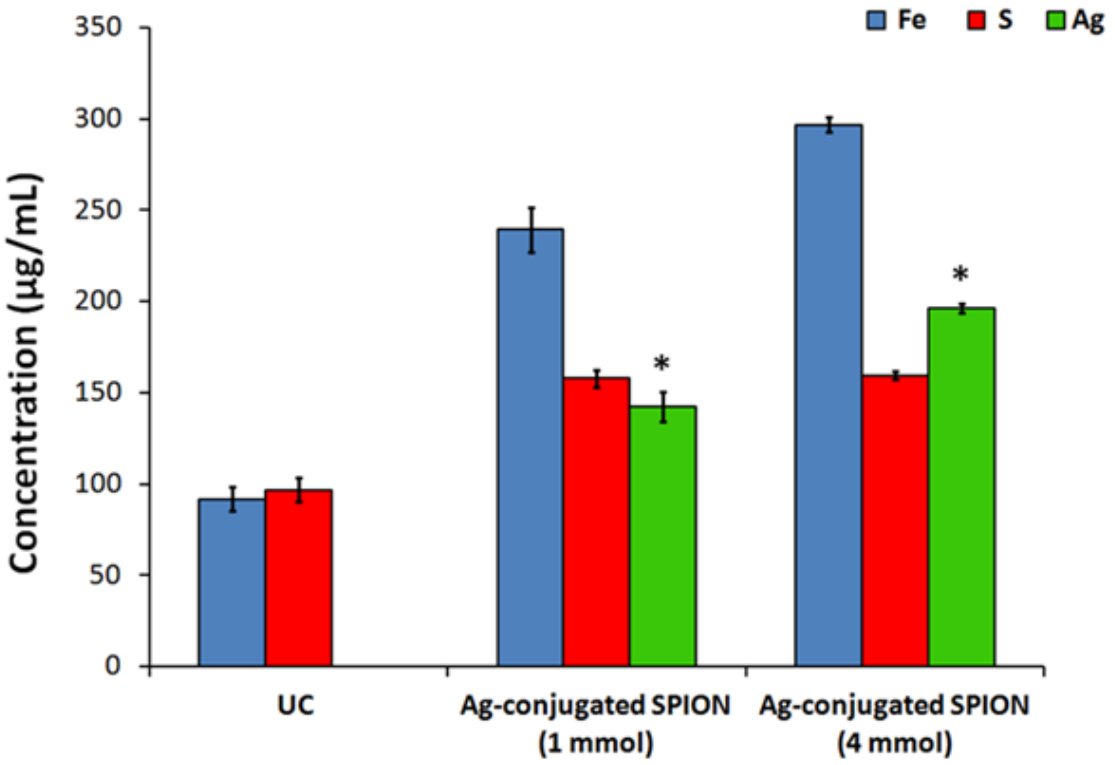

Figure 4.4. Characterization of unconjugated (UC) and silver-conjugated SPION. Elemental composition of unconjugated (UC) and silver-conjugated SPION determined by ICP-AES. 10 mg/mL of a SPION solution was conjugated with 1 mM or 4 mM salt of $AgNO_3$. ICP-AES indicated that silver was successfully conjugated to SPION. The concentration of silver (Ag^+) ions increased as the silver metal salt conjugations increased from 1 mmol to 4 mmol. Data represents mean ± standard error of the mean (SEM), N=3.

4.3.2. Characterization of Antibacterial Properties

Then, the antibacterial and anti-biofilm activity of silver-conjugated SPION against an antibiotic-resistant biofilm were investigated. The Mu50 strain which is a clinical isolate of MRSA with reduced susceptibility to vancomycin was used as the target organism. [201,202,232] The antibacterial properties against both planktonic (free-floating) MRSA and sessile MRSA biofilms were investigated by a high-throughput in vitro screening assay. Biofilms were established as the inoculated bacteria attached to the surface of a microtiter plate during 24 hours of incubation. Then, biofilms were treated with silver-conjugated SPION. After 24 hours of treatment, planktonic MRSA growth and sessile MRSA biofilm mass was analyzed.

4.3.2.1. Optimization of the Antibacterial Dose of Ag-conjugated SPION

First, the antibacterial activity of silver-conjugated SPION at three different concentrations (0.01 mg/mL, 0.1 mg/mL and 1 mg/mL) was assessed. As shown in **Figure 4.5**, when the concentration of silver-conjugated SPION in bacterial culture medium (tyrptic soy broth) increased from 0.1 to 1 mg/mL, planktonic MRSA growth significantly decreased from 88.14 ± 2.28% to 57.91 ± 1.57% ($p < 0.001$) whereas 0.01 mg/mL silver-conjugated SPION did not have any significant antibacterial effect. In addition, the concentration of SPION had a significant effect on planktonic MRSA growth. 1 mg/mL of silver-conjugated SPION was significantly more effective than 0.01 mg/mL and 0.1 mg/mL silver-conjugated SPION ($p < 0.001$). Therefore, 1 mg/mL was chosen as the optimal dose for further experiments to assess the anti-biofilm properties of the nanoparticles.

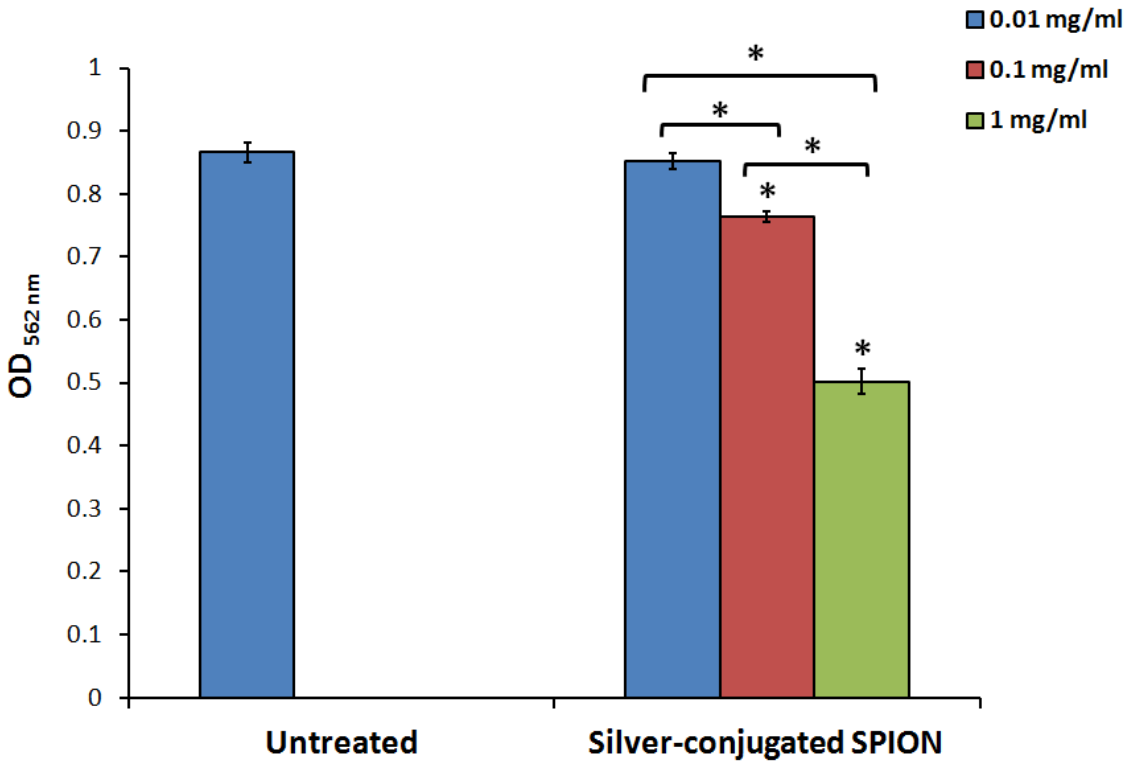

Figure 4.5. Optimization of the antibacterial dose of silver-conjugated SPION. Antibacterial activity of silver-conjugated SPION was assessed at three different concentrations (0.01 mg/mL, 0.1 mg/mL and 1 mg/mL). When the concentration of silver-conjugated SPION increased from 0.1 to 1 mg/mL, planktonic MRSA growth rate significantly decreased from 88.14 ± 2.28% to 57.91 ± 1.57% (* $p < 0.001$). On the other hand, 0.01 mg/mL silver-conjugated SPION did not have any significant antibacterial effect. In addition, the concentration of SPION had a significant effect on planktonic MRSA growth rate. 1 mg/mL was significantly more effective than 0.01 mg/mL and 0.1 mg/mL silver-conjugated SPION (*$p < 0.001$). Data represents mean ± standard error of the mean (SEM), N= 3.

4.3.2.2. Anti-biofilm Properties

The MRSA biofilm mass after silver-conjugated SPION treatment was quantified by crystal violet staining, Crystal violet stains the bacterial cells as well as the biofilm exopolysaccharide matrix (EPS) components, and thus quantifies the biofilm mass. A ~30% decrease in biofilm mass was observed when MRSA biofilms were treated with 1 mg/mL silver-conjugated SPION ($p < 0.01$) (**Figure 4.6**). Most importantly, this decrease in biofilm mass corresponded to a seven orders of magnitude (7 logs) decrease in viable bacteria numbers within the biofilm.

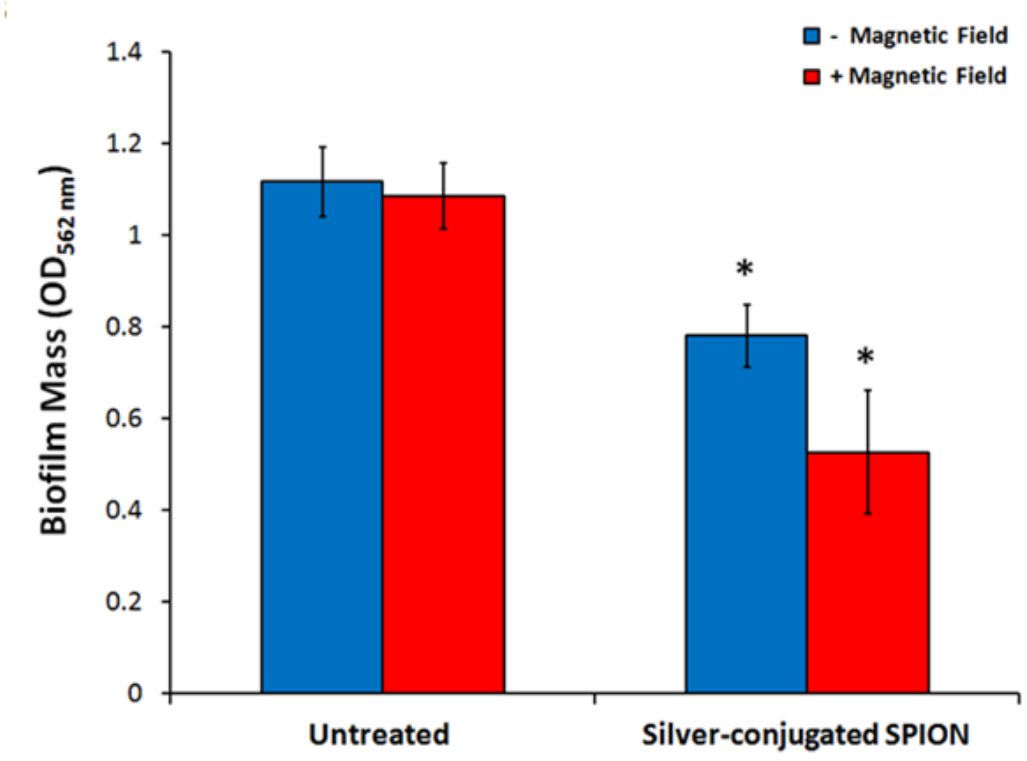

Figure 4.6. Antibacterial properties of silver-conjugated SPION against MRSA biofilms. Biofilm mass significantly decreased when MRSA biofilms were treated with 1 mg/mL silver-conjugated SPION. Biofilm mass further decreased when an external field was present (*$p < 0.01$).

Figure 4.7 shows bacterial colonies to represent the eradication of MRSA biofilms with the silver-conjugated SPION treatment. During viable cell count experiments, uncountable colonies were observed for the untreated MRSA biofilm at the 10-5 dilution. On the other hand, countable colonies were observed at the same dilution when antibiotic-resistant biofilms were treated with 1 mg/mL silver-conjugated SPION. These representative colony images clearly showed that silver-conjugated SPION significantly eradicated the antibiotic-resistant biofilms. In addition, fluorescent microscopy analysis also showed that silver-conjugated SPION better eradicated the MRSA biofilms (**Figure 4.8**).

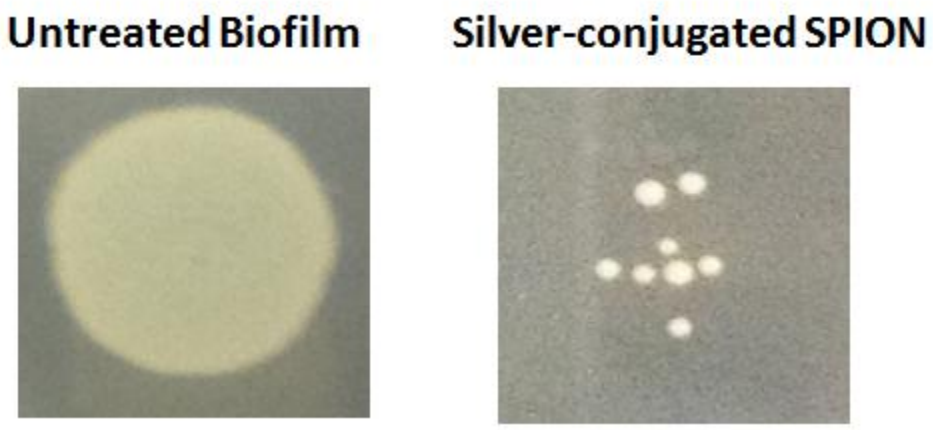

Figure 4.7. Representative colony forming units. An uncountable colony was observed for the untreated MRSA biofilm at a 10^{-5} dilution whereas countable colonies were observed at the same dilution when biofilms were treated with 1 mg/mL silver-conjugated SPION. Thus, silver-conjugated SPION treatment significantly eradicated the MRSA biofilms.

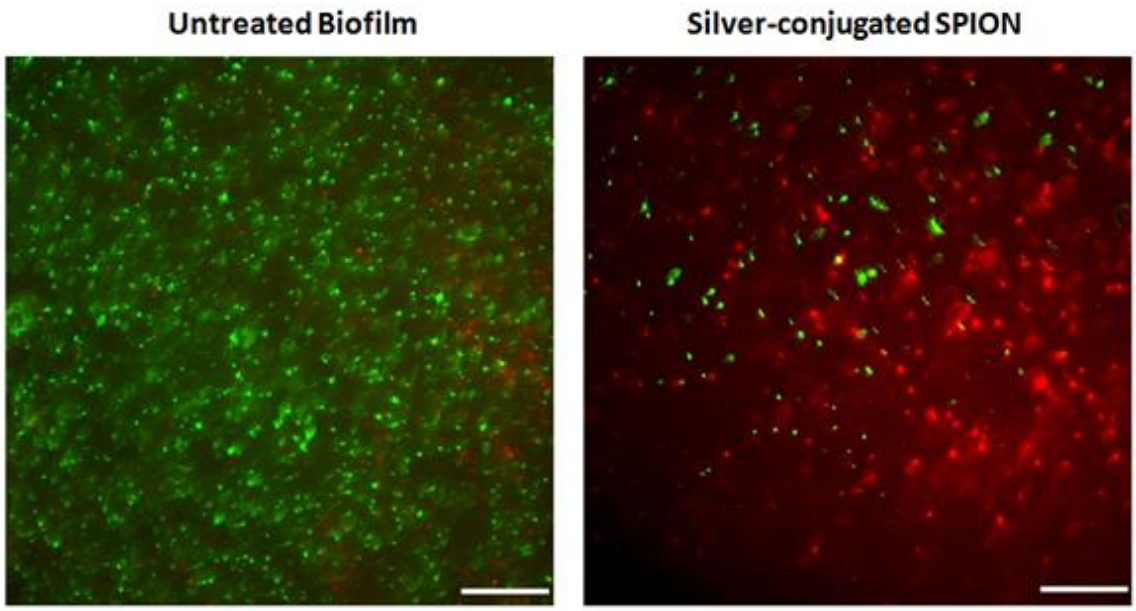

Figure 4.8. The eradication efficacy of silver-conjugated SPION against MRSA biofilms as compared to control biofilms. Live (green) and dead (red) cells were stained with Baclight Live/Dead utilizing Syto®9 and propidium iodide stains. Scale bars represent 20 µm.

The magnetic manipulation of silver-conjugated SPION has been also investigated, towards improving antibacterial properties *in vitro*. The anti-biofilm efficacy of silver-conjugated SPION was significantly improved when they were coupled with an external magnetic field (2.6 mm diameter x 5 mm thick magnet). Planktonic bacteria growth and biofilm mass significantly decreased in the presence of silver-conjugated SPION + magnetic field. For example, biofilm mass decreased to ~47 % when MRSA biofilms were treated with 1 mg/mL silver-conjugated SPION in the presence of an external field ($p < 0.01$) (Figure 5). Moreover, planktonic MRSA growth further decreased to 21.73 %

when an external magnetic field was present ($p < 0.001$) (**Figure 4.9**). Increases in the antibacterial activity of silver-conjugated SPION in the presence of an external magnetic field can be due to the improved penetration of the nanoparticles within the biofilm. Thus, this novel treatment has the potential to be targeted to the infection site, disrupt and eradicate the biofilm, in the presence of a magnetic field.

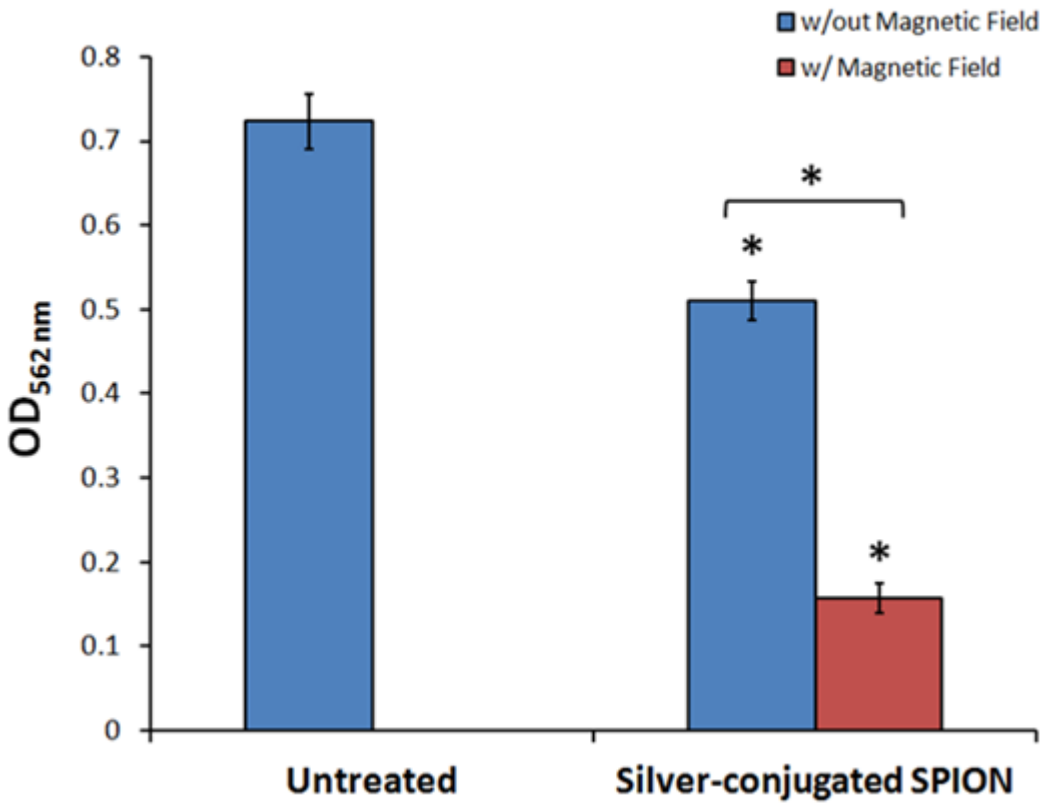

Figure 4.9. Planktonic MRSA growth further decreased when an external magnetic field was present (*p < 0.001). All of these results show that the anti-biofilm efficacy of silver-conjugated SPION treatment is improved in the presence of an external magnetic field.

Many studies have shown that the yield of nanoparticle uptake by the biofilms is low and nanoparticles cannot penetrate to the full depth of the biofilm. Therefore, the uptake of silver-conjugated SPION within the MRSA biofilms was analyzed by quantifying the presence of iron (Fe^{3+}), sulfur (S^{2-}) and silver (Ag^{+}) ions by ICP-AES (**Figure 4.10**). The uptake of SPION included the nanoparticles within the cell, attached to the bacterial cell surface as well as in the EPS matrix of the biofilm. The intracellular or membrane-bound iron (Fe^{3+}) concentration was 22.122 ± 4.590 µg/mL, which was significantly higher compared to untreated control biofilms ($p < 0.01$). Significant increases in intracellular or membrane-bound sulfur (S^{2-}) concentration were also observed, which increased from 2.601 ± 0.426 µg/mL to 5.939 ± 1.15 µg/mL ($p < 0.05$). Moreover, silver (Ag^{+}) concentration was 3.928 ± 0.718 µg/mL which was significantly higher compared to untreated control biofilms ($p < 0.001$). These results indicated that the anti-biofilm efficacy of silver-conjugated SPION treatment is mostly due to the significant increases in intracellular or membrane bound iron, sulfur and silver ion concentrations, and thus increased uptake of SPION within the MRSA biofilms.

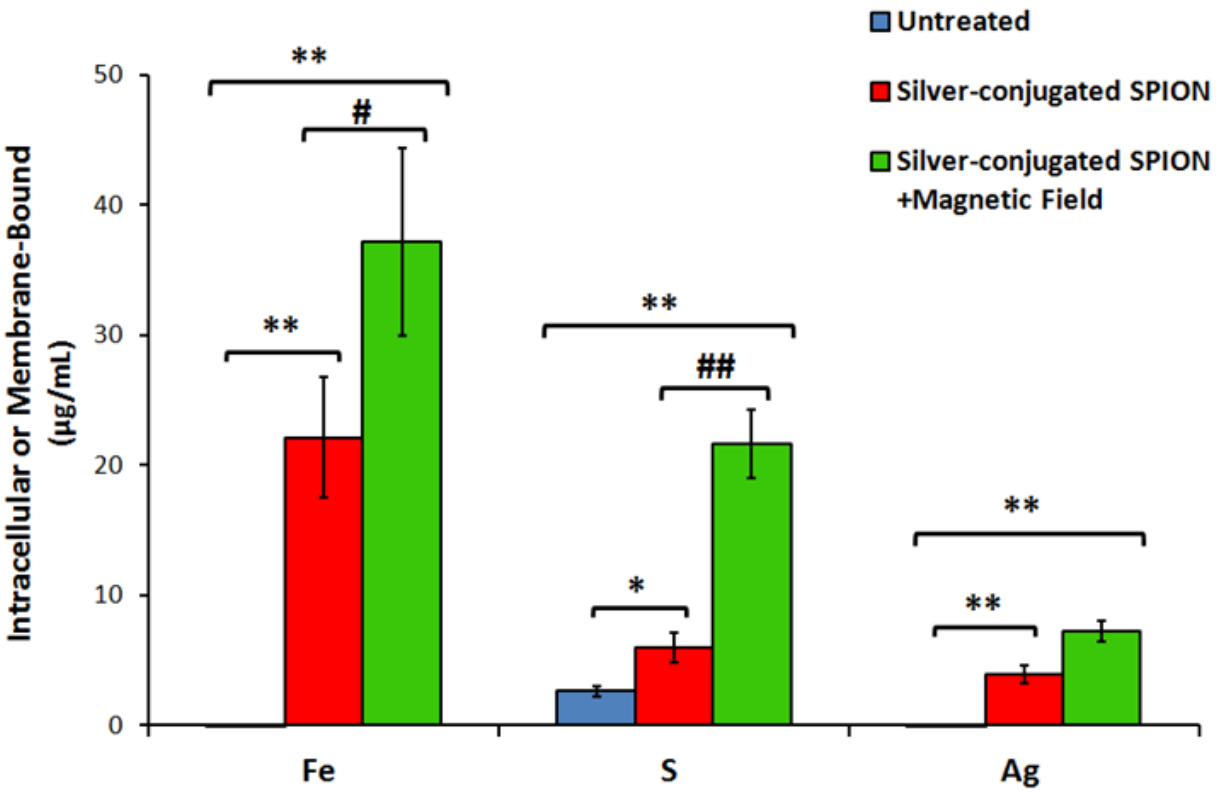

Figure 4.10. Analysis of the uptake of silver-conjugated SPION within the MRSA biofilms by quantifying the presence of iron (Fe^{3+}), sulfur (S^{2-}) and silver (Ag^{+}) ions by inductively coupled plasma atomic emission spectroscopy (ICP-AES). The enhanced anti-biofilm efficacy of SPION treatments are due to the significant increases in intracellular or membrane bound iron (Fe^{3+}) (**$p < 0.001$*), sulfur (S^{2-}) (**$p < 0.05$*) and silver (Ag^{+}) (**$p < 0.001$*), which indicates an increased uptake of silver-conjugated SPION within the MRSA biofilms. An external magnetic field further increased the intracellular or membrane-bound Fe^{3+} ($^{\#}p < 0.1$), S^{2-} ($^{\#\#}p < 0.01$) and Ag^{+} within the biofilm and improved the antimicrobial activity of silver-conjugated SPION. Data represents mean ± standard error of the mean (SEM), N= 3.

Iron oxide nanoparticles have been widely used for biomedical and clinical applications due to their desirable magnetic properties (i.e. superparamagnetism) and low cost. [107,169,172] In addition, SPION have been approved by the US Food and Drug Administration (FDA) for several applications as imaging agents [238] and their biocompatibility with mammalian cells has been demonstrated in many studies. [239,240] Silver nanoparticles also possess unique optical [241], catalytic [242] and antibacterial properties[146,207,243]. Silver has shown bactericidal activity even at very low concentrations, such as 35 parts per billion (ppb), without toxic effects to mammalian cells[244-246]. Silver antibacterial activity is generally attributed to the oxidative stress generated by reactive oxygen species (ROS) [247]. In addition, the electrostatic interactions between silver nanoparticles and bacterial cell membranes as well as membrane proteins could result in damages in cell membrane and lead to bacterial cell death.[124,248]

4.4. Conclusions

In this chapter, the unique magnetic and antibacterial properties of SPION and silver particles were combined through the design of silver-conjugated SPION. For the first time, it was demonstrated that MRSA biofilms can be eradicated by silver-conjugated SPION. In addition, SPION anti-biofilm efficacy was further improved in the presence of an external magnetic field. This novel SPION could be used as a targeted antibacterial therapy to the infection site and could be removed with an external magnetic field. Once their toxicity is completely understood, silver-conjugated SPION has a great potential to be an alternative infection therapy to vancomycin, the antibiotic of last resort. It is envisioned that this novel infection eradication strategy will result in a decrease in antibiotics usage, thus a decrease in antibiotic resistance in the clinical settings.

Chapter 5. Potential Applications of the Multifunctional Platform Nanotechnologies in the Healthcare Settings

5.1. Introduction

Medical devices (such as catheters, enteral feeding tubes, stethoscopes) have become an integral part of primary healthcare. While these devices are used in many areas of primary care, medical complications due to infections have been a critical concern. Due to increasing costs of accessing medical care and shortage of primary care physicians in community and rural areas[249], a transformation in the infection management and maintenance of medical devices to increase compliance with primary care protocols while reducing medical error needs to be addressed. Thus, infection control in primary care is critical for patient safety and there is an urgent need for innovative technologies to prevent infections in primary care settings.

The Centers for Disease Control and Prevention (CDC) determined that among the nearly 2 million annual infections, the majority (78%) were acquired in acute care facilities. Long-term care accounted for 100,000 infections. Most importantly, more than 250,000 patients acquired infections while receiving home healthcare.[250] For example, in primary and community healthcare settings, urinary catheterization commonly used in managing older people and those with neurological conditions, where alternative treatments for bladder dysfunction are unsuccessful.[251] In the US, approximately 4 million patients undergo urinary catheterization annually, which are commonly used by patients in home healthcare settings.[252] However, these patients face the high risk of developing catheter-

associated urinary tract infections (CAUTI). CAUTI are also associated with recurrent catheter blockage, urinary tract stones, and increased risk of bladder cancer.[252] Moreover, medical device infections put an economic burden on the healthcare system, which includes the cost of antibiotic therapy that is a major source of bacterial resistance, leading to an estimated total cost of more than $35 billion per year.[7,8]

The surfaces of medical devices serve as substrates for bacterial attachment, growth, colonization and biofilm formation. Contamination occurs by inoculation with only a few microorganisms during implantation. Pathogens could be acquired from the primary care setting as well as the hands of the healthcare workers, including the physicians, nurses and nurse practitioners. There are standard principles to provide guidance on infection control in primary care settings. These distinct interventions include hand hygiene, use of personal protective equipment, education of patients and healthcare personnel.[253] However, these principles have been hard to implement. In addition, little has been explored to control infections by manipulating surface properties of medical devices at the nanoscale. Recently, many studies have shown that changes in material properties at the nanometer level can provide antibacterial properties.[23,26,113,115,118] In addition, some specific metabolites, such as fructose, have been found to increase the efficiency of antibiotics[179] and have been used to treat *E. coli* and *S. aureus* infections Thus, infection control is critical for patient safety and there exists an urgent need for innovative studies to develop infection prevention strategies in the primary care settings as well as clinical settings.

In this chapter, first, the antibacterial properties of superparamagnetic iron oxide nanoparticles (SPION) were investigated when incorporated into a traditional polymeric biomaterial (polyvinyl chloride). Then, the potential applications of multifunctional SPION polymer nanocomposites in the healthcare settings have been covered.

5.2. Methods and Materials

5.2.1. Nanocomposite Preparation

Unconjugated SPION (~10 nm in size) synthesized in Chapter 3 were added to tetrahydrofuran (THF) dissolved PVC endotracheal tubes (Hudson RCI, Research Triangle Park, NC). Final SPION concentration in the nanocomposite solution was 1 mg/mL, which corresponds to the antibacterial dose of SPION, as shown in earlier chapters. Solution was sonicated to promote nanoparticle distribution, pipetted onto 12 mm diameter glass coverslips (Fisher Scientific, Pittsburgh, PA), and dried in a vacuum oven. For bacteria experiments, PVC+SPION nanocomposites were sterilized by immersing the samples in 95% ethanol and sonicating for 30 minutes.

5.2.2. Bacteria Cell Counts Determined by Optical Density

S. aureus (ATCC #25923, American Type Culture Collection, Mannassas, VA) was hydrated and streaked for isolation on a tryptic soy agar plate. Following growth, a single isolated colony was selected and inoculated in 3 mL tryptic soy broth (TSB) media (MP Biomedicals, Solon, OH). The bacteria culture was grown on an incubator shaker for 18

hours at 37^0C, 200 rpm until it reached the stationary phase. First, the optical density of the overnight culture at 562 nm (OD_{562}) was adjusted to 0.52, which corresponds to cell number of 10^9. Then, the cultures were serially diluted to get a 10^3 cells/mL bacteria solution. 1 mL of a 10^3 cells/mL bacteria solution was seeded onto a single well of a 24-well plate (BD, Franklin Janes, New Jersey) containing either PVC+SPION nanocomposite or an conventional PVC sample. The plate was then placed in a stationary incubator at 37^0C with 5% CO_2. After 24 hours, samples were removed with a pair of sterile forceps. Optical density of the plate was then measured at 562 nm using a SpectraMax M5 plate reader (Molecular Devices, Sunnyvale, CA) to analyze the planktonic bacteria growth.

5.2.3. Biofilm Formation Analysis by Viable Cell Counts

Biofilm formation on the nanocomposite surfaces was assessed by quantifying the colony forming units/mL (CFU/mL). Specifically, each sample was placed in 1 mL of PBS (Fisher Scientific, Pittsburg, PA) and vortexed at 3000 rpm for 10 minutes. The cells were then serially diluted in PBS (Fisher Scientific, Pittsburg, PA) over a 4-log range. 20 µL of each dilution were plated on tryptic soy agar plates and incubated at 37°C overnight. After overnight incubation, colony forming units were counted.

5.3. Results

We have synthesized PVC+SPION composites to decrease bacterial growth and biofilm formation. Final SPION concentration in the nanocomposite solution was 1 mg/mL, which corresponded to the antibacterial dose of SPION, which also corresponded to 2% w/w of the nanocomposite. **Figure 5.1** shows the *S. aureus* planktonic growth on PVC + 2% SPION nanocomposites after 24 hours. Planktonic bacteria growth on nanocomposite surfaces significantly decreased by 36 ± 13.6 %, compared to conventional PVC surfaces ($p < 0.001$).

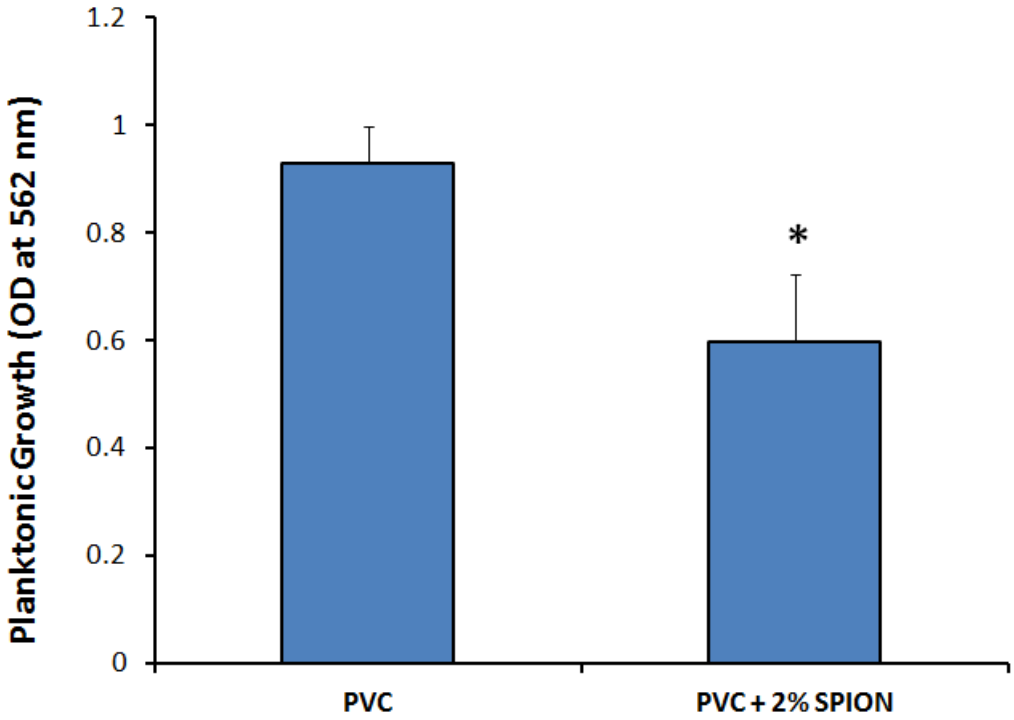

Figure 5.1. *S. aureus* optical density measurements after 24 hours. Planktonic bacteria growth significantly decreased on PVC+ 2% SPION nanocomposites, compared to conventional PVC surfaces (* $p < 0.001$). Data represents mean ± SEM, N=3.

In addition, *S. aureus* biofilm formation decreased on PVC+2% nanocomposites by ~73% compared to conventional PVC surfaces (**Figure 5.2**). Representative colony forming unit observed for the dilutions over the 4-log range during the viable cell count experiments are shown in **Figure 5.3**. For example, uncountable colony units were observed at 10^{-2} dilutions on conventional PVC surfaces. On the other hand, countable colonies were observed at the same dilution (10^{-2} dilution) when *S. aureus* was cultured on PVC+2% SPION nanocomposites.

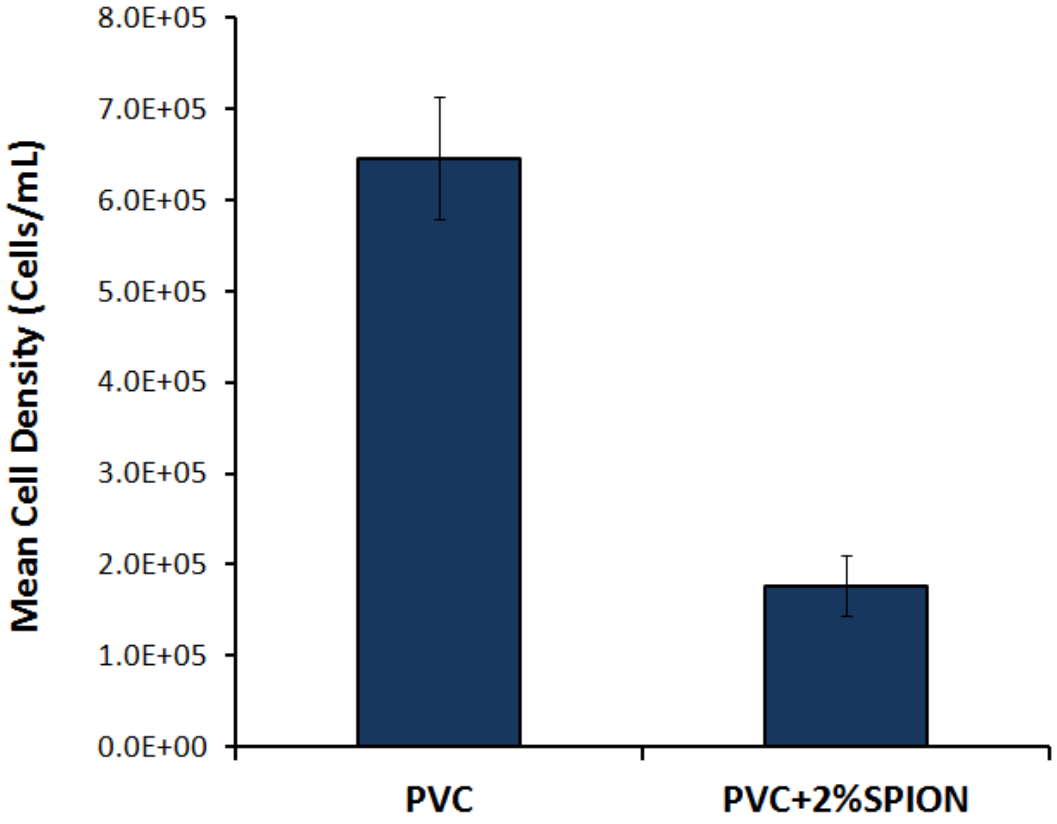

Figure 5.2. *S. aureus* biofilm formation on nanocomposite surfaces after 24 hours Biofilm formation decreases on PVC+ 2% nanocomposites by ~73%, compared to conventional PVC surfaces. Data represents mean ± SEM, N=3.

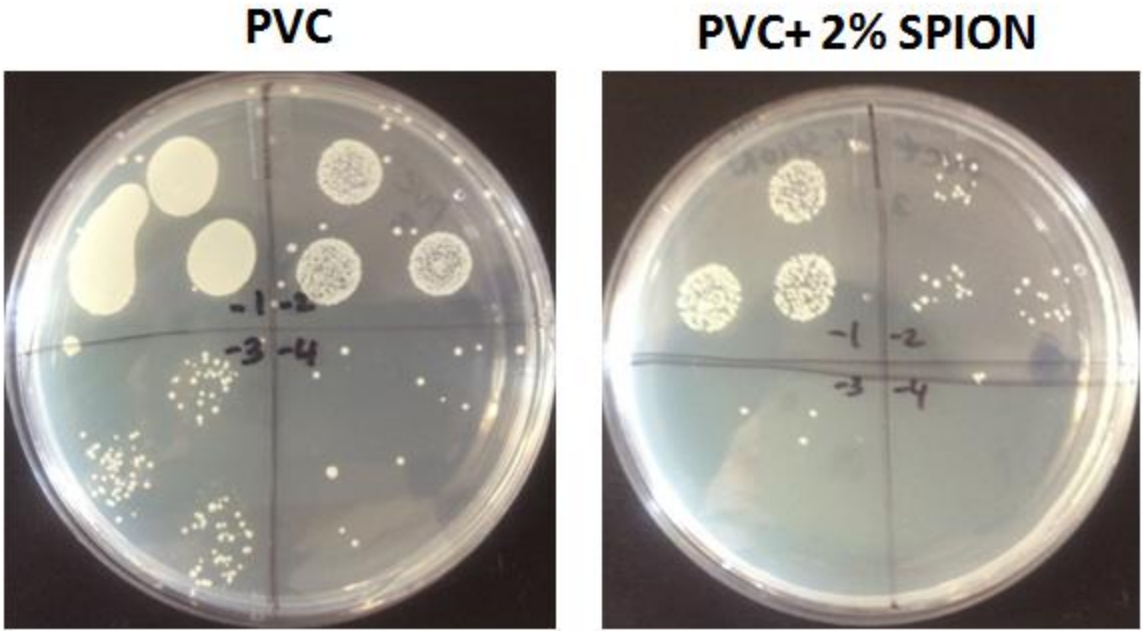

Figure 5.3. Representative colony forming unit observed for the dilutions over the 4-log range during the viable cell count experiments. Uncountable colony units were observed at 10^{-1} and 10^{-2} dilutions on conventional PVC surfaces. On the other hand, countable colonies were observed at the same dilution (10^{-2} dilution) when S. aureus was cultured on PVC+2% SPION nanocomposites.

In this chapter, magnetic iron oxide nanoparticles reduced the activity of *S. aureus* when incorporated into PVC, a polymer commonly used in endotracheal tube and catheter applications which frequently become contaminated. This suggests that the polymer and SPION nanocomposites could be used for biomaterial applications prone to excessive bacterial growth due to their ability to reduce biofilm formation without using antibiotics.

5.4. Potential Applications in Primary and Acute Healthcare Settings

Here, the possible applications of this broadly applicable infection prevention technology platform in healthcare settings will be covered. This multifunctional platform has a potential to **a)** decrease the initial bacterial attachment on the medical device surface (i.e. catheter surface); **b)** further reduce bacterial biofilm formation on the surface by using magnetic nanoparticles that can be targeted to the infected site on demand (**Figure 5.4**). When combined with metabolic approaches developed in Chapter 2 and 3, this platform might have a potential to monitor bacterial colonization by detecting bacterial metabolic activity after utilization of metabolites on the device surfaces, as shown in the literature. Moreover, this technology platform is broadly applicable to many other devices commonly used in clinical settings. Thus, proposed platform has the potential to impact the future of surface engineering and infection control of numerous biomedical devices leading to more successful clinical outcomes in terms of longer device lifetimes, minimized infections and decreased antibiotic usage; all of which can support decreased antibiotic resistance in the primary care setting as well as clinical settings.

In this chapter**,** the primary focus will be PVC-catheters, since catheter-associated infection is a significant problem in the primary care settings where patients perform self-catheterization or peritoneal dialysis at their home settings. There are also many catheter-related infections occur in nursing home patients. There is a much broader significance as well. There are thousands of ambulatory patients with catheters. These include the paraplegics, patients with multiple sclerosis (MS) and other neurological disorders and those post prostate surgery.

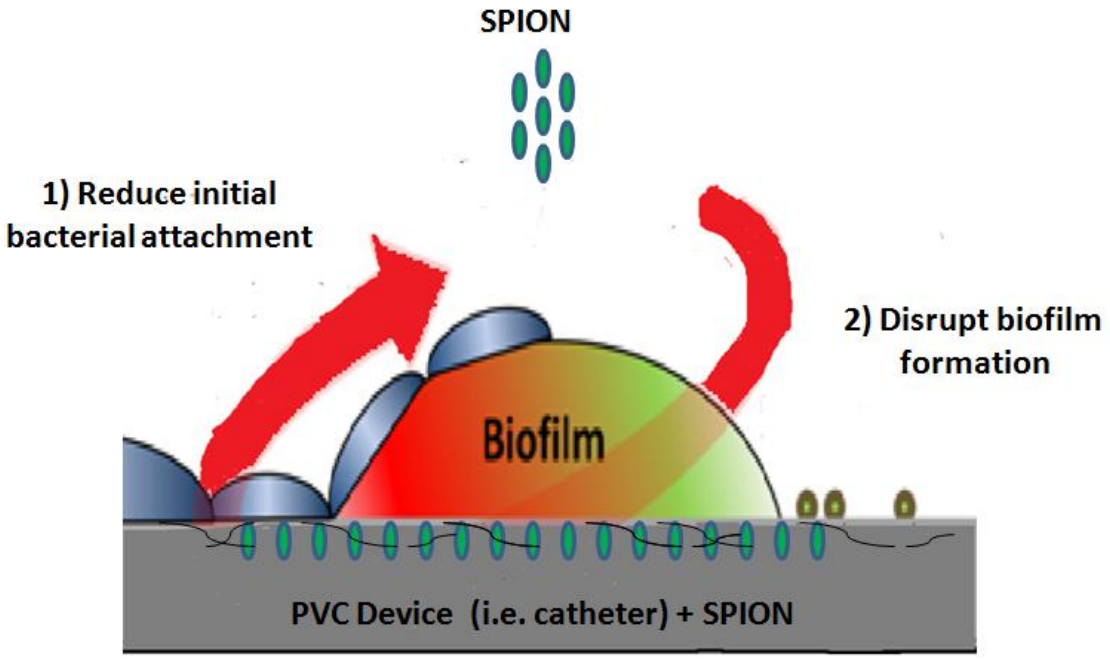

Figure 5.4. Schematic overview of the proposed infection prevention technology: PVC+SPION nanocomposites. This broadly applicable multifunctional platform technology will: **a)** decrease the initial bacterial attachment on the medical device surface (i.e. catheter surface); **b)** further reduce bacterial biofilm formation on the surface by using magnetic nanoparticles that can be targeted to the infected site on demand. Moreover, the nanoroughness of the nanocomposites surfaces can be increased to further improve the anti-biofilm properties (as shown in Chapter 2).

5.4.1. Infections Associated with Catheters in Primary Care Settings

CAUTI is currently one of the most common infections and comprises 40% of all institutionally acquired infections. In home healthcare settings, CAUTIs occur in 8% of patients.[251] The daily risk of developing CAUTI ranges from 3% to 7% and it cumulatively increases as the duration of the catheter use increases.[218] Moreover, according to research held in 11 European countries, the prevalence of indwelling catheter use was 5.4% and this went up to 40% in some countries, especially in nursing homes in the United Kingdom.[251,254,255] The risk of developing a urinary tract infection was 6.5 times greater than that for non-catheterized individuals.[255] Another study focused on frail elderly women living in the community and reported that the catheter prevalence rate was 38.1%. Prevalence of a urinary tract infection was 21% and catheterized patients were more likely to die within a year. [251,256]

For primary care applications, this proposed infection prevention technology could be applied to patients who perform self-catheterization at their home settings as well as for the patients in nursing homes. In addition, patients who perform peritoneal dialysis (PD) at home settings are at the risk of developing infections on the exit-sites of the dialysis catheters.

5.4.1.1. Intermittent Catheters (IC) (Self-catheterization)

As the care of long-term conditions has shifted from the hospital to the community settings, there is an associated increase in the use of urinary catheters within patients' homes. Intermittent catheterization (IC) is the insertion and removal of a catheter to

empty the bladder several times a day.[257,258] This self-catheterization method is the preferred method for adult and children patients with neurogenic bladder and is an integral part of urologic nursing care. A common cause of a neurogenic bladder is spinal cord injury, which occurs in more than 200,000 patients (10,000 cases per year) in the United States.[257-259] Other causes might include: a) upper motor neuron disease (i.e. stroke, Parkinson's disease, multiple sclerosis) and b) lower motor neuron disease (i.e. pelvic nerve injury, peripheral neuropathy, diabetes mellitus).[257]

Urologic nurses are at the forefront of educating and teaching patients how to self-catheterize. Catheterizations performed in institutions, such as acute and rehabilitation hospitals are usually done aseptically.[257] However, IC has been more frequently performed by the patient in the home settings using a clean technique involving the re-use of catheters. On the other hand, the introduction of a catheter several times a day can give rise to complications. Urinary tract infection (UTI) is the most frequent complication and patients who perform IC for long term face a higher risk of infection.[257,258] Moreover, patients who perform IC are at higher risk than the general population for developing a UTI and renal deterioration.[257] UTIs can be the result of poor catheterization technique or the passing of the catheter through a very contaminated area of the urethra before it reaches the bladder. Cross infection is another problem when the catheterization is done by the patients at home-based settings. [257]

5.4.1.2. Current Primary Care Practices for the Infection Prevention Control and Maintenance of IC

Several procedures that have been used to decrease the risk of infection are of no benefit. The most important prevention methods include the patient education and compliance, the use of appropriate catheter type and material, and consistent catheterization technique.[258] However, there are no clear guidelines about length of time for catheter use. Most patients re-use the catheters for up to 7 days.[257] In addition, cleaning techniques for catheter maintenance suggested by nurses are soap-and-water washing, boiling, microwave sterilization and soaking in an antiseptic solution (i.e. peroxide and povidone-iodine or Betadine®).[257] On the other hand, the comparative effectiveness of these methods is currently unknown. In addition, 8% of the nursing staff reported that daily meatal cleaning with an antiseptic actually might increase the risk of infection through irritation.[260,261] Thus, the result of current prevention strategies is the same: the colonization or infection of intermittent catheters with more resistant organisms.

Currently, the only available technology to reduce catheter-associated UTI is the use of silver-alloy urinary catheters. There are some studies which showed silver-alloy catheters reduce infections; at least in the short term.[212,251] However, silver-alloy catheters are not commonly used due to the significant difference in cost between silver-coated and uncoated catheters (~$6).[262] In addition, further research is needed to decide which patients are most likely to benefit from silver-coated catheters. Therefore, cost-effectiveness of using silver-coated catheters rather than the standard ones should be further studied.

As none of the currently available catheter materials is fully resistant to bacterial adherence and biofilm formation, there is a clinical need to create intermittent catheter surfaces that can resist bacteria attachment and biofilm formation to decrease the risk of UTI. Novel, simple and inexpensive prevention technologies that reduce the incidence of catheter-associated infections in primary care settings have a great potential to influence the safety of patients whom self-catheterize in their home settings or nursing homes.

5.4.1.3. Peritoneal Dialysis (PD) Catheters

Peritoneal dialysis (PD) is a simple home-based solution to big growing problem of end stage renal disease (ESRD) (**Figure 5.5**). In 2007, Medicare spent $8.6 billion on the the treatment and medications of dialysis patients. Despite the costs, a significant portion of the US dialysis patients die every year (20.1% in 2006). The prevalence of chronic kidney disease (CKD) in the US adult population was 16.8% of the US population aged >20 years according to 1999-2004 National Health and Nutrition Examination Survey (NHANES). For CKD patients with ESRD, kidney replacement or dialysis to preserve any residual renal function is required. According to the US Renal Data System (USRDS), 350,000 ESRD patients were on dialysis in 2006 and an estimated 530,000 people will need dialysis in 2020 in the US alone. As compared to the traditional hemodialysis (HD), peritoneal dialysis (PD) provides higher patient satisfaction in terms of cost, mobility, and convenience for medical treatment. HD costs $45,000 per month, where as PD costs $2500 per month.

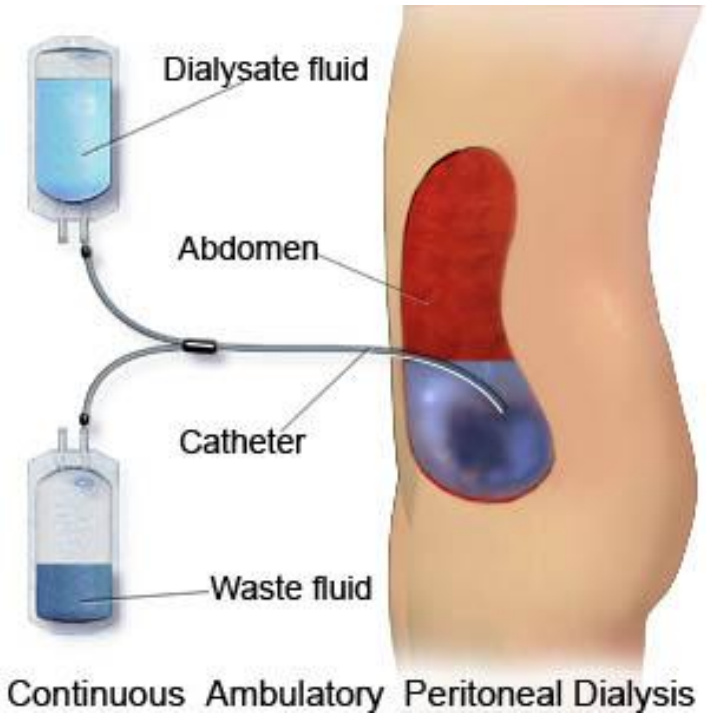

Figure 5.5. Schematic diagram of peritoneal dialysis (PD).[263] PD is a simple home-based solution to big growing problem of end stage renal disease. However, infections can occur on the catheter surface or at the catheter-exit sites while patients perform PD at their home setting.

On the other hand, infection is the most common complication of PD (**Figure 5.5**).[227,228] Infections on the PD catheter surfaces or on the catheter exit-sites lead to the occurrence of peritonitis, i.e. inflammation of the peritoneum[227]. Catheter infections contribute to PD failure, hospitalization of patients who perform PD at their homes and removal of the catheter, which significantly increases the overall cost of PD. In addition, there is a 6% mortality rate among those suffering from peritonitis. Mortality rate might increase to 25% if peritonitis develops due to fungal infections.[264] Thus, complications due to

infections at the patients' home settings create a clinical barrier in the widespread use of PD.

5.4.1.4. Current Primary Care Practices for the Infection Prevention Control and Maintenance of PD Catheters

Currently, patients are expected to look at the cloudiness of the fluid and initiate a call to their caregivers followed by an office visit. However, turbidity and visual cloudiness measurements are not enough and most of the time patients do not warn the caregiver until they feel pain, which is already too late. The routine care to prevent catheter exit-site infections is the proper hand hygiene.[264,265] Patients are advised to wash their hands thoroughly with antibacterial soap or alcohol-based cleaning agent prior to touching the exit site. The CDC recommends that when soap and water are not available, alcohol-based agents are acceptable if they contain at least 60% isopropanol or ethanol.[265] However, hand hygiene has been hard to implement. In addition, treatment of exit-sites with antibiotics is another approach to prevent infections.[228,264,265] However, the use of exit-site antibiotics has been criticized as fostering the development of resistant organisms. For example, resistance to mupirocin has been reported.[266] Moreover, patients with prolonged or repeated courses of antibiotics are at increased risk of fungal peritonitis, which significantly increase the mortality risk of the patient. [264]

5.5. Advantages of the Proposed Infection Prevention Technology over Current Primary Care Practice and Guidelines

In the past decades, control of environmental and personnel contamination has been the principal target to decrease both IC and PD catheter-associated infections in the primary care. In a population, i.e. nursing homes, where incontinence is common and many residents are confused and unable to maintain basic personal hygiene, hand hygiene has been hard to implement. On the other hand, this novel technology focuses on providing antibacterial medical device surfaces. This broadly applicable multifunctional platform technology will: **a)** decrease the initial bacterial attachment on the medical device surface (i.e. catheter surface); **b)** further reduce bacterial biofilm formation on the surface by using magnetic nanoparticles that can be targeted to the infected site on demand. Moreover, the nanoroughness of the nanocomposites surfaces can be increased to further improve the anti-biofilm properties (as shown in Chapter 2). Our chemical etching method to create nanomodified surfaces is simple, low cost and rapid. The surface chemistry of the material does not change after the chemical etching. In addition, Nanomodified surfaces could resist bacteria attachment and growth without relying on the proper hand hygiene of the patient or primary healthcare personnel. It will also offer better care and infection control when combined with a proper hygiene. Most significantly, this technology does not rely on antibiotic therapy. Common primary care practice recommends using antibacterial solutions in the urine drainage bags or using antibiotic-based creams (i.e. gentamicin cream) on the exit-sites of PD dialysis catheters. However, excessive antibiotic usage causes bacterial resistance. Gentamicin is even known to induce biofilm formation.[40] As nanomodified surfaces decrease bacterial

growth, our technology offers the unique advantage to decrease antibiotic usage, minimized infections and longer device lifetimes. All of these events can support decreased antibiotic resistance in the primary care settings. The advantages of the proposed infection prevention technology are summarized in **Table 5.1**.

Table 5.1. Summary of the Advantages of Proposed Invention Prevention Technology over the Current Primary Care Practice and Guidelines

Current Primary Care Practice		**Proposed Infection Prevention Technology**	
Guideline	**Disadvantage**	**Innovation**	**Advantage**
Hand Hygiene	Hard to implement	Creates nanostructures to resist bacterial growth	Does not rely on hygiene. More effective when combined with proper hygiene
Antibacterial agents	None is proven to be effective to prevent UTI	**No antibiotics, antibacterial agents or antiseptics used**	Significantly less risk of developing bacterial resistance Less antibiotic usage Minimized infections Longer device lifetime Decreased antibiotic resistance in primary care
Meatal cleaning with soap and water	Increases the risk of infection due to irrigation		
Antibacterial solutions in urine drainage bags	Not effective, increases bacterial resistance		
Exit-site care with antibiotic-cream	Not effective, increases bacterial resistance and fungal infection risk, as well as mortality risk		

Literature Cited

1. Furuya EY, Lowy FD. Antimicrobial-resistant bacteria in the community setting. *Nat. Rev. Microbiol.* Jan 2006;4(1):36-45.

2. Andersson DI, Hughes D. Antibiotic resistance and its cost: is it possible to reverse resistance? *Nat. Rev. Microbiol.* Apr 2010;8(4):260-271.

3. Levy SB, Marshall B. Antibacterial resistance worldwide: causes, challenges and responses. *Nat. Med.* Dec 2004;10(12):S122-S129.

4. Christof von Eiff BJ, Wolfgang Kohnen, Karsten Becker. Infections Associated with Medical Devices. *Drugs.* 2005;65(2):179.

5. Donlan RM. Biofilms and Device-Associated Infections. *Emerging Infectious Diseases.* 2001;7(2).

6. Pierce GE. Pseudomonas aeruginosa, Candida albicans, and device-related nosocomial infections: implications, trends, and potential approaches for control. *J Ind Microbiol Biotechnol.* 2005;32:309-318.

7. Burke JP. Infection Control - A Problem for Patient Safety. *N Engl J Med.* 2003;348(7):651-659.

8. Fears R, van der Meer JWM, Meulen VT. The Changing Burden of Infectious Disease in Europe. *Science.* 2011;3(103):1-4.

9. The Burden of Health Care-Associated Infection Worldwide: A Summary. *World Healtcare Organization (WHO).* 2010.

10. Ducel G, Fabry J, Nicolle L. Prevention of hospital-acquired infections. A practical guide. *World Healtcare Organization (WHO).* 2002.

11. Bordi C, de Bentzmann S. Hacking into bacterial biofilms: a new therapeutic challenge. *Annals of intensive care.* 2011 2011;1(1):19.

12. Boles BR, Thoendel M, Roth AJ, Horswill AR. Identification of Genes Involved in Polysaccharide-Independent Staphylococcus aureus Biofilm Formation. *PLos One.* Apr 2010;5(4).

13. del Pozo JL, Patel R. The challenge of treating biofilm-associated bacterial infection. *Clin. Pharmacol. Ther.* Aug 2007;82(2):204-209.

14. Otto M. Staphylococcus epidermidis - the 'accidental' pathogen. *Nat. Rev. Microbiol.* Aug 2009;7(8):555-567.

15. Tran N, Tran PA. Nanomaterial-Based Treatments for Medical Device-Associated Infections. *ChemPhysChem.* Jul 2012;13(10):2481-2494.

16. Mermel LA. Prevention of intravascular catheter-related infections (vol 132, pg 391, 2000). *Ann. Intern. Med.* Sep 2000;133(5):395-395.

17. Cardo D, Horan T, Andrus M, et al. National Nosocomial Infections Surveillance (NNIS) System Report, data summary from January 1992 through June 2004, issued October 2004. *Am. J. Infect. Control.* Dec 2004;32(8):470-485.

18. O'Grady NP, Alexander M, Burns LA, et al. Guidelines for the prevention of intravascular catheter-related infections. *Am. J. Infect. Control.* May 2011;39(4):S1-S34.

19. Rello J, Ochagavia A, Sabanes E, et al. Evaluation of outcome of intravenous catheter-related infections in critically ill patients. *Am. J. Respir. Crit. Care Med.* Sep 2000;162(3):1027-1030.

20. Dimick JB, Pelz RK, Consunji R, Swoboda SM, Hendrix CW, Lipsett PA. Increased resource use associated with catheter-related bloodstream infection in the surgical intensive care unit. *Arch. Surg.* Feb 2001;136(2):229-234.
21. Sanders J, Pithie A, Ganly P, et al. A prospective double-blind randomized trial comparing intraluminal ethanol with heparinized saline for the prevention of catheter-associated bloodstream infection in immunosuppressed haematology patients. *J. Antimicrob. Chemother.* Oct 2008;62(4):809-815.
22. Jean Chastre J-YF. Ventilator-associated Pneumonia. *Am J Respir Crit Care Med.* 2002;165:867–903.
23. Seil JT, Rubien NM, Webster TJ, Tarquinio KM. Comparison of quantification methods illustrates reduced Pseudomonas aeruginosa activity on nanorough polyvinyl chloride. *J Biomed Mater Res B Appl Biomater.* 2011;98(1):1-7.
24. Farah K. Bahrani-Mougeot BJP, Shirley Coleman,Sara Barbuto, Michael T. Brennan, Jenene Noll, Thomas Kennedy, Philip C. Fox, Peter B. Lockhart1. Molecular Analysis of Oral and Respiratory Bacterial Species Associated with Ventilator-Associated Pneumonia. *Journal of Clinical Microbiology.* 2007;45(5):1588–1593.
25. Raad II, Mohamed JA, Reitzel RA, et al. The prevention of biofilm colonization by multidrug-resistant pathogens that cause ventilator-associated pneumonia with antimicrobial-coated endotracheal tubes. *Biomaterials.* 2011;32(11):2689-2694.
26. Machado MC, Cheng D, Tarquinio KM, Webster TJ. Nanotechnology: pediatric applications. *Pediatr Res.* 2010;67(5):500-504.
27. Koerner R. Contribution of endotracheal tubes to the pathogenesis of ventilator-associated pneumonia *Journal of Hospital Acquired Infection.* 1997;35:83-89.
28. Fagon JY, Chastre J, Domart Y, Trouillet JL, Gibert C. Mortality due to ventilator-associated pneumonia or colonization with Pseudomonas or Acinetobacter species: assessment by quantitative culture of samples obtained by a protected specimen brush. *Clin Infect Dis.* 1996;23(3):538-542.
29. Adair CG, Gorman SP, Feron BM, et al. Implications of endotracheal tube biofilm for ventilator-associated pneumonia. *Intensive Care Med.* 1999;25(10):1072-1076.
30. Sottile FD, Marrie TJ, Prough DS, et al. Nosocomial pulmonary infection: possible etiologic significance of bacterial adhesion to endotracheal tubes. *Crit Care Med.* 1986;14(4):265-270.
31. Rello J, Torres A, Ricart M, et al. Ventilator-associated pneumonia by Staphylococcus aureus. Comparison of methicillin-resistant and methicillin-sensitive episodes. *Am J Respir Crit Care Med.* 1994;150(6):1545-1549.
32. Rutala WA, Weber DJ. Disinfection and sterilization in health care facilities: What clinicians need to know. *Clin. Infect. Dis.* Sep 1 2004;39(5):702-709.
33. Hetrick EM, Schoenfisch MH. Reducing implant-related infections: active release strategies. *Chem Soc Rev.* 2006;35(9):780-789.
34. Hopkins CG, McHugh PE, McGarry JP. Computational Investigation of the Delamination of Polymer Coatings During Stent Deployment. *Ann Biomed Eng.* Jul 2010;38(7):2263-2273.
35. Durmus NG, Webster TJ. Nanostructured titanium: the ideal material for improving orthopedic implant efficacy? *Nanomedicine.* Jun 2012;7(6):791-793.

36. Bernard L, Hoffmeyer P, Assal M, Vaudaux P, Schrenzel J, Lew D. Trends in the treatment of orthopaedic prosthetic infections. *J. Antimicrob. Chemother.* Feb 2004;53(2):127-129.

37. Campoccia D, Montanaro L, Speziale P, Arciola CR. Antibiotic-loaded biomaterials and the risks for the spread of antibiotic resistance following their prophylactic and therapeutic clinical use. *Biomaterials.* Sep 2010;31(25):6363-6377.

38. Neut D, van de Belt H, van Horn JR, van der Mei HC, Busscher HJ. Residual gentamicin-release from antibiotic-loaded polymethylmethacrylate beads after 5 years of implantation. *Biomaterials.* May 2003;24(10):1829-1831.

39. Hendriks JGE, van Horn JR, van der Mei HC, Busscher HJ. Backgrounds of antibiotic-loaded bone cement and prosthesis-related infection. *Biomaterials.* Feb 2004;25(3):545-556.

40. Hoffman LR, D'Argenio DA, MacCoss MJ, Zhang ZY, Jones RA, Miller SI. Aminoglycoside antibiotics induce bacterial biofilm formation. *Nature.* Aug 2005;436(7054):1171-1175.

41. O'Toole G, Kaplan HB, Kolter R. Biofilm formation as microbial development. *Annu. Rev. Microbiol.* 2000;54:49-79.

42. Henrici AT. Studies of freshwater bacteria I A direct microscopic technique. *J. Bacteriol.* Mar 1933;25(3):277-287.

43. Hall-Stoodley L, Costerton JW, Stoodley P. Bacterial biofilms: From the natural environment to infectious diseases. *Nat. Rev. Microbiol.* Feb 2004;2(2):95-108.

44. Xavier JB, Picioreanu C, Rani SA, van Loosdrecht MC, Stewart PS. Biofilm-control strategies based on enzymic disruption of the extracellular polymeric substance matrix-a modelling study. *Microbiology.* 2005;151:3817-3832.

45. Davey ME, O'toole GA. Microbial biofilms: from ecology to molecular genetics. *Microbiol Mol Biol Rev.* 2000;64(4):847-867.

46. Westall F, de Wit MJ, Dann J, van der Gaast S, de Ronde CEJ, Gerneke D. Early Archean fossil bacteria and biofilms in hydrothermally-influenced sediments from the Barberton greenstone belt, South Africa. *Precambrian Res.* Feb 2001;106(1-2):93-116.

47. Walsh MM, Lowe DR. FILAMENTOUS MICROFOSSILS FROM THE 3,500-MYR-OLD ONVERWACHT GROUP, BARBERTON MOUNTAIN LAND, SOUTH-AFRICA. *Nature.* 1985;314(6011):530-532.

48. Antoci V Jr, Adams CS, Parvizi J, et al. The inhibition of Staphylococcus epidermidis biofilm formation by vancomycin-modified titanium alloy and implications for the treatment of periprosthetic infection. *Biomaterials.* 2008;35:4684-4690.

49. Costerton JW, Stewart PS, Greenberg EP. Bacterial biofilms: a common cause of persistent infections. *Science.* 1999;284(5418):1318-1322.

50. Taylor E WT. Reducing infections through nanotechnology and nanoparticles. *Int J Nanomedicine.* 2011;6:1463-1473.

51. Stoodley P, Sauer K, Davies DG, Costerton JW. Biofilms as complex differentiated communities. *Annu. Rev. Microbiol.* 2002;56:187-209.

52. Sauer K, Camper AK, Ehrlich GD, Costerton JW, Davies DG. Pseudomonas aeruginosa displays multiple phenotypes during development as a biofilm. *J. Bacteriol.* Feb 2002;184(4):1140-1154.

53. Pratt LA, Kolter R. Genetic analysis of Escherichia coli biofilm formation: roles of flagella, motility, chemotaxis and type I pili. *Mol. Microbiol.* Oct 1998;30(2):285-293.

54. Dickinson GM, Bisno AL. INFECTIONS ASSOCIATED WITH INDWELLING DEVICES - INFECTIONS RELATED TO EXTRAVASCULAR DEVICES. *Antimicrob. Agents Chemother.* May 1989;33(5):602-607.

55. Katsikogianni M, Missirlis YF. Concise review of mechanisms of bacterial adhesion to biomaterials and of techniques used in estimating bacteria-material interactions. *European cells & materials.* 2004 Dec 2004;8:37-57.

56. Pavithra D, Doble M. Biofilm formation, bacterial adhesion and host response on polymeric implants - issues and prevention. *Biomed. Mater.* Sep 2008;3(3).

57. Heilmann C, Hussain M, Peters G, Gotz F. Evidence for autolysin-mediated primary attachment of Staphylococcus epidermidis to a polystyrene surface. *Mol. Microbiol.* Jun 1997;24(5):1013-1024.

58. Muller E, Hubner J, Gutierrez N, Takeda S, Goldmann DA, Pier GB. ISOLATION AND CHARACTERIZATION OF TRANSPOSON MUTANTS OF STAPHYLOCOCCUS-EPIDERMIDIS DEFICIENT IN CAPSULAR POLYSACCHARIDE ADHESIN AND SLIME. *Infect. Immun.* Feb 1993;61(2):551-558.

59. Herrmann M, Vaudaux PE, Pittet D, et al. FIBRONECTIN, FIBRINOGEN, AND LAMININ ACT AS MEDIATORS OF ADHERENCE OF CLINICAL STAPHYLOCOCCAL ISOLATES TO FOREIGN MATERIAL. *J. Infect. Dis.* Oct 1988;158(4):693-701.

60. Darouiche RO. Device-associated infections: A macroproblem that starts with microadherence. *Clin. Infect. Dis.* Nov 2001;33(9):1567-1572.

61. Archer NK, Mazaitis MJ, Costerton JW, Leid JG, Powers ME, Shirtliff ME. Staphylococcus aureus biofilms Properties, regulation and roles in human disease. *Virulence.* Sep-Oct 2011;2(5):445-459.

62. Debeer D, Stoodley P, Lewandowski Z. LIQUID FLOW IN HETEROGENEOUS BIOFILMS. *Biotechnol. Bioeng.* Aug 1994;44(5):636-641.

63. Davies DG, Chakrabarty AM, Geesey GG. EXOPOLYSACCHARIDE PRODUCTION IN BIOFILMS - SUBSTRATUM ACTIVATION OF ALGINATE GENE-EXPRESSION BY PSEUDOMONAS-AERUGINOSA. *Appl. Environ. Microbiol.* Apr 1993;59(4):1181-1186.

64. Stewart PS. A review of experimental measurements of effective diffusive permeabilities and effective diffusion coefficients in biofilms. *Biotechnol. Bioeng.* Aug 1998;59(3):261-272.

65. Vrany JD, Stewart PS, Suci PA. Comparison of recalcitrance to ciprofloxacin and levofloxacin exhibited by Pseudomonas aeruginosa bofilms displaying rapid-transport characteristics. *Antimicrob. Agents Chemother.* Jun 1997;41(6):1352-1358.

66. Anderl JN, Franklin MJ, Stewart PS. Role of antibiotic penetration limitation in Klebsiella pneumoniae biofilm resistance to ampicillin and ciprofloxacin. *Antimicrob. Agents Chemother.* Jul 2000;44(7):1818-1824.

67. Stone G, Wood P, Dixon L, Keyhan M, Matin A. Tetracycline rapidly reaches all the constituent cells of uropathogenic Escherichia coli biofilms. *Antimicrob. Agents Chemother.* Aug 2002;46(8):2458-2461.

68. Darouiche RO, Dhir A, Miller AJ, Landon GC, Raad, II, Musher DM. VANCOMYCIN PENETRATION INTO BIOFILM COVERING INFECTED PROSTHESES AND EFFECT ON BACTERIA. *J. Infect. Dis.* Sep 1994;170(3):720-723.

69. Stewart PS, Costerton JW. Antibiotic resistance of bacteria in biofilms. *Lancet.* Jul 2001;358(9276):135-138.

70. Shigeta M, Tanaka G, Komatsuzawa H, Sugai M, Suginaka H, Usui T. Permeation of antimicrobial agents through Pseudomonas aeruginosa biofilms: A simple method. *Chemotherapy.* Sep-Oct 1997;43(5):340-345.

71. Davies D. Understanding biofilm resistance to antibacterial agents. *Nat. Rev. Drug Discov.* Feb 2003;2(2):114-122.

72. Brozel VS, Strydom GM, Cloete TE. A METHOD FOR THE STUDY OF DE-NOVO PROTEIN-SYNTHESIS IN PSEUDOMONAS-AERUGINOSA AFTER ATTACHMENT. *Biofouling.* 1995;8(3):195-201.

73. Whiteley M, Bangera MG, Bumgarner RE, et al. Gene expression in Pseudomonas aeruginosa biofilms. *Nature.* Oct 2001;413(6858):860-864.

74. Bagge N, Hentzer M, Andersen JB, Ciofu O, Givskov M, Hoiby N. Dynamics and spatial distribution of beta-lactamase expression in Pseudomonas aeruginosa biofilms. *Antimicrob. Agents Chemother.* Apr 2004;48(4):1168-1174.

75. Mah TF, Pitts B, Pellock B, Walker GC, Stewart PS, O'Toole GA. A genetic basis for Pseudomonas aeruginosa biofilm antibiotic resistance. *Nature.* Nov 2003;426(6964):306-310.

76. Shoemaker NB, Vlamakis H, Hayes K, Salyers AA. Evidence for extensive resistance gene transfer among Bacteroides spp. and among Bacteroides and other genera in the human colon. *Appl. Environ. Microbiol.* Feb 2001;67(2):561-568.

77. Rani SA, Pitts B, Beyenal H, et al. Spatial patterns of DNA replication, protein synthesis, and oxygen concentration within bacterial biofilms reveal diverse physiological states. *J. Bacteriol.* Jun 2007;189(11):4223-4233.

78. Lewis K. Persister cells, dormancy and infectious disease. *Nat. Rev. Microbiol.* Jan 2007;5(1):48-56.

79. Lee SW, Foley EJ, Epstein JA. Mode of action of penicillin l Bacterial growth and penicillin activity - Staphylococcus aureus FDA. *J. Bacteriol.* Oct 1944;48(4):393-399.

80. Levin BR, Rozen DE. Opinion - Non-inherited antibiotic resistance. *Nat. Rev. Microbiol.* Jul 2006;4(7):556-562.

81. Jose L. Martınez FR. Metabolic regulation ofantibiotic resistance. *FEMS Microbiol Rev.* 2011;35:768–789.

82. Tack KJ, Sabath LD. INCREASED MINIMUM INHIBITORY CONCENTRATIONS WITH ANAEROBIASIS FOR TOBRAMYCIN, GENTAMICIN, AND AMIKACIN, COMPARED TO LATAMOXEF,

PIPERACILLIN, CHLORAMPHENICOL, AND CLINDAMYCIN. *Chemotherapy.* 1985;31(3):204-210.

83. Anderl JN, Zahller J, Roe F, Stewart PS. Role of nutrient limitation and stationary-phase existence in Klebsiella pneumoniae biofilm resistance to ampicillin and ciprofloxacin. *Antimicrob. Agents Chemother.* Apr 2003;47(4):1251-1256.

84. Zhang LJ, Webster TJ. Nanotechnology and nanomaterials: Promises for improved tissue regeneration. *Nano Today.* Feb 2009;4(1):66-80.

85. Liu H, Webster TJ. Nanomedicine for implants: A review of studies and necessary experimental tools. *Biomaterials.* Jan 2007;28(2):354-369.

86. Harrison BS, Atala A. Carbon nanotube applications for tissue engineering. *Biomaterials.* 2007;28:344-353.

87. Wagner V, Dullaart A, Bock AK, Zweck A. The emerging nanomedicine landscape. *Nat. Biotechnol.* Oct 2006;24(10):1211-1217.

88. Alivisatos AP. Semiconductor clusters, nanocrystals, and quantum dots. *Science.* Feb 1996;271(5251):933-937.

89. Gao XH, Cui YY, Levenson RM, Chung LWK, Nie SM. In vivo cancer targeting and imaging with semiconductor quantum dots. *Nat. Biotechnol.* Aug 2004;22(8):969-976.

90. Niemeyer CM. Nanoparticles, proteins, and nucleic acids: Biotechnology meets materials science. *Angew. Chem.-Int. Edit.* 2001;40(22):4128-4158.

91. Gao XH, Yang LL, Petros JA, Marshal FF, Simons JW, Nie SM. In vivo molecular and cellular imaging with quantum dots. *Curr. Opin. Biotechnol.* Feb 2005;16(1):63-72.

92. Variola F, Vetrone F, Richert L, et al. Improving Biocompatibility of Implantable Metals by Nanoscale Modification of Surfaces: An Overview of Strategies, Fabrication Methods, and Challenges. *Small.* 2009;5:996-1006.

93. Nanci A, Wuest JD, Peru L, et al. Chemical modification of titanium surfaces for covalent attachment of biological molecules. *J. Biomed. Mater. Res.* May 1998;40(2):324-335.

94. Webster TJ, Ejiofor JU. Increased osteoblast adhesion on nanophase metals: Ti, Ti6Al4V, and CoCrMo. *Biomaterials.* Aug 2004;25(19):4731-4739.

95. Yao C, Perla V, McKenzie J, Slamovich EB, Webster TJ. Anodized Ti and Ti6Al4V possessing nanometer surface features enhances osteoblast adhesion. *J Biomed Nano.* 2005;1(1):68–73.

96. Oh S, Brammer KS, Li YSJ, et al. Stem cell fate dictated solely by altered nanotube dimension. *Proc. Natl. Acad. Sci. U. S. A.* Feb 2009;106(7):2130-2135.

97. Puckett SD. Select Nanofabricated Titanium Materials for Enhancing Bone and Skin Growth of Intraosseous Transcutaneous Amputation Prostheses. *PhD Thesis, Brown University.* 2010.

98. Bjursten LM, Rasmusson L, Oh S, Smith GC, Brammer KS, Jin S. Titanium dioxide nanotubes enhance bone bonding in vivo. *J. Biomed. Mater. Res. Part A.* Mar 2010;92A(3):1218-1224.

99. Puckett S, Webster TJ. Greater in vivo bone growth on anodized nanotubular titanium. *Ortho Res Soc Proc.* 2009:887.

100. Ercan B, Kummer KM, Tarquinio KM, Webster TJ. Decreased Staphylococcus aureus biofilm growth on anodized nanotubular titanium and the effect of electrical stimulation. *Acta Biomaterialia.* Jul 2011;7(7):3003-3012.
101. Ercan B, Webster TJ. The effect of biphasic electrical stimulation on osteoblast function at anodized nanotubular titanium surfaces. *Biomaterials.* May 2010;31(13):3684-3693.
102. Popat KC, Eltgroth M, LaTempa TJ, Grimes CA, Desai TA. Decreased Staphylococcus epidermis adhesion and increased osteoblast functionality on antibiotic-loaded titania nanotubes. *Biomaterials.* Nov 2007;28(32):4880-4888.
103. Puckett SD, Taylor E, Raimondo T, Webster TJ. The relationship between the nanostructure of titanium surfaces and bacterial attachment. *Biomaterials.* Feb 2010;31(4):706-713.
104. Li ML, Gu HC, Zhang CF. Highly sensitive magnetite nano clusters for MR cell imaging. *Nanoscale Res. Lett.* Mar 2012;7.
105. Veiseh O, Gunn JW, Zhang MQ. Design and fabrication of magnetic nanoparticles for targeted drug delivery and imaging. *Adv. Drug Deliv. Rev.* Mar 2010;62(3):284-304.
106. Mahmoudi M, Hosseinkhani H, Hosseinkhani M, et al. Magnetic Resonance Imaging Tracking of Stem Cells in Vivo Using Iron Oxide Nanoparticles as a Tool for the Advancement of Clinical Regenerative Medicine. *Chem. Rev.* Feb 2011;111(2):253-280.
107. Xu F, Inci F, Mullick O, et al. Release of Magnetic Nanoparticles from CellEncapsulating Biodegradable Nanobiomaterials. *ACS Nano.* 2012.
108. Xu F, Wu CAM, Rengarajan V, et al. Three-Dimensional Magnetic Assembly of Microscale Hydrogels. *Adv. Mater.* Oct 2011;23(37):4254-4260.
109. Gu HW, Xu KM, Xu CJ, Xu B. Biofunctional magnetic nanoparticles for protein separation and pathogen detection. *Chem. Commun.* 2006(9):941-949.
110. Kang S, Mauter MS, Elimelech M. Microbial Cytotoxicity of Carbon-Based Nanomaterials: Implications for River Water and Wastewater Effluent. *Environ. Sci. Technol.* Apr 2009;43(7):2648-2653.
111. Hao R, Xing RJ, Xu ZC, Hou YL, Gao S, Sun SH. Synthesis, Functionalization, and Biomedical Applications of Multifunctional Magnetic Nanoparticles. *Adv. Mater.* Jul 2010;22(25):2729-2742.
112. Huh AJ, Kwon YJ. "Nanoantibiotics": A new paradigm for treating infectious diseases using nanomaterials in the antibiotics resistant era. *J. Control. Release.* Dec 2011;156(2):128-145.
113. Mitik-Dineva N, Wang J, Mocanasu RC, Stoddart PR, Crawford RJ, Ivanova EP. Impact of nano-topography on bacterial attachment. *Biotechnol J.* 2008;3(4):536-544.
114. Mitik-Dineva N, Wang J, Truong VK, et al. Escherichia coli, Pseudomonas aeruginosa, and Staphylococcus aureus attachment patterns on glass surfaces with nanoscale roughness. *Curr Microbiol.* 2009;58(3):268-273.
115. Truong VK, Rundell S, Lapovok R, et al. Effect of ultrafine-grained titanium surfaces on adhesion of bacteria. *Appl Microbiol Biotechnol.* 2009;83(5):925-937.

116. Ivanova EP, Truong VK, Wang JY, et al. Impact of nanoscale roughness of titanium thin film surfaces on bacterial retention. *Langmuir.* 2010;26(3):1973-1982.
117. Puckett SD, Taylor E, Raimondo T, Webster TJ. The relationship between the nanostructure of titanium surfaces and bacterial attachment. *Biomaterials.* 2010;31(4):706-713.
118. Colon G, Ward BC, Webster TJ. Increased osteoblast and decreased Staphylococcus epidermidis functions on nanophase ZnO and TiO2. *J Biomed Mater Res A.* 2006;78(3):595-604.
119. Scardino AJ, Zhang H, Cookson DJ, Lamb RN, de Nys R. The role of nano-roughness in antifouling. *Biofouling.* 2009;25(8):757-767.
120. Hajipour MJ, Fromm KM, Ashkarran AA, et al. Antibacterial properties of nanoparticles. *Trends Biotechnol.* Oct 2012;30(10):499-511.
121. Li QL, Mahendra S, Lyon DY, et al. Antimicrobial nanomaterials for water disinfection and microbial control: Potential applications and implications. *Water Res.* Nov 2008;42(18):4591-4602.
122. Taylor E, Webster TJ. Reducing infections through nanotechnology and nanoparticles. *Int J Nanomedicine.* 2011;6:1463 - 1473.
123. Durmus NG, Webster TJ. Eradicating Antibiotic-Resistant Biofilms with Silver-Conjugated Superparamagnetic Iron Oxide Nanoparticles. *Advanced Healthcare Materials.* 2012.
124. Mahmoudi M, Serpooshan V. Silver-Coated Engineered Magnetic Nanoparticles Are Promising for the Success in the Fight against Antibacterial Resistance Threat. *ACS Nano.* Mar 2012;6(3):2656-2664.
125. Park H, Park HJ, Kim JA, et al. Inactivation of Pseudomonas aeruginosa PA01 biofilms by hyperthermia using superparamagnetic nanoparticles. *J. Microbiol. Methods.* Jan 2011;84(1):41-45.
126. Rabea EI, Badawy MET, Stevens CV, Smagghe G, Steurbaut W. Chitosan as antimicrobial agent: Applications and mode of action. *Biomacromolecules.* Nov-Dec 2003;4(6):1457-1465.
127. Raafat D, von Bargen K, Haas A, Sahl HG. Insights into the mode of action of chitosan as an antibacterial compound. *Appl. Environ. Microbiol.* Jun 2008;74(12):3764-3773.
128. Ma YL, Zhou T, Zhao CS. Preparation of chitosan-nylon-6 blended membranes containing silver ions as antibacterial materials. *Carbohydr. Res.* Feb 2008;343(2):230-237.
129. Sanpui P, Murugadoss A, Prasad PVD, Ghosh SS, Chattopadhyay A. The antibacterial properties of a novel chitosan-Ag-nanoparticle composite. *Int. J. Food Microbiol.* May 2008;124(2):142-146.
130. Fernandes JC, Tavaria FK, Fonseca SC, Ramos OS, Pintado ME, Malcata FX. In Vitro Screening for Antimicrobial Activity of Chitosans and Chitooligosaccharides, Aiming at Potential Uses in Functional Textiles. *J. Microbiol. Biotechnol.* Feb 2010;20(2):311-318.
131. Shameli K, Bin Ahmad M, Yunus W, et al. Green synthesis of silver/montmorillonite/chitosan bionanocomposites using the UV irradiation

method and evaluation of antibacterial activity. *International Journal of Nanomedicine.* 2010;5:875-887.

132. Qi LF, Xu ZR, Jiang X, Hu CH, Zou XF. Preparation and antibacterial activity of chitosan nanoparticles. *Carbohydr. Res.* Nov 2004;339(16):2693-2700.

133. Liu XF, Guan YL, Yang DZ, Li Z, De Yao K. Antibacterial action of chitosan and carboxymethylated chitosan. *J. Appl. Polym. Sci.* Feb 2001;79(7):1324-1335.

134. Rai MK, Deshmukh SD, Ingle AP, Gade AK. Silver nanoparticles: the powerful nanoweapon against multidrug-resistant bacteria. *J. Appl. Microbiol.* May 2012;112(5):841-852.

135. Lara HH, Garza-Trevino EN, Ixtepan-Turrent L, Singh DK. Silver nanoparticles are broad-spectrum bactericidal and virucidal compounds. *J. Nanobiotechnol.* Aug 2011;9.

136. Ingle A, Gade A, Pierrat S, Sonnichsen C, Rai M. Mycosynthesis of silver nanoparticles using the fungus Fusarium acuminatum and its activity against some human pathogenic bacteria. *Curr. Nanosci.* May 2008;4(2):141-144.

137. Birla SS, Tiwari VV, Gade AK, Ingle AP, Yadav AP, Rai MK. Fabrication of silver nanoparticles by Phoma glomerata and its combined effect against Escherichia coli, Pseudomonas aeruginosa and Staphylococcus aureus. *Lett. Appl. Microbiol.* Feb 2009;48(2):173-179.

138. Shahverdi AR, Fakhimi A, Shahverdi HR, Minaian S. Synthesis and effect of silver nanoparticles on the antibacterial activity of different antibiotics against Staphylococcus aureus and Escherichia coli. *Nanomed.-Nanotechnol. Biol. Med.* Jun 2007;3(2):168-171.

139. Lara HH, Ayala-Nunez NV, Turrent LDI, Padilla CR. Bactericidal effect of silver nanoparticles against multidrug-resistant bacteria. *World J. Microbiol. Biotechnol.* Apr 2010;26(4):615-621.

140. Feng QL, Wu J, Chen GQ, Cui FZ, Kim TN, Kim JO. A mechanistic study of the antibacterial effect of silver ions on Escherichia coli and Staphylococcus aureus. *J. Biomed. Mater. Res.* Dec 2000;52(4):662-668.

141. Sondi I, Salopek-Sondi B. Silver nanoparticles as antimicrobial agent: a case study on E-coli as a model for Gram-negative bacteria. *J. Colloid Interface Sci.* Jul 2004;275(1):177-182.

142. Lkhagvajav N, Yasa I, Celik E, Koizhaiganova M, Sari O. ANTIMICROBIAL ACTIVITY OF COLLOIDAL SILVER NANOPARTICLES PREPARED BY SOL-GEL METHOD. *Dig. J. Nanomater. Biostruct.* Jan-Mar 2011;6(1):149-154.

143. Fayaz AM, Balaji K, Girilal M, Yadav R, Kalaichelvan PT, Venketesan R. Biogenic synthesis of silver nanoparticles and their synergistic effect with antibiotics: a study against gram-positive and gram-negative bacteria. *Nanomed.-Nanotechnol. Biol. Med.* Feb 2010;6(1):103-109.

144. Amro NA, Kotra LP, Wadu-Mesthrige K, Bulychev A, Mobashery S, Liu GY. High-resolution atomic force microscopy studies of the Escherichia coli outer membrane: Structural basis for permeability. *Langmuir.* Mar 2000;16(6):2789-2796.

145. Morones JR, Elechiguerra JL, Camacho A, et al. The bactericidal effect of silver nanoparticles. *Nanotechnology.* Oct 2005;16(10):2346-2353.

146. Panacek A, Kvitek L, Prucek R, et al. Silver colloid nanoparticles: Synthesis, characterization, and their antibacterial activity. *J. Phys. Chem. B.* Aug 2006;110(33):16248-16253.
147. Pal S, Tak YK, Song JM. Does the antibacterial activity of silver nanoparticles depend on the shape of the nanoparticle? A study of the gram-negative bacterium Escherichia coli. *Appl. Environ. Microbiol.* Mar 2007;73(6):1712-1720.
148. Roe D, Karandikar B, Bonn-Savage N, Gibbins B, Roullet JB. Antimicrobial surface functionalization of plastic catheters by silver nanoparticles. *J. Antimicrob. Chemother.* Apr 2008;61(4):869-876.
149. Lv M, Su S, He Y, et al. Long-Term Antimicrobial Effect of Silicon Nanowires Decorated with Silver Nanoparticles. *Adv. Mater.* Dec 2010;22(48):5463-5467.
150. Jones N, Ray B, Ranjit KT, Manna AC. Antibacterial activity of ZnO nanoparticle suspensions on a broad spectrum of microorganisms. *FEMS Microbiol. Lett.* Feb 2008;279(1):71-76.
151. Seil JT, Webster TJ. Antibacterial effect of zinc oxide nanoparticles combined with ultrasound. *Nanotechnology.* Dec 2012;23(49).
152. Kuhn KP, Chaberny IF, Massholder K, et al. Disinfection of surfaces by photocatalytic oxidation with titanium dioxide and UVA light. *Chemosphere.* Oct 2003;53(1):71-77.
153. Lee SH, Pumprueg S, Moudgil B, Sigmund W. Inactivation of bacterial endospores by photocatalytic nanocomposites. *Colloid Surf. B-Biointerfaces.* Feb 2005;40(2):93-98.
154. Maness PC, Smolinski S, Blake DM, Huang Z, Wolfrum EJ, Jacoby WA. Bactericidal activity of photocatalytic TiO2 reaction: Toward an understanding of its killing mechanism. *Appl. Environ. Microbiol.* Sep 1999;65(9):4094-4098.
155. Sunada K, Kikuchi Y, Hashimoto K, Fujishima A. Bactericidal and detoxification effects of TiO(2) thin film photocatalysts. *Environ. Sci. Technol.* Mar 1998;32(5):726-728.
156. Anpo M, Kishiguchi S, Ichihashi Y, et al. The design and development of second-generation titanium oxide photocatalysts able to operate under visible light irradiation by applying a metal ion-implantation method. *Res. Chem. Intermed.* 2001;27(4-5):459-467.
157. Tian Y, Tatsuma T. Plasmon-induced photoelectrochemistry at metal nanoparticles supported on nanoporous TiO2. *Chem. Commun.* 2004(16):1810-1811.
158. Seery MK, George R, Floris P, Pillai SC. Silver doped titanium dioxide nanomaterials for enhanced visible light photocatalysis. *J. Photochem. Photobiol. A-Chem.* Jun 2007;189(2-3):258-263.
159. Reddy MP, Venugopal A, Subrahmanyam M. Hydroxyapatite-supported Ag-TiO2 as Escherichia coli disinfection photocatalyst. *Water Res.* Jan 2007;41(2):379-386.
160. MacMicking J, Xie QW, Nathan C. Nitric oxide and macrophage function. *Annu. Rev. Immunol.* 1997;15:323-350.
161. Ghaffari A, Miller CC, McMullin B, Ghahary A. Potential application of gaseous nitric oxide as a topical antimicrobial agent. *Nitric Oxide-Biol. Chem.* Feb 2006;14(1):21-29.

162. Fang FC. Mechanisms of nitric oxide-related antimicrobial activity. *J. Clin. Invest.* Jun 1997;99(12):2818-2825.
163. Hetrick EM, Shin JH, Stasko NA, et al. Bactericidal efficacy of nitric oxide-releasing silica nanoparticles. *ACS Nano.* Feb 2008;2(2):235-246.
164. Gupta AK, Gupta M. Synthesis and surface engineering of iron oxide nanoparticles for biomedical applications. *Biomaterials.* Jun 2005;26(18):3995-4021.
165. Mahmoudi M, Hofmann H, Rothen-Rutishauser B, Petri-Fink A. Assessing the In Vitro and In Vivo Toxicity of Superparamagnetic Iron Oxide Nanoparticles. *Chem. Rev.* Apr 2012;112(4):2323-2338.
166. Peng S, Wang C, Xie J, Sun SH. Synthesis and stabilization of monodisperse Fe nanoparticles. *J. Am. Chem. Soc.* Aug 2006;128(33):10676-10677.
167. Sun C, Lee JSH, Zhang MQ. Magnetic nanoparticles in MR imaging and drug delivery. *Adv. Drug Deliv. Rev.* Aug 2008;60(11):1252-1265.
168. Lee JH, Huh YM, Jun Y, et al. Artificially engineered magnetic nanoparticles for ultra-sensitive molecular imaging. *Nat. Med.* Jan 2007;13(1):95-99.
169. Tran N, Mir A, Mallik D, Sinha A, Nayar S, Webster TJ. Bactericidal effect of iron oxide nanoparticles on Staphylococcus aureus. *International Journal of Nanomedicine.* 2010;5:277-283.
170. Taylor EN, Webster TJ. The use of superparamagnetic nanoparticles for prosthetic biofilm prevention. *International Journal of Nanomedicine.* 2009;4:145-152.
171. Azam A, Ahmed AS, Oves M, Khan MS, Habib SS, Memic A. Antimicrobial activity of metal oxide nanoparticles against Gram-positive and Gram-negative bacteria: a comparative study. *International Journal of Nanomedicine.* 2012;7:6003-6009.
172. Prucek R, Tucek J, Kilianova M, et al. The targeted antibacterial and antifungal properties of magnetic nanocomposite of iron oxide and silver nanoparticles. *Biomaterials.* Jul 2011;32(21):4704-4713.
173. Zhao LZ, Wang HR, Huo KF, et al. Antibacterial nano-structured titania coating incorporated with silver nanoparticles. *Biomaterials.* Aug 2011;32(24):5706-5716.
174. Megan S. Lorda, Morten Foss, Flemming Besenbacher. Influence of nanoscale surface topography on protein adsorption and cellular response. *Nanotoday.* 2010;5(1):66-78.
175. Woo KM, Chen VJ, Ma PX. Nano-fibrous scaffolding architecture selectively enhances protein adsorption contributing to cell attachment. *J Biomed Mater Res A.* 2003;67(2):531-537.
176. Khang D, Kim SY, Liu-Snyder P, Palmore GT, Durbin SM, Webster TJ. Enhanced fibronectin adsorption on carbon nanotube/poly(carbonate) urethane: independent role of surface nano-roughness and associated surface energy. *Biomaterials.* 2007;28(32):4756-4768.
177. Webster TJ, Ergun C, Doremus RH, Siegel RW, Bizios R. Specific proteins mediate enhanced osteoblast adhesion on nanophase ceramics. *J Biomed Mater Res.* 200;51(3):475-483.

178. Singh AJ, Vyas V, Patil R, et al. Quantitative Characterization of the Influence of the Nanoscale Morphology of Nanostructured Surfaces on Bacterial Adhesion and Biofilm Formation. *PLos One.* 2011;6(9).
179. Allison KR, Brynildsen MP, Collins JJ. Metabolite-enabled eradication of bacterial persisters by aminoglycosides. *Nature.* 2011;73(7346):216-220.
180. Davey ME, O'Toole GA. Microbial biofilms: from ecology to molecular genetics. *Microbiol. Mol. Biol. Rev.* Dec 2000;64(4):847-+.
181. Costerton JW, Stewart PS, Greenberg EP. Bacterial biofilms: A common cause of persistent infections. *Science.* May 1999;284(5418):1318-1322.
182. Fabrega J, Renshaw JC, Lead JR. Interactions of Silver Nanoparticles with Pseudomonas putida Biofilms. *Environ. Sci. Technol.* Dec 2009;43(23):9004-9009.
183. Rello J, Ollendorf DA, Oster G, et al. Epidemiology and outcomes of ventilator-associated pneumonia in a large US database. *Chest.* 2002;122:2155-2121.
184. Richards MJ, Edwards JR, Culver DH, Gaynes RP. Nosocomial infections in medical intensive care units in the United States. National Nosocomial Infections Surveillance System. *Crit Care Med.* 1999;27(5):887-892.
185. Vincent JL, Bihari DJ, Suter PM, et al. The prevalence of nosocomial infection in intensive care units in Europe. Results of the European Prevalence of Infection in Intensive Care (EPIC) Study. EPIC International Advisory Committee. *JAMA.* 1995 274(8):639-644.
186. Sean P. Gorman JGM, A. David Woolfson, Colin G. Adair, David S. Jones. The concomitant development of poly(vinyl chloride)-related biofilm and antimicrobial resistance in relation to ventilator-associated pneumonia. *Biomaterials.* 2001;22:2741-2747.
187. K. Triandafillua DJB, B.-O. Aronssonc, P. Descoutsc, P. Tu Quocd, C. van Deldend, H.J. Mathieub, H. Harmsa. Adhesion of Pseudomonas aeruginosa strains to untreated and oxygen-plasma treated poly(vinyl chloride) (PVC) from endotracheal intubation devices. *Biomaterials.* 2003;24:1507–1518.
188. Divison BM. *Agento Silver Coated Endotracheal Tube Brochure.*
189. Kuehnert MJ, Kruszon-Moran D, Hill HA, et al. Prevalence of Staphylococcus aureus nasal colonization in the United States, 2001-2002. *J Infect Dis.* 2006;193(2):172-179.
190. McHale G, Shirtcliffe NJ, Aqil S, Perry CC, Newton MI. Topography driven spreading. *Phys Rev Lett.* 2005;93(3):036102.
191. Kenneth K. S. Lau, José Bico, Kenneth B. K. Teo, et al. Superhydrophobic Carbon Nanotube Forests. *Nano Letters.* 2003;3(12):1701-1705.
192. Chow TS. Wetting of rough surfaces. *J Phys-Condens Matter.* 1998;10(27):L445–L451.
193. Borgs C, De Coninck J, Kotecký R, Zinque M. Does the roughness of the substrate enhance wetting? *Phys Rev Lett. .* 1995;74(12):2292-2294.
194. Fears R, van der Meer JWM, ter Meulen V. The Changing Burden of Infectious Disease in Europe. *Sci. Transl. Med.* Oct 2011;3(103).
195. Burke JP. Infection control - A problem for patient safety. *N. Engl. J. Med.* Feb 2003;348(7):651-656.

196. Klevens RM, Morrison MA, Nadle J, et al. Invasive methicillin-resistant Staphylococcus aureus infections in the United States. *Jama-Journal of the American Medical Association.* Oct 17 2007;298(15):1763-1771.
197. Chambers HF, DeLeo FR. Waves of resistance: Staphylococcus aureus in the antibiotic era. *Nat. Rev. Microbiol.* Sep 2009;7(9):629-641.
198. McKenna M. Man vs MRSA. *Nature.* Feb 2012;482(7383):23-25.
199. Hersh AL, Chambers HF, Maselli JH, Gonzales R. National trends in ambulatory visits and antibiotic prescribing for skin and soft-tissue infections. *Arch. Intern. Med.* Jul 2008;168(14):1585-1591.
200. Hiramatsu K, Hanaki H, Ino T, Yabuta K, Oguri T, FC. T. Methicillin-resistant Staphylococcus aureus clinical strain with reduced vancomycin susceptibility. *J Antimicrob Chemother.* 1997;40(1):135.
201. Nelson JL, Rice KC, Slater SR, et al. Vancomycin-intermediate Staphylococcus aureus strains have impaired acetate catabolism: implications for polysaccharide intercellular adhesin synthesis and autolysis. *Antimicrob Agents Chemother.* . 2007;51(2):616-622.
202. Hiramatsu K, Aritaka N, Hanaki H, et al. Dissemination in Japanese hospitals of strains of Staphylococcus aureus heterogeneously resistant to vancomycin. *Lancet.* 1997;350(9092):1670-1673.
203. Staphylococcus aureus with reduced susceptibility to vancomycin-United States. *Morb. Mortal. Wkly. Rep.* 1997;46:765-766.
204. Liu SB, Wei L, Hao L, et al. Sharper and Faster "Nano Darts" Kill More Bacteria: A Study of Antibacterial Activity of Individually Dispersed Pristine Single-Walled Carbon Nanotube. *ACS Nano.* Dec 2009;3(12):3891-3902.
205. Gunawan P, Guan C, Song XH, et al. Hollow Fiber Membrane Decorated with Ag/MWNTs: Toward Effective Water Disinfection and Biofouling Control. *ACS Nano.* Dec 2011;5(12):10033-10040.
206. Hu WB, Peng C, Luo WJ, et al. Graphene-Based Antibacterial Paper. *ACS Nano.* Jul 2010;4(7):4317-4323.
207. Shrivastava S, Bera T, Roy A, Singh G, Ramachandrarao P, Dash D. Characterization of enhanced antibacterial effects of novel silver nanoparticles. *Nanotechnology.* Jun 2007;18(22).
208. Cui Y, Zhao YY, Tian Y, Zhang W, Lu XY, Jiang XY. The molecular mechanism of action of bactericidal gold nanoparticles on Escherichia coli. *Biomaterials.* Mar 2012;33(7):2327-2333.
209. Makhluf S, Dror R, Nitzan Y, Abramovich Y, Jelinek R, Gedanken A. Microwave-assisted synthesis of nanocrystalline MgO and its use as a bacteriocide. *Adv. Funct. Mater.* Oct 2005;15(10):1708-1715.
210. Raghupathi KR, Koodali RT, Manna AC. Size-Dependent Bacterial Growth Inhibition and Mechanism of Antibacterial Activity of Zinc Oxide Nanoparticles. *Langmuir.* Apr 2011;27(7):4020-4028.
211. Lee D, Cohen RE, Rubner MF. Antibacterial properties of Ag nanoparticle loaded multilayers and formation of magnetically directed antibacterial microparticles. *Langmuir.* Oct 2005;21(21):9651-9659.

212. Schumm K, Lam TBL. Types of urethral catheters for management of short-term voiding problems in hospitalised adults. *Cochrane database of systematic reviews (Online).* 2008 2008(2):CD004013.

213. Yantasee W, Warner CL, Sangvanich T, et al. Removal of heavy metals from aqueous systems with thiol functionalized superparamagnetic nanoparticles. *Environ. Sci. Technol.* Jul 2007;41(14):5114-5119.

214. Yamaura M, Camilo RL, Sampaio LC, Macedo MA, Nakamura M, Toma HE. Preparation and characterization of (3-aminopropyl) triethoxysilane-coated magnetite nanoparticles. *J. Magn. Magn. Mater.* Aug 2004;279(2-3):210-217.

215. Chatterjee J, Haik Y, Chen CJ. Size dependent magnetic properties of iron oxide nanoparticles. *J. Magn. Magn. Mater.* Feb 2003;257(1):113-118.

216. Park TJ, Papaefthymiou GC, Viescas AJ, Moodenbaugh AR, Wong SS. Size-dependent magnetic properties of single-crystalline multiferroic BiFeO3 nanoparticles. *Nano Letters.* Mar 2007;7(3):766-772.

217. Qiang Y, Antony J, Sharma A, Nutting J, Sikes D, Meyer D. Iron/iron oxide core-shell nanoclusters for biomedical applications. *Journal of Nanoparticle Research.* 2006;8(3):489-496.

218. Lo E, Nicolle L, Classen D, et al. Strategies to prevent catheter-associated urinary tract infections in acute care hospitals. *Infection control and hospital epidemiology : the official journal of the Society of Hospital Epidemiologists of America.* 2008 2008;29 Suppl 1:S41-50.

219. Durmus NG, Taylor EN, Inci F, Kummer KM, Tarquinino KM, Webster TJ. Fructose enhanced reduction of bacterial growth on nanorough surfaces. *Int Journal of Nanomedicine* 2012.

220. Bell JM, Turnidge JD, Participants SA. High prevalence of oxacillin-resistant Staphylococcus aureus isolates from hospitalized patients in Asia-Pacific and South Africa: Results from SENTRY antimicrobial surveillance program, 1998-1999. *Antimicrob. Agents Chemother.* Mar 2002;46(3):879-881.

221. Martins A, Couto I, Aagaard L, et al. Prolonged exposure of methicillin-resistant Staphylococcus aureus (MRSA) COL strain to increasing concentrations of oxacillin results in a multidrug-resistant phenotype. *Int. J. Antimicrob. Agents.* Mar 2007;29(3):302-305.

222. Herold BC, Immergluck LC, Maranan MC, et al. Community-acquired methicillin-resistant Staphylococcus aureus in children with no identified predisposing risk. *Jama-Journal of the American Medical Association.* Feb 1998;279(8):593-598.

223. Howden BP, Ward PB, Charles PGP, et al. Treatment outcomes for serious infections caused by methicillin-resistant Staphylococcus aureus with reduced vancomycin susceptibility. *Clin. Infect. Dis.* Feb 2004;38(4):521-528.

224. Burton E, Yakandawala N, LoVetri K, Madhyastha MS. A microplate spectrofluorometric assay for bacterial biofilms. *J. Ind. Microbiol. Biotechnol.* Jan 2007;34(1):1-4.

225. Dahlback B, Pedersen K. VIABILITY OF A MARINE MICROBIAL BIOFILM. *Curr. Microbiol.* 1982;7(4):209-212.

226. Bakke A. Clean intermittent catheterization--physical and psychological complications. *Scandinavian journal of urology and nephrology. Supplementum.* 1993 1993;150:1-69.
227. Gokal R, Mallick NP. Peritoneal dialysis. *Lancet.* Mar 1999;353(9155):823-828.
228. Bernardini J, Bender F, Florio T, et al. Randomized, double-blind trial of antibiotic exit site cream for prevention of exit site infection in peritoneal dialysis patients. *J. Am. Soc. Nephrol.* Feb 2005;16(2):539-545.
229. Taylor EN, Kummer KM, Durmus NG, Leuba K, Tarquinio KM, Webster TJ. Superparamagnetic Iron Oxide Nanoparticles (SPION) for the Treatment of Antibiotic-Resistant Biofilms. *Small.* 2012.
230. Dwyer DJ, Kohanski MA, Collins JJ. Role of reactive oxygen species in antibiotic action and resistance. *Curr. Opin. Microbiol.* Oct 2009;12(5):482-489.
231. Kohanski MA, Dwyer DJ, Hayete B, Lawrence CA, Collins JJ. A common mechanism of cellular death induced by bactericidal antibiotics. *Cell.* Sep 2007;130(5):797-810.
232. Hiramatsu K, Hanaki H, Ino T, Yabuta K, Oguri T, Tenover FC. Methicillin-resistant Staphylococcus aureus clinical strain with reduced vancomycin susceptibility. *J. Antimicrob. Chemother.* Jul 1997;40(1):135-136.
233. Wan J, Cai W, Meng X, Liu E. Monodisperse water-soluble magnetite nanoparticles prepared by polyol process for high-performance magnetic resonance imaging. *Chem. Commun.* 2007(47):5004-5006.
234. Dobrovolskaia MA, Patri AK, Zheng JW, et al. Interaction of colloidal gold nanoparticles with human blood: effects on particle size and analysis of plasma protein binding profiles. *Nanomed.-Nanotechnol. Biol. Med.* Jun 2009;5(2):106-117.
235. Murdock RC, Braydich-Stolle L, Schrand AM, Schlager JJ, Hussain SM. Characterization of nanomaterial dispersion in solution prior to In vitro exposure using dynamic light scattering technique. *Toxicol. Sci.* Feb 2008;101(2):239-253.
236. Liu JY, Sonshine DA, Shervani S, Hurt RH. Controlled Release of Biologically Active Silver from Nanosilver Surfaces. *ACS Nano.* Nov 2010;4(11):6903-6913.
237. Alt V, Bechert T, Steinrucke P, et al. An in vitro assessment of the antibacterial properties and cytotoxicity of nanoparticulate silver bone cement. *Biomaterials.* Aug 2004;25(18):4383-4391.
238. LaConte L, Nitin N, Bao G. Magnetic nanoparticle probes. *Materials Today.* 2005;8(5):32-38.
239. Ito A, Ino K, Kobayashi T, Honda H. The effect of RGD peptide-conjugated magnetite cationic liposomes on cell growth and cell sheet harvesting. *Biomaterials.* Nov 2005;26(31):6185-6193.
240. Huang DM, Hsiao JK, Chen YC, et al. The promotion of human mesenchymal stem cell proliferation by superparamagnetic iron oxide nanoparticles. *Biomaterials.* Aug 2009;30(22):3645-3651.
241. Evanoff DD, Chumanov G. Synthesis and optical properties of silver nanoparticles and arrays. *ChemPhysChem.* Jul 2005;6(7):1221-1231.
242. Fujiwara Y, Kobayashi Y, Kita K, et al. Ag nanoparticle catalyst for electroless Cu deposition and promotion of its adsorption onto epoxy substrate. *J. Electrochem. Soc.* 2008;155(5):D377-D382.

243. Baker C, Pradhan A, Pakstis L, Pochan DJ, Shah SI. Synthesis and antibacterial properties of silver nanoparticles. *J. Nanosci. Nanotechnol.* Feb 2005;5(2):244-249.
244. Pratten J, Nazhat SN, Blaker JJ, Boccaccini AR. In vitro attachment of Staphylococcus epidermidis to surgical sutures with and without Ag-containing bioactive glass coating. *J. Biomater. Appl.* Jul 2004;19(1):47-57.
245. Chambers C, Proctor C, Kabler P. Bactericidal effects of low concentrations of silver. *J Am Waterworks Assoc.* 1962;54(2):208-216.
246. Hardes J, Ahrens H, Gebert C, et al. Lack of toxicological side-effects in silver-coated megaprostheses in humans. *Biomaterials.* Jun 2007;28(18):2869-2875.
247. Choi O, Hu ZQ. Size dependent and reactive oxygen species related nanosilver toxicity to nitrifying bacteria. *Environ. Sci. Technol.* Jun 2008;42(12):4583-4588.
248. Liu LH, Xu KJ, Wang HY, et al. Self-assembled cationic peptide nanoparticles as an efficient antimicrobial agent. *Nature Nanotechnology.* Jul 2009;4(7):457-463.
249. Recent Studies and Reports on Physician Shortages in the US. *Association of American Medical Colleges.* May 2011.
250. Kenneley IL. Infection control and prevention in home healthcare: prevention activities are the key to desired patient outcomes. *Home Healthcare Nurse.* 2007 2007;25(7):459-467; quiz 468-459.
251. Getliffe K, Newton T. Catheter-associated urinary tract infection in primary and community health care. *Age and Ageing.* 2006;35:477–481.
252. Herter R, Wallace Kazer M. Best Practices in Urinary Catheter Care. *Home Healthcare Nurse.* 2010;28(6):342-349.
253. National, Institute, for, Clinical, Excellence. Clinical Guideline 2: Infection control Prevention of healthcare-associated infection in primary and community care. 2003.
254. McNulty C, Freeman E, Smith G, et al. Prevalence of urinary catheterization in UK nursing homes. *J. Hosp. Infect.* Oct 2003;55(2):119-123.
255. Sorbye LW, Finne-Soveri H, Ljunggren G, Topinkova E, Bernabei R. Indwelling catheter use in home care: elderly, aged 65+, in 11 different countries in Europe. *Age and Ageing.* Jul 2005;34(4):377-381.
256. Landi F, Cesari M, Onder G, et al. Indwelling urethral catheter and mortality in frail elderly women living in community. *Neurourol. Urodyn.* 2004;23(7):697-701.
257. Newman DK, Willson MM. Review of intermittent catheterization and current best practices. *Urologic nursing.* 2011 2011;31(1):12-28, 48; quiz 29.
258. Wyndaele JJ. Complications of intermittent catheterization: their prevention and treatment. *Spinal Cord.* Oct 2002;40(10):536-541.
259. Consortium for Spinal Cord M. Bladder management for adults with spinal cord injury: a clinical practice guideline for health-care providers. *The journal of spinal cord medicine.* 2006 2006;29(5):527-573.
260. Pellowe CM PR, Harper P , Loveday HP , Robinson N , Jones SR , MacRae ED , Mulhall A , Smith GW , Bray J , Carroll A , Chieveley Williams S , Colpman D , Cooper L , McInnes E , McQuarrie I , Newey JA , Peters J , Pratelli N , Richardson G , Shah PJ , Silk D , Wheatley C , Guideline Development Group, . Infection control: prevention of healthcare-associated infections in primary and

community care. Guidelines for preventing healthcare-associated infections during long-term urinary catheterisation in primary and community care. *Journal of Hospital Infection.* 2003;55(Supp 2):S61 – S87.

261. McNulty C.A.M. Reducing urinary catheter related infections in care homes: a review of the literature. *Journal of Infection Prevention.* 2009;10(2):70-75.

262. Beattie M. Can silver alloy catheters reduce infection rates? *Nursing Times.* 2011;107(29):19-22.

263. http://www.drugs.com/cg/continuous-ambulatory-peritoneal-dialysis.html.

264. Piraino B, Bailie GR, Bernardini J, et al. Peritoneal dialysis-related infections recommendations: 2005 update. *Perit. Dial. Int.* Mar-Apr 2005;25(2):107-131.

265. Bender FH, Bernardini J, Piraino B. Prevention of infectious complications in peritoneal dialysis: best demonstrated practices. *Kidney Int.* Nov 2006;70:S44-S54.

266. Perez-Fontan M, Rosales M, Rodriguez-Carmona N, Falcon TG, Valdes F. Mupirocin resistance after long-term use for Staphylococcus aureus colonization in patients undergoing chronic peritoneal dialysis. *Am. J. Kidney Dis.* Feb 2002;39(2):337-341.